AN ABSTRACT OF THE DISSERTATION OF

David B. DeVallance for the degree of Doctor of Philosophy in Wood Science presented on April 24, 2009.

Title: Non-Destructive Evaluation of Veneer Using Optical Scanning and Ultrasonic Stress Wave Analysis Systems

Abstract approved:

James W. Funck

Non-destructive commercial ultrasonic grading provides laminated veneer lumber (LVL) manufacturers a means for sorting veneer based on average ultrasonic propagation time (UPT) and/or average dynamic modulus of elasticity (MOE_d). While this may provide reliable estimations of modulus of elasticity (MOE), little is known about the influence of veneer defects on strength properties of veneer and LVL. It was hypothesized that inclusion of veneer defect and growth ring pattern measures, obtained via optical scanning, would improve veneer and LVL static tensile MOE and strength (F_t) property predictions. Non-destructive and destructive testing on Douglas-fir (*Pseudotsuga menziesii*) veneer and LVL was performed to evaluate improvements in veneer and LVL tensile MOE and F_t property predictions. Various models based solely on density, optical, and ultrasonic system measures, as well as various combinations of systems measures, were developed for individual veneer and LVL property predictions.

The integration of optical and ultrasonic measures (i.e., combined system model) best explained the variation in veneer static tensile MOE and F_t. The combined system model best predicted average LVL static tensile MOE. LVL static F_t was best predicted by using overall average veneer measures comprising the entire LVL material, rather than the average of individually predicted veneer F_t used in assembling the LVL. Specifically, the combined system model, which included various specific average defect, growth ring pattern, and MOE_d measures comprising the LVL material, best explained the variation in LVL static F_t values ($R^2 = 0.65$) as compared to all other models. Results from this study suggest improved veneer and LVL F_t predictions can be achieved by integrating the existing ultrasonic and optical systems already existing in many manufacturing facilities.

Additionally, the optical model which included average defect, growth ring, and density measurements within the LVL material better explained the variation in LVL static F_t values ($R^2 = 0.58$), as compared to the MOE_d ($R^2 = 0.52$) and UPT ($R^2 = 0.31$) models. As a result, the developed optical system showed promise as a suitable veneer grading system. A need was identified for future research on optically grading full-size veneer sheets and manufacturing and testing full-size LVL billets.

Non-Destructive Evaluation of Veneer Using Optical Scanning and Ultrasonic Stress Wave Analysis Systems

by
David B. DeVallance

A DISSERTATION

submitted to

Oregon State University

in partial fulfillment of
the requirements for the
degree of

Doctor of Philosophy

Presented April 24, 2009
Commencement June 2009

Doctor of Philosophy dissertation of David B. DeVallance presented on April 24, 2009.

APPROVED:

Major Professor, representing Wood Science

Head of the Department of Wood Science and Engineering

Dean of the Graduate School

I understand that my dissertation will become part of the permanent collection of Oregon State University libraries. My signature below authorizes release of my dissertation to any reader upon request.

David B. DeVallance, Author

ACKNOWLEDGEMENTS

I would first like to express my sincere appreciation to my major professor, Dr. James W. Funck, for his continued support, assistance, patience, and input throughout my entire PhD program. His knowledge and expertise was invaluable in the successful completion of this research.

Also, I would like to convey my gratitude to my committee members, Dr. Sundar Atre, Dr. Rakesh Gupta, Dr. Glen Murphy, Dr. James Reeb, and Dr. Willie (Skip) Rochefort for their guidance throughout my endeavors at Oregon State University. I would like to especially thank Milo Clauson, not only for his amazing amount of knowledge, but whose valuable assistance made completing this research possible. In addition, I would like to thank Dr. Charles Brunner, Dr. Lech Muszyński, Dr. Jim Wilson, Dr. Jun-Won Seo, Matthew Peterson, and Joseph McRae for all their assistance.

I would also like to express my deepest appreciation to TECO for allowing me to continue to work within the wood industry throughout my PhD program and for providing much needed equipment and support. Special thanks are given to Freres Lumber Co., Inc, Hexion Specialty Chemicals, Murphy Engineered Wood Division, and Weyerhaeuser for contributing laboratory equipment, materials, and assistance.

Last, but certainly not least, to all my friends and family. In particular, Elizabeth Dickinson, who has stood by me through some very trying times with nothing but love and continual encouragement.

TABLE OF CONTENTS

Page

1. INTRODUCTION 1

1.1 Graded Veneer Use in Engineered Wood Products 2

1.2 Research Objectives 3

1.3 Hypothesis 4

2. LITERATURE REVIEW 7

2.1 Benefits and Implications of Laminating Veneers 7

2.2 Background – Non-Destructive Evaluation of Wood 10

2.3 General Stress Wave Theory for Non-Destructive Evaluation 12

2.4 Stress Wave Testing of Veneer for Use in Laminated Veneer Lumber 14

2.4.1 Veneer: Dynamic MOE in Relation to Static MOE and Strength 15
2.4.2 Veneer Dynamic MOE in Relation to LVL MOE and Strength 18
2.4.3 Strengths and Limitations of Stress Wave Veneer Grading 21

2.5 Using Stress Waves to Locate Defects 24

2.6 Influence of Moisture and Temperature on Stress Waves 25

2.7 Non-Destructive Evaluation Using Optical Scanning/Imaging Systems 27

2.8 Additional Non-Destructive Evaluation Techniques for Wood 30

2.8.1 High Resolution Ultrasonic and Acousto-Ultrasonic Systems 31
2.8.2 Nuclear Magnetic Resonance and Near Infrared Spectroscopy Systems 32

2.9 Need for Additional Veneer NDE Techniques 34

3. PRELIMINARY STUDIES 37

3.1 Preliminary Study One: Optical Scanning and Ultrasonic Systems Trials 43

TABLE OF CONTENTS (Continued)

Page

3.1.1 Preliminary Study One Test Methods 38
3.1.2 Preliminary Study One Results 45

3.1.2.1 Preliminary Findings on Predicting Veneer Tensile MOE 45
3.1.2.2 Preliminary Findings on Predicting Veneer F_t 49

3.2 Preliminary Study Two: Additional Optical and Spectral Analysis 55

3.2.1 Preliminary Study Two Procedures 55
3.2.2 Preliminary Study Results with Inclusion of Spectral Analysis and Additional Defect Measurements 56

3.3 Preliminary Study Significance 58

4. VENEER MILL VERSUS LABORATORY GRADING 60

4.1 Comparison of Mill and Lab Ultrasonic Grading 60

4.1.1 Production Facility: Veneer Grading, Sampling, and Measurements 61
4.1.2 Laboratory Setting: Veneer Grading 62
4.1.3 Comparison of Mill and Laboratory Ultrasonic Testing 63

4.2 Comparison of Mill Optical Scanning and Past Research 66

4.2.1 Production Facility: Veneer Image Capturing and Processing 66
4.2.2 Comparison of Image Measurements with Past Research Results 69

5. VENEER NON-DESTRUCTIVE EVALUATION (NDE) SYSTEM DEVELOPMENT AND DESTRUCTIVE TESTING 75

5.1 Veneer Material & Specimen Preparation for Predicting Veneer Properties 75

5.2 Non Destructive and Destructive Evaluation of Veneer Specimens 77

5.2.1 Testing of Final Veneer NDE Systems 77
5.2.2 Non Destructive Evaluation of Veneer 78

5.2.2.1 Ultrasonic System NDE on Veneer 78

TABLE OF CONTENTS (Continued)

Page

5.2.2.2 Optical Scanning System NDE on Veneer 85

5.2.3 Destructive Evaluation of Veneer 59

5.3 Veneer Non-Destructive and Destructive Evaluation Results and Discussion 91

5.3.1 Destructive Veneer Results and Relation Between MOE and F_t 92
5.3.2 Ability of Waveform Spectral Analysis Measures to Locate Defects and High Versus Low Strength Veneer 96

6. OPTICAL, ULTRASONIC, AND COMBINED NDE MODEL PREDICTIONS OF VENEER TENSILE MOE AND F_t DEVELOPMENT AND COMPARISONS 100

6.1 Methodology for Determining Statistically Significant Veneer Measures and Selecting the Most Appropriate Prediction Model for Each System 101

6.2 Veneer Density as a Predictor of Veneer Properties 102

6.3 Optical System: Development of Veneer Property Predictions 104

6.3.1 Veneer Tensile Property Model Development Using Latewood and Defect Optical Data (i.e., Basic Optical) 104
6.3.2 Veneer Tensile Property Model Development by Inclusion of Growth Ring Pattern (GRP) Measurements 109
6.3.3 Veneer Tensile Property Model Development by Inclusion of Density, Optical, and Growth Ring Pattern Measures 113
6.3.4 Veneer Tensile Property Model Development by Density and Optical Measures 118

6.4 Ultrasonic System: Development of Veneer Property Predictions 121

6.4.1 Veneer Tensile Property Model Development Using Metriguard Stress Wave Timer Data 121
6.4.2 Veneer Tensile Property Model Development Using Average MOE_d and Waveform Spectral Analysis Data 128

6.5 Combined Systems: Development of Veneer Property Predictions 132

TABLE OF CONTENTS (Continued)

Page

6.6 Comparison of Models Developed to Predict Veneer Tensile MOE and F_t 136

7. PREDICTION MODEL VALIDATION AND LVL ASSEMBLY AND PROPERTY PREDICTION 140

7.1 Veneer Specimen Preparation for Model Validation and LVL Assembly 140

7.2 Prediction Model Validation Study 142

7.2.1 Model Validation Testing Procedures 142
7.2.2 Model Validation Testing Results 142
7.2.3 Model Validation Prediction Results and Discussion 145

7.2.3.1 Veneer Tensile MOE Model Validation 146
7.2.3.2 Veneer F_t Model Validation 151
7.2.3.3 Improvements in Veneer Grading and Property Predictions 156

7.3 Laminated Veneer Lumber Assembly and Property Prediction Study 158

7.3.1 Veneer for LVL: Non-Destructive Testing and Property Prediction 159
7.3.2 LVL Assembly Procedures and Property Predictions 160

7.3.2.1 LVL Sorting and Property Predictions 160
7.3.2.2 LVL Assembly Procedures 162

7.3.3 LVL Specimen Destructive Tension Testing 165
7.3.4 LVL Property Prediction Results and Discussion 167

7.3.4.1 LVL Test Results 167
7.3.4.2 LVL Tensile MOE Property Prediction Using Developed Models 172
7.3.4.3 LVL F_t Property Prediction Using Developed Models 177

7.3.5 LVL Property Prediction via Overall Average Veneer Measures Within a Specimen 181

TABLE OF CONTENTS (Continued)

Page

7.3.6 LVL Property Prediction via NDE on LVL Material 188

7.3.7 Improvements in LVL Property Predictions 191

8. CONCLUSIONS AND FUTURE RESEARCH RECOMMENDATIONS 195

8.1 Conclusions on Each System's Ability to Predict Veneer Tensile MOE and F_t 196

8.2 Conclusions on Each System's Ability to Predict LVL Tensile MOE and F_t 198

8.3 Conclusions on Implications for Veneer and LVL Manufacturers 200

8.4 Recommendations for Future Research 201

BIBLIOGRAPHY 204

APPENDICES 211

Appendix A Model Development Study: Individual Veneer Tension Test Results, Cross Correlation Between Basic Optical, Growth Ring Pattern, Basic Ultrasonic, and Veneer Static Tensile MOE and F_t Values, and Cross Correlation Between Defect and Waveform Measures 212

Appendix B Model Validation Study: Individual Veneer Tension Test Results and Plots of Predicted Veneer Tensile MOE and F_t Values via Each Model Versus Static (actual) Tensile MOE and F_t Values 230

Appendix C Laminated Veneer Study: Individual LVL Tension Test Results, Plots of Predicted LVL Tensile MOE via Each Model Versus Static (actual) Tensile MOE, and Linear Regression Plots for Prediction of LVL Static F_t for Each System Model 242

LIST OF FIGURES

Figure — Page

3.1 Optical image lettering system layout 39

3.2 Optical image system output 40

3.3 Ultrasonic system setup 42

3.4 Destructive tensile testing system setup 44

3.5 Typical load versus deformation curve from veneer tension tests 44

3.6 Preliminary study: Veneer static tensile MOE versus average MOE_d 46

3.7 Preliminary study: Veneer static tensile MOE versus average UPT 46

3.8 Preliminary study: Veneer static tensile MOE versus density 47

3.9 Preliminary study: Veneer static F_t versus average MOE_d 49

3.10 Preliminary study: Veneer static F_t versus average UPT 50

3.11 Preliminary study: Veneer static F_t versus density 50

3.12 Preliminary study: Optically predicted veneer F_t versus static F_t 51

3.13 Preliminary study: Density and optically predicted veneer F_t versus static F_t 52

3.14 Preliminary study: Average MOE_d and optically predicted veneer F_t versus static F_t 53

3.15 Failure when growth rings were oriented parallel to specimen length 54

3.16 Specimen failure at knot and sloped growth ring pattern locations 54

4.1 Mill facility Metriguard 2800DME ultrasonic veneer grading 62

4.2 Laboratory ultrasonic stress wave system setup 63

4.3 Veneer scanning using a Ventek GS2000 scanning system 67

LIST OF FIGURES (Continued)

Figure		Page
4.4	Windowed veneer image captured via a Ventek GS2000 scanning system	68
4.5	Veneer image thresholding for percent earlywood (black) and latewood (white)	68
4.6	Veneer image thresholding for percent defect area (white)	68
4.7	Predicted veneer average UPT (using Funck et al. formula) versus mill average UPT	70
4.8	Predicted veneer average UPT using latewood percentage and defect area versus mill average UPT	72
4.9	Predicted veneer average MOE_d using latewood percentage and defect area versus mill average MOE_d	73
5.1	Example of purposely selected specimens containing specific features	76
5.2	Modified ultrasonic stress wave testing setup	80
5.3	Setup of oscilloscope voltage capturing system	82
5.4	Example clipped waveform data used to perform spectral analysis	83
5.5	Example spectral analysis output for PS and PSD on linear scale	83
5.6	Example spectral analysis output for PEAK and RMS on linear scale	84
5.7	Example spectral analysis output for PS and PSD on dB scale	84
5.8	Example spectral analysis output for PEAK and RMS on dB scale	85
5.9	Setup of final optical scanning system	86
5.10	Close-up of camera and veneer specimen in optical scanning system	86
5.11	Original and threshold veneer images	88
5.12	Original and defect threshold veneer images	89

LIST OF FIGURES (Continued)

Figure — Page

5.13 Growth ring pattern measurement images showing analysis along the veneer image length (E) and across the veneer width (E90) 90

5.14 Veneer static F_t versus static tensile MOE from model development study destructive testing 95

5.15 Three highest strength veneer specimens (relatively defect free and straight failure patterns) with arrows indicating failure locations 95

5.16 Three lowest strength veneer specimens (numerous, large defects and highly sloped failure patterns) with arrows indicating failure locations 96

5.17 Cumulative sum versus frequency of power spectrum output data on veneer with minimum, maximum, and average values of maximum defect width 98

5.18 Cumulative sum versus frequency of power spectrum output data on veneer with minimum, maximum, and average values of F_t 98

6.1 Veneer static tensile MOE versus density 103

6.2 Veneer static tensile strength versus density 103

6.3 Predicted veneer tensile MOE from the basic optical model (latewood and defect measures) versus veneer static tensile MOE 107

6.4 Predicted veneer tensile strength from the basic optical model (latewood and defect measures) versus veneer static F_t 108

6.5 Predicted veneer tensile MOE from the optical and growth ring pattern measures model versus veneer static tensile MOE 110

6.6 Predicted veneer F_t from the optical and growth ring pattern measures model versus veneer static F_t 112

6.7 Predicted veneer tensile MOE from the optical, growth ring pattern measures and density model versus veneer static tensile MOE 114

6.8 Predicted veneer F_t from the optical, growth ring pattern measures and density model versus veneer static F_t 116

LIST OF FIGURES (Continued)

Figure — Page

6.9 Predicted veneer tensile MOE from the basic optical and density model versus veneer static tensile MOE 119

6.10 Predicted veneer F_t from the basic optical and density model versus veneer static F_t 120

6.11 Veneer static tensile MOE versus average MOE_d 123

6.12 Veneer static F_t versus average MOE_d 124

6.13 Veneer static tensile MOE versus average UPT 126

6.14 Veneer static F_t versus average UPT 126

6.15 Predicted veneer tensile MOE from the basic ultrasonic and waveform spectral analysis measures model versus veneer static tensile MOE 129

6.16 Predicted veneer F_t from the basic ultrasonic and waveform spectral analysis measures model versus veneer static F_t 130

6.17 Predicted veneer tensile MOE from combined system measures model versus destructively determined veneer tensile MOE 133

6.18 Predicted veneer F_t from combined system measures model versus veneer static F_t 136

7.1 Model validation and LVL lay up specimen preparation layout 141

7.2 Box and whisker plots for veneer tensile MOE test results from the model development and validation studies 144

7.3 Box and whisker plots for veneer F_t test results from the model development and validation studies 144

7.4 Box and whisker plots for veneer density test results from the model development and validation studies 145

7.5 Box and whisker plots for veneer tensile MOE from all prediction models and static (destructive) results 149

LIST OF FIGURES (Continued)

Figure Page

7.6 Box and whisker plots for veneer F_t from all prediction models and static results 154

7.7 EPI adhesive application using laboratory-style adhesive spreader 163

7.8 Assembled LVL specimens prior to cold pressing 163

7.9 Cold pressed LVL specimens during manufacturing 164

7.10 LVL tension test setup 166

7.11 LVL specimen and strain gauge placement during tension tests 167

7.12 LVL static F_t versus static tensile MOE as destructively determined 169

7.13 Typical LVL tension failures showing failure through layers 170

7.14 Typical LVL tension failures observed on surface layers (A-large defects spaced apart, B-grouping of defects, C-small defect combined with diving grain) 171

7.15 Additional typical LVL tension failures observed on surface layers (A-relatively free of defects and fairly straight grain pattern, B- highly sloped grain pattern, C-two large defects combined with diving grain) 171

7.16 Box and whisker plots for LVL tensile MOE from all prediction models and static (destructive) results 174

7.17 Box and whisker plots for predicted LVL F_t using the average of individually predicted veneer F_t values under each model as compared to static (destructive) test results 178

7.18 Box and whisker plots of fitted LVL F_t values from all prediction models in comparison to static (destructive) results 181

7.19 Predicted LVL F_t from average optical measures (including growth ring pattern measures) and density versus LVL static F_t 183

LIST OF FIGURES (Continued)

Figure Page

7.20 Predicted LVL F_t from average optical (no growth ring pattern) and density measures versus LVL static F_t 184

7.21 Predicted LVL F_t from average combined system measures (average basic optical, growth ring pattern, MOE_d, and peak variance - dB scale) versus LVL static F_t 186

7.22 LVL static F_t versus non-destructively measured UPT on LVL specimens 189

7.23 LVL static F_t versus non-destructively measured MOE_d on LVL specimens 190

LIST OF TABLES

Table		Page
3.1	Optical measures determined in preliminary study one	40
3.2	Additional optical measures determined in preliminary study two	55
3.3	Statistically significant measures in preliminary study two	57
4.1	Cross correlation table	69
5.1	Oscilloscope specifications and settings	81
5.2	Veneer destructively determined tension test results	92
6.1	Statistically significant correlation coefficients from individual correlation analysis between veneer tensile MOE and various optical measurements	105
6.2	Statistically significant correlation coefficients from individual correlation analysis between veneer static tensile strength and various optical measurements	106
6.3	Statistically significant basic optical model variables, regression coefficients, and p-values from regression analysis for predicting veneer static tensile MOE	107
6.4	Statistically significant basic optical model variables, regression coefficients, and p-values from regression analysis for predicting veneer static F_t	108
6.5	Statistically significant optical including growth ring pattern measures model variables, regression coefficients, and p-values from regression analysis for predicting veneer static tensile MOE	110
6.6	Statistically significant optical including growth ring pattern measures model variables, regression coefficients, and p-values from regression analysis for predicting veneer static F_t	111
6.7	Statistically significant optical including growth ring pattern measures and density model variables, regression coefficients, and p-values from regression analysis for predicting veneer static tensile MOE	114

LIST OF TABLES (Continued)

Table — Page

6.8 Statistically significant optical including growth ring pattern measures and density model variables, regression coefficients, and p-values from regression analysis for predicting veneer static F_t 116

6.9 Statistically significant basic optical and density model variables, regression coefficients, and p-values from regression analysis for predicting veneer static tensile MOE 119

6.10 Statistically significant basic optical and density model variables, regression coefficients, and p-values from regression analysis for predicting veneer static F_t 120

6.11 Statistically significant correlation coefficients from individual correlation analysis between veneer static tensile MOE and F_t and basic ultrasonic measurements 122

6.12 Statistically significant basic ultrasonic and waveform spectral analysis measures model variables, regression coefficients, and p-values from regression analysis for predicting veneer tensile MOE 129

6.13 Statistically significant basic ultrasonic and waveform spectral analysis measures model variables, regression coefficients, and p-values from regression analysis for predicting veneer static F_t 130

6.14 Statistically significant combined system measures model variables, regression coefficients, and p-values from regression analysis for predicting veneer static tensile MOE 133

6.15 Statistically significant combined system measures model variables, regression coefficients, and p-values from regression analysis for predicting veneer static F_t 135

6.16 Comparison of R-squared values and rank for each model developed from regression analysis to predict veneer tensile MOE 137

6.17 Comparison of R-squared values and rank for each model developed from regression analysis to predict veneer F_t 138

7.1 Veneer destructively determined tension test results from validation study 142

LIST OF TABLES (Continued)

Table		Page
7.2	Comparison of R-squared values of the prediction model and validation model test when predicting veneer tensile MOE	147
7.3	Comparison of percent error of predicted average veneer tensile MOE from each model as compared to average veneer static tensile MOE	150
7.4	Comparison of average percent error for each prediction model on an individual veneer specimen basis as related to veneer static tensile MOE	151
7.5	Comparison of R-squared values of the prediction model and validation model test when predicting veneer F_t	152
7.6	Comparison of average population predictions to static values of veneer tensile F_t	155
7.7	Comparison of average percent error for each prediction model on an individual veneer specimen basis as related to veneer static F_t	155
7.8	Outline of LVL specimen assembly process variables	164
7.9	LVL destructively determined tension test results	168
7.10	Comparison of R-squared values of each prediction model in comparison to LVL static tensile MOE	173
7.11	Multiple range comparison output on tests for differences in average LVL tensile MOE between groups, showing homogeneous groups (those in bold were not statistically different from LVL static tensile MOE)	175
7.12	Comparison of average percent error for each prediction model on an individual LVL specimen basis as related to LVL static tensile MOE	176
7.13	Comparison of R-squared values of each prediction model in comparison to LVL static F_t	180
7.14	Statistically significant variables, regression coefficients, and p-values from regression analysis on average optical (including growth ring pattern measures) and density data for predicting LVL static F_t	182

LIST OF TABLES (Continued)

Table		Page
7.15	Statistically significant variables, regression coefficients, and p-values from regression analysis on average basic optical and density data for predicting LVL static F_t	184
7.16	Statistically significant variables, regression coefficients, and p-values from regression analysis on combined system measures for predicting LVL static F_t	185
7.17	Comparison of R-squared values of models using average of predicted individual veneers in comparison when using average measures within an LVL specimen to predict LVL static F_t	187

LIST OF APPENDIX FIGURES

Figure — Page

B-1 Density model: Predicted veneer tensile MOE vs. static MOE 233

B-2 Density model: Predicted veneer F_t vs. static F_t 233

B-3 Basic optical model: Predicted veneer tensile MOE vs. static MOE 234

B-4 Basic optical model: Predicted veneer F_t vs. static F_t 234

B-5 Optical + density model: Predicted veneer tensile MOE vs. static MOE 235

B-6 Optical + density model: Predicted veneer F_t vs. static F_t 235

B-7 Optical + GRP model: Predicted veneer tensile MOE vs. static MOE 236

B-8 Optical + GRP model: Predicted veneer F_t vs. static F_t 236

B-9 Optical + GRP + density model: Predicted veneer tensile MOE vs. static MOE 237

B-10 Optical + GRP + density model: Predicted veneer F_t vs. static F_t 237

B-11 Average MOE_d model: Predicted veneer tensile MOE vs. static MOE 238

B-12 Average MOE_d model: Predicted veneer F_t vs. static F_t 238

B-13 Average UPT model: Predicted veneer tensile MOE vs. static MOE 239

B-14 Average UPT model: Predicted veneer F_t vs. static F_t 239

B-15 Ultrasonic + spectral analysis model: Predicted veneer tensile MOE vs. static MOE 240

B-16 Ultrasonic + spectral analysis model: Predicted veneer F_t vs. static F_t 240

B-17 Combined Optical + ultrasonic model: Predicted veneer tensile MOE vs. static MOE 241

B-18 Combined optical + ultrasonic model: Predicted veneer F_t vs. static F_t 241

C-1 Density model: Predicted LVL tensile MOE vs. static MOE 245

LIST OF APPENDIX FIGURES (Continued)

Figure — Page

C-2 Basic optical model: Predicted LVL tensile MOE vs. static MOE 245

C-3 Optical + density model: Predicted LVL tensile MOE vs. static MOE 246

C-4 Optical + GRP model: Predicted LVL tensile MOE vs. static MOE 246

C-5 Optical + GRP + density model: Predicted LVL tensile MOE vs. static MOE 247

C-6 Average MOE_d model: Predicted LVL tensile MOE vs. static MOE 247

C-7 Average UPT model: Predicted LVL tensile MOE vs. static MOE 248

C-8 Ultrasonic + spectral analysis model: Predicted LVL tensile MOE vs. static MOE 248

C-9 Combined optical + ultrasonic model: Predicted LVL tensile MOE vs. static MOE 249

C-10 Density model: Regression equation for predicting LVL static F_t based on calculated average of predicted F_t for veneer comprising a LVL specimen 249

C-11 Basic optical model: Regression equation for predicting LVL static F_t based on calculated average of predicted F_t for veneer comprising a LVL specimen 250

C-12 Optical + density model: Regression equation for predicting LVL static F_t based on calculated average of predicted F_t for veneer comprising a LVL specimen 250

C-13 Optical + GRP model: Regression equation for predicting LVL static F_t based on calculated average of predicted F_t for veneer comprising a LVL specimen 251

C-14 Optical + GRP + density model: Regression equation for predicting LVL static F_t based on calculated average of predicted F_t for veneer comprising a LVL specimen 251

LIST OF APPENDIX FIGURES (Continued)

Figure Page

C-15 Average MOE_d model: Regression equation for predicting LVL static F_t based on calculated average of predicted F_t for veneer comprising a LVL specimen 252

C-16 Average UPT model: Regression equation for predicting LVL static F_t based on calculated average of predicted F_t for veneer comprising a LVL specimen 252

C-17 Ultrasonic + spectral analysis model: Regression equation for predicting LVL static F_t based on calculated average of predicted F_t for veneer comprising a LVL specimen 253

C-18 Combined Optical + ultrasonic model: Regression equation for predicting LVL static F_t based on calculated average of predicted F_t for veneer comprising a LVL specimen 253

LIST OF APPENDIX TABLES

Tables		Page
A-1	Individual veneer static tension MOE and F_t test results from model development study	213
A-2	Cross correlation table (correlation and p-values) for variables 1-7	216
A-3	Cross correlation table (correlation and p-values) for variables 8-14	218
A-4	Cross correlation table (correlation and p-values) for variables 15-21	220
A-5	Cross correlation table (correlation and p-values) for variables 22-28	222
A-6	Cross correlation table (correlation and p-values) for variables 29-34	224
A-7	Cross correlation table (correlation and p-values) between defect and waveform measures	226
B-1	Individual veneer static tension MOE and F_t test results from model validation study	231
C-1	Individual LVL static tension MOE and F_t test results	243

This work is dedicated to my best friend and partner in life, Elizabeth Dickinson. Words cannot express all she means to me and how blessed I am to be able spend my days with someone who is so adventurous, thoughtful, and caring.

NON-DESTRUCTIVE EVALUATION OF VENEER USING OPTICAL SCANNING AND ULTRASONIC STRESS WAVE ANALYSIS SYSTEMS

CHAPTER 1. INTRODUCTION

Veneer utilized to manufacture wood-based composite products (e.g., laminated veneer lumber and plywood) are generally evaluated and sorted based on a specific set of criteria. Typically, veneer sorting is performed to produce a product with given properties. Veneer used in manufacturing structural plywood for the United States market has to meet a particular visually determined grade dependent upon the final panel grade designation (NIST 2007). Laminated veneer lumber (LVL), however, is less of commodity product, as compared to structural plywood and many manufacturers have their own set of veneer grade designations. Regardless of the specific requirements, most manufacturers employ some type of veneer grading system. Early means of veneer grading were based on visual classification, later followed by automated stress wave grading, and, in some instances, optical scanning systems. Typically, optical information (e.g., defect size) obtained in today's industry is used to make decisions regarding veneer grade and is dependent upon having a particular defect present within an individual veneer. While this method assigns a visual grade to veneer, very little research has been performed to utilize veneer defect information in an attempt to predict veneer and composite material elastic and strength properties.

1.1 Graded Veneer Use in Engineered Wood Products

LVL is an engineered wood product consisting of individual veneer layers adhesively bonded together to form a billet. Each veneer comprising an LVL billet is aligned with the grain oriented toward the billet's long axis. This ensures veneer defects within the billet are randomized; therefore, individual localized defects are less likely to limit LVL mechanical properties. Within each veneer sheet, however, localized defects and density variability influence the strength and stiffness of each sheet, and therefore mechanical properties of LVL. To aid in predicting LVL mechanical properties, most manufacturers use ultrasonic stress wave systems to place veneer into strength categories (e.g., G1, G2, and G3). By using non-destructive stress waves, the ultrasonic propagation time (UTP) and/or the dynamic modulus of elasticity (MOE_d) are determined and used as the basis for classifying veneer into a group. More recent commercial systems allow for determining veneer sheet density to calculate MOE_d and also the ability to measure veneer moisture content and temperature. Calculated MOE_d is then adjusted for the influence of moisture content and temperature and veneer is assigned to a strength category. Once assigned to strength categories, veneer is laid-up in specific arrangements to produce LVL billets with certain predicted mechanical properties.

While commercially available grading systems allow LVL manufacturers to produce less variable products, opportunities exist to use alternative non-destructive techniques to better quantify defects, and in turn, increase overall strength by using improved lay-up patterns. Past research on large size veneer sheets determined the

MOE_d of individual veneer sheets, classified veneer into strength categories, constructed LVL billets based on categories, and determined static modulus of elasticity (MOE_s) and strength of LVL specimens. From this process, correlations were made between average veneer sheet MOE_d used in LVL billets and the resulting MOE_s and strength values. This allows for prediction of average LVL properties based on the average veneer MOE_d. Current technology, however, does not incorporate variation within veneer sheet density, grain angle, growth ring angle, and localized defects when assessing veneer modulus of elasticity and strength. Additionally, when using stress wave analysis systems, a gap exists, as there is no theoretical relationship between MOE_s and various strength properties (Bodig 2000). By utilizing optical scanning (i.e., machine vision) systems to quantify defects, there exists a possibility to improve veneer sorting and better predict LVL mechanical properties based on individual veneer sheets comprising a billet.

1.2 Research Objectives

The objectives of this research are to:

1. Determine which characteristics influence a veneer specimen's tensile modulus of elasticity (MOE) and strength (F_t).
2. Determine if individual veneer specimens can be non-destructively evaluated using an optical scanning system to accurately predict veneer tensile MOE and F_t, and provide reliable sorting for lay-up of LVL billets.
3. Determine whether or not using results from an optical scanning system to sort veneer and select the lay-up pattern for laminated veneer lumber results in

improved mechanical properties as compared to currently used systems that sort on the basis of MOE_d.

4. Determine whether or not combining information obtained from an optical scanning system and commercial type ultrasonic veneer grading system results in improved predictions of individual veneer sheet mechanical properties.

1.3 Hypotheses

1. Defects within veneer will influence individual veneer specimen tensile MOE and F_t.

While individual defects may not greatly influence the MOE of full size veneer sheets, the cumulative area of such defects may. In particular, knots represent an area of weakness in veneer sheets and need to be accounted for when assessing veneer mechanical properties. Researchers have suggested that both localized defects and overall defect area contribute to veneer strength (James 1964, Funck et al. 1991). Additionally, Gerhards (1982a) reported static MOE of lumber increased as knot-area ratio was decreased.

2. Using an optical scanning system will allow for quantifying certain veneer defects and characteristics that are not suitably detected using ultrasonic veneer grading systems.

Optical scanning (i.e., machine vision) systems are capable of locating and quantifying certain defects in veneer and lumber. Research has shown the ability of optical scanning systems to identify and quantify veneer characteristics (Schmidt 1978, Funck et al. 1991, Boardman et al. 1992, Brunner et al. 1992). Additionally, optical scanning allows for determining earlywood and latewood percentages within veneer. By optically scanning veneer and applying various threshold values to output signals, veneer characteristics (including defects such as knots) can be identified and quantified. Conversely, ultrasonic stress wave systems have shown less reliability in locating defects when solely using velocity measurements (as employed in commercial veneer grading systems). Stress wave attenuation shows the ability to identify defects (Burmester 1967), but is not incorporated into commercially available ultrasonic veneer grading systems. Additionally, for wide, long veneer sheets, the influence of knots on overall stress wave velocity is minimal (Gerhards 1982a), so current ultrasonic techniques may not properly account for localized defects when grading veneer.

3. By combining quantified defect information from an optical scanning system with ultrasonic system data, static tensile MOE and F_t will be better predicted for individual veneer specimen and LVL material.

While stress wave velocity has been used to reliably predict veneer MOE and strength, published research focuses on clear veneer specimens and very small veneer strips with some defects (Koch and Woodson 1968, Pellerin and Galligan 1973, McAlister 1976). However, McDonald (1978) suggested that inclusion of optical

scanning techniques that locate defects when non-destructively evaluating wood would complement current ultrasonic systems. Research (Funck et al. 1991) has shown correlations between veneer characteristics and ultrasonic stress wave propagation time (UPT). Specifically, veneer defect area and latewood percentage, determined optically on full-size sheets, were statistically significant when predicting UPT. While this research did not destructively evaluate veneer, it suggests that there is some relationship between veneer characteristics and MOE_d values from ultrasonic stress wave evaluated veneer. By combining veneer characteristic measurements from optical methods with ultrasonic measurements (in particular, the calculated MOE_d), it is likely that better predictions of overall veneer static elastic and strength properties can be developed. Once developed, these predictions should lead to better sorting and improved predictions of LVL mechanical properties.

CHAPTER 2. LITERATURE REVIEW

Specific background information is required to assess strengths, limitations, and areas of opportunities for non-destructive evaluation of veneer used in producing laminated veneer lumber (LVL). In particular, a background review of technology and research currently used in commercial ultrasonic stress wave systems is warranted. Also important is a review of the research and principles behind using ultrasonic stress wave systems to predict LVL elastic and strength properties. Furthermore, the ability of commercially used systems to identify and quantify various veneer defects (e.g., knots, splits, checks, etc.) needs to be addressed. Finally, alternative non-destructive techniques that allow for detection and quantifying veneer defects need to be evaluated. In doing so, limitations and areas for improvement can be identified and other non-destructive techniques can be explored. This review allowed for identifying areas where other non-destructive techniques may provide an opportunity to improve veneer sorting and predictions of LVL mechanical properties. Before reviewing various non-destructive techniques employed to predict veneer and LVL properties, principles behind laminating effects needed to be explored.

2.1 Benefits and Implications of Laminating Veneers

Veneers are laminated into a composite material to reduce the likelihood of having defects located in one specific area, thus a lower strength material (Uskoski and Bechtel 1993). Additionally, strength is increased by adhesive between each

laminate acting to reduce shear failures, which are typically responsible for tension failure (Preston 1950). In general, higher strength properties can be achieved by utilizing different laminates of veneer and horizontally randomizing defects when making LVL. While this produces a stronger material, it does not necessarily result in higher stiffness (Bodig and Jayne 1992). Furthermore, the assumption that LVL possesses a tensile strength distribution equivalent to the distribution of the laminates average strength is not strictly valid (Uskoski and Bechtel 1993). In terms of LVL strength in bending, further enhancement of strength properties can be achieved by vertical arrangement and placing laminates with larger defects at the neutral axis where stress is minimized (Bodig and Jayne 1992).

One of this study's objectives is to predict LVL mechanical properties based on individual veneer property predictions, therefore lamination effects are of importance. Serrano et al. (1996) described the lamination effect and how it relates to layered composites. Lamination effect indicates that a multi-layer composite results in higher bending strength than expected from the laminates' tensile strengths. This occurs by various means. First, a defect is more likely to reduce strength of specific laminate by itself, more so than when the same laminate is contained within a layered composite (Serrano et al. 1996). The second lamination effect, reinforcing effect, suggests a laminate possessing low strength (and usually lower elasticity) receives less stress in a layered composite, as more stress is shifted to adjacent, higher strength laminations (Serrano et al. 1996). The last effect, so called testing effect, deals with how individual veneer laminates react when tested individually versus in a layered composite. When testing an individual veneer in tension, localized bending is likely to

occur in areas containing knots and grain deviations. Such localized bending will likely influence a veneer's ultimate tensile strength. Once a laminate is placed in a composite and tested in tension, adjacent laminations confine any localized bending at knots and grain deviations (Serrano et al. 1996). Barnes (2000) reported, however, tensile strength and stiffness of veneer composites decreased as grain angle (in respect to applied stress) increased and the rate of decrease was higher for parallel oriented (e.g., LVL) versus cross-oriented (e.g., plywood) composites. This suggests overall grain pattern within a composite material still influences tensile strength and stiffness.

In terms of predicting composite material properties, in particular LVL, Bejo and Lang (2004) developed a model to predict bending and compressive MOE. The model included some measure of veneer strand orientation, indicating grain angle of individual laminates would be important in terms of MOE. Although they provided no model for LVL strength properties, grain angle of individual laminates likely have an even greater influence on strength properties than for elastic properties. Some measure of grain pattern described from an optical scanning system would likely provide significant information for improving LVL composite MOE and strength properties.

In terms of this study, lamination effect principles are important when using individual veneer predicted properties to predict LVL material properties. First, veneer characteristics influential in individual veneer properties may not be as significant when predicting LVL strength properties. Second, it may be possible the LVL strength properties are more related to measures of minimum, maximum, or variation of veneer laminae strength comprising the LVL, rather than overall average

laminae strength. Finally, while nothing feasible can be done in terms of localized bending in individual veneer tension tests, this influence will hopefully be accounted for by determining which veneer characteristics are statistically significant in terms of predicting LVL mechanical properties.

2.2 Background – Non-Destructive Evaluation of Wood

Ross et al. (1998) defined non-destructive evaluation (NDE) as "the science of identifying the physical and mechanical properties of a piece of material without altering its end-use capabilities and using this information to make decisions regarding appropriate applications". Non-destructive evaluation of wood has been practiced for some time to assess wood product quality. The earliest use of non-destructive evaluation comes in the form of grading and sorting wood products on a visual basis (Bodig 2000). Furthermore, assessment of lumber quality via visual means is likely the most prevalent NDE method (Ross et al. 1998). By determining the size, amount, and defect location, lumber and veneer is categorized into different grades for both structural and non-structural (appearance) use. While visual grading has been a historical practice, much attention and research focuses on finding new and alternative non-destructive techniques to better predict physical and mechanical properties of wood products.

Jayne's (1959) hypothesis, that wood's static behavior is dictated by the same mechanisms that control wood's ability to store and dissipate energy, led to investigating relationships between static behavior and energy. More recent

developments in NDE techniques focused on using various methods to better predict wood stiffness and strength. In terms of physical NDE of lumber, many techniques exist including: electrical resistance, dielectric and vibrational properties, acoustical emission, wave propagation, and X-ray (Ross et al. 1998). Additionally, mechanically proof loading lumber in bending, tension, and compression to determine stiffness provides alternative NDE approaches (Ross et al. 1998). Once stiffness is determined, relationships between wood stiffness and strength are then used to predict strength. Bodig (2000) points out that while this is commonly done, there exists only a partial relationship between stiffness and strength and that there is, to date, no theoretical relationship between the two properties. This is because strength is controlled by localized defects and stiffness is a function of the overall material characteristics.

In terms of this study, ultrasonic stress wave systems are the primary non-destructive method used to judge veneer quality when manufacturing laminated veneer lumber. Ultrasonic stress waves are used to determine veneer MOE_d and assign veneer to strength categories. The use of ultrasonic stress wave technology has been related to the growth of the LVL industry (Ross et al. 1998, Pellerin and Ross 2002). Ultrasonic stress wave technology is similar to sonic stress wave systems, but is applied at higher frequencies. Research using stress waves encompasses investigation that relates stress wave speed to wood properties and stress wave attenuation to wood defect detection. The fundamental NDE research using stress waves covers a variety of wood products including log quality, lumber, glue-laminated beams, wood composites (e.g., particleboard), and engineered structural lumber (e.g., laminated veneer lumber). As research progressed, there became a need to determine how stress

waves are influenced by moisture content, temperature, grain angle, and growth ring angle. A combination of prior research on sonic and ultrasonic stress waves led to the development of ultrasonic stress wave systems employed in today's LVL manufacturing facilities.

2.3 General Stress Wave Theory for Non-Destructive Evaluation

Before looking at ultrasonic stress wave evaluation of veneer and LVL, a basic understanding of stress wave theory and relationships to material properties is warranted. Specifically, one must first understand the theory behind stress wave propagation speed, particle movement, and energy dissipation (i.e., wave attenuation). Ross (1985) provided a detailed explanation of general stress wave behavior principles. In doing so, he described stress wave motion in a long, thin viscoelastic bar with an applied compression force at one end. When subjected to a compressive force, molecular particles at the end begin moving longitudinally in a wave fashion down the bar. As the wave travels, particles at the leading edge become excited and those at the trailing edge come to rest. As a result of wave travel through the rod, slight longitudinal particle movement is produced. Once the wave travels to the rod's end, it is reflected and the wave movement changes direction. Even though the wave direction changes, particle movement direction remains the same because there is now a tensile force on the particles. Ross (1985) further details that during this process the wave speed remains constant, but the energy associated with each pass dissipates.

With each successive wave, particle motion decreases until all particles come to rest. The rate at which particle motion decreases is a measure of stress wave attenuation.

From the theory of how stress waves travel through materials, a generally accepted formula to calculate wood's dynamic modulus of elasticity (MOE_d) using stress wave velocity (c) and measured density is as follows (Pellerin and Ross 2002):

$$MOE_d = c^2 \times \rho$$

Where: MOE_d = dynamic modulus of elasticity

c = stress wave velocity

ρ = mass density

Even though wood is an anisotropic, non-homogenous material and this relationship is based on theory for a one-dimensional case, it has been adopted by the wood science field. Adoption of this relationship has been explored by researchers in wood science and specifically in early work by Bertholf, (1965) on clear wood specimens and Pellerin and Galligan (1973) who patented a NDE stress wave system based on this relationship. Numerous NDE research projects on wood materials utilized stress waves and calculated the dynamic modulus of elasticity (Koch and Woodson 1968, Pellerin and Galligan 1973, Gerhards 1982a, Ross 1985, Ross and Pellerin 1988 and 1994, Pellerin and Ross 2002, Ross et al. 2004). Research using this relationship as a foundation to correlate MOE_d to other physical and mechanical properties exists in many areas of wood science including: log quality, solid lumber, wood degradation, veneer, and wood-based composite materials.

From the basic stress wave theory summarized previously, it is apparent that stress wave speed is constant within a material and that energy associated with particle motion diminishes with each pass of the wave through a material. Using this basis, researchers focused on determining regression equations (i.e., relationship) between dynamic modulus of elasticity and static properties (both MOE and strength) of various wood products. While stress wave velocity (i.e., transit or propagation time over a given length) is the basis for current commercial systems that grade veneer, stress wave attenuation has been the focus of much research when analyzing wood for defect characteristics. In general, for wood, stress waves are used to quantify energy storage and dissipation by using low molecular motion (Ross and Pellerin 1988). Stress wave transit time is a measure of energy storage, and stress waves travel at higher speed (i.e., faster transit times) through stronger material. Furthermore, stress wave attenuation (i.e., particle velocity amplitude over time) measures the relative amount of energy dissipation in wood, and stronger materials attenuate at a slower rate than weaker materials (Ross 1985, Ross and Pellerin 1988).

2.4 Stress Wave Testing of Veneer for Use in Laminated Veneer Lumber

Dynamic modulus of elasticity is one currently used basis for assessing veneer quality when manufacturing laminated veneer lumber. Metriguard, Inc. produces the only commercial system to ultrasonically grade veneer (Pellerin and Ross 2002). The Metriguard system grades veneer into strength categories by using the fundamental relationship that MOE_d is a function of density and longitudinal stress wave velocity.

The current Metriguard system measures ultrasonic velocity, specific gravity, moisture content, veneer sheet width, and compensates for veneer temperature (Logan 2000). From these measurements, the newest system allows for sorting veneer based on computed MOE_d, ultrasonic wave velocity, or veneer density. Since this system is commercially produced, much of the information and research surrounding the development is proprietary. The system evolved from early research performed on veneer and lumber using sonic stress waves to evaluate MOE_d and relate it to static MOE. Much of the current research focuses on using the Metriguard system to evaluate veneer, assign it to categories, lay-up LVL billets based on strength categories, and test the static properties of LVL. Some early research provided the fundamental basis for developing relationships between veneer MOE_d and MOE_s (static modulus of elasticity).

2.4.1 Veneer: Dynamic MOE in Relation to Static MOE and Strength

Koch and Woodson (1968) reported a strong correlation (r-squared = 0.888) between the MOE_d and static tensile MOE in southern pine veneer strips (2.75-inches wide) using a sample size of 177 observations. Similarly, Pellerin and Galligan (1973) reported a correlation of 0.955 (r-squared = 0.91) between veneer MOE_d and static tensile MOE with a sample size of 120 in their patented method for NDE evaluation method for grading wood. McAlister (1976) reported a coefficient of determination (r-squared) of 0.971 between MOE_d and MOE_s in tension when testing loblolly pine; however, here the sample size of sixteen was much smaller. One interesting note from

the McAlister study was that veneer specific gravity and MOE_d had a coefficient of correlation 0.497, but concluded using specific gravity as a tool to select veneer would not result in reduced variability within a composite veneer product. Logan (2000) indicated veneer sorting solely by density (or specific gravity) is useful in controlling the average grade of a population, but may not be appropriate for sorting individual veneers. Furthermore, Logan (2000) pointed out that in some wood species, there is a strong correlation between micro fibril angle and specific gravity. This correlation allows for veneer sorting solely by density when line speeds are greater than what an ultrasonic stress wave grading system can achieve.

Other research (Hunt et al. 1989) reported density as a poor predictor of yellow-poplar veneer strand tensile strength ($R^2 = 0.006$). Hunt et al. (1989) also reported a high correlation between yellow-poplar veneer strand tensile MOE_s versus MOE_d ($R^2 = 0.699$) and a correlation between veneer tensile strength and static MOE ($R^2 = 0.472$). However, there was no report of the correlation (if any) between veneer MOE_d and static tensile strength, and in the study, the yellow-poplar strands were clear, straight grain veneer material.

More recent research conducted by Lang et al. (2003) on five different hardwood species compared tensile MOE_s to MOE_d. Results from this research indicated the traditional MOE_d formula is applicable for larger sheets, as propagation times on small strips were not different from propagation times on larger sheets. Additionally, tensile MOE_d versus MOE_s showed a first order linear relationship with an $R^2 = 0.91$. Further analysis indicated by using a second order approach resulted in a slight improvement ($R^2 = 0.94$) in MOE_s from MOE_d information. Again, this

research utilized small strips (25-mm wide by 100-mm long) free from defects. They reported low variation in MOE results, which could be a function of testing clear material. It was also reported that MOE_d decreased significantly with increasing grain under 45-degrees, and then leveled off above 45-degrees. This indicates MOE_d is significantly influenced by grain angle within a veneer. Of note in this research was a reasonably successful prediction model incorporating grain angle to predict MOE_s (Lang et al. 2003). Because specimens were clear of defects, localized grain angle patterns around knots, which are likely to also influence MOE, were not included in the model.

While strong correlations between MOE_d and static MOE in tension have been reported, little information is available on the relationship between veneer ultrasonic stress wave velocity and strength. Additionally, most research focused on small veneer strips, rather than larger specimens, including larger size veneer sheets used in manufacturing LVL. Results on small veneer strips would not account for within-sheet variation and overall defect area encountered when assessing full size veneer sheet properties. Furthermore, past research on LVL mechanical properties focused specifically on correlating LVL elastic and strength properties to average MOE_d of veneer sheets used in manufacturing LVL. While this method is common when assessing veneer, there exists a gap within grading an individual full size veneer based on strength, and limits current systems used to manufacture LVL to specific lay-up patterns. Better prediction of individual veneer strength (which includes defect and growth ring pattern information) would allow for lay-up patterns to be changed and

result in better predictions of LVL mechanical properties without physical testing and development of many regression equations.

2.4.2 Veneer Dynamic MOE in Relation to LVL MOE and Strength

In early research, Kunesh (1978b) described a lack of consistency in producing high grades of parallel laminated veneer lumber when using visually graded C and D veneer. Additionally, Kunesh (1978b) concluded visual classifications resulted in poor correlation to LVL strength. In terms of transit time, faster transit times (i.e., higher stress wave velocity) are generally representative of stronger material (Ross 1985). From a visually graded standpoint, C grade veneer is assumed to be stronger than D grade veneer, and should result in faster stress wave transit time. However, Pieters (1979) reported that stress wave time of flight (i.e., transit time) for D grade veneer was faster, in many cases, than for C grade veneer; therefore there is a need for a more efficient NDE system when grading veneer. In response to this, use of a Metriguard system (Model 239 Stress Wave Timer) to grade veneer was initiated. Kunesh (1978b) reported that veneer longitudinal stiffness (as measured from a dynamic stress wave system) and LVL tension and bending strengths resulted in a correlation of 0.92 and 0.91, respectively. Furthermore, a strong correlation existed between LVL dynamic longitudinal stiffness and tensile and bending strengths. As a result of these findings, Kunesh (1978b) reported similar high correlations were obtained using ultrasonic stress waves (Metriguard model 2600) instead of shock energy when using stress waves.

Pieters (1979) reported results on average LVL billet ultrasonic propagation time (UPT) computed by averaging the individual veneer's UPT values within a billet. He reported correlations between average billet UPT to LVL tensile, edge-wise bending, compression parallel, and edge-wise bending stiffness, of 0.80, 0.88, 0.68, and 0.80, respectively. In the same study, laying-up LVL based on ultrasonically graded veneer did not result in higher mean strength as compared to using a visual lay-up method (i.e., lay-up based on C and D grade visually sorted veneer). However, the UPT lay-up method resulted in LVL billets with a better predicted mean strength and reduction in variability (i.e., lower coefficient of variation).

Jung (1982) investigated LVL MOE and strength in edge-wise bending, flat-wise bending, and tension produced from Douglas-fir veneer. Predicted veneer and billet modulus of elasticity (referred to as MOE_p) was calculated using an ultrasonic stress wave system. Additionally, when evaluating flat-wise bending, a weighted MOE_p (value that weighted each veneer's MOE_d by their corresponding amount of inertia) was calculated. High correlations were found between MOE_p and static MOE for edge-wise bending, flat-wise bending, flat-wise bending (weighted), and tension with r-squared values of 87.9%, 82.3%, 78.6%, and 65.9%, respectively. While high correlations were found between MOE_p and static MOE, the same was not true in terms of static strength. Jung (1982) reported that ultrasonic stress wave prediction provided poor correlation to strength (r-squared from 0.4% to 30.6%). Additionally, he reported that static MOE did not correlate well with static strength (r-squared from 8.1% to 37.1%). He hypothesized that poor correlations may have been influenced by not having any low-quality material in the study. Nonetheless, in terms of strength

prediction, Jung's (1982) results appear to contradict what has been found by other research (Kunesh 1978b, Pieters 1979). Moreover, poor correlations between static MOE and static strength may suggest that defects need to be considered when relating these two properties.

More current research focused on using ultrasonic veneer grading, in particular the Metriguard veneer system, to evaluate alternative species (i.e., red maple and yellow-poplar) for producing LVL. Kimmel and Janowiak (1995) used ultrasonic graded veneers to lay-up LVL based on optimized and mixed strategies. They reported statistically significant higher average flat-wise flexural MOE for LVL when using an optimized lay-up pattern of veneer sorted by ultrasonic propagation time. For average flat-wise flexural MOR (modulus of rupture), they reported higher values for optimized lay-ups, but found no statistically significant difference in average MOR for mixed lay-ups. For flexure properties, however, optimized sorting resulted in lower variation around the mean. In terms of shear properties (parallel and perpendicular to the glueline) they reported higher average shear values and lower coefficient of variation for mixed lay-ups, but no statistically significant difference to optimized lay-ups.

Wang et al. (2003) further studied using red maple veneer for manufacturing LVL. Their results showed strong linear relationships between both average ultrasonic propagation time and average MOE_d with average flat-wise billet MOE, average edge-wise (using small specimens) MOE, and average edge-wise MOR (small specimen). In all cases, MOE_d provided higher correlation coefficients, indicating inclusion of density improved relationships to static properties. However, the authors

indicated that further research was necessary to investigate effects of other factors, including grain angle. This suggestion indicates that ultrasonic stress wave systems do not properly identify differences in veneer grain angle which can influence mechanical properties of LVL.

2.4.3 Strengths and Limitations of Stress Wave Veneer Grading

Tensile strength is an important property and considered by some in industry as an indication of product and process quality (Kunesh 1978a). While much attention in sorting veneer via MOE_d concentrates on elasticity, tensile strength may be the limiting factor in some design applications. The premise behind laminating veneers together is defects are spread throughout a billet. While average MOE in tension for LVL may represent average veneer MOE in a billet, the same cannot be stated for tensile strength, as individual veneers do not always have an equivalent strength ratio to elasticity (Uskoski and Bechtel 1993). Elasticity generally represents overall material characteristics, but strength is controlled by localized defects (Bodig 2000); therefore other factors such as localized knots and grain angle could play an important role in determining individual veneer and LVL tensile strength. Pellerin (1965) reported energy dissipation was unreliable for predicting bending strength of construction lumber. Mainly, the influence of defects and cross grain was not accurately accounted for by energy dissipation amount. However, energy dissipation was found to be a better predictor of bending MOE.

Jung (1979) reported stress wave techniques did not detect steep grain angles in veneer. Additionally, he concluded while stress waves become impeded when going through a knot, in wide veneers, the impeded stress wave will catch up with the overall stress wave. Gerhards (1982b) indicated when evaluating lumber, while knots and curved grain around them, tend to slow stress waves, if straight grain is located around knots, overall knot influence on stress waves is minimal. Furthermore, Jung (1979) pointed out when measuring stress wave velocity only at the veneer's end grain, defect location and size characteristics, most likely, cannot be established. He made this finding when assessing veneers with a 10-inch width. Lastly, his findings suggested as veneer sheets become narrower, stress wave path is increasingly restricted; therefore veneer grading via stress waves provide better approximation of quality as width is reduced. This finding may help explain why such high correlations between stress wave and tensile strength existed in earlier studies on veneer strips. Because the strips were narrow, better correlations could be developed for tensile strength. In current ultrasonic stress wave systems, however, measurements are made on much wider sheets (typically, 4-foot width) and at the sheet's end (typically, 8-foot in length). Based on Jung's (1979) findings, current ultrasonic stress wave systems would not be able to estimate location and size of defects which may be the limiting factor controlling veneer tensile strength.

While tensile strength may be influenced by localized defects, it is likely that when a veneer contains numerous defects, it affects modulus of elasticity. Ross et al. (2004) measured MOE_d on veneer peeled from number 1, 2, and 3 logs. In general, veneer peeled from number 3 logs should be expected to contain a higher degree of

defects. Veneer from number 3 logs, using material from the Great Lakes States, appeared to have MOE_d distributions in the upper two-thirds of a normally distributed population. Veneer peeled from number 3 logs, using material from Eastern States, showed a low tail in MOE_d as they expected. While no mention was made regarding differences in defect amount (i.e., knots) in the veneer from the two regions, the discrepancy led them to remove veneer from number 3 logs in their overall analysis. It could be argued, based on Jung's (1979) observations, the inability of stress wave systems to approximate defects on wide sheets led to discrepancies in MOE_d as measured by Ross et al. (2004).

Although ultrasonic stress wave veneer grading has some limitations, it is evident the current system reduces overall variability in strength and elasticity from billet to billet and production run to production run as compared to visual human grading. Sharp (1985) reported a historical variation in LVL strength properties from 16-18% with visual grading techniques to a reduction of 10-12% using ultrasonic stress wave systems. Since strength design values are typically based on the lower 5^{th} percentile of a distribution, a reduction in the coefficient of variation by using ultrasonic stress wave systems allows for increasing LVL design values. Past research has not proved the ability of ultrasonic stress wave systems to increase LVL mean strength as compared to traditional visual grading techniques (Pieters 1979). An automated optical scanning system capable of estimating defect size and location combined with an ultrasonic system to reduce variability should result in both higher average LVL strength and elasticity; and therefore it would allow for a further increase in design values.

2.5 Using Stress Waves to Locate Defects

It is apparent that defects play an important role in determining both elasticity and strength of wood. In particular, defects are likely to influence strength properties to a higher degree than elastic properties (James 1964). Furthermore, when using regression equations to relate elasticity to strength, different regression coefficients are likely needed depending upon the amount of defects in the wood material (James 1964). This suggests inclusion of defect characteristics into regression equations is needed when relating elasticity to strength. When investigating knot detection in Scots pine (*Pinus sylvestris L.*), Burmester (1967) concluded ultrasonic sound reduction over time better detected knots as compared to sound velocity. Using transverse stress waves, Fuller et al. (1994 and 1995) determined a small increase in transit time occurred when knots were located in red oak lumber. While increase in transit time due to knots was small when measured over the lumber's entire length, larger localized transit time increases at knot locations were observed.

A similar finding was made by Gerhards (1982a) when using longitudinal stress waves to calculate MOE_d of southern pine and Douglas-fir lumber containing various size knots. MOE_d was determined over various distances (i.e., spans) between sensors that included a knot within the test span. After stress wave testing was completed, the lumber's bending MOE_s was determined. The results showed a statistically significant relationship between MOE_d and MOE_s when stress waves were measured over a span of one-foot, but not over a span of two-foot and greater. This suggests longitudinal stress wave systems are unable to detect knot presence when

velocity is measured over a distance of two-feet or greater, as done when evaluating full size veneer sheets. Additionally, he determined knot-area ratio was not statistically correlated to stress wave transit time, but MOE_s increased as knot-area ratio decreased (Gerhards 1982a). Other research (McDonald 1978) reported defects were not adequately identified in lumber's width when using a longitudinal stress wave system, but suggested inclusion of optical scanning techniques, to locate visible surface defects, would complement ultrasonic systems. This suggestion is important in the context of this study, as defects (e.g., knots, hole, splits, etc.) likely to influence veneer mechanical properties are visible because of the relative thickness of veneer.

2.6 Influence of Moisture and Temperature on Stress Waves

When non-destructively evaluating wood, both moisture content and temperature influence stress wave velocity. Past research agrees as moisture content of wood decreases, stress wave velocity increases (James 1961, Gerhards 1975, Sakai 1990, Brashaw et al. 1996, Kang and Booker 2002, Brashaw et al. 2004). Brashaw et al. (2004) reported a strong correlation (correlation coefficient = 0.91) between green and dry veneer stress wave values. Kang and Booker (2002) reported stress wave velocity decreases at a high rate when moisture content increases from zero to wood's fiber saturation point (FSP). After reaching fiber saturation, stress wave velocity continues to decrease as moisture content increases, but at a slower rate. While there is a relationship between moisture content and changes in stress wave velocity, the question would be whether or not this known relationship allows for proper prediction

of LVL properties at various moisture contents. Pu and Tang (1997) reported that as southern pine LVL moisture content increased, edge-wise bending static MOE decreased much more significantly than indicated by the decrease in dynamic MOE, determined via stress wave testing. Furthermore, Lee et al. (2001) reported NDT methods (i.e., stress wave and transverse-vibration) did not reliably demonstrate the actual effect of relative humidity (RH) on yellow-poplar LVL static bending test results.

While the relationship between moisture content and stress wave speed allows for commercial systems to adjust for moisture content, localized wet pockets will also result in slower stress wave velocity (Gerhards 1975). This may be of importance if veneer is adjusted for an overall sheet moisture content, while the localized wet pockets influence the stress wave values. When this occurs, calculated veneer dynamic modulus of elasticity may be underestimated. In cases where veneer is stress wave evaluated at moisture contents above fiber saturation, higher moisture contents can dampen the signal of commercially used stress wave timers (Brashaw et al. 1996). Additionally, Sakai (1990) determined abrupt transition between Douglas-fir earlywood and latewood resulted in more scattered data when evaluating influences of moisture content on stress wave velocity.

While moisture content influences stress wave velocity, temperature is also important to a lesser degree, but needs to be accounted for during veneer grading via stress waves (Kang and Booker 2002). Stress wave velocity decreases with increasing wood temperature (James 1961, Kang and Booker 2002). Additionally, transducer temperature can change stress wave transit time (i.e., stress wave velocity) and as

temperature increases, transducer sensitivity decreases (Kang and Booker 2002). Because of this, both wood and transducer temperature may influence stress wave velocity when assessing veneer quality. To date, little research has been published on the influence of temperature during ultrasonic veneer grading. For this study, using an optical scanning system to grade veneer would remove temperature influence. From a mill production standpoint, however, temperature during non-destructive veneer evaluation will influence moisture content and still needs to be considered when using an optical scanning system.

2.7 Non-Destructive Evaluation Using Optical Scanning/Imaging Systems

Most important, for this research, are NDE techniques associated with optical scanning (i.e., machine vision). Since inherent veneer defects likely influence strength properties, quantitative data on defect size and location needs to be determined during non-destructive evaluation. While human visual grading is historically the oldest method of NDE, limitations include things such as human graders are only able to evaluate features they are trained to identify, and their results can be influence by experience, lighting, and fatigue (Boardman et al. 1992). Schmidt (1978) pointed out that optical techniques are viable at high speeds and able to be used in conjunction with various types of ultraviolet, visible, and infrared light. Furthermore, he concluded an optical system (called SYDAT) was able to detect knots in veneer by using visible light. While he did not present any data to back his conclusions, other research has determined optical scanning as a viable means to detect defects.

Color is of particular importance when scanning veneer for defects. By utilizing color camera systems, defects could be classified more efficiently than when using gray-scale optical systems (Lebow et al. 1996, Boardman et al. 1992, Brunner et al. 1990). Brunner et al. (1990) provides an in-depth outline of how information from optical scanning with color is used to quantify signals into useable information for classifying defects. They point out the first quantitative color measurement standard was developed by the Commission Internationale de l'Eclairage (CIE) based on three primary monochromic lights with various wavelengths. Light having wavelengths of 700nm, 546.1nm, and 435.8nm are classified as "red", "green", and "blue", respectively (commonly referred to as the RGB system) and color cameras can separate RGB signals for each pixel of an image (Brunner et al. 1990). Advancements in cameras (e.g., extended-color and multi-spectral) led to newer systems utilizing both higher and lower wavelengths of color than RGB (Brunner et al. 2001). With these newer systems, careful consideration needs to be given in terms of light sources, focusing, and post-imaging processing when classifying defects (Butler et al. 2002). Using both gray-scale and color optical systems, much research has focused on grading lumber for aesthetics and defects. For this study, however, research pertaining to locating and quantifying defects (e.g., knots, splits, holes, etc.) and determining ratios of earlywood versus latewood in veneer are of particular importance.

Boardman et al. (1992) reported an optical system, which combined signals of a three color system (light-dark, red-green, and yellow-blue), was able to detect defects in black walnut veneer at a 78% success rate. Additionally, 98% of the time knots were successfully classified as such, rather than another type of defect. In

general, they pointed out defects tended to be darker and different in color than clear wood material. Lebow et al. (1996), using spectral reflectance (i.e., percentage of incident light for each wavelength reflected back from an object's surface), concluded that Douglas-fir veneer sapwood/earlywood had an average brighter appearance than sapwood/latewood. This suggests earlywood could be differentiated from latewood as areas with a brighter appearance when using spectral reflectance techniques. Brunner et al. (1992) showed the three color system, RGB, could be useful in measuring brightness if color space was computed by dividing each primary color (RGB) by their cumulative sum. In particular, when investigating Douglas-fir veneer, "R" performed the best in differentiating between knots and clear wood material, and thus, only one-dimensional analysis (i.e., brightness) is required to detect knots (Brunner et al. 1992). They pointed out, however, a commercial system would require two-dimensional analysis (i.e., measures of brightness and chromaticity) to identify multiple defects (e.g., knots and pitch streaks).

Since one of the objectives in this study is to use optical scanning to quantify veneer defects and earlywood/latewood percentages and relate them to mechanical properties, of particular interest was research performed by Funck et al. (1991). While previous research showed optical scanning techniques could identify defects and features in veneer, no relationship to mechanical properties has been reported. Funck et al. (1991) optically scanned Douglas-fir veneer sheets (2-feet wide by 8-feet long) and found certain features as being statistically correlated to ultrasonic propagation time (UPT) measurements from a commercial Metriguard UPT system. Their results indicated UPT measurements could be predicted (with an R-squared of 0.77) using

veneer defect area and latewood percentage obtained from optical imaging. Specifically, by applying a threshold to green channel signals, images were converted from color to black and white (i.e., binary), then latewood and defect pixels were counted. While these results are promising for development of an optical scanning system to measure mechanical properties of individual veneer sheets, their results relied on relationships between UPT and mechanical properties of veneer. As previously discussed, there is limited published research on full size veneer UPT measurements in relation to static material properties, other than studies on small veneer strip mechanical properties. This being said, optical systems show potential for measuring defects and latewood percentages on full size veneer sheets, and then performing mechanical tests on full veneer sheets to determine if a relationship exists.

2.8 Additional Non-Destructive Evaluation Techniques for Wood

While other NDE techniques are utilized to evaluate wood properties, as previously stated, only one commercially available system exists that measures veneer MOE non-destructively. Common NDE techniques used to estimate physical and mechanical properties of wood include electrical resistance, dielectric, vibration, wave propagation, acoustic emissions, x-ray, and flexural stiffness (proof loading) (Pellerin and Ross 2002). While the most common type of proof loading, machine stress rating (MSR), is typical in lumber evaluation, it would be extremely difficult to use when categorizing veneer because of veneer's character (e.g., waviness and relatively

thinness) (Logan 1978). That being said, in terms of this study, some other relevant systems were evaluated on how they pertain to solid wood and veneer.

2.8.1 High Resolution Ultrasonic and Acousto-Ultrasonic Systems

In evaluating detection of earlywood and latewood, Berndt et al. (1999) used high resolution ultrasonic imaging. They investigated ultrasonic transit time (i.e., propagation velocity), attenuation, reflective properties, and backscatter emitted from wood inhomogeneities. By recording signals from a digital oscilloscope and taking high quality photographs of southern pine specimens, they concluded latewood areas had a high ultrasonic reflectivity and lower optical reflectivity. Conversely, earlywood was distinguished as areas exhibiting lower ultrasonic reflectivity and higher optical reflectivity. A similar method that uses a combination of acoustic and ultrasonic techniques is acousto-ultrasonic (AU). Specifically, AU techniques investigate waveform patterns, rather than measuring ultrasonic reflections from material discontinuities, when a stress wave is subjected to wood (Biernacki and Beall 1993). Kawamoto, S. and R. Sam. Williams (2002) define AU as "a non-destructive method that uses stress waves to detect and evaluate diffuse defects, damage, and variations in mechanical properties of materials."

Wang et al. (2001) used AU measurement to locate lathe checks and knots in veneer. Their research focused on AU techniques parallel and perpendicular to grain in veneer. They concluded that while perpendicular AU waves did not detect knots, parallel AU waves identified knot existence, but was not sensitive to knot size when

considering wave attenuation and transit time separately. Additionally, lathe checks were difficult to measure parallel to grain with longitudinal stress waves because waves did not cross lathe checks. Perpendicular wave velocity, however, was responsive to lathe check presence. If identifying both lathe checks and knot location were of importance for veneer, it would require taking AU measurements in both the parallel and perpendicular direction. In this same study (Wang et al. 2001), it was determined that an X-Ray system was able to detect knot existence, but not lathe checks. In terms of AU, more research is needed to identify influences of grain angle, grain orientation, species difference, attenuation, and other growth characteristics before a suitable system capable of measuring defects can be achieved (Beall 2002).

2.8.2 Nuclear Magnetic Resonance and Near Infrared Spectroscopy Systems

Nuclear magnetic resonance (NMR) is another NDE techniques used for evaluating wood properties. NMR surmises that differences in normal and abnormal cells can be determined (Chang et al. 1989). Chang et al. (1989) outlined basic NMR principles as nuclei (with odd number protons and/or neutrons) under strong magnetic field randomly will align their moments toward the external magnetic field. Then by subjecting a material (in this case wood) to radio frequency (RF), nuclei would absorb RF waves and re-align their moment away from the external magnetic field. This process is termed resonance. Once RF is removed, nuclei re-align themselves toward the magnetic field (relaxation) and give off energy (RF signals). During relaxation, a small magnetic field is imposed and nuclei at unlike positions emit signals at different

frequencies. By analyzing received RF signals, spatial distributions of the imaged nuclei are determined and a 2-d image constructed (Chang et al. 1989). Using an NMR system, images are created that allow for the detection of defects such as knots, worm holes, ring shank, decayed areas, wetwood, and tension wood (Chang et al. 1989). Additionally, NMR has been used to distinguish between heartwood and sapwood amounts in wood (Wang and Chang 1986).

While the previously listed techniques are utilized for evaluating wood, their use on veneer has been somewhat limited. One other method, near infrared (NIR) spectroscopy, has been used for identifying veneer defects. Meder et al. (2002) used NIR spectroscopy to predict radiata pine (*Pinus radiata*) veneer stiffness. Using commercially available NIR scanning systems, they investigated both small veneer strips (38mm wide by 190mm long) and larger veneer sheets (1.2m by 1.2m) to compare with static bending MOE. Veneer was scanned on both the tight and loose (side in contact with the knife during peeling) veneer faces and the data was averaged. Results from small veneer strips provided a correlation of 0.77 (R-squared of 0.59) between the first derivative of average spectral data and static bending MOE on an individual veneer strip basis. Due to waviness of veneer in larger sheets, they were unable to evaluate individual veneer sheet static bending MOE; rather, they produced small LVL specimens from NIR scanned sheets. The individual sheet spectral data (average of four scans) comprising the LVL specimen was averaged and regressed against static MOE. Results provided a strong relationship between average veneer spectral data and static bending MOE (r-squared of 0.96 for their calibration model, and r-squared of 0.74 for their validation model). These results are promising as

predictions improved when scanning larger areas. Because individual veneer static bending MOE could not be predicted (due to unavailable method to test static bending MOE on large sheets), this prediction would only pertain to overall LVL billets, and does not hold great promise for sorting on individual sheet basis.

2.9 Need for Additional Veneer NDE Techniques

From the literature review, it is evident using current ultrasonic systems in commercial production results in a relatively reliable means to determine elastic properties of veneer. However, the current ultrasonic system is limited when it comes to predicting veneer strength properties. It appears that ultrasonic systems, as they stand today, cannot properly detect the presence of defects within veneer. Defects within a veneer sheet are likely to have a large influence on strength properties. To accurately detect defects, an appropriate optical scanning system and/or better understanding of ultrasonic signals needs to be evaluated. While many other NDE techniques were reviewed in Section 2.8, for this research the focus was on optical techniques suitable for locating and quantifying defects. Optical technology, in comparison to those listed in Section 2.8, is commonplace in current veneer peeling and LVL production facilities. By gaining knowledge of how optically acquired measures influence veneer properties, the findings could be relatively quickly incorporated into many existing production facilities, without much investment. Hoover et al. (1988) indicated stress wave sorting systems would likely not be economical for LVL (specifically hardwood LVL) used in manufacturing furniture, so

it is unlikely techniques outlined in Section 2.8 could be implemented without a high cost to manufacturers, especially in comparison to optical scanning systems. The goal of this research is to use an optical system to detect, quantify, and account for defects and other veneer features (e.g., annual growth ring patterns) and thus improve the prediction of veneer strength properties, and ultimately strength properties of commercial products containing veneer.

Past published research on relating NDE measurement with veneer destructive properties has focused on small size specimens, many of which contained little to no amount of defects. Generally, veneer used in making most commercial veneer products would contain a significant degree of defects. Another gap exists as there is little to no research indicating small size veneer specimens and full size veneer sheets are related in terms of mechanical properties. This study was initiated to look at influence of defects on smaller veneer sheets. If future research on full-size sheets is conducted, this research would provide a means to compare small and large veneer specimens when accounting for optically measured variables and predicting veneer mechanical properties.

In terms of LVL production, past research has focused on ultrasonically testing veneer sheets, producing billets, testing specimens destructively, and correlating NDE measurements to destructive properties. This being said, production factors could influence the mechanical property predictions and depending on raw material source, there may be different correlations needed for different production runs. By destructively testing individual veneer, containing a varying degree of defects and growth ring patterns, and correlating the results to NDE measurements, veneer could

be sorted with greater precision. Furthermore, more reliable predictions of composite product (e.g., LVL) mechanical properties could be obtained and it would allow for improving overall elastic and strength properties of final products.

Due to continuous changes in veneer raw material supply (likely containing more defects), to reliably predict LVL mechanical strength properties requires defects and other veneer features to be detected and quantified. Additionally, to improve predictions of LVL properties based on NDE measurements, destructive testing on veneer specimens, with various degrees of defects, needs to be performed. The following study is designed to address viable means to identify and quantify veneer features (e.g., defects, growth ring pattern) and use this information to predict veneer mechanical properties.

CHAPTER 3. PRELIMINARY STUDIES

Prior to evaluating whether or not an optical scanning system was capable of better predicting veneer mechanical properties, as compared to current commercial ultrasonic systems, suitable optical techniques needed to be developed. Additionally, preliminary research was needed to determine which veneer properties influence mechanically determined tensile modulus of elasticity and strength. To do so, the preliminary research focused on non-destructive and destructive testing of veneer specimens without conditioning or a specific sampling pattern. Two different preliminary studies were performed, as after the first study, it was determined more investigation was needed. The preliminary study allowed for resolution of many issues related to developing suitable non-destructive techniques prior to investing time and effort in measuring individual veneer NDE properties and producing LVL in the primary study.

3.1 Preliminary Study One: Optical Scanning and Ultrasonic Systems Trials

This particular preliminary study was initiated to get an idea of how well current ultrasonic systems predict veneer tensile strength and MOE. Additionally, an initial optical scanning system was setup and evaluated in terms of reliability in predicting veneer tensile properties. Finally, veneer tensile failure patterns were evaluated, and veneer characteristics appearing to influence tensile strength were noted. Using information from this preliminary study, specific characteristics were determined as

being important and a set of characteristics needing measurement during the primary study sections (i.e., Chapters 5 through 7) was developed.

3.1.1 Preliminary Study One Test Methods

Twenty-four (24), Douglas-fir (*Pseudotsuga menziesii*) veneer half sheets were randomly selected from a set of previously optically and ultrasonically evaluated samples. The half sheet dimensions were, approximately, 26-inches wide by 102-inches long by nominal 1/8-inches thick. From these half sheets, ninety (90) test specimens were prepared to a final size of 6-inches wide be 31-inches long. Specimen preparation was performed in a manner where some specimens contained various defects (e.g., knots, holes, splits), while other were free from defects. For each specimen, half-sheet number, UPT, and any other significant marking were recorded.

Sixty (60) veneer test specimens were first scanned using an optical scanning system to obtain digital images of the veneer's surface. The remaining thirty (30) veneer specimens were saved. Each specimen was imaged using a Hitachi HV-C20 video camera connected to an AT&T Targa-32 image acquisition card. Halogen lighting was used to illuminate the veneer surface. A spatial resolution of 26 pixels per inch was used when capturing veneer images. Due to the specimen's size, four images (two per face), indicated as A, B, C, and D (Figure 3.1), were taken per specimen to cover the entire area under investigation (i.e., the areas which were under tensile loading during destructive tests). For each individual veneer, data from image A and B were combined to allow for analysis and calculations based on the veneer's

top face (i.e., tight-side). Images C and D were saved in the event further analysis was need utilizing the bottom face (i.e., loose-side) of the veneer.

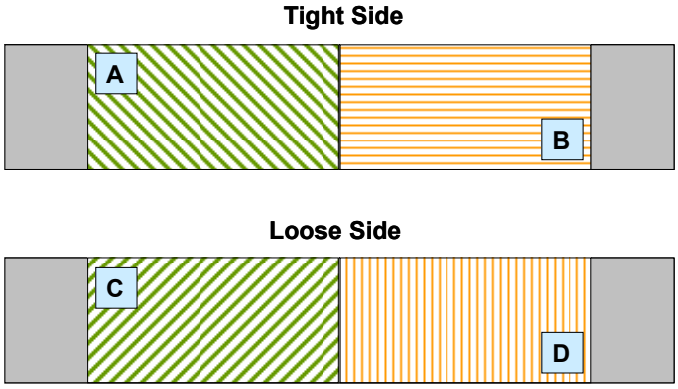

Figure 3.1. Optical image lettering system layout.

The resulting images were analyzed using two Otsu classification algorithms (single and dual threshold of the "green" signal) to determine percent latewood and earlywood. The single threshold Otsu classification algorithm outputted latewood areas as black pixels (Figure 3.2). The dual threshold outputted latewood areas as black pixels, along with the interpretation of earlywood/latewood transition zone areas as green pixels (Figure 3.2). Individual defects within each specimen were located by using various hand-selected threshold values on each veneer image (Figure 3.2).

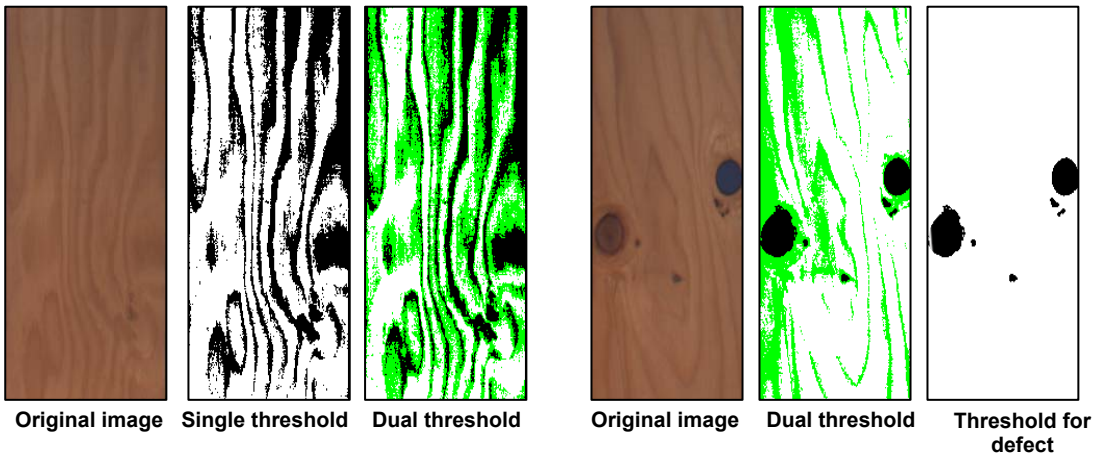

Figure 3.2. Optical image system output.

Once defects were located, percent defect area was calculated based on the percentage of black pixels within the analyzed image. Additionally, total number of defects and average percent area per defect was determined on each veneer specimen. A complete list of optically determined measures is provided in Table 3.1.

Table 3.1. Optical measures determined in preliminary study one.

Latewood Characteristics	Defect Characteristics
Percent Latewood: Single Threshold	Total Defect Area Percentage
Percent Latewood - Green and Black Area: Dual Threshold	Average Defect Area Percentage
Percent Latewood: Black Area: Dual Threshold	Total Number of Defects
Percent Transition Area - Green Area: Dual Threshold	

Veneer test specimens were then evaluated using a Metriguard Model 239A, lab-style stress wave timer to determine ultrasonic propagation time (UPT) (Figure 3.3). Specimen dimensions, moisture content, and weight were measured and recorded. Specimen width and thickness were determined at three and six different locations, respectively. UPT was measured longitudinally at five different locations across the specimen width. The accelerometers (i.e., sensors) were placed at 3.5-inches from the specimen ends, thus resulting in an overall transit distance of 24-inches. UPT at each location was recorded and an average specimen UPT was calculated. Dynamic MOE (MOE_d) was calculated for each specimen using Equation 3.1.

$$MOE_d = c^2 \times \rho \qquad \textbf{Equation 3.1}$$

Where:

MOE_d = dynamic modulus of elasticity (lb/in^2)

c = ultrasonic stress wave velocity (in/s) = transit distance (in.) / UPT (s)

ρ = mass density ($lb\text{-}s^2/in^4$)

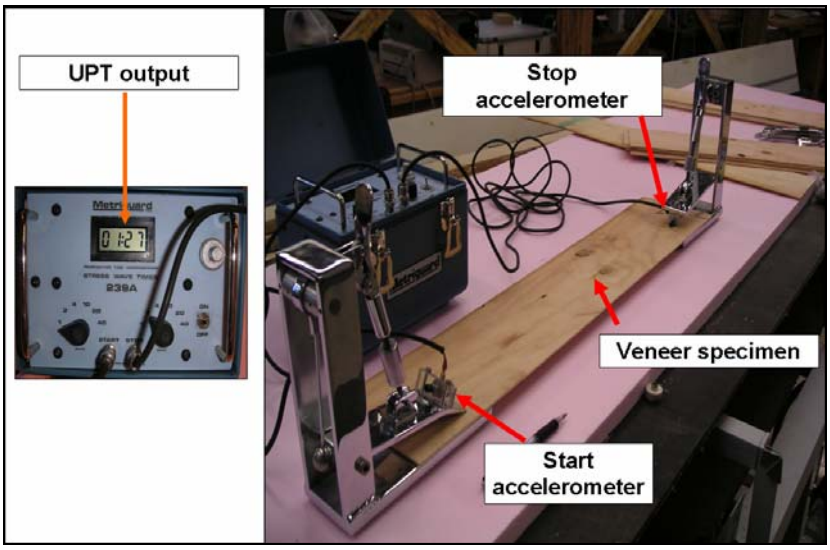

Figure 3.3. Ultrasonic system setup.

Finally, the veneer specimens were tested destructively in tension. Both static tensile modulus of elasticity (MOE) and strength (F_t) was evaluated. Tension testing was performed using a modified version of ASTM D3500, Method B (2003). While this method typically pertains to structural-based panels, it was found to be the most relevant for this study given the specimen's size. Modifications were made to the specimen length and grip area to accommodate for the tension test machine's capability, while still maintaining the correct test area between grips. The grip area was 3.5-inches on each end, leaving 24-inches as the overall length between grips. Specimen width and thickness measurements were taken from values measured during ultrasonic evaluation. Specimens were tested in tension parallel to grain at a rate of 0.075-inches per minute of cross head motion using a Baldwin Universal Test Machine (UTM) located at TECO's Eugene, Oregon test laboratory. Load was measured by an Interface 25K load cell, and deformation was recorded on each face of

the specimens over a gauge length of 9-inches using two Macrosensor linear variable differential transformers (LVDTs). Upon test completion, veneer tensile strength and modulus of elasticity were calculated using Equation 3.2 and 3.3, respectively.

$$F_t = \frac{P_{max}}{A}$$ **Equation 3.2**

$$MOE_s = \frac{stress}{strain} = \frac{\sigma}{\varepsilon} = \frac{\frac{P}{A}}{\frac{\Delta L}{L_o}} = \frac{P \times L_o}{A \times \Delta L} = \frac{Slope \times L_o}{A}$$ **Equation 3.3**

Where:

F_t = veneer static tensile strength (psi)

MOE_s = veneer static tensile modulus of elasticity (psi)

σ = stress (lbf./in.^{2})

ε = strain (in./in.)

ΔL = change in length (in.) = actual deformation (average of 2 faces)

L_o = original length, gauge length = 9 in.

P_{max} = failure force (lbf.)

P = force (lbf.)

A = cross sectional area under load (in.^{2}) = spec. thickness (in.) x width (in.)

Slope = P/ΔL in the linear region, set to 5% to 35% of ultimate load (lbf./in.)

Figure 3.4 and Figure 3.5 show the tension test setup and typical resulting load versus deformation output, respectively.

Figure 3.4. Destructive tensile testing system setup.

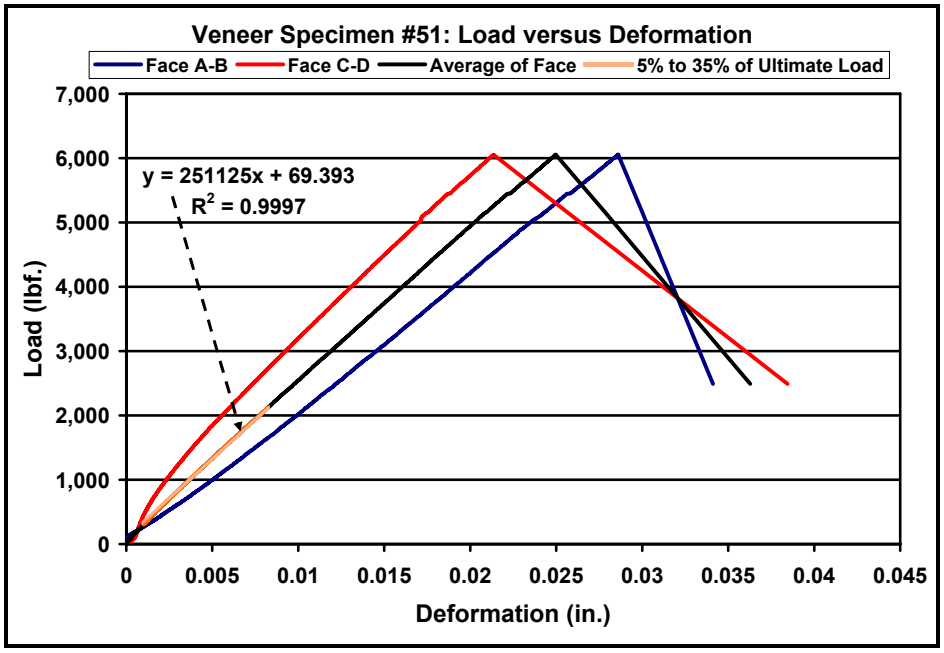

Figure 3.5. Typical load versus deformation curve from veneer tension tests.

3.1.2 Preliminary Study One Results

Various linear regression analysis techniques (single, multiple, robust, and step-wise) were utilized to examine which ultrasonic and optical NDE measures were influential when predicting veneer tensile properties. Analysis was also preformed to provide an initial indication of which system best predicted veneer mechanical properties. This analysis allowed for determining if any of the systems utilized needed improvement prior to beginning the primary study. Additionally, specimen failure patterns were evaluated to determine how specific veneer features may have influenced tensile strength results.

3.1.2.1 Preliminary Findings on Predicting Veneer Tensile MOE

In terms of predicting veneer static tensile MOE, ultrasonic MOE_d (Figure 3.6) resulted in better prediction ($R^2 = 0.77$) as compared to UPT ($R^2 = 0.55$) (Figure 3.7). It was apparent that inclusion of veneer density (when calculating MOE_d) improved the prediction of veneer static tensile MOE. This result stands to reason as density is, in general, significantly correlated to elastic properties of wood materials (Figure 3.8).

Step-wise regression was used to determine which, if any, selected optical measurements are likely to influence veneer mechanical properties once the primary study was conducted. When analyzing optical only NDE measurements listed in Table 3.1, the resulting predictions of veneer static tensile MOE from stepwise regression were rather weak ($R^2 = 0.11$) and only number of defects was statistically significant (at a 5% level).

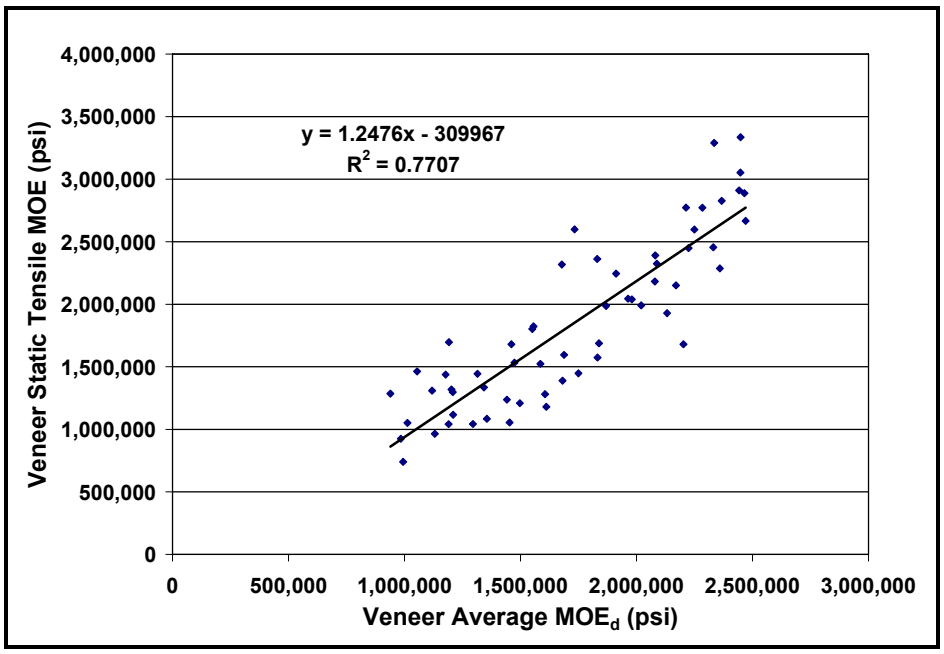

Figure 3.6. Preliminary study: Veneer static tensile MOE versus average MOE_d.

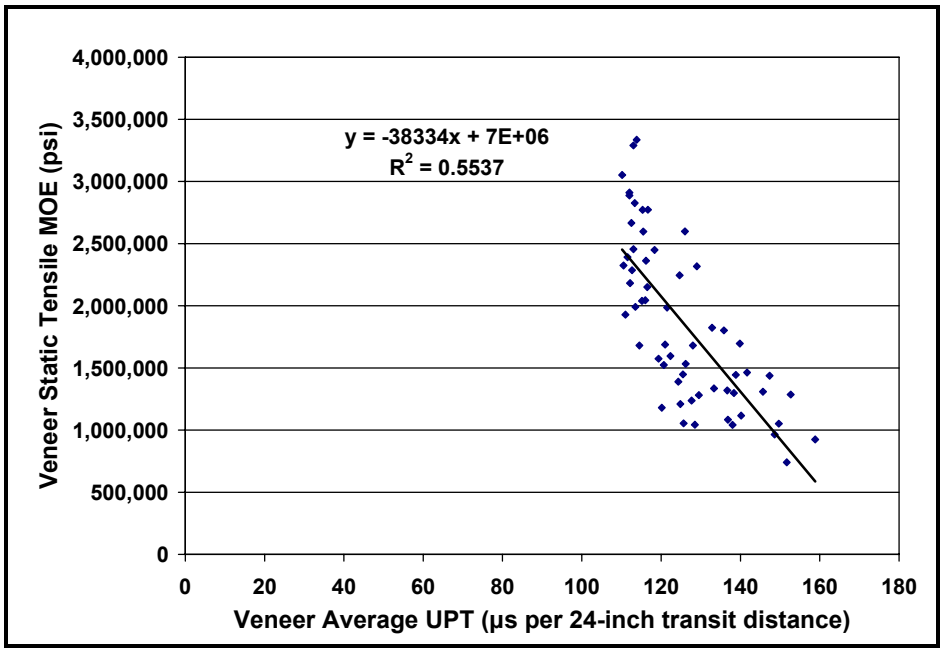

Figure 3.7. Preliminary study: Veneer static tensile MOE versus average UPT.

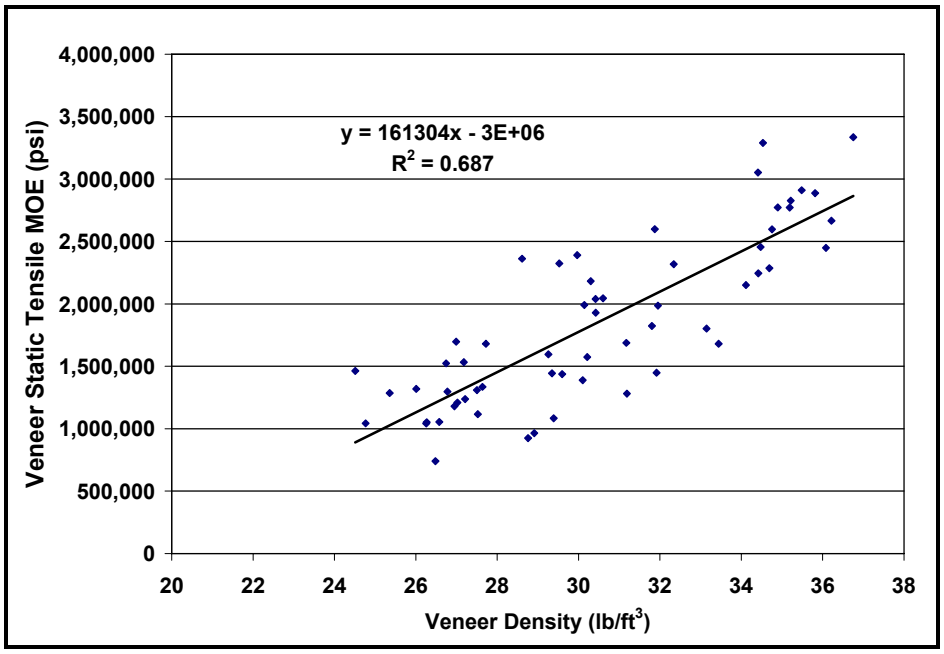

Figure 3.8. Preliminary study: Veneer static tensile MOE versus density.

It was anticipated that some measure of latewood percentage would be related to veneer density, and if so, would be significant in terms of predicting veneer static tensile MOE, however, this was not the case. Stepwise regression was then performed to determine whether or not numbers of defects was still statistically significant once density was included in with optical data. The results of this analysis indicated density was the only statistically significant measure (at a 5% level), and number of defects was no longer included in the model. Additionally, robust regression was performed to reduce any influence of outliers on the results of the optical predictions. Once performed, while a few optical measures were statistically significant, there was minimal improvement in predicting veneer static tensile MOE using robust regression analysis.

Finally, optical measures were combined with MOE_d in step-wise analysis to see if there was any improvements in predicting veneer static tensile MOE. Results of this analysis indicated MOE_d was the only statistically significant measure (at a 5% level), and no optical measures were included in the model. This indicated, at this point, to have a reliable optical system capable of predicting veneer static tensile MOE, further preliminary research needed to be conducted with other optical measures included. When predicting veneer static tensile MOE, optical measures included in the first preliminary study were not as reliable as MOE_d. It was initially considered that percent latewood values determined by the optical system would be correlated to ultrasonic values. As previously stated, it was thought the optical system could adequately determine density by measuring latewood percentage and provide a good prediction of tensile MOE. However, percent latewood values obtained from the optical system, as setup, did not provide good correlation to ultrasonic or veneer density measurements.

Upon further analysis one source of error in the preliminary study's optical methodology was using a spatial resolution of 26 pixels per inch. Funck et at. (1991), reported a spatial resolution of 10 pixels per inch (as opposed to 15, 20, and 25) provided the best results for determining latewood percentage. In the primary study, determining latewood percentage via optical means (both spatial resolution and threshold methods) and correlation to ultrasonic and veneer density measurements needed to be re-evaluated and spatial resolution set near 10 pixels per inch.

3.1.2.2 Preliminary Findings on Predicting Veneer F_t

In terms of predicting veneer static tensile strength (F_t), ultrasonic MOE_d (Figure 3.9) resulted in better prediction (r-value = 0.67) as compared to UPT (r-value = 0.62) (Figure 3.10). Density, by itself, was not very reliable in predicting veneer static F_t (r-value = 0.52) (Figure 3.11). This suggests other factors influence veneer F_t properties.

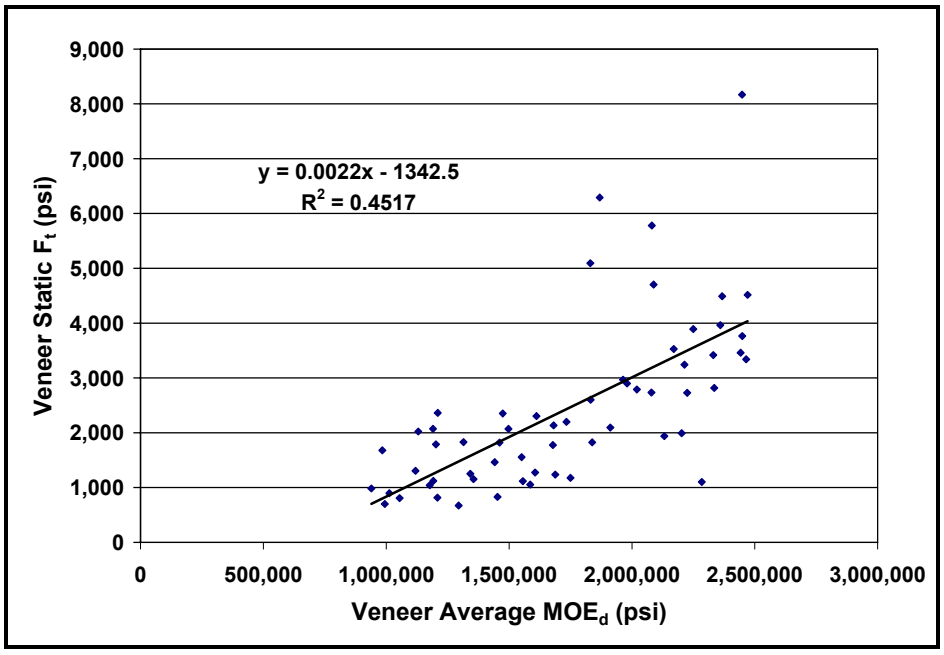

Figure 3.9. Preliminary study: Veneer static F_t versus average MOE_d.

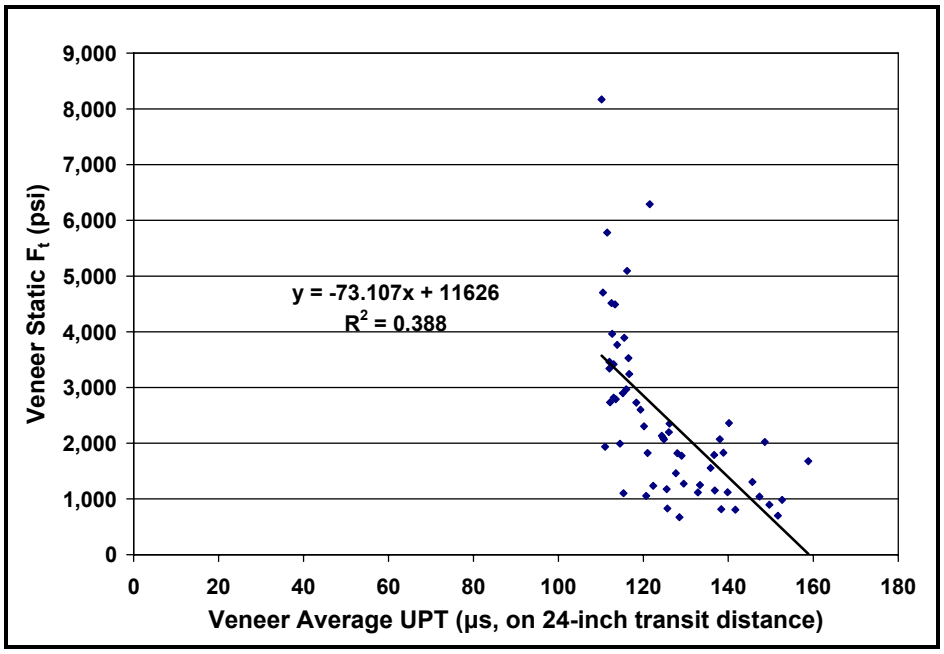

Figure 3.10. Preliminary study: Veneer static F_t versus average UPT.

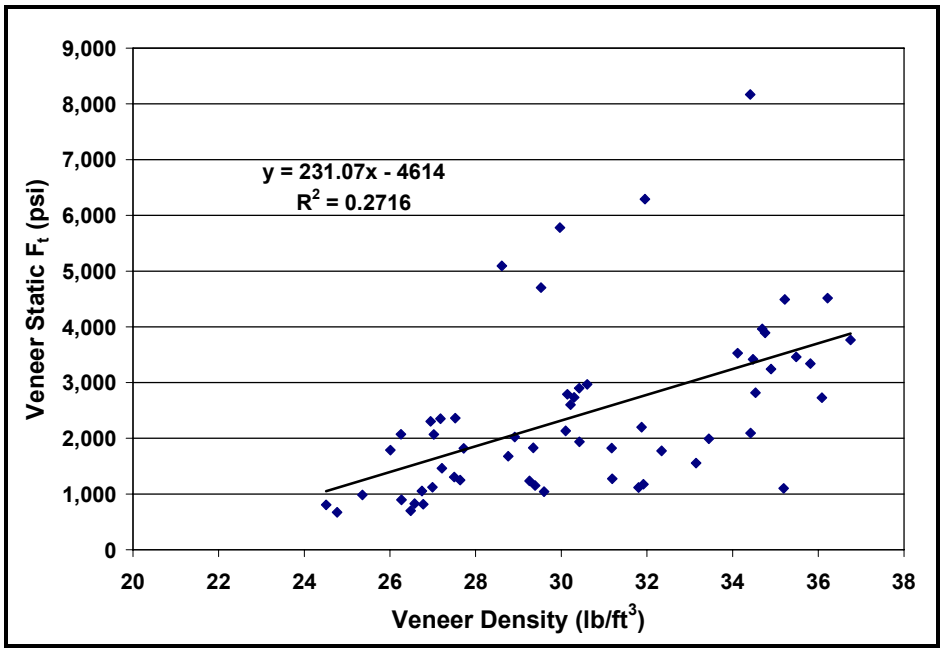

Figure 3.11. Preliminary study: Veneer static F_t versus density.

In terms of optical measurements, stepwise regression indicated two measurements, number of defects and average defect area percentage, as being statistically significant (at a 5% level) with a $R^2 = 0.29$ (Figure 3.12). When predicting veneer static F_t, optical characteristics listed in Table 3.1 performed slightly better than density, but worse than MOE_d and UPT. A particular limitation of this model was for specimens containing no defects. When specimens contained no defects, the same F_t value was predicted. Given this, and the optical model's low reliability, it was evident more optical measures were needed to adequately predict veneer F_t.

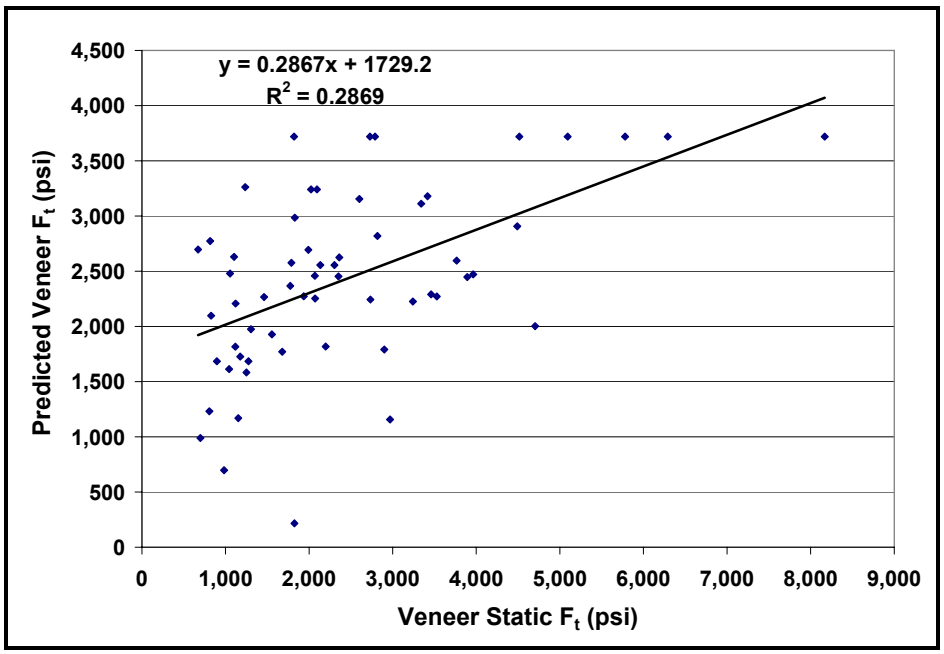

Figure 3.12. Preliminary study: Optically predicted veneer F_t versus static F_t.

Stepwise regression was then performed to determine if combining density with optical measures would improve veneer static F_t prediction. The results of this analysis showed an improved prediction of veneer static F_t ($R^2 = 0.40$), as both density and number of defects were statistically significant (at a 5% level) (Figure 3.13). In comparison to MOE_d, however, the combined density and optical model was slightly less reliable. Finally, optical measures were combined with MOE_d in step-wise analysis to see if any improvement was made in predicting veneer F_t. Results of this analysis provided the best prediction of veneer F_t ($R^2 = 0.52$), as both MOE_d and number of defects were statistically significant (at a 5% level) (Figure 3.14).

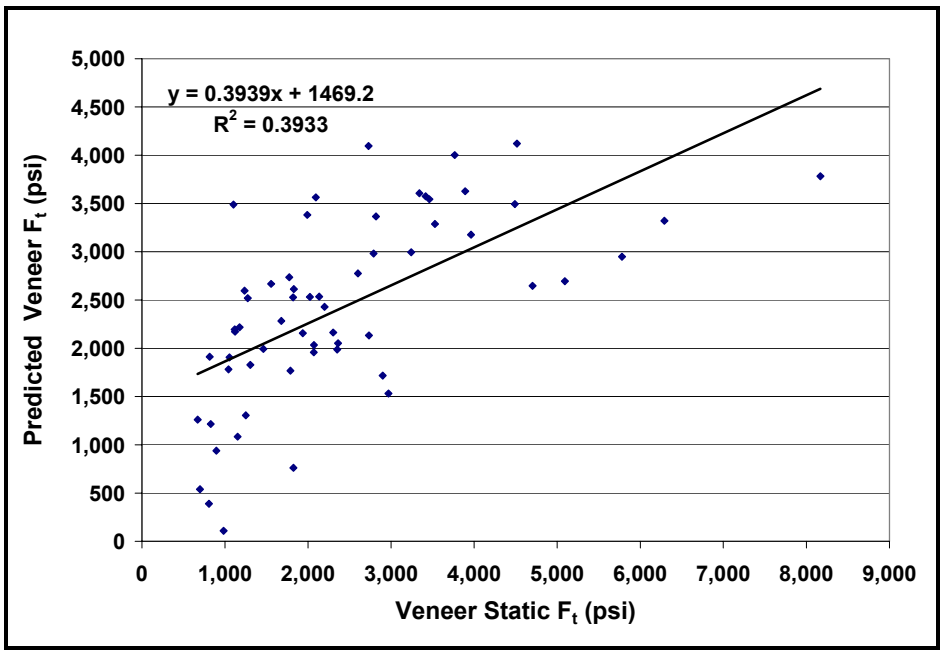

Figure 3.13. Preliminary study: Density and optically predicted veneer F_t versus static F_t.

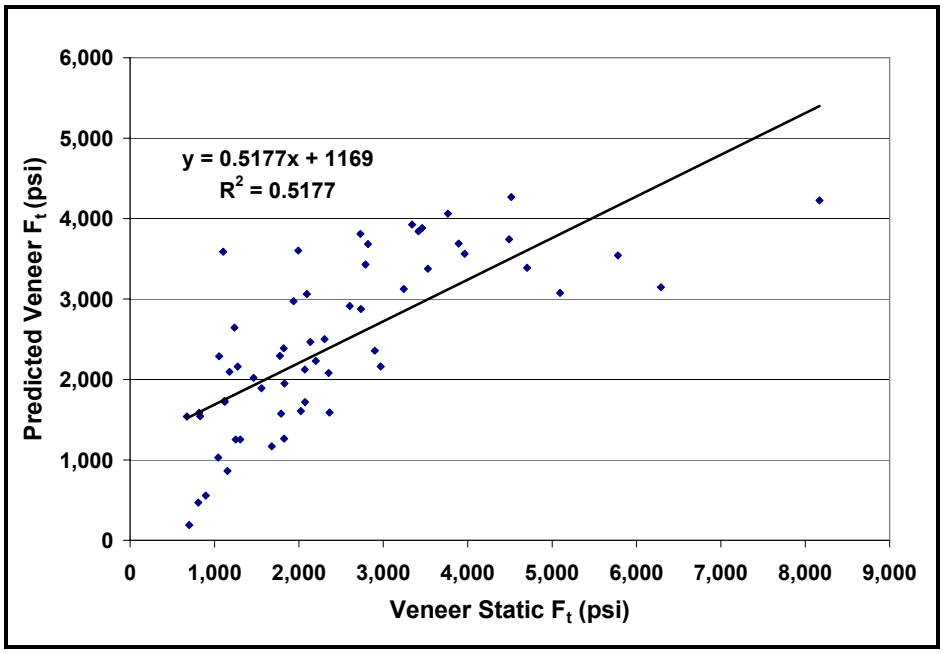

Figure 3.14. Preliminary study: Average MOE_d and optically predicted veneer F_t versus static F_t.

In all prediction models generated, analysis of predicted versus veneer static F_t indicated some results as being distinctly different (Figures 3.9 to 3.14). Specifically, specimens with extremely low and extremely high strength, in comparison to the general trend, exhibited a distinctly different relationship. To further investigate the nature of differences between these outliers and the overall trend, failure patterns were observed. Upon analysis, it was determined that specimens possessing a fairly straight growth ring pattern exhibited, in some cases, higher tensile strength and tended to fail in a vertical pattern (i.e., parallel to specimen length) (Figure 3.15). Additionally, specimens containing many knots and highly sloped annual growth ring patterns, in general, tended to result in lower tensile strength (Figure 3.16). Based on these observations, it became apparent veneer annual growth ring pattern was influential in

tensile strength. Furthermore, to reliably predict veneer tensile strength, annual growth ring patterns need to be determined. This being said, for the primary study, a method needed to be developed to determine and quantify annual growth ring patterns from optical image analysis.

Figure 3.15. Failure when growth rings were oriented parallel to specimen length.

Figure 3.16. Specimen failure at knot and sloped growth ring pattern locations.

3.2 Preliminary Study Two: Additional Optical and Spectral Analysis

3.2.1. Preliminary Study Two Procedures

The remaining thirty (30) veneer specimens were used to determine whether or not including some additional optical measurements improved veneer mechanical property predictions and/or were at a minimum, statistically significant. Also, further research was performed to determine if spectral analysis of ultrasonic waveform data provided an indication of veneer defects or growth ring patterns. The methods outlined in Section 3.1.1 for optical and ultrasonic scanning and mechanical testing was used for this particular section. In addition, for each point at which UPT was determined, raw ultrasonic stress wave data was captured using a Tektronix 2430A Digital Oscilloscope. In terms of optical data, for this particular section, further defect measurements, to those listed in Table 3.1, were collected. Specifically, additional information regarding veneer's defect width and volume characteristics were determined and recorded (Table 3.2).

Table 3.2. Additional optical measures determined in preliminary study two.

Additional Defect Characteristics	
Average Defect Width	Average Defect Volume
Total Defect Width	Total Defect Volume
Minimum Defect Width	Maximum Defect Volume
Maximum Defect Width	

Waveform data was collected from the Metriguard Model 239A, lab-style stress wave timer output at the start and stop accelerometers. Waveform capturing

was triggered based on the start accelerometer. Once the trigger was activated, 1024 voltage and corresponding time measurements (128 of which were pre-trigger data) were sampled from both the start and stop accelerometers. The data was then sent via a National Instruments GPIB-USB-HS cable and acquired and saved by a LabVIEW data acquisition program.

Once captured, limited spectral analysis was performed on waveform data acquired from the stop accelerometer. Specifically, magnitude peak spectral analysis was performed. Since magnitude peak spectral analysis returns output in terms of peak amplitude of the overall spectrum, it was thought a difference in grain pattern or defect presence may result in dissimilar peak amplitudes. Data from the start accelerometer was determined to contain a waveform indicative of the ball impactor assembly's ringing pattern, and therefore was not used in any analysis. For each veneer specimen, various spectral value statistics (e.g., average, minimum, maximum, median, mode, etc.) were determined at each of the six locations tested. The six resulting magnitude peak spectral analysis values were then averaged to obtain one measure of the various spectral values for each specimen.

3.2.2. Preliminary Study Results with Inclusion of Spectral Analysis and Additional Defect Measurements

The intention of the second set of preliminary tests was to analyze whether or not any additional spectral analysis and defect measurements were statistically significant in predicting veneer mechanical properties. The results of this section indicated additional spectral analysis and defect measurements as being statistically

significant (from stepwise regression analysis at a 5% level) when predicting both veneer static tensile MOE and F_t. Table 3.3 outlines statistically significant measures determined from analyzing the second set of preliminary tests. Additionally, which property was being predicted and the type of information included in each separate analysis (i.e., System Used) are outlined in Table 3.3.

Table 3.3. Statistically significant measures in preliminary study two.

System Used	Statistically Significant (at 5% level) Measures
Predicting Veneer Tensile MOE	
Optical	Percent Latewood: Single Threshold
Optical + Density	Density, Number of Defects
Ultrasonic (including spectral analysis)	MOE_d, Magnitude Peak Maximum
Combined Ultrasonic and Optical	MOE_d, Number of Defects, Magnitude Peak Amplitude and Minimum
Predicting Veneer F_t	
Optical	Total Defect Width
Optical + Density	Total Defect Width
Ultrasonic (including spectral analysis)	MOE_d, Magnitude Peak Mode and Minimum
Combined Ultrasonic and Optical	Total Defect Width, Magnitude Peak Minimum

From the stepwise regression analysis, total defect width was statistically significant in the optical only, optical and density, and combined ultrasonic and optical systems. Also of note, percent latewood using a single threshold technique was found to be statistically significant when predicting veneer static tensile MOE as previously

hypothesized in the first preliminary study section. In terms of additional spectral analysis, four different measures (magnitude peak amplitude, minimum, maximum, and mode) were found to be statistically significant when predicting veneer tensile MOE and F_t when using the ultrasonic and combined systems. Because this was a new set of tests, and involved a smaller sample size, the extent of any model prediction improvement could not be strictly identified, rather was used as a tool to identify other statistically significant measures.

3.3 Preliminary Study Significance

Results from the preliminary study indicated that ultrasonic techniques provided a reliable prediction of veneer static tensile MOE. MOE_d provided the best correlation to veneer static tensile MOE as compared to UPT, density, and the optical system. In terms of predicting veneer F_t, however, ultrasonic and optical scanning (which included density) methods, while each being weakly reliable, performed rather similar. It was evident density alone was not a reliable predictor of veneer F_t. When defect width and volume measures, as well as spectral analysis values, were included in the analysis, various measures proved to be statistically significant in terms of predicting veneer static tensile MOE and F_t. This suggested the optical scanning system used in the primary study should include measurement of defect width and volume, along with area and number of defects. Furthermore, for the primary study, not only should the ultrasonic system include UPT and MOE_d values, but stop accelerometer waveform data needed to be collected and spectral analysis performed.

Additionally, specimen failure patterns revealed annual growth ring patterns likely influenced veneer F_t. Given this, a means to measure and quantify annual growth ring patterns from optically obtained images needed to be developed in the primary study to better predict veneer F_t.

Based on preliminary results and conclusions, the primary study had to address various aspects to reliably predict veneer tensile strength. Specifically, the following items needed investigation:

- Changes in optical scanning techniques, including adjustment of image spatial resolution.
- Further correlation between optical measures, ultrasonic values, and veneer density.
- Development of an optical system capable of quantifying annual growth ring patterns.
- Further analysis of ultrasonic stress wave signal patterns to determine if annual growth ring and defect (i.e., knots, holes, etc.) characteristics could be detected.

CHAPTER 4 VENEER MILL VERSUS LABORATORY GRADING

An underlying goal of this research was to provide manufacturers with a means to use both optical and ultrasonic data to better predict veneer mechanical properties. Since most of the primary study research focused on testing in a laboratory environment, one area which needed further investigation was any measurable difference in ultrasonic data measured at a production facility versus in the laboratory. Therefore, a comparison was performed to determine if any differences existed between ultrasonic data obtained at a veneer manufacturing facility (i.e., mill) and in a laboratory setting. Additionally, there was a need to determine the feasibility of utilizing images captured from current in-use optical systems. Using mill acquired veneer images, analysis was performed to explore whether or not simple image processing was able to identify and measure certain veneer characteristics which were to be used during the primary study.

4.1 Comparison of Mill and Lab Ultrasonic Grading

Prior to comparing laboratory non-destructive techniques (i.e., ultrasonic scanning) when predicting veneer mechanical properties, a study was conducted to evaluate any differences in ultrasonic scanning between mill and laboratory settings with the following purposes:

1) To determine any differences between ultrasonic data collected from a veneer mill and ultrasonic data obtained in a laboratory setting.

2) To determine if any particular grade of veneer was more prone to error when grading in a production environment.

4.1.1 Production Facility: Veneer Grading, Sampling, and Measurements

One-hundred (100) ultrasonically graded Douglas-fir veneer sheets (1/8-inches in thickness, full sheets) were selected from a local veneer production facility. The sheets were selected based on MOE_d to represent typical grades of material used in manufacturing LVL (i.e., G1, G2, and G3). Within each grade, at least thirty (30) sheets were obtained. Each veneer was run through a Metriguard Ultrasonic Veneer Tester (Model 2800DME), which collected ultrasonic data from approximately forty-two (42) points across the width of the veneer (Figure 4.1). For each point, the UPT was calculated along the veneer's longitudinal direction over a distance of eighty-seven (87) inches. The Metriguard output a total of twelve (12) UPT scan values (i.e., it averaged 42 points into a total of 12 scan lines). Additionally, a final average UPT and MOE_d was calculated and recorded for the entire veneer sheet. The following information for each veneer sheet, as determined by a Metriguard Ultrasonic Veneer Tester (Model 2800DME), was logged into a file and recorded:

- Grade category (i.e., G1, G2, and G3)
- Overall sheet ultrasonic propagation time
- Within sheet scan line ultrasonic propagation time
- Dynamic modulus of elasticity (MOE_d)
- Specific gravity
- Moisture content
- Temperature

Figure 4.1. Mill facility Metriguard 2800DME ultrasonic veneer grading.

4.1.2 Laboratory Setting: Veneer Grading

A total of ninety-two (92) veneer sheets were tested for ultrasonic propagation time using a Metriguard Model 239A, lab-style stress wave timer setup (Figure 4.2). UPT was then measured at forty-two (42) points across the specimen width. The first reading was taken 5-inches from the edge, followed by readings in increments of 1-inch thereafter. At each location, only one measurement was taken. Based on earlier testing, the UPT value did not significantly change (if there was any change at all) when repeatedly tested at the same location given the setup used (i.e., foam base and appropriate gain settings). The start and stop gains on the Metriguard Model 239A were set at ten (10) and forty (40), respectively. For each point, the UPT was calculated along the veneer's longitudinal direction over a distance of 92-inches. To

match the UPT determined over a shorter distance at the mill, the Lab UPT was divided by 92-inches and then multiplied by 87-inches. Points at specific locations were averaged together to obtain a total of twelve (12) UPT scan values (i.e., averaged the 42 points into a total of 12 scan lines), in a manner to match the process performed by the Metriguard DME2800 in section 4.1.1. Additionally, a final average UPT was calculated and recorded for the entire veneer sheet.

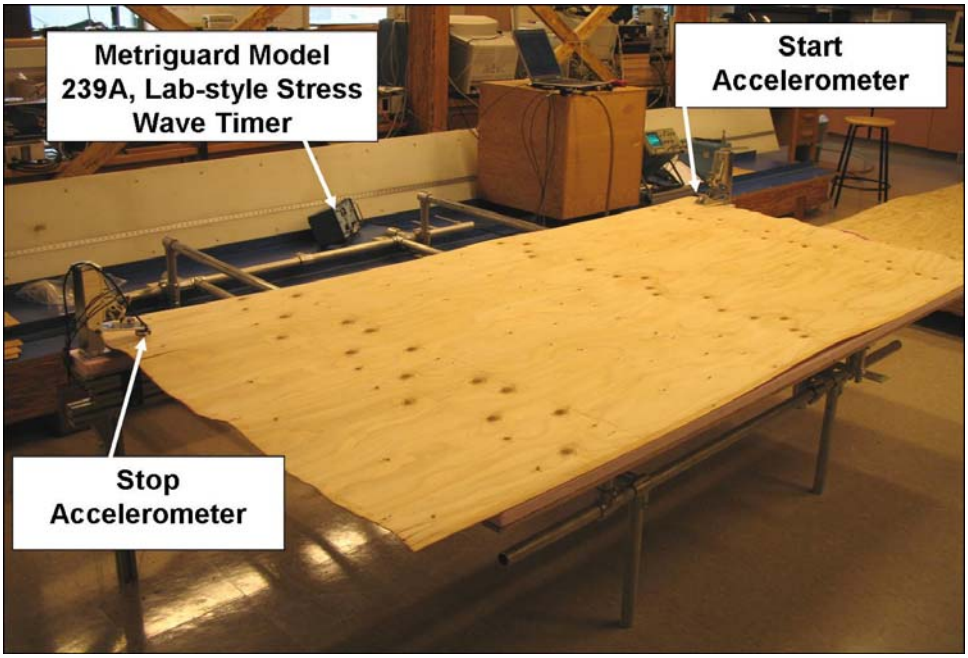

Figure 4.2. Laboratory ultrasonic stress wave system setup.

4.1.3 Comparison of Mill and Laboratory Ultrasonic Testing

To compare differences in average UPT when veneer grading was performed at the mill versus in a laboratory setting, a paired comparison statistical test was performed. When all the data was compared without regard to veneer grade category,

results from the paired t-test indicated there was a statistically significant difference (two-sided p-value = 0.0123) in average UPT between values obtained in the mill as compared to the laboratory. The average laboratory UPT (423 μs) was slightly higher than the average mill UPT (415 μs). Results from the sign test and signed rank test indicated there was no statistically significant difference (two-sided p-value = 0.8321 and 0.174, respectively) in median UPT between values obtained in the mill as compared to the laboratory.

The UPT data was further analyzed by separately performing paired comparison statistical tests on results within each veneer grade category. For G1 veneer, results indicated there was a statistically significant difference (two-sided p-value = 0.0042) in average UPT between values obtained in the mill as compared to the laboratory. The G1 veneer average laboratory UPT (418 μs) was slightly higher than the average mill UPT (400 μs). Results from the sign test indicated there was no statistically significant difference (two-sided p-value = 0.2812) in median UPT between values obtained in the mill as compared to the laboratory. Results from the signed rank test, however, indicated there was a statistically significant difference (two-sided p-value = 0.0049) in median UPT between values obtained in the mill as compared to the laboratory.

Differences in G1 veneer's mill and laboratory average UPT values could be partly explained by the number of scan lines included under each system. Not every scan line was included in the mill overall average UPT, while in the laboratory study, all scan lines were included. Specifically, upon analysis of mill ultrasonic data it was determined some high UPT values were omitted when determining veneer sheet

average UPT. The extent of differences in scan lines utilized was not fully explored, but the laboratory maximum UPT (535 μs) was significantly higher than the mill maximum UPT (423 μs). The minimum laboratory and mill UPT were 375 μs and 377, respectively and were determined to be very similar.

For G2 and G3 veneer, results indicated there was no statistically significant difference (two-sided p-value = 0.2933 and 0.8968, respectively) in average UPT between values obtained in the mill as compared to the laboratory. For G2 and G3 veneer, results from the sign test indicated there was no statistically significant difference (two-sided p-value = 0.3768 and 0.5563, respectively) in median UPT between values obtained in the mill as compared to the laboratory. Additionally, for G2 and G3 veneer, results from the signed rank test indicated there was no statistically significant difference (two-sided p-value = 0.8979 and 0.5587, respectively) in median UPT between values obtained in the mill as compared to the laboratory.

In general, the laboratory and mill ultrasonic testing was comparable. One exception was G1 veneer grading. Even though the mill grading system appeared to discard high UPT values, for this study's primary testing section (Chapters 5 through 7), it was determined these high values should not be removed. High UPT values were included to determine if they are somehow related to knot or highly sloped grain pattern identification. If they are, then they could possibly lead to better veneer mechanical property predictions.

4.2 Comparison of Mill Optical Scanning and Past Research

Prior to performing optical scanning in a laboratory setting, veneer images from a production facility were obtained and analyzed for the following purposes:

1) To determine if images captured from in-line mill equipment can be used to determine percent latewood and defect area using various image processing techniques.
2) To determine how well latewood percentage, defect area, and number of defects correlate to ultrasonic properties, and how the correlations compare to past research.

4.2.1 Production Facility: Veneer Image Capturing and Processing

After each veneer sheet sampled in Section 4.1 went through the Metriguard scanning system, they were graded for visual classification (e.g., A, C, D, etc.) by a Ventek GS2000 visual scanning system (Figure 4.3). For each veneer sheet, a Tagged Image File Format (.tiff) image was created and saved (Figure 4.4). Each image was then processed through various routines using ImageJ software to determine percent latewood and defect area. For determining latewood percentage, images were fitted to a set window size (to match the area scanned in Section 4.1), passed through a bandpass filter, and thresheld by using an Otsu algorithm. The resulting images were saved for determining percent earlywood/latewood (Figure 4.5) and defect area (Figure 4.6). Earlywood and latewood percentages were calculated using a program

written in MATLAB to output the number of black (earlywood) and white (latewood) pixels. Because defects also showed up as white pixels, defect percentage was subtracted from latewood percentage to get a true representation of actual latewood percentage. For determining defect percentage, images were again fitted to the set window size, passed through a bandpass filter, and thresholded at a value of seventy-three (73). Percent defect area was calculated using a program written in MATLAB to output the number of white (defect area) and black (defect free) pixels.

Figure 4.3. Veneer scanning using a Ventek GS2000 scanning system.

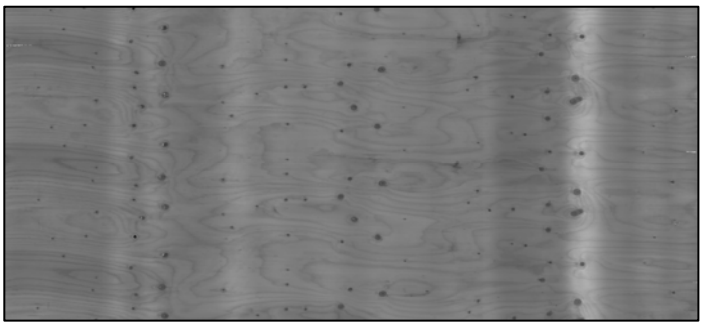

Figure 4.4. Windowed veneer image captured via a Ventek GS2000 scanning system.

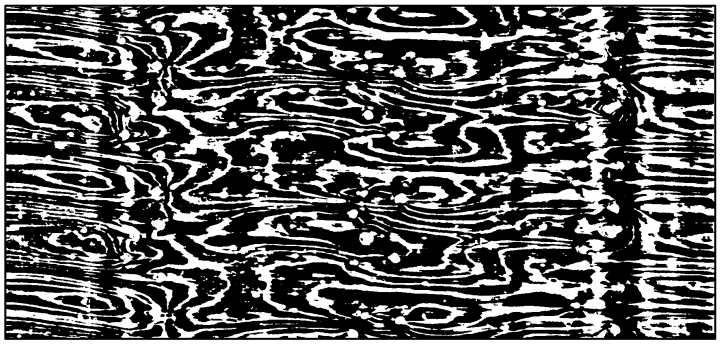

Figure 4.5. Veneer image thresholding for percent earlywood (black) and latewood (white).

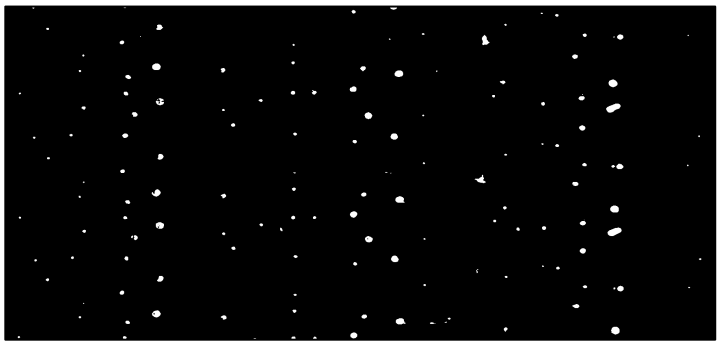

Figure 4.6. Veneer image thresholding for percent defect area (white).

4.2.2 Comparison of Image Measurements with Past Research Results

Correlation analysis results, including correlation coefficients and significance level, are shown in Table 4.1. Past research (Funck et al. 1991) indicated latewood and defect percentages as being statistically significant in predicting UPT values obtained using a Metriguard System. Results from correlation analysis in this study differed from Funck et al. (1991), as defect area was not found to have a statistically significant (at a 0.01 level) correlation to UPT (both mill and lab results). Latewood percentage, however, was found to have a statistically significant correlation to both UPT (mill and lab results) and MOE_d.

Table 4.1. Cross correlation table.

Variable	Lab UPT	Mill UPT	Percent Defect Area	Percent Latewood	MOE_d
Lab UPT	1.00 0.00	0.57 0.00	0.14 0.18	-0.40 0.00	-0.37 0.00
Mill UPT	0.57 0.00	1.00 0.00	-0.02 0.83	-0.66 0.00	-0.82 0.00
Percent Defect Area	0.14 0.18	-0.02 0.83	1.00 0.00	-0.08 0.44	-0.02 0.83
Percent Latewood	-0.40 0.00	-0.66 0.00	-0.08 0.44	1.00 0.00	0.64 0.00
MOE_d	-0.37 0.00	-0.82 0.00	-0.02 0.83	0.64 0.00	1.00 0.00

Further analysis was performed using multiple linear regression techniques to predict mill UPT from optical scanning data (i.e., latewood and defect percentage). The first analysis used the prediction equation from Funck et al. (1991) to calculate

UPT and compare it to average UPT determined at both mill and laboratory settings. To do so, measured average UPT was first converted, for consistency purposes, to a transit over distance of 8-feet by dividing the measured UPT by 87-inches and multiplying by 96-inches (basis of Funck et al. formula). Figure 4.7 shows a relatively weak prediction ($R^2 = 0.25$) of mill UPT using the prediction equation from Funck et al. (1991) who reported a $R^2 = 0.77$. Comparison of predicted versus actual laboratory average UPT resulted in an even lower correlation ($R^2 = 0.15$).

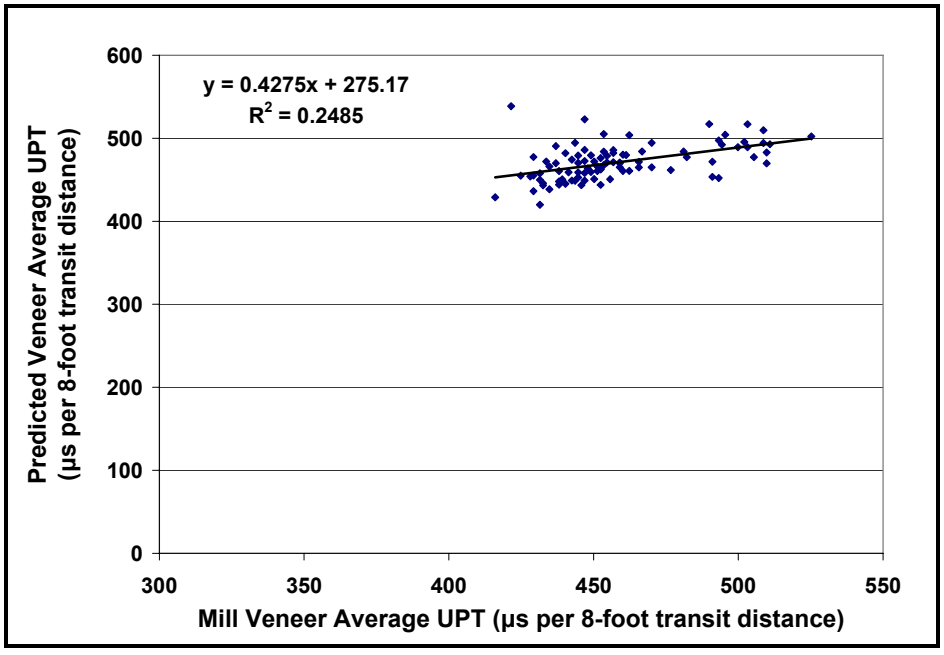

Figure 4.7. Predicted veneer average UPT (using Funck et al. formula) versus mill average UPT.

There are many possible reasons for the apparent weakness of the prediction equation in determining average veneer sheet UPT during this study. Some possible explanations were differences in image resolution, thresholding techniques, and

general variability of measured veneer UPT. During this study, captured images were of a higher resolution than the optimal value (10 pixels per inch) suggested by Funck et al. (1991). This higher image resolution in this study could have resulted in different latewood percentage determination as compared to Funck et al. (1991). Additionally, this study utilized different thresholding methods and could have resulted in dissimilar latewood percentages to those measured by Funck et al. (1991). Furthermore, average veneer UPT may be more variable and possibly a less reliable measure of actual veneer properties. With the advent of in-line techniques to measure veneer density and calculate MOE_d, it appears UPT is less likely the best predictor of veneer properties.

Given this study's different methodology for determining latewood percentage and higher image resolution, there was a likelihood different regression coefficients would result in better UPT prediction. To test this, multiple regression analysis was used to develop a new prediction equation of UPT given the measurements of optical data obtained in this study. Using percent latewood and defect area, mill UPT from the Metriguard 2800DME was predicted. As shown in Figure 4.8, the prediction of UPT was improved ($R^2 = 0.44$ or r-value = 0.66) as compared to the analysis in Figure 4.7 ($R^2 = 0.25$). This analysis also verified that in this particular part of the study, inclusion of defect area did not improve the prediction of UPT. Specifically, the same correlation coefficient (r-value = 0.66) was obtained when predicting UPT both when defect area was (Figure 4.8) and was not included (Table 4.1).

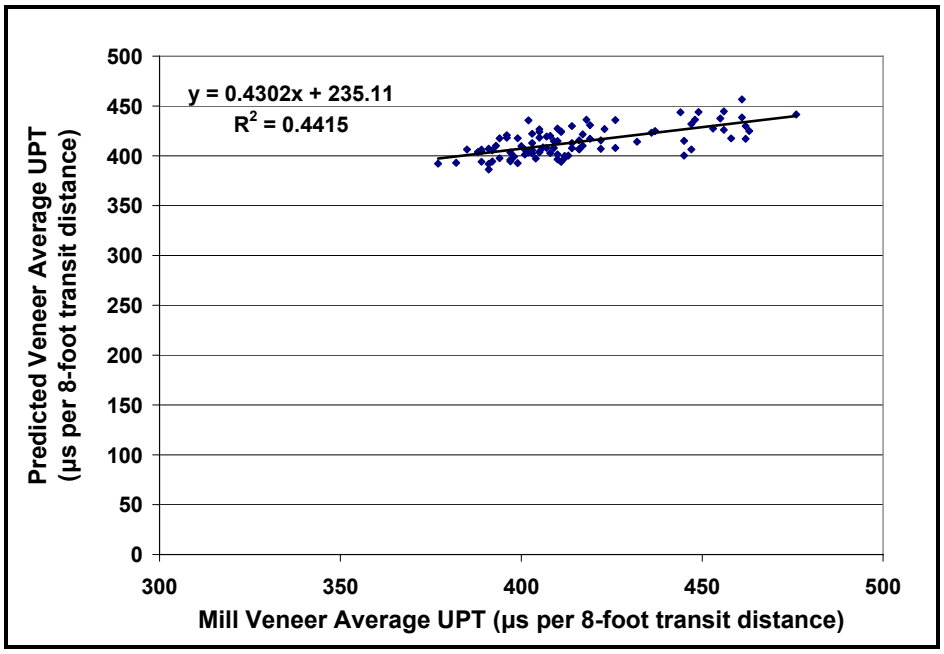

Figure 4.8. Predicted veneer average UPT using latewood percentage and defect area versus mill average UPT.

While Funck et al. (1991) did not relate optical values to MOE_d, many manufacturers grade veneer based on MOE_d. Given this, it was important to determine how well optical values could predict MOE_d. To do so, multiple regression analysis was used to develop a new prediction equation of MOE_d given the measurements of optical data obtained in this study. Using percent latewood and defect area, MOE_d from the Metriguard 2800DME was predicted. As shown in Figure 4.9, the prediction of MOE_d using both percent latewood and defect area was rather weak ($R^2 = 0.41$ or r-value = 0.64). Again, the analysis verified that in this particular part of the study, inclusion of defect area did not improve the prediction of MOE_d. Specifically, the same correlation coefficient (r-value = 0.66) was obtained when

predicting MOE_d both when defect area was (Figure 4.9) and was not included (Table 4.1).

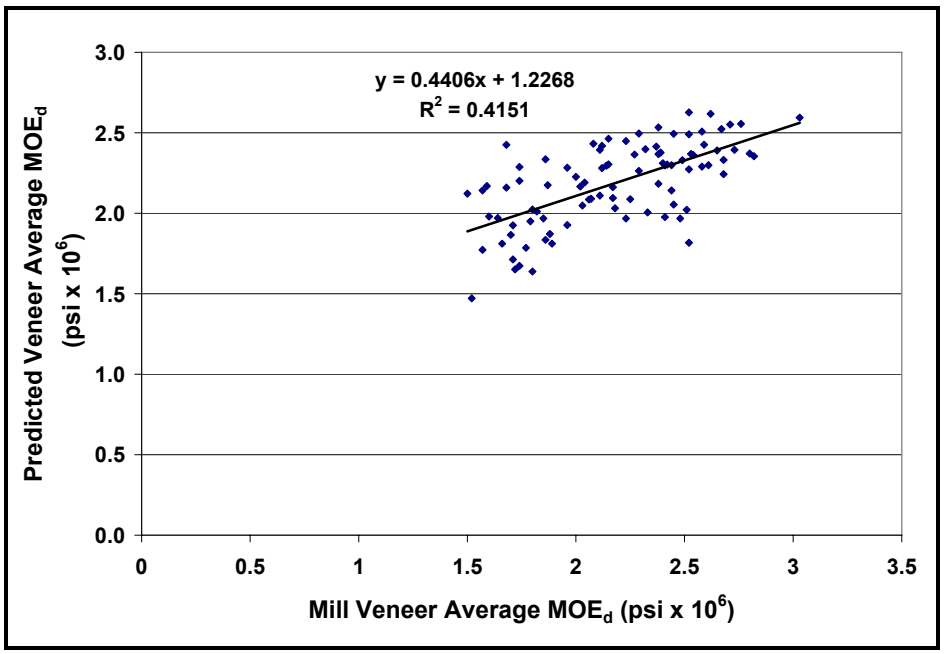

Figure 4.9. Predicted veneer average MOE_d using latewood percentage and defect area versus mill average MOE_d.

Results of this section indicate percent latewood is related to both UPT and MOE_d. In terms of defect area, while it is not statistically significant in predicting UPT and MOE_d, it still may be important in terms of actual veneer mechanical properties. As UPT and MOE_d are hypothesized, in this study, as being only somewhat reliable predictors of veneer mechanical properties, it is still likely both percent latewood and defect area are statistically significant when related to veneer static mechanical properties. This assumption was tested in the primary study section. The images acquired from existing mill optical scanning systems, however, were

successfully utilized to determine latewood percentage and defect area. This capability could, without much additional cost, provide manufacturers with existing optical scanning equipment an enhanced method of incorporating latewood and defect characteristics when grading veneer. Before this type of system can be incorporated, however, any possible relationship between latewood and defect measures on veneer mechanical properties needs further investigation. Chapter 5 and 6 of this study was designed to use an optical scanning system to measure veneer characteristics and determine if their relationship to veneer static mechanical properties.

CHAPTER 5 VENEER NON-DESTRUCTIVE EVALUATION (NDE) SYSTEM DEVELOPMENT AND DESTRUCTIVE TESTING

Prior to developing prediction models of veneer mechanical properties, non-destructive and destructive evaluation of veneer needed to be performed. Based on the preliminary study section findings (Chapter 3), modifications were made to the optical and ultrasonic scanning systems. Research was then conducted on small veneer sheets for the following purposes:

1) To quantify veneer latewood percentage, defect measures, and growth ring patterns using non-destructive optical techniques.

2) To measure veneer ultrasonic properties and determine if waveform spectral analysis was able to identify veneer containing different amounts of defects.

3) To determine veneer tensile elasticity (MOE) and strength (F_t) and investigate the relationship between MOE and strength of veneer.

4) To obtain sufficient NDE and destructive veneer data to be used in the development of veneer tensile MOE and F_t property prediction models.

5.1 Veneer Material & Specimen Preparation for Predicting Veneer Properties

Eighteen (18) ultrasonically graded Douglas-fir veneer sheets (1/8-inches in thickness, full sheets) were selected from the previously sampled veneer in Section

4.1.1. The sheets were selected based on MOE_d to represent typical grades of material used in manufacturing LVL (i.e., G1, G2, and G3). Six (6) sheets per grade were selected, therefore each grade was adequately represented and high grading of the population did not occur.

From each veneer sheet, six (6) specimens, having a dimension of 6-inches wide by 31-inches long, were purposely selected to obtain specimens either containing distinctive defects or ones clear of defects. The purpose of hand-selecting representative specimens was to determine whether or not non-destructive evaluation techniques were capable of identifying defects, and which defects influence veneer tensile MOE and strength. An example of specimen selection lay-out is shown in Figure 5.1.

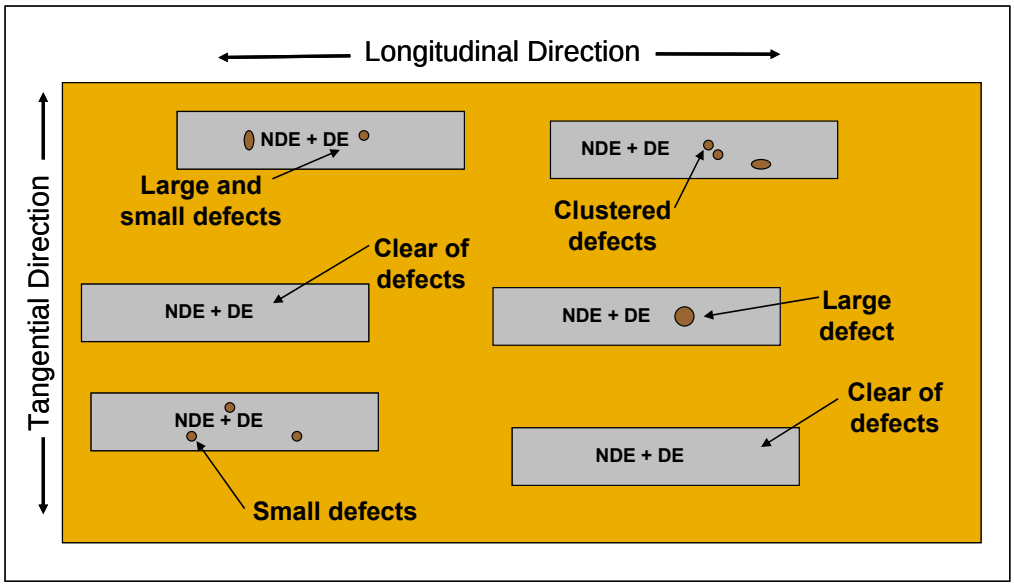

Figure 5.1. Example of purposely selected specimens containing specific features.

For the purpose of this study, defects included tight knots, loose knots, and holes. No distinction was made between the types of defect. Rather any tight knot, loose knot, or hole within the veneer was labeled as a defect. Very small splits along the longitudinal direction (likely due to lathe checks) were allowed in specimens, but generally were minimal. Specimens containing splits along the veneer's width were discarded, unless the specific split was associated with grain pattern at a localized defect. Defects were located within 12-inches from the center, in each direction, to be included in the tension test area (i.e., not within the grip area). After being processed from full sheets, specimens were conditioned to equilibrium at 60 percent relative humidity and 20^{o}C.

5.2 Non Destructive and Destructive Evaluation of Veneer Specimens

5.2.1 Testing of Final Veneer NDE Systems

For the ultrasonic system, tests were repeated on the same veneer specimen to verify results (in terms of UPT and waveform data) were not statistically different in a given run. Furthermore, various oscilloscope settings for volts/division (amplitude) and seconds/division (sampling rate) were evaluated. The optimal oscilloscope settings were determined as those allowing capture of entire waveform (until dissipation) from the stop accelerometer. The final oscilloscope settings are outlined in Table 5.1.

For the optical system, repeated images were captured on an individual veneer specimen positioned at 0-degrees. Additionally, images of an individual veneer were

captured with the veneer rotated 180-degrees. The resulting images (0-degrees and 180-degrees) were all thresholded and assessed to verify the optical system captured the same image when repeated (0-degree images), and also that the lighting was as uniform as possible (difference between 0-degree and 180-degree images).

Additionally, as evident from the preliminary study, a means was needed to quantify the growth ring pattern on each veneer. To do so, resulting entropy images (edge detection images), as shown in Figure 5.13, were used to determine a measure of growth ring pattern. Various types of analysis using entropy images were examined, and a final method to measure growth ring pattern was developed, as discussed in Section 5.2.2.2. With the operational systems in place, non-destructive and destructive testing of veneer specimens was then initiated.

5.2.2 Non Destructive Evaluation of Veneer

5.2.2.1 Ultrasonic System NDE on Veneer

The resulting one-hundred-eight (108) veneer specimens were tested for ultrasonic propagation time using a Metriguard Model 239A, lab-style stress wave timer (Figure 5.2). The stress wave setup was similar to that used in preliminary research (Section 3.1.1), with the addition of pneumatically controlled clamping and a moveable table. The pneumatically controlled clamping system was set at 40 pounds per square-inch (psi) to assure adequate and consistent contact pressure between veneer surface and stop and start accelerometers. A moveable table was utilized to provide consistent linear movement at set points across the veneer. Prior to stress

wave testing, specimen width (at three locations), thickness (at six locations), and weight was measured and recorded.

UPT (i.e., transit time) was then measured at six points across the specimen width, with the first reading taken 0.5-inches from the edge and in increments of 1-inch thereafter. At each location, only one measurement was taken. Based on earlier testing, the UPT value did not significantly change (if there was any change at all) when repeatedly tested at the same location given the setup used (i.e., foam base and appropriate gain settings). The start and stop gains on the Metriguard Model 239A were set at four (4) and forty (40), respectively. The accelerometers were located 3.5-inches from the specimen ends, thus resulting in an overall transit distance of 24-inches. Individual UPT was measured and recorded. For each specimen, UPT measurements were averaged to calculate final average specimen UPT. MOE_d was calculated for each specimen using Equation 3.1 and was based on velocity (i.e., final UPT divided by transit distance) and measured specimen density. No adjustment for moisture content was used, as all the veneer utilized in the primary study was subjected to the same conditioning environment.

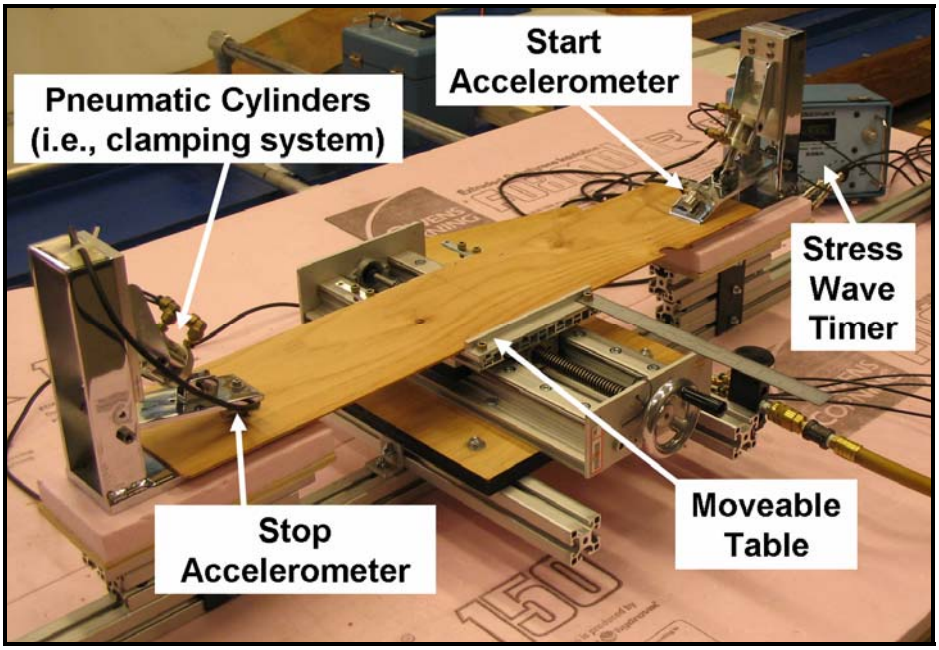

Figure 5.2. Modified ultrasonic stress wave testing setup.

In addition, for each point at which UPT was determined, raw ultrasonic stress wave data was captured using a Tektronix 2430A Digital Oscilloscope setup as outlined in Table 5.1. Waveform data was collected from the start and stop accelerometer outputs of the Metriguard Model 239A (Figure 5.3). Waveform capturing was triggered based on the start accelerometer. Once the trigger was activated, 1024 voltage values (maximum for a Tektronix 2430A oscilloscope) were sampled from both the start (channel 1) and stop (channel 2) accelerometers. Based on the digital oscilloscope specifications, from the 1024 voltage values recorded, 128 were pre-trigger data, while the remaining 896 represented voltage measurements after a stress wave was initiated in the veneer. The resulting triggered voltage data was sent

via a National Instruments GPIB-USB-HS cable and acquired and saved by a LabVIEW data acquisition program.

Table 5.1. Oscilloscope specifications and settings.

TEKTRONIX 2430A SPECIFICATIONS			
Horizontal		**Vertical**	
Points/Division =	50	Resolution =	8-bit
Record Length =	1024	Digitization Levels/Div. =	25
Number of Divisions =	20.48	Number of Divisions =	10.24
TEKTRONIX 2430A SETTINGS - Vertical			
Parameter		**CH1**	**CH2**
Setting V/Division		1V	50mV
Volts/Division (VAC)		1.000	0.050
Min. Change Detected (VAC)		0.04	0.002
+/- Range (VAC)		5.12	0.256
TEKTRONIX 2430A SETTINGS - Horizontal			
Time Per Division Setting	500us		
Trigger Setting	2.03 V - CH1		
Coupling	AC		

The waveform data was first clipped to remove pre-trigger data (Figure 5.4). Once captured, spectral analysis using power spectrum (PS), power spectrum density (PSD), magnitude peak (PEAK), and magnitude RMS (RMS) methods was performed on individual waveform data acquired at the stop accelerometer location. Analysis was performed on both a linear (Figure 5.5 and 5.6) and decibel (dB) (Figure 5.7 and 5.8) scale basis.

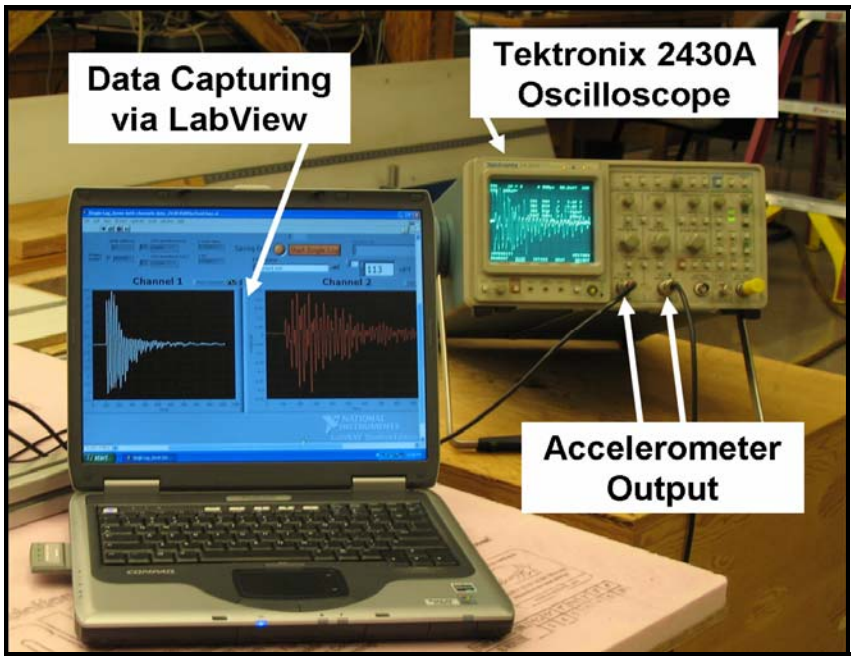

Figure 5.3. Setup of oscilloscope voltage capturing system.

An automated LabVIEW program was created and used to perform the spectral analysis. Various spectral value statistics (average, minimum, maximum, median, mode, standard deviation, variance, summation, kurtosis, and skewness) were determined at each of the six locations tested within an individual veneer. The six resulting spectral analysis values, within each method of analysis, were then averaged to obtain one measure of the various spectral values for each specimen. Additionally, raw waveform statistics were recorded. Upon completion of stress wave testing, specimens were placed back into the conditioning chamber.

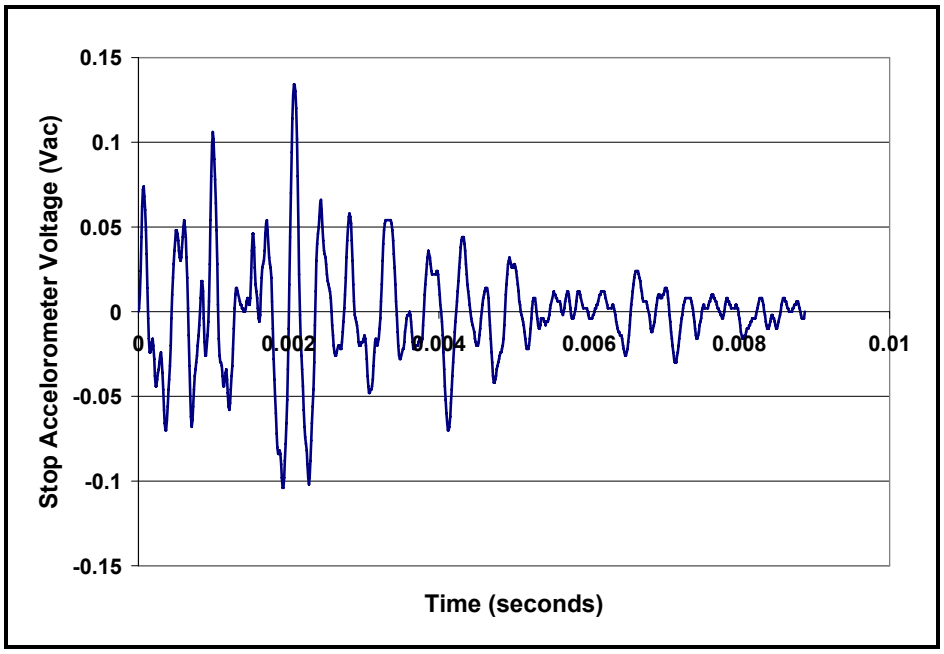

Figure 5.4. Example clipped waveform data used to perform spectral analysis.

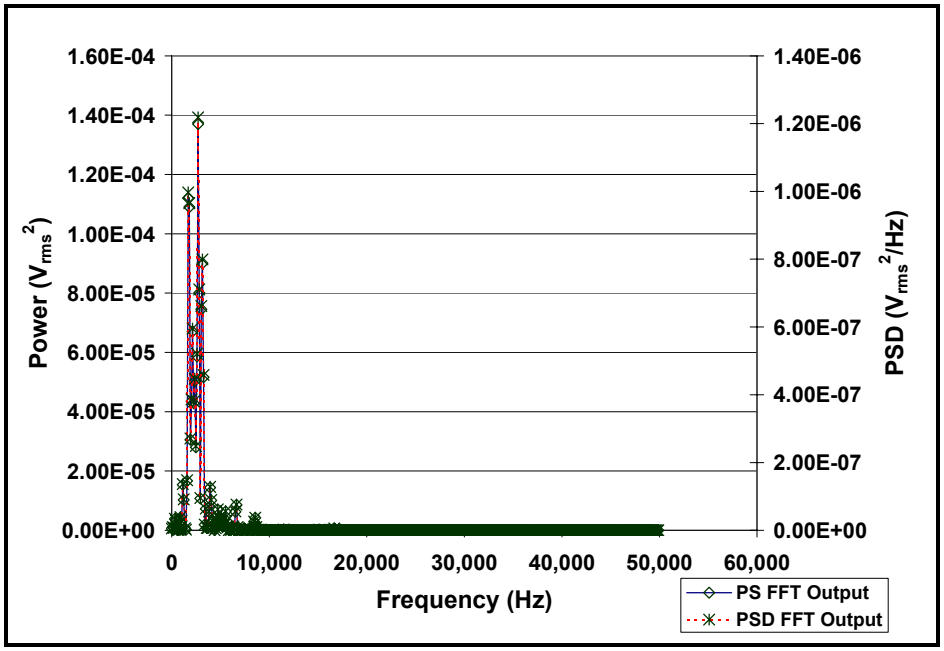

Figure 5.5. Example spectral analysis output for PS and PSD on linear scale.

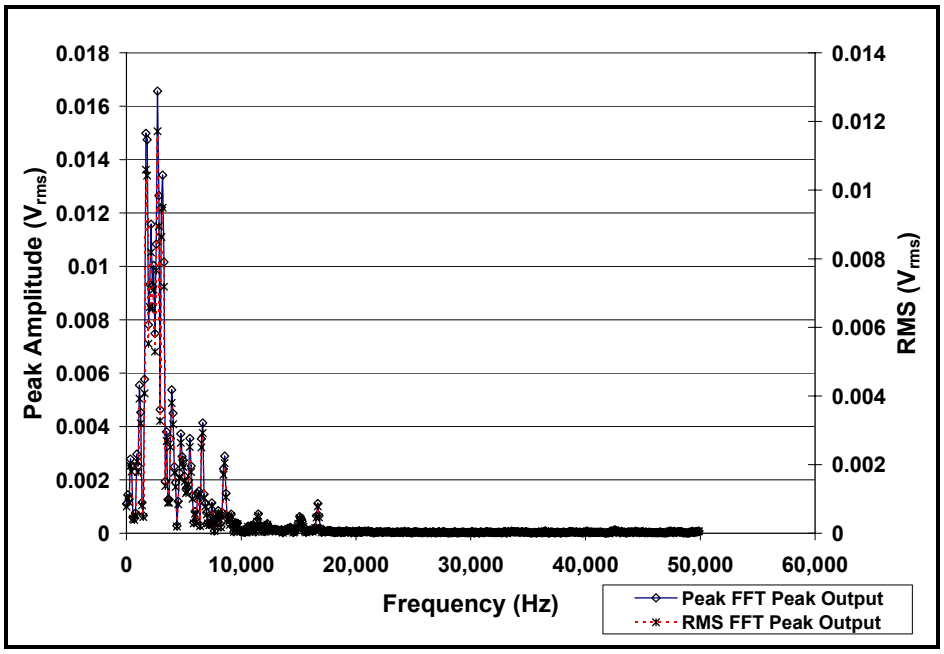

Figure 5.6. Example spectral analysis output for PEAK and RMS on linear scale.

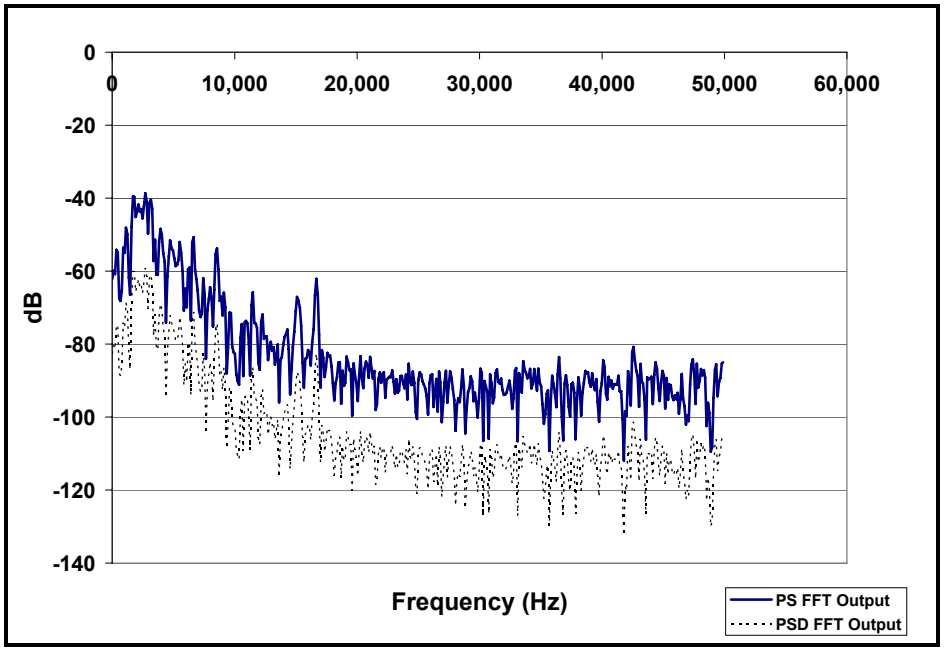

Figure 5.7. Example spectral analysis output for PS and PSD on dB scale.

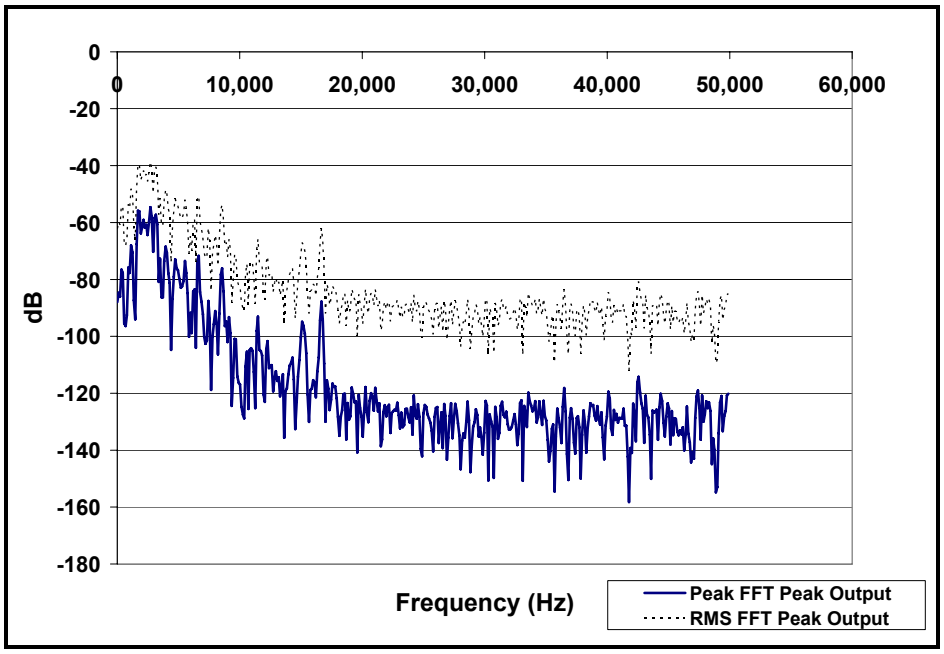

Figure 5.8. Example spectral analysis output for PEAK and RMS on dB scale.

5.2.2.2 Optical Scanning System NDE on Veneer

Specimens were then tested non-destructively using an optical scanning system (Figure 5.9 and 5.10). Each specimen was imaged by using a Hitachi HV-C20 video camera (with a Pentax 8-48mm F/1.0 lens) connected to an AT&T Targa-32 image acquisition card. Both halogen (overhead lamps) and fluorescent (room) lighting was used to uniformly illuminate the veneer surface. A spatial resolution of 13 pixels and 12 pixels per inch along the length and across the veneer width, respectively, was used when capturing images. By utilizing a different camera lens than in the preliminary study (and a lower resolution), only one image per veneer side had to be captured to cover the entire area under investigation (i.e., area subjected to tensile loading in

destructive tests). After optical scanning was completed, specimens were placed back into the conditioning chamber.

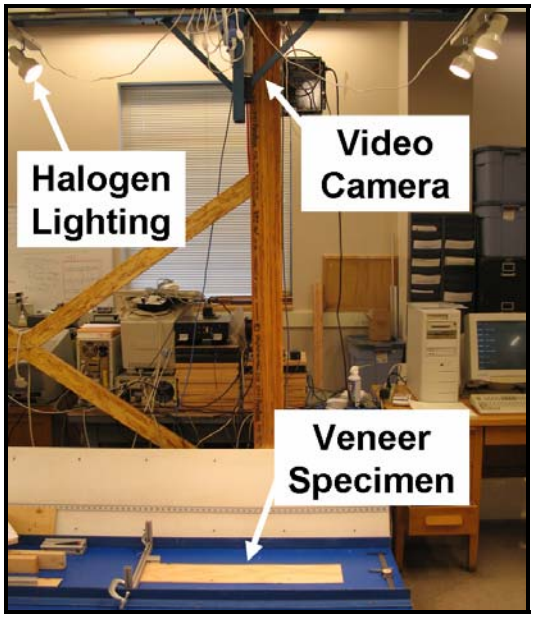

Figure 5.9. Setup of final optical scanning system.

Figure 5.10. Close-up of camera and veneer specimen in optical scanning system.

For determining earlywood and latewood percentages, images were analyzed through a batch routine in Zmenu (proprietary program developed at OSU). The captured images were analyzed using two Otsu classification algorithms (single and dual threshold of the "green" and "blue" signal) to determine percent latewood and earlywood. Both "green" and "blue" signals were utilized, because when one signal failed to determine the percent latewood (i.e., only thresholded for defect area), the other signal was able to correctly threshold for latewood percentage.

The single threshold Otsu classification algorithm outputted latewood areas as black pixels (Figure 5.11). The dual threshold method denoted latewood areas as black pixels, along with interpretation of earlywood/latewood transition zone areas as green pixels (Figure 5.11). Additionally, the Zmenu program output an edge tracing grayscale image (i.e., entropy image) (Figure 5.11). The resulting images were first saved as Targa (.tga) files and then converted to bitmap (.bmp) files for determining earlywood and latewood percentage. Earlywood and latewood percentages were calculated using a program written in MATLAB to output the number of white (earlywood), black (latewood), and green (transition between earlywood and latewood) pixels.

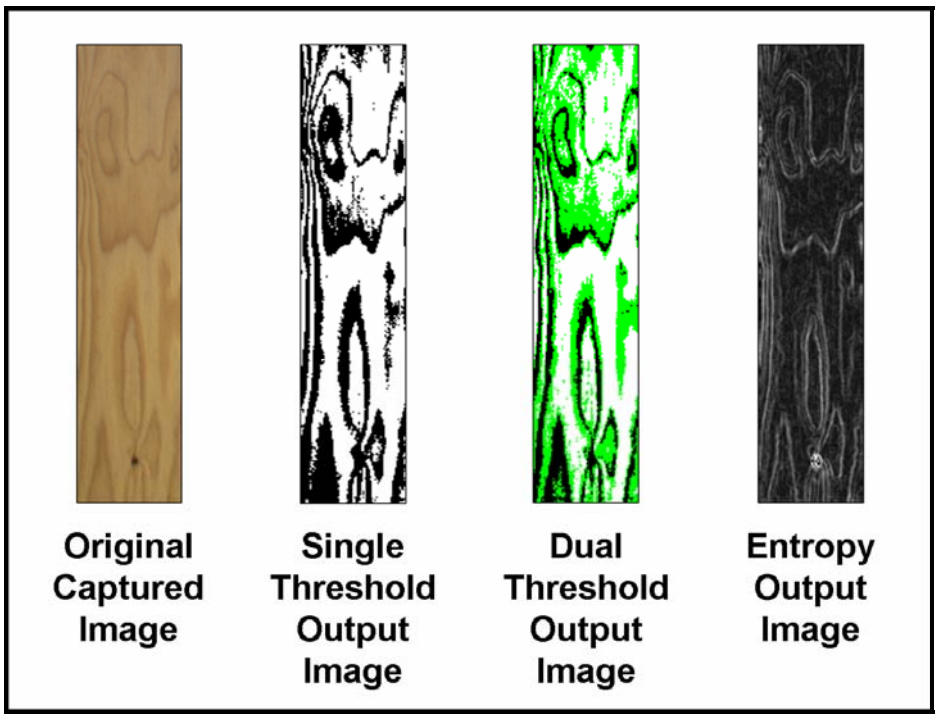

Figure 5.11. Original and threshold veneer images.

Defect area was determined from each image by using ImageJ, which first converted images to 8-bit, followed by the application of a maximum entropy threshold scheme (Figure 5.12). The resulting images were saved as bitmap files for determining percent defect. Defect area was calculated using a program written in MATLAB to output the number of white (defect free area) and black (defect area) pixels. Defect number and width was determined using Photoshop. Defect volume (both for knots and holes and assuming a relatively circular shape) was then calculated based on the average veneer thickness and defect width using the Equation 5.1 for volume of a cylinder.

$$V = \pi \times r^2 \times h$$ **Equation 5.1**

Where:

V = Defect volume (in^3)

π = 3.114159

r = Radius of defect (in.)

h = Veneer thickness (in)

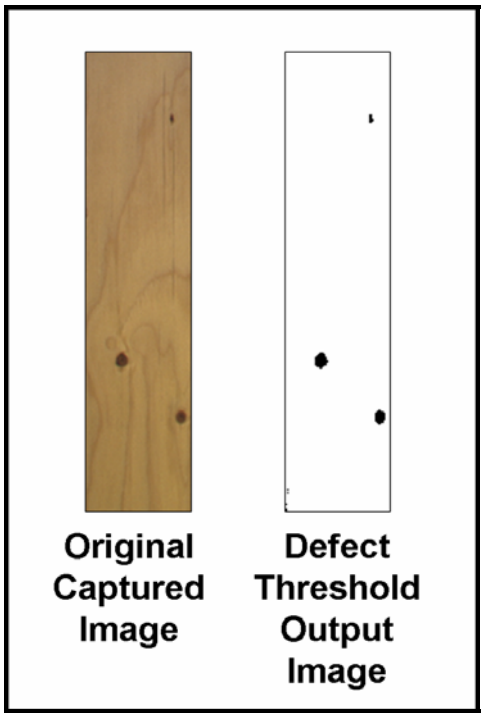

Figure 5.12. Original and defect threshold veneer images.

Measures of growth ring pattern were determined using the resulting entropy images from the Zmenu program. The resulting veneer entropy images consisted of 312 pixels along the veneer's length and 71 pixels across the veneer's width. To

measure growth ring patterns, entropy images were analyzed along the length and across the veneer width (Direction 1 and 2, respectively as shown in Figure 5.13). The color value of each individual pixel within a line along the entropy image's length and across the width were summed and recorded. When growth ring pattern image analysis was done along the veneer image's length, the output consisted of 71 summation lines (with 312 pixel values summed per line). Growth ring pattern image analysis done across the veneer image's length resulted in an output of 312 summation lines (with 71 pixel values summed per line).

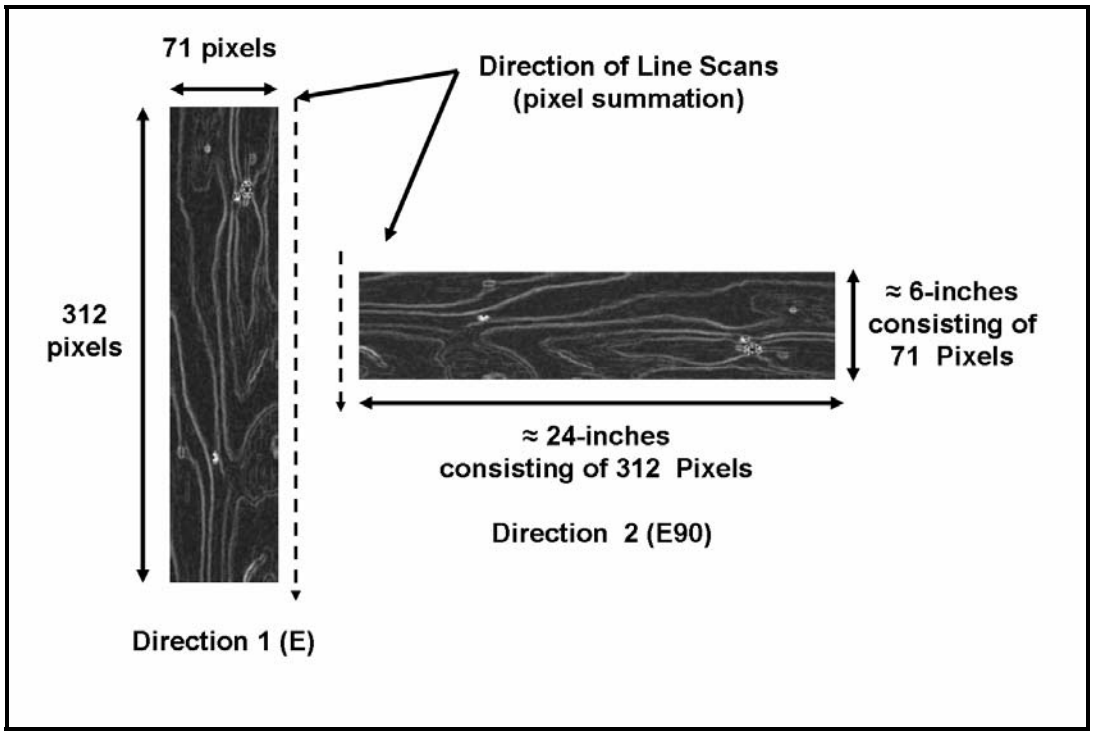

Figure 5.13. Growth ring pattern measurement images showing analysis along the veneer image length (E) and across the veneer width (E90).

Using the summation result for each line within the entropy image, overall image statistics of mean, minimum, maximum, standard deviation, and median were determined and recorded as the measure of growth ring pattern. Statistical values were determined for both Direction 1 (labeled as E) and Direction 2 (labeled as E90). The process of analyzing and calculating entropy image statistics was done using an automated process via a program written in Matlab.

5.2.3 Destructive Evaluation of Veneer

Specimens were then tested destructively in tension. Both veneer tensile MOE and F_t was determined. Tension testing was performed using the same fixture setup as outlined in Section 3.1.1. Specimens were tested in tension parallel to grain at a rate of 0.075-inches per minute of cross head motion using a Tinius Olsen UTM. The grip area was 3.5-inches on each end, leaving 24-inches as the overall length between grips (i.e., area imaged in Section 5.1.2 above). Specimen width and thickness measurements were taken from values measured during ultrasonic evaluation, as the specimen weight was verified as being equal at time of ultrasonic and tension testing. Deformation was recorded on each face of the specimens over a gauge length of 9-inches as shown in Figure 3.4 and 3.5.

5.3 Veneer Non-Destructive and Destructive Evaluation Results and Discussion

Using the non-destructive and destructive evaluation techniques, a set of quantified veneer measures was successfully determined under both the optical and

ultrasonic system. The relationship between veneer tensile MOE and F_t was evaluated. Additionally, analysis was performed to determine if waveform spectral data could be easily used to distinguish between high and low strength veneer, and veneer consisting of large defects.

5.3.1 Destructive Veneer Results and Relation Between MOE and F_t

Table 5.2 provides a summary of destructively determined veneer tensile MOE and F_t. Complete results for each individual specimen are located in Appendix A.

Table 5.2. Veneer destructively determined tension test results.

Summary Statistic	Density (lb/ft^3)	Tensile MOE (psi)	F_t (psi)
Average	32.1	1,776,568	2,884
St. Dev.	3.0	447,488	1,481
COV %	9.4	25.2	51.4
Min.	27.9	775,341	545
Max.	40.2	3,211,719	8,756
Sample Size	106	106	106

Of the 108 specimens tested, two specimens had to be removed from the analysis. One specimen failed partially within the grip area. This failure was associated with a defect near the grip that failed into the grip area, leaving the remainder of the veneer specimen intact. The other specimen removed was determined to have a high degree of failure before testing. This resulted in a total of 106 specimens destructively evaluated.

The coefficient of variation percentage (COV%) of the test results, especially for F_t, was noted as being quite high (Table 5.2). The average COV for clear wood tensile parallel to grain has been reported as 25 percent (Forest Products Laboratory 1999). Green et al. (1990) reported COV percentage for Douglas-fir lumber tensile properties based on testing of various grades of lumber. They reported COV percentages ranging from 17 to 27 percent and 28 to 59 percent for tensile MOE and ultimate tensile strength (i.e., F_t), respectively, when testing various grades of Douglas-fir lumber at 10 percent moisture content. Given this, a high COV was to be expected, in this study, given sampling was performed in a manner to include specimens with high and low numbers of defects and highly sloped and straight grain patterns. The high COV percentage, therefore, allowed for determining which veneer characteristics influence mechanical properties. If the COV percentage had been very small, it would have likely indicated not enough variation between veneer specimens was present, and thus would not allow for an adequate set of data to perform prediction model development.

When using ultrasonic values to predict veneer properties, MOE_d is typically regressed against static MOE. In establishing this relationship, the correlation between veneer MOE is used to predict veneer and LVL strength properties. Past researchers have suggested that when localized defects and grain deviations are included in wood, there is, however, only a partial relationship between wood elasticity and strength (Barnes 2000, Bodig 2000). To test this assumption in the context of this study, the relationship between veneer static tensile MOE and F_t was determined. Figure 5.14 shows the relationship between destructively evaluated

veneer tensile MOE and F_t. In this regression, 46.4 percent of the variation (R-squared = 0.464) in veneer F_t was explained by veneer tensile MOE. This relationship was very similar to previous research by Hunt et al. (1989), who reported a linear relationship with an R-squared value = 0.472 between yellow-poplar veneer tensile strength and static MOE.

While some relationship existed between veneer tensile MOE and F_t, analysis of specimen failure provided some insight that inclusion of defect and growth ring pattern measures may improve prediction of veneer strength properties. In particular, very high strength veneers were relatively free from defects and consisted of straighter growth ring patterns (Figure 5.15). In comparison, very low strength veneers contained defects, more numerous and/or larger and sloped veneer growth ring patterns (Figure 5.16). Based on the manner in which veneer tension failure occurred, it appeared both defect and growth ring pattern measurements were important in determining final veneer F_t. Using defect and growth ring pattern measurements in regression analysis would likely result in better prediction of veneer F_t values as compared to using tensile MOE as a predictor.

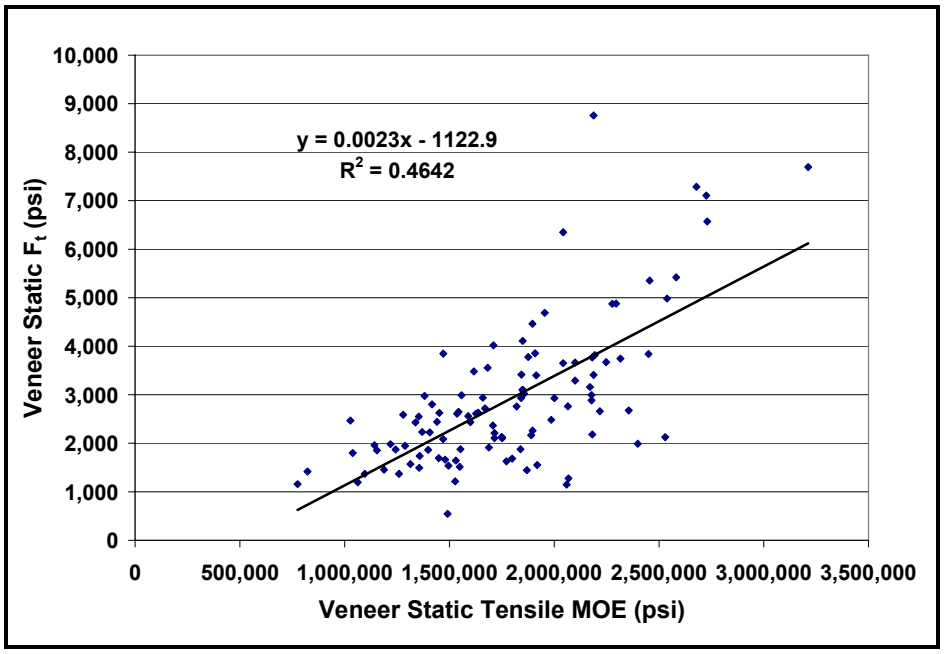

Figure 5.14. Veneer static F_t versus static tensile MOE from model development study destructive testing.

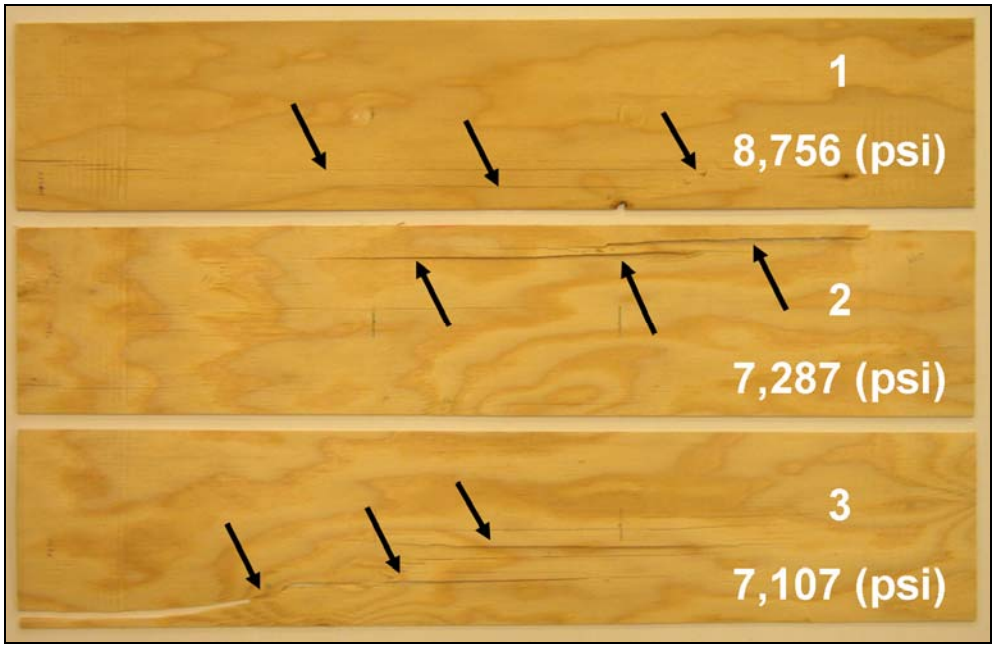

Figure 5.15. Three highest strength veneer specimens (relatively defect free and straight failure patterns) with arrows indicating failure locations.

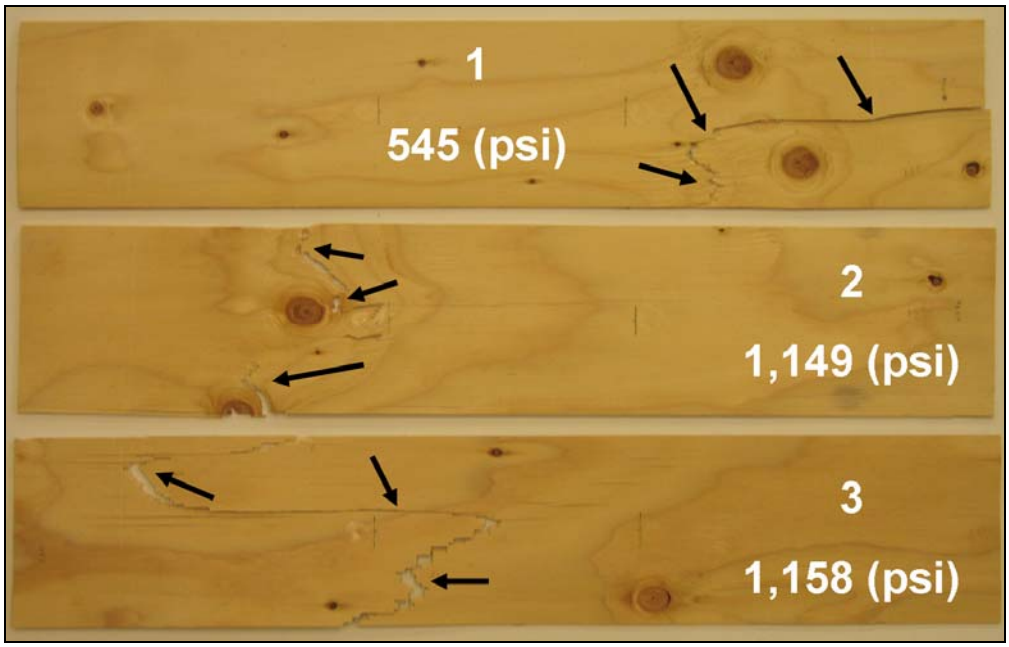

Figure 5.16. Three lowest strength veneer specimens (numerous, large defects and highly sloped failure patterns) with arrows indicating failure locations.

5.3.2 Ability of Waveform Spectral Analysis Measures to Locate Defects and High Versus Low Strength Veneer

In addition to using waveform spectral analysis data to better predict veneer mechanical properties, analysis was performed to see if any difference existed in waveforms obtained from veneer with large versus small defects and high versus low F_t. To do this, raw data output from waveform spectral analysis using power spectrum analysis was analyzed. Specifically, raw power spectrum data was compared for veneer specimens having the highest, average, and lowest measure of maximum defect width. Maximum defect width was chosen for comparison as it was thought the largest defect (i.e., the one containing the maximum width) in a veneer specimen

would be the most influential in determining veneer F_t. Additionally, raw power spectrum data was compared for veneer specimens with highest, average, and lowest F_t.

Comparisons were made by using the raw data output by the power spectrum analysis and producing a cumulative sum plot of waveform frequency. The goal was to determine if differences existed in the cumulative sum versus frequency plots for veneer with different defect and F_t properties. If differences existed in the plots, the frequency (i.e., harmonic nature) at which the plots differed may have provided a means to use waveform peak amplitude values at a given frequency as a measure of high versus low defect width and veneer F_t. Furthermore, given any noticeable difference in the plots, principle components analysis could then be performed to identify specific frequencies and how they related to veneer properties.

Little to no difference was observed in cumulative sum versus frequency plots. Specifically, there was little difference in cumulative sum versus frequency plots for veneer with the maximum, average, and minimum measures of maximum defect width (Figure 5.17). Furthermore, there was little difference in cumulative sum versus frequency plots for veneer with the maximum, average, and minimum value of veneer F_t (Figure 5.18). As shown in Figures 5.17 and 5.18, the maximum waveform frequency measured was 50,000 Hz (i.e., 50 kHz). Given no difference in cumulative sum versus frequency was observed from the plots on veneer with highly different defect and F_t properties, no further principle components analysis was performed.

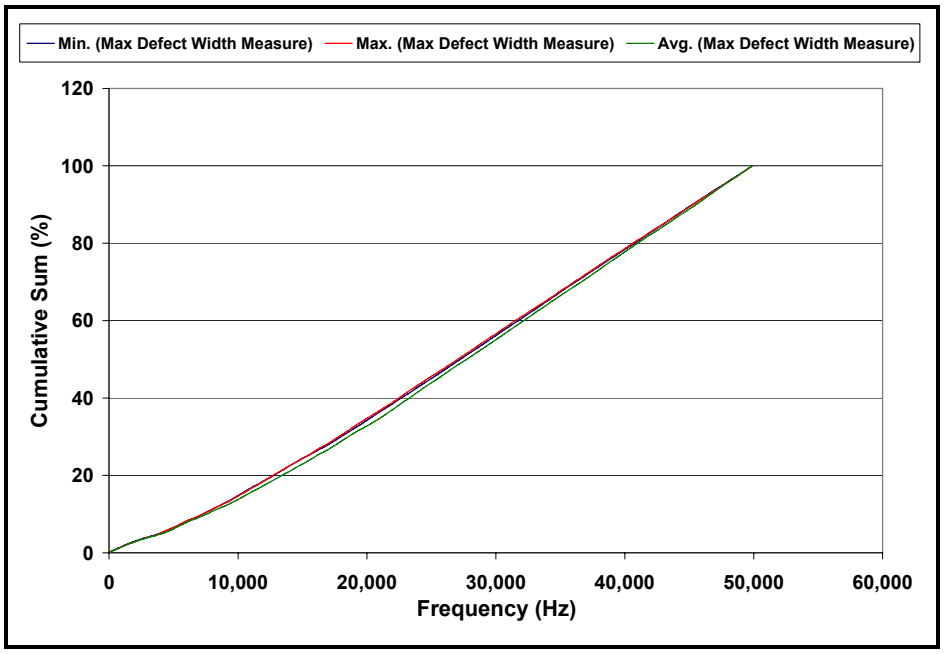

Figure 5.17. Cumulative sum versus frequency of power spectrum output data on veneer with minimum, maximum, and average values of maximum defect width.

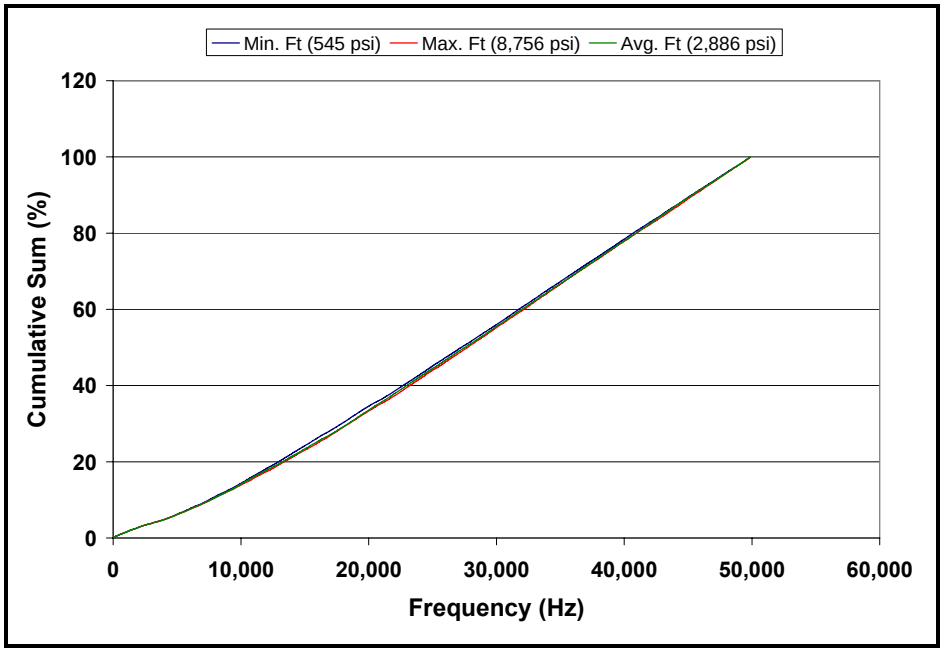

Figure 5.18. Cumulative sum versus frequency of power spectrum output data on veneer with minimum, maximum, and average values of F_t.

Additionally, correlation analysis was performed between waveform (raw waveform and spectral analysis measures) and defect measures. While many defect and waveform measurements showed a significant individual correlation (at a 0.01 level) to each other, the highest correlation (-0.544) was between maximum defect volume and power spectrum arithmetic mean (i.e., average) on the decibel scale. Based on this being the best correlation between defect and waveform measures, it was unlikely the ultrasonic system alone provided a reliable means of quantifying defect information. A complete correlation table between defect and waveform measures is provided in Appendix A.

Attempts made during the preliminary study and ultrasonic system development sections to capture the entire waveform of the first stress wave when using the Tektronix 2430A oscilloscope were not successful, at least with any high degree of accuracy. It is possible a faster sampling, higher resolution oscilloscope, capable of capturing only the first pass of the stress wave, or more of each waveform as it passed the stop accelerometer, may better detect differences in veneer properties.

CHAPTER 6 OPTICAL, ULTRASONIC, AND COMBINED NDE MODEL PREDICTIONS OF VENEER TENSILE MOE AND F_t DEVELOPMENT AND COMPARISONS

Prior to performing non-destructive and destructive evaluation of veneer for the purpose of manufacturing LVL specimens and predicting their mechanical properties, research using small veneer sheets was conducted for the following purposes:

1) To determine how features, measured using an optical scanning system, influence veneer tensile MOE and strength when destructively testing veneer.

2) To determine if information obtained from an optical scanning system resulted in accurate prediction equations of veneer destructively determined (i.e., static) tensile elastic and strength properties.

3) To determine whether or not ultrasonic stress wave systems were able to identify defects in small veneer sheets and if UPT and/or MOE_d values resulted in significant correlations with tensile MOE and strength of destructively tested veneers.

4) To determine whether or not a combined optical and ultrasonic scanning system resulted in significantly better predictions of veneer's tensile MOE and strength properties.

6.1 Methodology for Determining Statistically Significant Veneer Measures and Selecting the Most Appropriate Prediction Model for Each System

Destructive properties evaluated in Section 5.1.2 were analyzed to determine which non-destructive measurements were statistically significant in predicting tensile strength and MOE. Correlation analysis was performed to determine if specific ultrasonic and optical scanning measurements are correlated with one another. Linear, variable selection (i.e., stepwise and all possible combination), and multiple linear regression techniques were used to determine the most appropriate prediction equations for static properties based on NDE measurements. Finally, the influence of defects on tensile strength and MOE was evaluated, and the non-destructive techniques ability to identify defects was investigated.

In terms of prediction model development, when many possible explanative variables were included, both stepwise and all possible combination regression techniques were employed. The resulting prediction model output from both stepwise and all possible combination analysis were compared. While stepwise regression output one final model, all possible combination analysis provided a list of various models with a different number of variables present. The most appropriate all possible combination regression output was determined by analyzing the Cp, R-squared, and Root MSE (mean squared error) values for the various model combinations and number of variables. Once the best estimation model was found from both stepwise and all possible combination analysis, selection between which two models to use was determined. When both techniques resulted in the same prediction model, it was then

selected as the best possible model. If the two models differed in output, then the most appropriate all possible combination model was selected.

6.2 Veneer Density as a Predictor of Veneer Properties

Relationship between density and veneer mechanical properties was an important aspect for this research. Specifically, density was used in calculation of MOE_d from ultrasonic testing and as a variable in portions of the optical system prediction models. Density has long been regarded as having a relationship to wood mechanical properties (Panshin and deZeeuw 1964). In this study, the relationship of veneer density to both elastic and strength properties was evaluated. Results indicated density was a better predictor of tensile MOE (Figure 6.1) as compared to strength (Figure 6.2). The relationship between density and veneer F_t (R-squared = 0.313), from this portion of the study, was much higher than reported by Hunt et al. (1989) who found density as being a poor predictor of yellow-poplar veneer strand tensile strength ($R^2 = 0.006$). While density did not predict strength all that reliably, however, it was still likely to be a statistically significant factor in terms of the optical, ultrasonic, and combined prediction models.

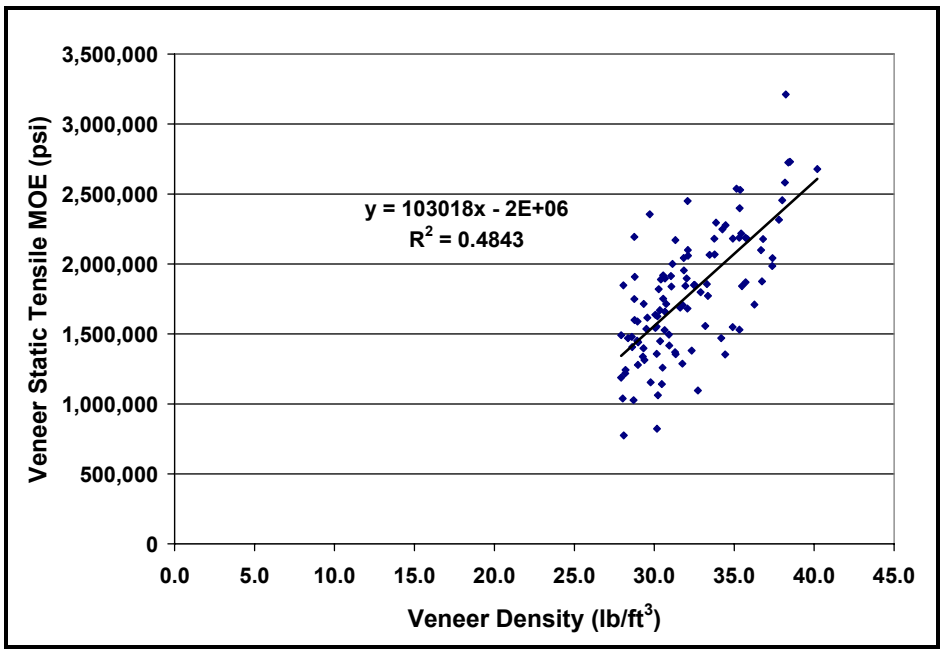

Figure 6.1. Veneer static tensile MOE versus density.

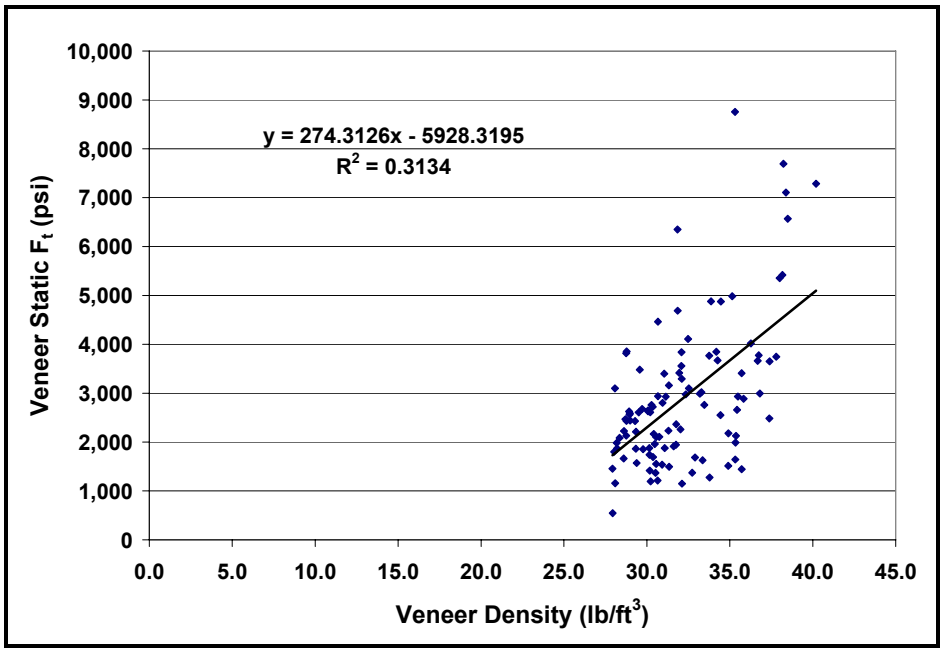

Figure 6.2. Veneer static tensile strength versus density.

6.3 Optical System: Development of Veneer Property Predictions

The first objective of the optical system study was to determine which veneer features were statistically significant in terms of influencing veneer tensile modulus of elasticity (MOE) and strength (F_t) properties. The second objective of the optical system study was to determine whether or not the developed optical system could be used to reliably predict destructively determined (i.e., static) veneer tensile MOE and F_t.

6.3.1 Veneer Tensile Property Model Development Using Latewood and Defect Optical Data (i.e., Basic Optical)

Correlation analysis was performed between veneer tensile MOE and all basic optical (latewood and defect) measurements (Appendix A). Table 6.1 shows the coefficients for optical measures having a significant individual correlation (at a 0.01 level) with veneer static tensile MOE. Latewood percentage (dual threshold) showed a statistically significant positive correlation to veneer static tensile MOE. This suggests that as latewood percentage increases, so does MOE. This would stand to reason as latewood possesses a higher density and as density increases, in most cases, so does elasticity of wood. The remaining statistically significant optical measures showed a negative correlation to veneer static tensile MOE. Because these optical measures were all defect measurements, this suggests that MOE decreases as the amount of defect increases. Furthermore, it was apparent that the amount of defect in a veneer sheet does have some influence on MOE.

Table 6.1. Statistically significant correlation coefficients from individual correlation analysis between veneer tensile MOE and various optical measurements.

Characteristic	Correlation Coefficient	Characteristic	Correlation Coefficient
Maximum Defect Volume	-0.433	**Total Defect Width**	-0.333
Maximum Defect Width	-0.391	**Average Defect Volume**	-0.317
Defect Percentage	-0.356	**Average Defect Width**	-0.310
Latewood Percentage - Dual Threshold (Black)	0.336	**Average Surface Area per Defect**	-0.259
Total Defect Volume	-0.336		

Correlation analysis was performed between veneer tensile F_t and all optical measurements (Appendix A). Table 6.2 shows the coefficients for optical measures having a significant individual correlation (at a 0.01 level) with veneer tensile strength. Latewood percentage (dual threshold black pixel area) showed a statistically significant positive correlation to veneer static tensile strength. This suggests that as latewood percentage increases, so does strength. This would stand to reason as latewood possesses a higher density and as density increases, in most cases, so does the strength of wood. The remaining statistically significant optical measures showed a negative correlation to veneer static tensile strength. Again, all negatively correlated optical measures were defect measurements and suggested veneer tensile strength decreases as the amount of defect increases. It was apparent that the amount of defect in a veneer sheet influences tensile strength.

Table 6.2. Statistically significant correlation coefficients from individual correlation analysis between veneer static tensile strength and various optical measurements.

Characteristic	Correlation Coefficient	Characteristic	Correlation Coefficient
Maximum Defect Width	-0.439	**Average Surface Area per Defect**	-0.355
Maximum Defect Volume	-0.412	**Total Defect Width**	-0.347
Average Defect Width	-0.394	**Average Defect Volume**	-0.334
Latewood Percentage - Dual Threshold (Black)	0.390	**Total Defect Volume**	-0.288
Defect Percentage	-0.383		

The second objective of the optical system study was to determine whether or not the developed optical system could be used to reliably predict veneer mechanical properties, specifically, tensile strength and MOE. In terms of veneer tensile MOE, while Table 6.1 lists nine variables as having significant individual correlations to MOE, regression analysis indicated that only two of those characteristics were statistically significant (at an alpha level = 0.05) in predicting veneer tensile MOE (Table 6.3). Figure 6.3 shows the relationship between predicted MOE using statistically significant optical measures versus veneer static tensile MOE. In this regression, only 23.7 percent of the variation (R-squared = 0.237) in veneer static tensile MOE was explained by the linear regression coefficients.

Table 6.3. Statistically significant basic optical model variables, regression coefficients, and p-values from regression analysis for predicting veneer static tensile MOE.

Independent Variable	Regression Coefficient	p-value
Constant	1.70E+06	0.000
Latewood Percentage – Dual Thresh, Black (v13)	16,925.6	0.012
Maximum Defect Volume (v23), in.^{3}	-4.04E+06	0.000

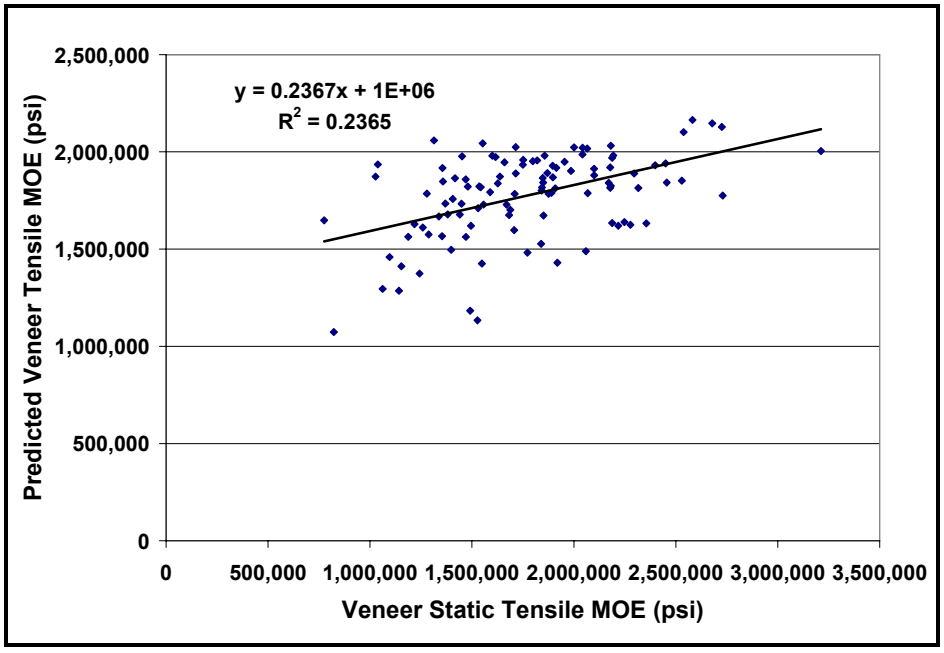

Figure 6.3. Predicted veneer tensile MOE from the basic optical model (latewood and defect measures) versus veneer static tensile MOE.

In terms of veneer strength properties, while Table 6.2 lists nine variables as having significant individual correlations to static F_t, regression analysis indicated that only two of those characteristics were statistically significant (at an alpha level = 0.05) in predicting veneer F_t (Table 6.4). Figure 6.4 shows the relationship between

predicted veneer F_t using statistically significant optical measures versus veneer static F_t. In this regression, only 27.6 percent of the variation (R-squared = 0.276) in veneer F_t was explained by the linear regression coefficients.

Table 6.4. Statistically significant basic optical model variables, regression coefficients, and p-values from regression analysis for predicting veneer static F_t.

Independent Variable	Regression Coefficient	p-value
Constant	2,790.4	0.000
Latewood Percentage – Dual Thresh, Black (v13)	72.8	0.001
Maximum Defect Width (v18), in.	-1,733.2	0.000

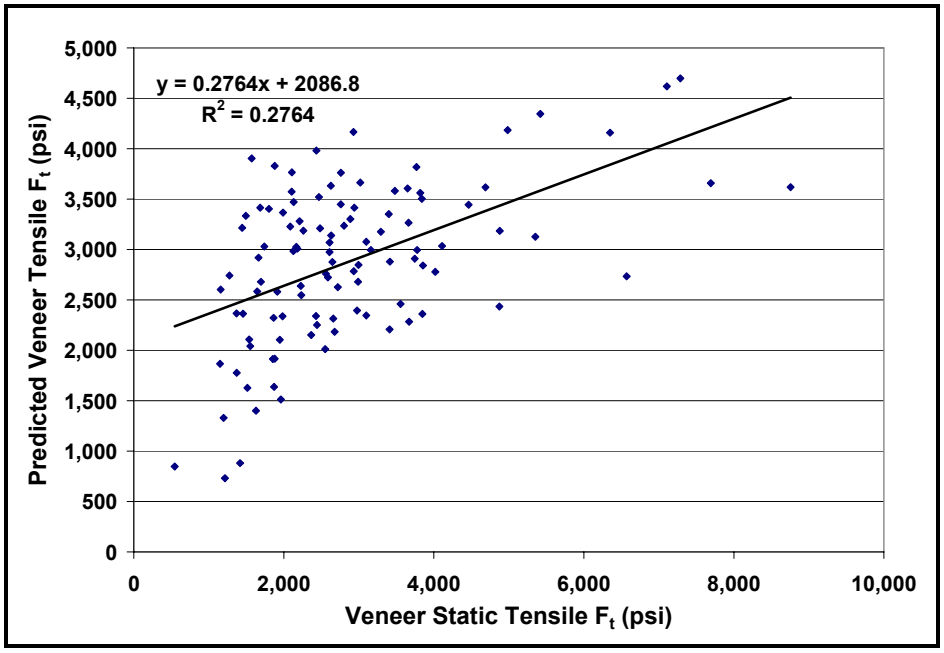

Figure 6.4. Predicted veneer tensile strength from the basic optical model (latewood and defect measures) versus veneer static F_t.

One of the objectives was to determine whether or not the developed optical system could be a stand alone reliable means of predicting veneer mechanical properties. The regression analysis in Tables 6.3 and 6.4 indicated an optical system which utilized only latewood and defect information was somewhat weak. To improve the optical system's reliability, inclusion of the quantified measures of veneer growth ring pattern and density was investigated when performing regression analysis.

6.3.2 Veneer Tensile Property Model Development by Inclusion of Growth Ring Pattern (GRP) Measurements

Latewood and defect measurements, by themselves, did not explain a large amount of variation in veneer tensile MOE and F_t. Given this, the next step was to include measurements of growth ring pattern obtained by summation along the length and across the veneer entropy images (referred to as E and E90, respectively) to investigate any improved prediction of veneer tensile MOE and F_t.

When evaluating veneer tensile MOE by including entropy image growth ring pattern statistics with optical measures from Section 6.3.1, regression indicated five characteristics were statistically significant (at an alpha level = 0.05) in predicting veneer tensile MOE (Table 6.5). Figure 6.5 shows the relationship between predicted veneer tensile MOE using statistically significant optical and entropy image growth ring pattern measures versus veneer static tensile MOE. In this regression, 42.2 percent of the variation (R-squared = 0.423) in veneer tensile MOE was explained by the linear regression coefficients.

Table 6.5. Statistically significant optical including growth ring pattern measures model variables, regression coefficients, and p-values from regression analysis for predicting veneer static tensile MOE.

Independent Variable	Regression Coefficient	p-value
Constant	1,202,015	0.000
Maximum Defect Volume (v23), in.^{3}	-5,333,605	0.000
E Mean (v25)	-748.1	0.008
E90 Standard Deviation (v31)	1,774.1	0.024
E90 Minimum (v33)	1,039.9	0.007
E90 Median (v34)	2,776.6	0.005

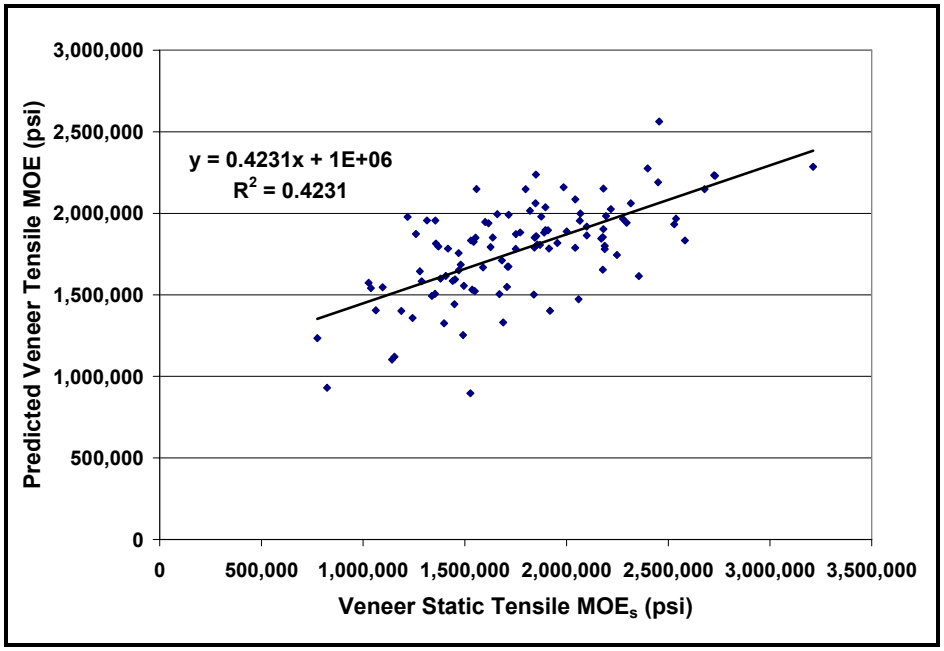

Figure 6.5. Predicted veneer tensile MOE from the optical and growth ring pattern measures model versus veneer static tensile MOE.

Prediction of veneer tensile MOE improved with inclusion of entropy image growth ring pattern statistics, as compared to basic optical (latewood and defect)

model (Figure 6.3). Inclusion of entropy image growth ring pattern statistics, however, were not as reliable in predicting veneer tensile MOE, as compared to density (Figure 6.1).

When evaluating veneer F_t and including entropy image growth ring pattern statistics with optical measures from Section 6.3.1, regression indicated three characteristics were statistically significant (at an alpha level = 0.05) in predicting veneer F_t (Table 6.6). Figure 6.6 shows the relationship between predicted veneer F_t using statistically significant optical and entropy image growth ring pattern measures versus veneer static F_t. In this regression, 38.7 percent of the variation (R-squared = 0.387) in veneer static F_t was explained by the linear regression coefficients.

Table 6.6. Statistically significant optical including growth ring pattern measures model variables, regression coefficients, and p-values from regression analysis for predicting veneer static F_t.

Independent Variable	Regression Coefficient	p-value
Constant	1,465.7	0.008
Latewood Percentage – Dual Thresh, Black (v13)	44.77	0.032
Maximum Defect Width (v18), in.	-2,095.9	0.000
E90 Minimum (v33)	1.5513	0.000

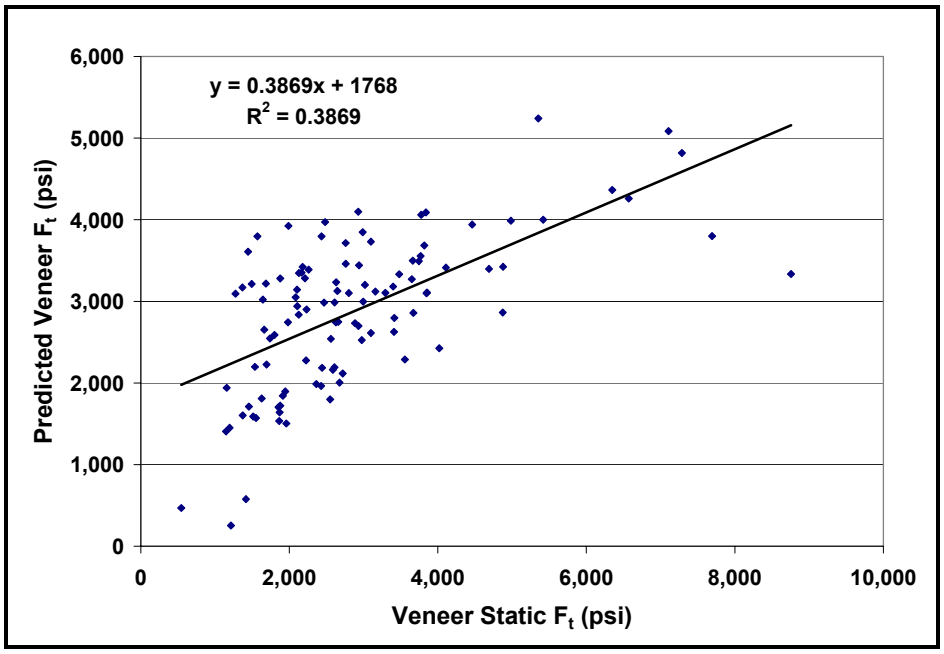

Figure 6.6. Predicted veneer F_t from the optical and growth ring pattern measures model versus veneer static F_t.

Inclusion of entropy image growth ring pattern statistics improved the prediction of veneer F_t, as compared to both density and basic optical (latewood and defect) models (Figures 6.2 and 6.4, respectively). While veneer F_t predictions improved, it was not known, at this point, how repeatable this method of measuring growth ring patterns would be in predicting future values of veneer F_t. The validity of including growth ring measures, as determined by the pixel color line summation method, is later investigated further in the model validation section (Chapter 7).

6.3.3 Veneer Tensile Property Model Development by Inclusion of Density, Optical, and Growth Ring Pattern Measures

Inclusion of growth ring pattern statistics improved the prediction of veneer tensile MOE, but was not as reliable as using density alone (Figure 6.1). Density was then included with optically determined measures (basic optical and growth ring pattern) to further investigate improvement of veneer tensile property predictions.

When evaluating veneer MOE by including density, basic optical (latewood and defect), and entropy growth ring pattern measurements, regression indicated seven characteristics were statistically significant (at an alpha level = 0.05) in predicting veneer MOE (Table 6.7). Figure 6.7 shows the relationship between predicted veneer tensile MOE using statistically significant density, basic optical, and growth ring pattern measures versus veneer static tensile MOE. In this regression, 71.7 percent of the variation (R-squared = 0.717) in veneer tensile MOE was explained by the linear regression coefficients.

Predictions of veneer tensile MOE improved once density was included in regression analysis with basic optical and growth ring pattern measures. The regression model including basic optical, growth ring pattern, and density measures explained the highest amount of variation, as compared to all other models, when predicting veneer tensile MOE (R-squared = 0.72). This was a significant improvement in predicting veneer tensile MOE as compared to using only basic optical and growth ring pattern measurement values (Figure 6.5) or density (Figure 6.1).

Table 6.7. Statistically significant optical including growth ring pattern measures and density model variables, regression coefficients, and p-values from regression analysis for predicting veneer static tensile MOE.

Independent Variable	Regression Coefficient	p-value
Constant	-1,415,976.8	0.000
Density (v3), lb./ft.^{3}	100,347.6	0.000
Number of Defects (v16)	67,134.5	0.000
Total Defect Width (v20), in	-275,769.5	0.000
E Mean (v25)	-810.5	0.000
E90 Standard Deviation (v31)	1,707.8	0.002
E90 Minimum (v33)	1,013.6	0.000
E90 Median (v34)	2,712.8	0.000

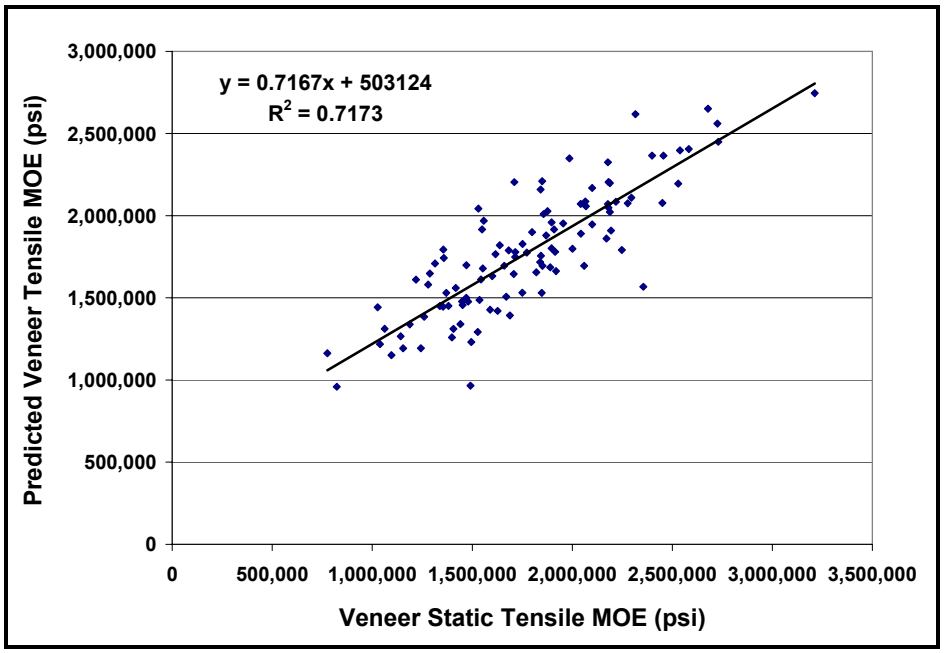

Figure 6.7. Predicted veneer tensile MOE from the optical, growth ring pattern measures and density model versus veneer static tensile MOE.

It was also noted that when density was included in the regression model with basic optical and growth ring pattern measures, latewood percentage was no longer a statistically significant measure in predicting veneer tensile MOE. While it was hoped latewood percentage would perform as well as density when predicting veneer tensile MOE, it appears that using density, rather than latewood percentage, greatly improves prediction of veneer tensile MOE.

Inclusion of growth ring pattern statistics with basic optical measures improved the prediction of veneer F_t, as compared to just density and/or basic optical. To further investigate any possible improvement in veneer F_t predictions, density was then included with all optically determined measures. Therefore, density, basic optical, and growth ring patterns measurements were all analyzed and the best prediction model was identified.

When evaluating veneer F_t with inclusion of density, basic optical (latewood and defect), and entropy growth ring pattern measurements, regression indicated five characteristics were statistically significant (at an alpha level = 0.05) in predicting veneer F_t (Table 6.8). In addition to density, one measure was from the basic optical system, while the remaining three measures were from growth ring pattern analysis. Figure 6.8 shows the relationship between predicted veneer F_t using statistically significant density, basic optical, and entropy image growth ring pattern measures versus veneer static F_t. In this regression, 56.1 percent of the variation (R-squared = 0.561) in veneer F_t was explained by the linear regression coefficients.

Table 6.8. Statistically significant optical including growth ring pattern measures and density model variables, regression coefficients, and p-values from regression analysis for predicting veneer static F_t.

Independent Variable	Regression Coefficient	p-value
Constant	3,259.0	0.005
Density (v3), lb./ft.^{3}	256.85	0.000
Average Defect Width (v21), in.	-2,633.5	0.000
E Median (v29)	0.9631	0.000
E90 Maximum (v32)	-1.0190	0.001
E90 Median (v34)	-2.9770	0.000

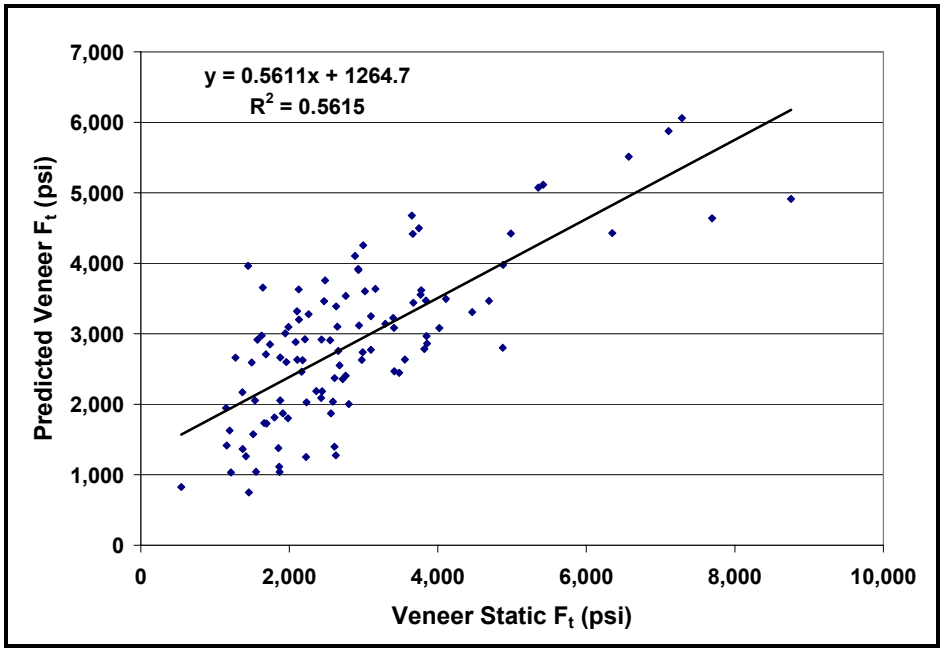

Figure 6.8. Predicted veneer F_t from the optical, growth ring pattern measures and density model versus veneer static F_t.

When analyzing the most appropriate regression model with density included, percent latewood was included in many of the best selected all possible combination models. Percent latewood, however, was not statistically significant (at an alpha level = 0.05) in the best all possible combination output, so it was removed from the model as shown in Table 6.8. When density was not included in the analysis (Table 6.3, 6.4, and 6.6), percent latewood was statistically significant, but the models R-squared was lower.

One of limitations of scanning the veneer surface for determining a measure of density by overall latewood percentage is the possibility exists that an area exhibiting earlywood and/or latewood on the surface may be relatively thin. An attempt to overcome this limitation was made by using the dual threshold approach to measures the amount of transition area between earlywood and latewood (i.e., green pixel area). Neither measure including the amount of earlywood/latewood transition zone (i.e., dual threshold black and green or dual threshold green only) was significant in predicting veneer tensile MOE or F_t. Some hope exists, however, that future refinement in determining latewood percentage using optical techniques could result in improved optical only system predictions of veneer mechanical properties.

Average defect width was statistically significant in regressions including density when predicting F_t. Specifically, as average defect width increased, veneer F_t decreased. This would stand to reason as larger defects (thus larger average defect width) would result in less solid continuous wood fiber in the veneer cross section, resulting in weaker veneer. Given this, veneer specimen defect size appears to have a significant influence on tensile strength capacity of veneer and thus should be

considered when grading veneer for strength categories. Values of average, rather than minimum and maximum, veneer defect properties proved to be influential in determining veneer strength and should be useful for predicting LVL mechanical properties. Specifically, average defect measures are likely to be more useful in predicting LVL strength due to lamination effects (Section 2.1) and defect randomization.

6.3.4 Veneer Tensile Property Model Development by Density and Optical Measures

To determine the amount of improvement made in predicting veneer tensile properties when including growth ring pattern measures, further analysis on predicting veneer tensile MOE and F_t was performed using only basic optical and density measurements. This analysis removed growth ring pattern measures as possible variables in the regressions and allowed for comparison of the results in Section 6.3.3 to results in this section.

When evaluating veneer MOE with inclusion of density and basic optical (latewood and defect) measurements, regression results indicated three characteristics were statistically significant (at an alpha level = 0.05) in predicting veneer tensile MOE (Table 6.9). In this regression, 65.6 percent of the variation (R-squared = 0.656) in veneer static tensile MOE was explained by the linear regression coefficients. Figure 6.9 shows the relationship between predicted veneer tensile MOE using statistically significant basic optical and density measures versus veneer static tensile MOE.

Table 6.9. Statistically significant basic optical and density model variables, regression coefficients, and p-values from regression analysis for predicting veneer static tensile MOE.

Independent Variable	Regression Coefficient	p-value
Constant	-1,444,030	0.000
Density (v3), lb./ft.^{3}	105,109.5	0.000
Number of Defects (v16)	69,877.3	0.000
Total Defect Width (v20), in.	-299,074.9	0.000

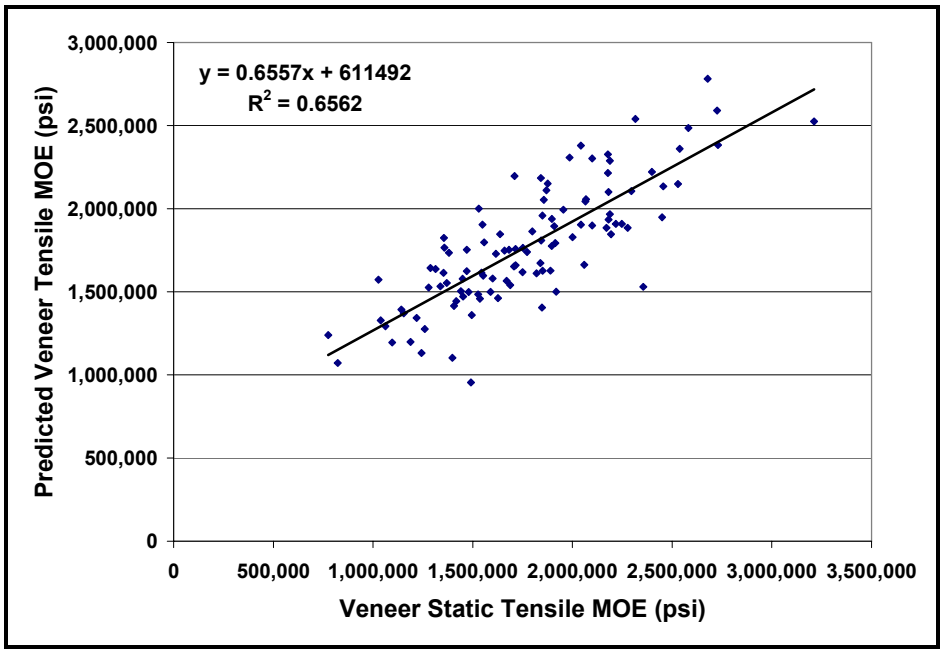

Figure 6.9. Predicted veneer tensile MOE from the basic optical and density model versus veneer static tensile MOE.

When evaluating veneer F_t with inclusion of basic optical and density measurements, regression results indicated three characteristics were statistically significant (at an alpha level = 0.05) in predicting veneer F_t (Table 6.10). Figure 6.10 shows the relationship between predicted veneer F_t using statistically significant basic

optical and density measures versus veneer static F_t. In this regression, 49.5 percent of the variation (R-squared = 0.495) in veneer static F_t was explained by the linear regression coefficients.

Table 6.10. Statistically significant basic optical and density model variables, regression coefficients, and p-values from regression analysis for predicting veneer static F_t.

Independent Variable	Regression Coefficient	p-value
Constant	-4,251.0	0.000
Density (v3), lb./ft.^{3}	279.1	0.000
Average Defect Width (v21), in.	-7,392.0	0.000
Average Defect Volume (v24), in.^{3}	53,229.0	0.018

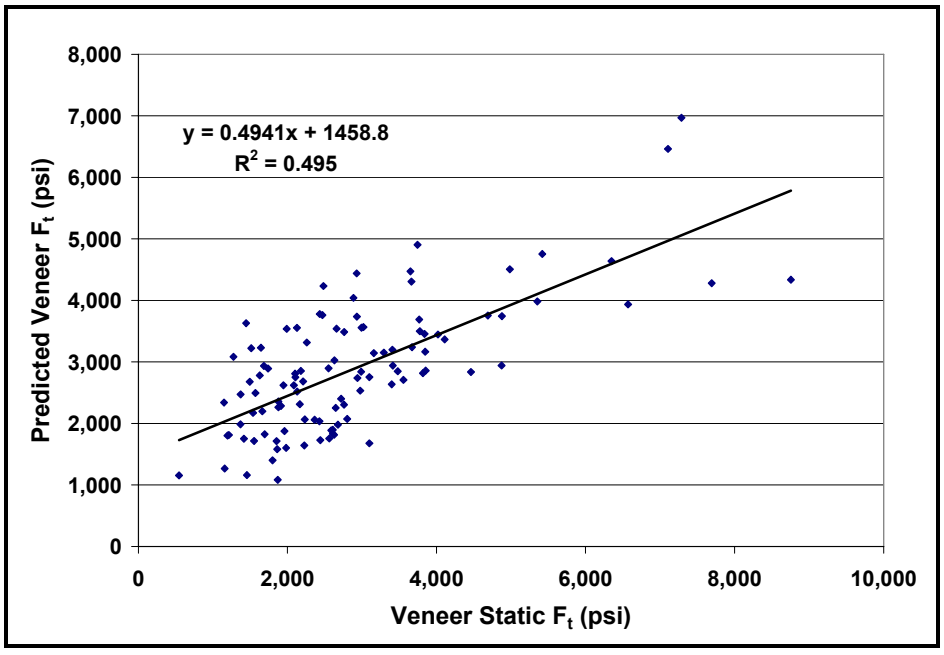

Figure 6.10. Predicted veneer F_t from the basic optical and density model versus veneer static F_t.

The results of the regression analysis on basic optical and density, growth ring measures removed, showed a reduction in R-squared values in predictions of both veneer static tensile MOE and F_t. This indicated that inclusion of growth ring measures better explained the variation in veneer static tensile MOE and F_t values.

6.4 Ultrasonic System: Development of Veneer Property Predictions

The first objective of the ultrasonic system study was to determine which ultrasonic measurements were statistically significant in terms of influencing veneer tensile MOE and F_t. The second objective of the optical system study was to determine whether or not the developed optical system could be used to reliably predict veneer tensile MOE and F_t. In particular, models were first developed using basic ultrasonic data obtained and calculated from output obtained by using the Metriguard Model 239A, lab-style stress wave timer. Additional analysis was then performed to identify any improvements when including spectral analysis measurements of waveform data acquired at the stop accelerometer.

6.4.1 Veneer Tensile Property Model Development Using Metriguard Stress Wave Timer Data

The first set of ultrasonic measurements investigated were those determined using output values from the Metriguard 239A Stress Wave Timer and measurement of density. Specifically, average ultrasonic propagation time (UPT), minimum and maximum UPT, dynamic modulus of elasticity (MOE_d), and minimum and maximum

MOE_d values were analyzed. Correlation analysis was performed between veneer static tensile MOE and F_t as compared to ultrasonic measurements (Appendix A). Table 6.11 shows the coefficients for ultrasonic measures having a significant individual correlation (at a 0.01 level) with veneer static tensile MOE and F_t.

Table 6.11. Statistically significant correlation coefficients from individual correlation analysis between veneer static tensile MOE and F_t and basic ultrasonic measurements.

Characteristic	Tensile MOE Correlation Coefficient	Tensile Strength Correlation Coefficient
Average MOE_d (v7)	0.780	0.670
Minimum MOE_d (v8)	0.745	0.658
Maximum MOE_d (v9)	0.749	0.628
Average UPT (v4)	-0.586	-0.513
Minimum UPT (v5)	-0.523	-0.444
Maximum UPT (v6)	-0.520	-0.472

Average MOE_d resulted in the highest correlation coefficient in relation to both veneer tensile MOE and strength. Among UPT measurements, average UPT resulted in the highest correlation coefficient in relation to both veneer tensile MOE and strength. These results are in agreement with industry methods for ultrasonically grading veneer based on either average MOE_d or average UPT, as opposed to minimum or maximum value, as they provided the best correlation to veneer static properties.

Regression analysis (linear, multiple, stepwise, and all possible combinations) was also employed to see which ultrasonic measures are statistically significant in

predicting veneer properties. In terms of both veneer tensile MOE and F_t, while Table 6.12 lists six variables as having significant individual correlations to veneer static MOE and F_t, regression analysis indicated only average MOE_d was statistically significant (at an alpha level = 0.05) in predicting both veneer static tensile MOE and F_t. Figure 6.11 and 6.12 show the relationships between average MOE_d (i.e., average MOE_d model) and veneer static tensile MOE and F_t, respectively. In terms of veneer static tensile MOE, 60.8 percent of the variation (R-squared = 0.608) was explained by using average MOE_d (Figure 6.11). In terms of veneer static F_t, 44.9 percent of the variation (R-squared = 0.449) was explained by using average MOE_d (Figure 6.12).

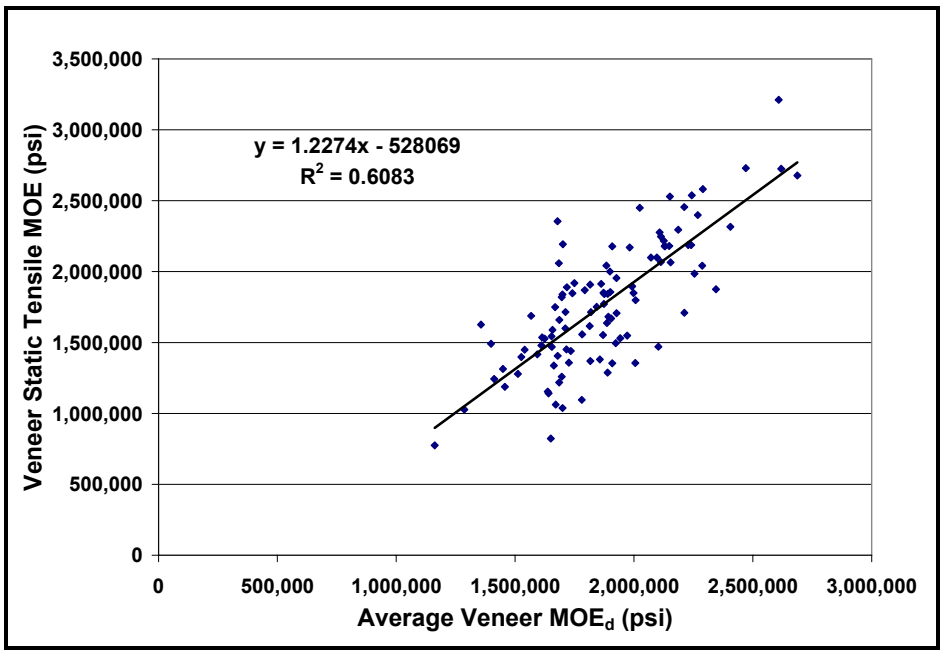

Figure 6.11. Veneer static tensile MOE versus average MOE_d.

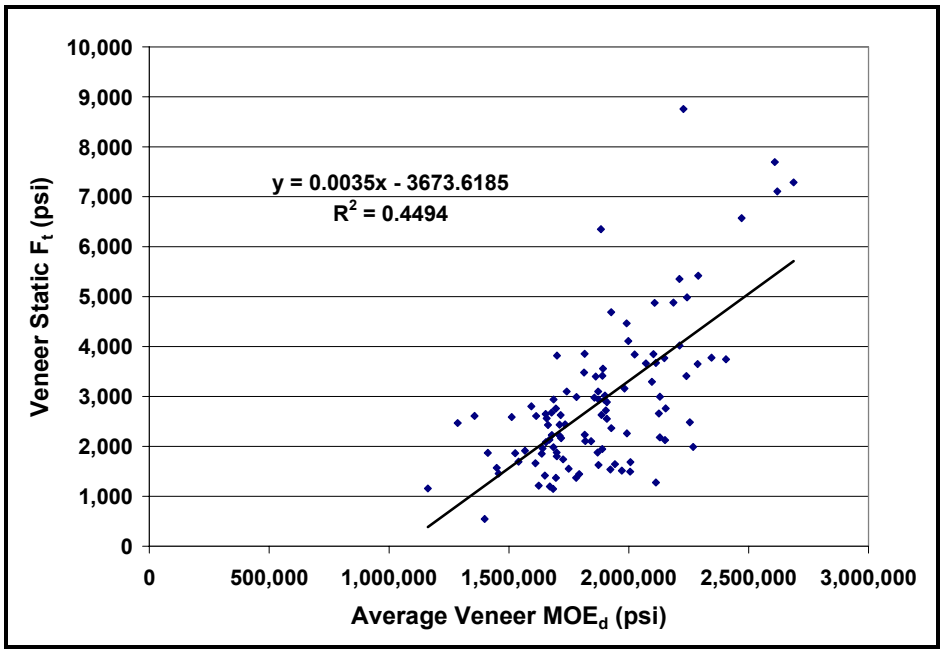

Figure 6.12. Veneer static F_t versus average MOE_d.

Some past research comparing ultrasonically determined MOE_d to veneer static tensile MOE reported very high R-squared values of 0.888 (Koch and Woodson 1968), 0.91 (Pellerin and Galligan 1973), and 0.971 (McAlister 1976). Other research by Hunt et al. (1989) and McAlister (1982) reported R-squared values of 0.669 and 0.65, between yellow-poplar veneer tensile MOE_s versus MOE_d, respectively. The results from this study indicated a weaker relationship (R-squared = 0.61) between MOE_d and veneer static tensile MOE, but were more in agreement with Hunt et al. (1989) and McAlister (1982).

In past research where high R-squared values were obtained, testing focused on narrower veneer strips which were likely to have less variation in grain angle and very few, if any, defects. In this study, wider veneer sheets which contained defects

and diving grain were tested. Jung (1979) concluded stress wave techniques used in his study were not able to detect diving grain. Furthermore, in wider veneers, while knots initially delayed a portion of the induced stress wave, the delayed portion caught up with the rest of the wave (Jung 1979). This suggests when using wider veneer sheets, as in this study, the previously reported high correlations would not be expected for the ultrasonic system. Specifically, veneer features such as diving grain and knots which influence veneer tensile MOE are not likely to be accounted for when using stress wave techniques on wider sheets. Given this, results from this study are more likely to represent the relationship between tensile MOE and MOE_d of typical veneer, which consists of diving grain and defect presence within veneer.

While MOE_d may provide the best ultrasonic method prediction of veneer tensile MOE and F_t, many veneer and LVL manufacturers still grade veneer based solely on UPT. In terms of this study's results, Figures 6.13 and 6.14 show the relationships between average UPT and veneer static tensile MOE and strength, respectively. In terms of veneer static tensile MOE, 34.3 percent of the variation (R-squared = 0.343) was explained by using average UPT (i.e., average UPT Model) (Figure 6.13). In terms of veneer static F_t, 26.3 percent of the variation (R-squared = 0.263) was explained by using average UPT (Figure 6.14).

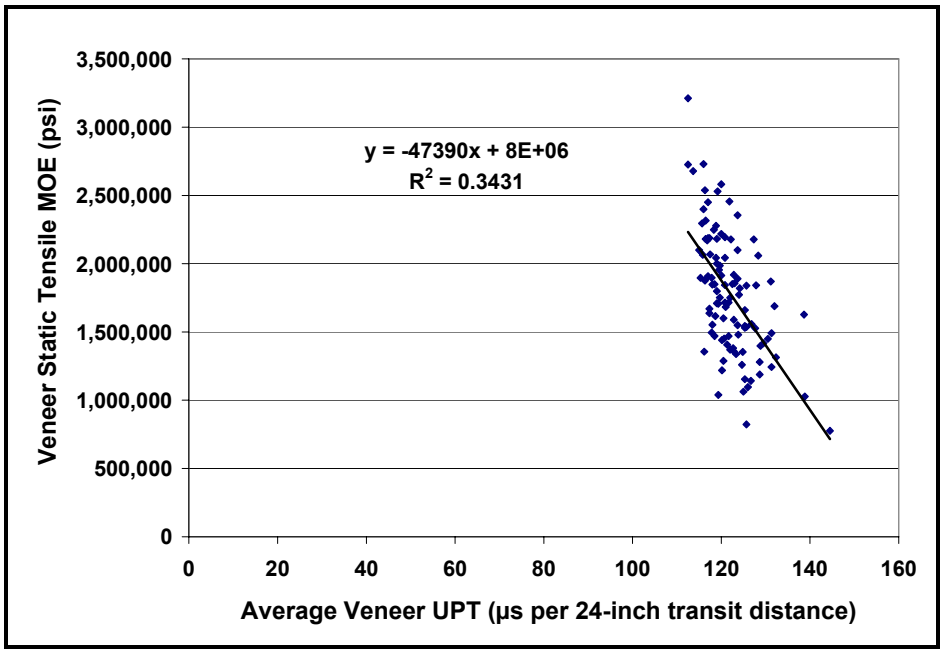

Figure 6.13. Veneer static tensile MOE versus average UPT.

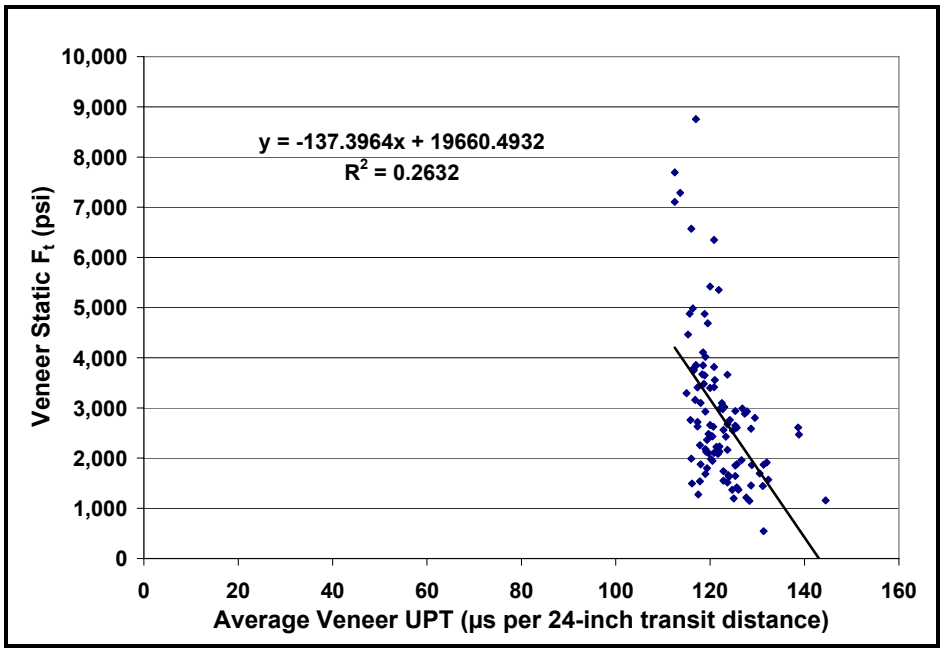

Figure 6.14. Veneer static F_t versus average UPT.

From the results comparing average MOE_d and average UPT, in this study, MOE_d resulted in a more reliable predictor of both veneer tensile MOE and F_t. This finding could justify a veneer manufacturer's decision to sort and grade veneer based on average MOE_d, rather than average UPT. While UPT showed a poor relationship to veneer static tensile properties, past research indicated grading veneer via UPT resulted in the manufacture of LVL with a reduced coefficient of variation, as compared to visual grading (Pieters 1979, Sharp 1985). Furthermore, while grading veneer by UPT did not result in higher LVL mean strength values, as compared to visual grading (Pieters 1979), the reduced variation allowed for increase in LVL design values (Sharp 1985). This reduction in variation around the mean justified why ultrasonic grading via average veneer UPT was widely adopted by industry as a replacement to visual human grading. In terms of this study, whether or not using MOE_d versus UPT results in better future predictions of both veneer and LVL properties is addressed in Chapter 7.

MOE_d models explained more of the variation in veneer static tensile MOE and F_t, as compared to basic optical and basic optical including growth ring pattern prediction models (Section 6.3.2). Models which included density and basic optical (Section 6.3.4) explained more of the variation in veneer static tensile MOE and F_t, as compared to the MOE_d model. Models which included density, basic optical, and growth ring patterns (Section 6.3.3) were better predictors of veneer tensile MOE and F_t, as compared to the MOE_d and UPT models. The UPT model explained more of the variation in veneer tensile MOE only when compared to the basic optical model. Additionally, all other models explained more of the variation in veneer F_t, as

compared to the UPT model. To investigate the possibility of improving ultrasonically predicted veneer properties, waveform data collected during ultrasonic testing was then analyzed.

6.4.2 Veneer Tensile Property Model Development Using Average MOE_d and Waveform Spectral Analysis Data

The collected waveform data analyzed using spectral analysis resulted in a very large set of measurements. Because of its large size, all possible regression analysis was not appropriate for this data set. Stepwise regression was used instead to determine the best prediction models using ultrasonic and waveform spectral analysis measures.

Regression results using ultrasonic and waveform spectral analysis measures indicated three characteristics were statistically significant (at an alpha level = 0.05) in predicting veneer tensile MOE (Table 6.12). Figure 6.15 shows the relationship between predicted veneer tensile MOE using statistically significant ultrasonic and waveform spectral analysis measures versus veneer static tensile MOE. In this regression, 65.4 percent of the variation (R-squared = 0.654) in veneer static tensile MOE was explained by the linear regression coefficients.

Table 6.12. Statistically significant basic ultrasonic and waveform spectral analysis measures model variables, regression coefficients, and p-values from regression analysis for predicting veneer tensile MOE.

Independent Variable	Regression Coefficient	p-value
Constant	380,772	0.592
Average MOE_d (v7), psi	1.1473	0.000
Avg. Power Spectrum Kurtosis – dB scale (v35)	-362,161	0.033
Average Peak Kurtosis – Linear scale (v36)	11,436.8	0.001

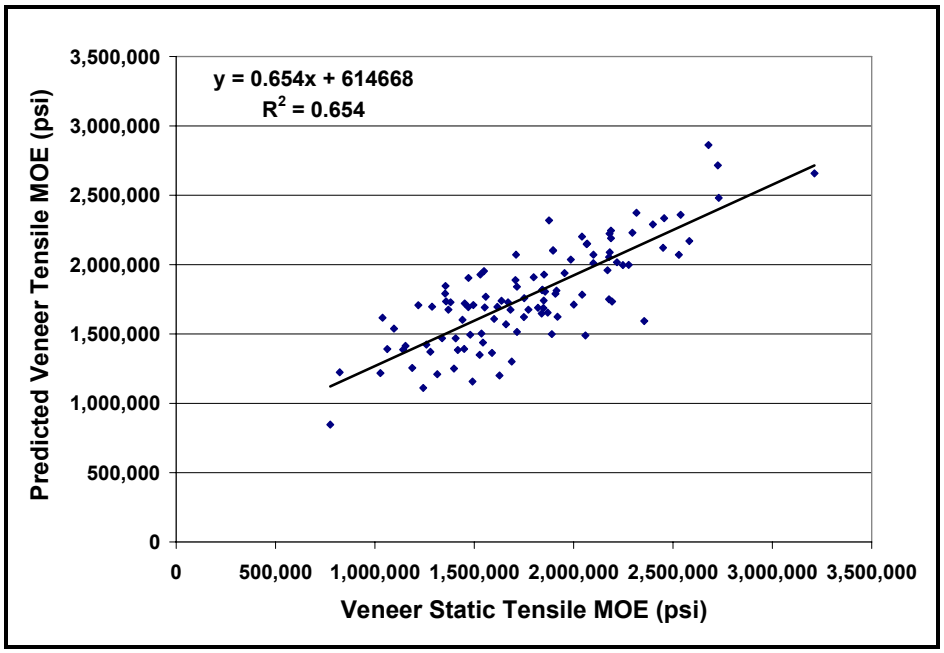

Figure 6.15. Predicted veneer tensile MOE from the basic ultrasonic and waveform spectral analysis measures model versus veneer static tensile MOE.

Regression results using ultrasonic and waveform spectral analysis measures indicated two characteristics were statistically significant (at an alpha level = 0.05) in predicting veneer F_t (Table 6.13). Figure 6.16 shows the relationship between

predicted veneer F_t using statistically significant ultrasonic and waveform spectral analysis measures versus veneer static F_t. In this regression, 51.1 percent of the variation (R-squared = 0.511) in veneer static F_t was explained by the linear regression coefficients.

Table 6.13. Statistically significant basic ultrasonic and waveform spectral analysis measures model variables, regression coefficients, and p-values from regression analysis for predicting veneer static F_t.

Independent Variable	Regression Coefficient	p-value
Constant	83,050	0.001
Average MOE_d (v7), psi	0.0028	0.000
Avg. Power Spectrum Density – dB Scale (v37)	824.64	0.000

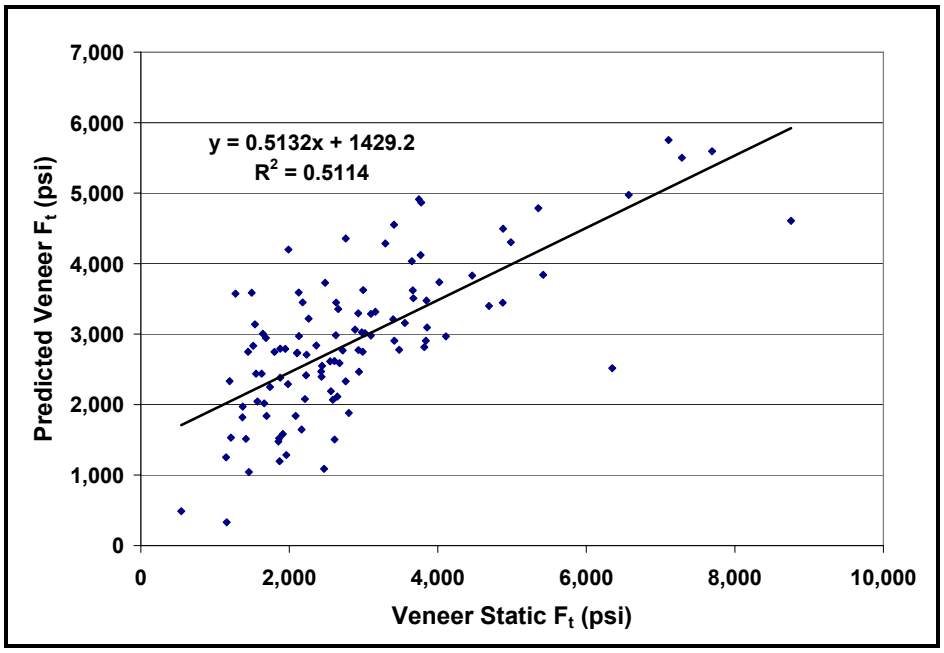

Figure 6.16. Predicted veneer F_t from the basic ultrasonic and waveform spectral analysis measures model versus veneer static F_t.

Inclusion of waveform spectral analysis measures improved veneer tensile MOE and F_t predictions when using the ultrasonic NDE system. The full ultrasonic system model explained less of the variation in veneer tensile MOE, as compared to the optical system model which included basic optical, growth ring pattern, and density measures (Figure 6.7). The ability of the full ultrasonic system model to predict veneer tensile MOE was, however, very similar as compared to the optical system including density and basic optical measures (Figure 6.9).

The full ultrasonic system model explained less of the variation in veneer tensile F_t, as compared to the optical system model which included basic optical, growth ring pattern, and density measures (Figure 6.8). The ability of the full ultrasonic system model to predict veneer F_t was, however, slightly better as compared to the optical system including density and basic optical measures (Figure 6.10).

The inclusion of growth ring pattern and waveform spectral analysis measures improved predictions of veneer tensile MOE and F_t under both the optical and ultrasonic systems, respectively. Because many veneer producers have both some type of ultrasonic and optical system in-line, it may be of benefit to combine information from both systems when grading veneer. Specifically, by combining ultrasonic and optical system measures, this research aims to further improve the prediction of veneer properties and grading of veneer at the mill level.

6.5 Combined Systems: Development of Veneer Property Predictions

Stepwise and all possible combination regression analysis was used to develop prediction models of veneer tensile MOE and F_t by including all measured veneer properties from the integration of data from both the optical system and the ultrasonic system. Because density is incorporated in calculations of MOE_d, it was not utilized as a possible variable in the combined systems model analysis. First, stepwise regression was used to determine which variables were statistically significant (at an alpha level = 0.05) from the entire set of possible variables. Secondly, all possible combination regression was used to compare the best possible models with the stepwise regression output. When performing all possible regression analysis, only veneer characteristics previously determined as being statistically significant were utilized, due to the high number of possible spectral analysis and optical measures. The best possible model was selected by comparing stepwise and all possible combination output. Once the best model was selected, multiple regression analysis was used to determine the final combined system prediction model for veneer tensile MOE and F_t.

Regression results using combined system measures indicated three characteristics were statistically significant (at an alpha level = 0.05) in predicting veneer tensile MOE (Table 6.14). Figure 6.17 shows the relationship between predicted veneer tensile MOE using statistically significant combined system measures versus veneer static tensile MOE. In this regression, 67.4 percent of the

variation (R-squared = 0.674) in veneer static tensile MOE was explained by the linear regression coefficients.

Table 6.14. Statistically significant combined system measures model variables, regression coefficients, and p-values from regression analysis for predicting veneer static tensile MOE.

Independent Variable	Regression Coefficient	p-value
Constant	-750,354.1	0.004
Average MOE_d (v7), psi	1.2178	0.000
Total Defect Volume (v22), $in.^3$	-288,020.6	0.001
Average Peak Kurtosis – Linear Scale (v36)	7,259.3	0.034

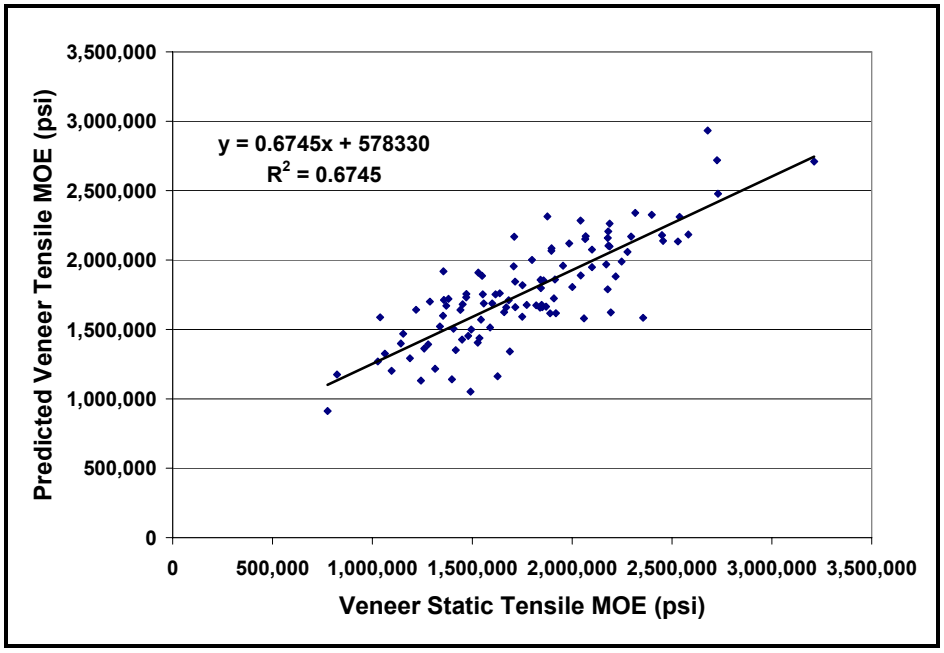

Figure 6.17. Predicted veneer tensile MOE from combined system measures model versus destructively determined veneer tensile MOE.

Integration of optical and ultrasonic system measures slightly improved veneer tensile MOE predictions as compared to the ultrasonic NDE system. The combined system model explained less of the variation in veneer tensile MOE, as compared to the optical system model which included basic optical, growth ring pattern, and density measures (Figure 6.7). The ability of the combined system model to predict veneer tensile MOE was, however, slightly better as compared to the optical system including density and basic optical measures (Figure 6.9).

While the combined optical and ultrasonic system prediction of veneer tensile MOE was slightly lower in comparison to the optical system model which included basic optical, growth ring pattern, and density measures, it was still comparable. When predicting veneer tensile MOE, the combined system incorporated only one optical measure, total defect volume. In comparison to the full ultrasonic system for predicting veneer tensile MOE (Table 6.12), the combined model was similar, except that total defect volume now replaced power spectrum kurtosis (dB scale). It was likely power spectrum kurtosis measures gave some indication of total defect area and was cross correlated with total defect volume when predicting veneer tensile MOE.

Correlation analysis results were used to determine if power spectrum kurtosis and total defect volume were related. Results from correlation analysis between total defect volume and power spectrum kurtosis (dB scale) resulted in a statistically significant correlation coefficient of 0.353 (two sided p-value < 0.001). While the two measures are correlated, their relationship is rather weak, so it was unlikely power spectrum kurtosis (dB scale) measures could be used as a reliable predictor of total defect volume in a veneer sheet without further investigation. It was, however, likely

the correlation between the two resulted in the substitution of total defect area by power spectrum kurtosis when developing the combined model.

Regression results using combined system measures indicated six characteristics were statistically significant (at an alpha level = 0.05) in predicting veneer F_t (Table 6.15). Figure 6.18 shows the relationship between predicted veneer F_t using statistically significant combined system measures versus veneer static F_t. In this regression, 63.1 percent of the variation (R-squared = 0.631) in veneer static F_t was explained by the linear regression coefficients.

Table 6.15. Statistically significant combined system measures model variables, regression coefficients, and p-values from regression analysis for predicting veneer static F_t.

Independent Variable	Regression Coefficient	p-value
Constant	-6,930.0	0.002
Average MOE_d (v7), psi	0.0026	0.000
Average Defect Width (v21), in.	-6,525.0	0.000
Average Defect Volume (v24), $in.^3$	63,896	0.002
E90 Maximum (v32)	-0.4887	0.006
E90 Minimum (v33)	1.0109	0.006
Average Peak Variance – dB Scale (v38)	13.846	0.006

Integration of optical and ultrasonic system measures improved the prediction of veneer F_t as compared to all other systems investigated. The combined system explained the greatest amount of variation when predicting veneer F_t as compared against all other models. The combined optical and ultrasonic system does show some possibility of improving veneer F_t prediction as compared to other systems, separately.

The reliability of the combined system to predict both individual veneer and LVL F_t properties is tested in Chapter 7.

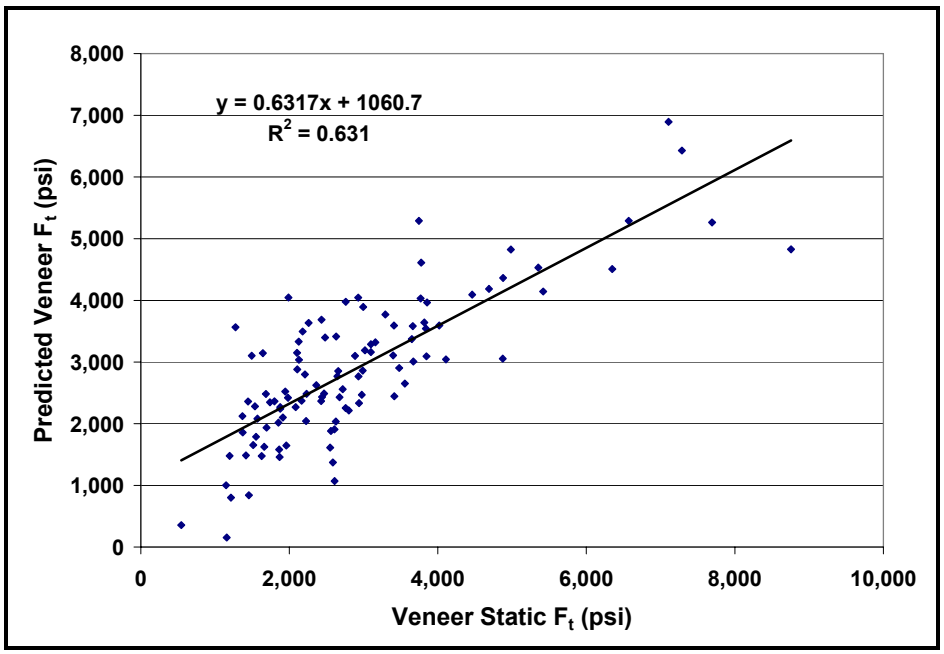

Figure 6.18. Predicted veneer F_t from combined system measures model versus veneer static F_t.

6.6 Comparison of Models Developed to Predict Veneer Tensile MOE and F_t

Many different models were constructed using measurements obtained by various NDE systems and combination of systems. Comparison of R-squared values for each individual model was performed to determine how likely each model was to predict future veneer tensile MOE and F_t properties. A summary of each model's R-square values for both veneer tensile MOE and F_t is shown in Table 6.16 and 6.17,

respectively. Variables used for predicting veneer properties under each model are shown in parenthesis.

Table 6.16. Comparison of R-squared values and rank for each model developed from regression analysis to predict veneer tensile MOE.

System	Model (included variables)	Prediction of Veneer Tensile MOE	
		R^2	Rank
Material Property	**Density** (v3)	**0.48**	**6**
Optical	**Basic Optical** (v13, v23)	**0.24**	**9**
	Optical + Density (v3, v16, v20)	**0.66**	**3**
	Optical + Growth Ring Pattern (v23, v25, v31, v33, v34)	**0.42**	**7**
	Optical + Density + Growth Ring Pattern (v3, v16, v20, v25, v31, v33, v34)	**0.72**	**1**
Ultrasonic	**Average MOE_d** (v7)	**0.61**	**5**
	Average UPT (v4)	**0.34**	**8**
	Ultrasonic + Spectral Analysis (v7, v35, v36)	**0.65**	**4**
Combined	**All Combined Systems** (v7, v22, v36)	**0.68**	**2**

Based on the R-squared values in Table 6.16, the optical system model which included optical, density, and growth ring pattern measures was most likely to best predict future veneer tensile MOE values. The basic optical model was most likely to perform the worst of all the models when predicting future veneer tensile MOE values.

In comparison with the UPT model, all other models, with the exception of the basis optical model, were more likely to better predict future veneer tensile MOE values.

Table 6.17. Comparison of R-squared values and rank for each model developed from regression analysis to predict veneer F_t.

System	Model (included variables)	Prediction of Veneer Tensile F_t	
		R^2	Rank
Material Property	**Density** (v3)	**0.31**	**7**
Optical	**Basic Optical** (v13, v18)	**0.28**	**8**
	Optical + Density (v3, v21, v24)	**0.50**	**4**
	Optical + Growth Ring Pattern (v13, v18, v33)	**0.39**	**6**
	Optical + Density + Growth Ring Pattern (v3, v21, v29, v32, v34)	**0.56**	**2**
Ultrasonic	**Average MOE_d** (v7)	**0.45**	**5**
	Average UPT (v4)	**0.26**	**9**
	Ultrasonic + Spectral Analysis (v7, v37)	**0.51**	**3**
Combined	**All Combined Systems** (v7, v21, v24, v32, v33, v38)	**0.63**	**1**

Based on the R-squared values in Table 6.17, the combined model, which integrated measurements from the optical and ultrasonic systems, was most likely to best predict future veneer F_t values. The UPT model was less likely, of all the models, to adequately predict future veneer F_t values. While R-squared values give some indication of how well future veneer tensile properties will be predicted for each

individual model, an assessment of each model's validity was needed. To do so, further research was conducted in Chapter 7.

CHAPTER 7 PREDICTION MODEL VALIDATION AND LVL ASSEMBLY AND PROPERTY PREDICTION

After non-destructive and destructive testing of selected veneer specimens was completed and prediction models were developed for each scanning system, research on randomly selected veneers specimens was conducted to determine the following:

1) How well predicted veneer mechanical properties compared to destructive results when veneer contains random defects (i.e., veneer specimens selected regardless of defects) and specimens were not hand selected.

2) How well results from optical scanning veneer grading, ultrasonic veneer grading, and the combination of the two related to destructively evaluated LVL mechanical properties.

7.1 Veneer Specimen Preparation for Model Validation and LVL Assembly

Forty-two (42) ultrasonically graded Douglas-fir veneer sheets (1/8-inches in thickness, full sheets) were selected from previously sampled veneer in Section 4.1.1. Sheets were selected based on MOE_d to represent typical grades of material used in manufacturing LVL (i.e., G1, G2, and G3). For this section, fourteen (14) sheets per grade were selected so each grade was adequately represented and high grading of the population did not occur.

From each veneer sheet, four (4) specimens, having a dimension of 6-inches wide by 31-inches long (for model validation), and ten (10) specimens, having a

dimension of 6-inches wide by 48-inches long (for LVL lay-up) were randomly processed. A general processing layout diagram is shown in Figure 7.1. While this cutting pattern was ideal, not every sample could be processed from each sheet, given many specimens were split the entire length. The large number of veneer sheets selected, however, allowed for successfully processing more than the required amount of specimens for both the model validation and LVL assembly section. All specimens were labeled with the corresponding full sheet identification number and specimen letter (a,b,c,d,e, etc.). Once all possible specimens were processed, ninety (90) specimens for the model validation section and three-hundred ten (310) specimens for the LVL assembly section were randomly selected. After being processed from full sheets, specimens were conditioned to equilibrium at 60 percent relative humidity and 20^{o}C.

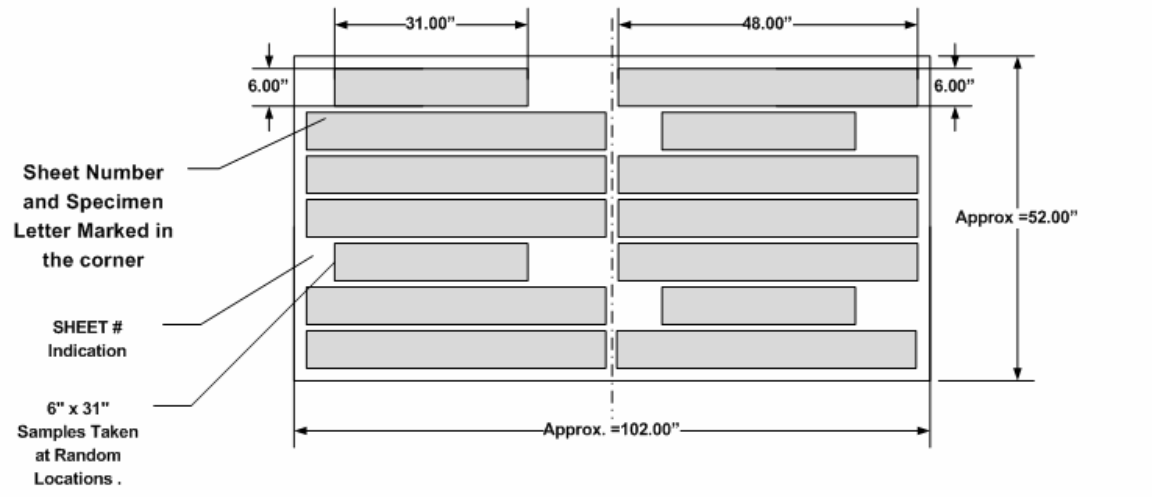

Figure 7.1. Model validation and LVL lay up specimen preparation layout.

7.2 Prediction Model Validation Study

7.2.1 Model Validation Testing Procedures

The ninety (90) veneer specimens sampled for analyzing validity of prediction models developed in Chapter 6 were first non-destructively tested following the methods in Section 5.2.2 when using both the optical system and ultrasonic system. Each specimen was then tested destructively, following the methods in Section 5.2.3, to determine static tensile MOE and F_t. In this section, the only veneer measurements needed were those used to predict veneer tensile MOE and F_t via various prediction models. All other remaining veneer measurements, however, were still determined and recorded. After being tested, specimens were placed back in the conditioning room set at 60 percent relative humidity and 20^{o}C.

7.2.2 Model Validation Testing Results

Table 7.1 provides a summary of destructively determined veneer tensile MOE and F_t. Complete results for each individual specimen are located in Appendix B.

Table 7.1. Veneer destructively determined tension test results from validation study.

Summary Statistic	Density (lb/ft^3)	Tensile MOE (psi)	F_t (psi)
Average	31.7	1,754,206	2,796
St. Dev.	2.8	475,619	1,591
COV %	8.9	27.1	56.9
Min.	24.0	529,433	702
Max.	38.4	2,782,359	8,445
Sample Size	89	87	89

Of the 90 specimens tested, one specimen was removed from the analysis, due to failure within the grip area. This resulted in a total of 89 veneer static F_t results. In terms of veneer static tensile MOE, when testing two of the specimens, the LVDT on one face of the veneer fell off prematurely during testing. This resulted in a total of 87 veneer static tensile MOE results. The percent coefficient of variation (COV%) for both veneer tensile MOE and F_t, was slightly higher than in the model development study tests (Table 5.2). The average veneer tensile MOE and F_t was similar between both sets of tests. Average veneer density values were also comparable.

Results from one-way ANOVA tests showed no statistically significant difference for average veneer tensile MOE, F_t, and density (p-values = 0.737, 0.691, and 0.343, respectively) between the test results generated in the model development (Chapter 5) and validation (Chapter 7) studies. Box and whisker plots from the one-way ANOVA tests for differences in veneer tensile MOE, F_t, and density are shown in Figures 7.2, 7.3, and 7.4, respectively.

Variance testing (Cochran's C, Bartlett's, Hartley's, and Levene's tests) indicated no statistically significant difference in standard deviation for average veneer tensile MOE, F_t, and density between the test results generated in the model development and validation study. Furthermore, results from the Kruskal-Wallis test indicated no statistically significant difference for median veneer tensile MOE, F_t, and density (p-values = 0.936, 0.289, and 0.543, respectively) between the test results generated in the model development and validation study.

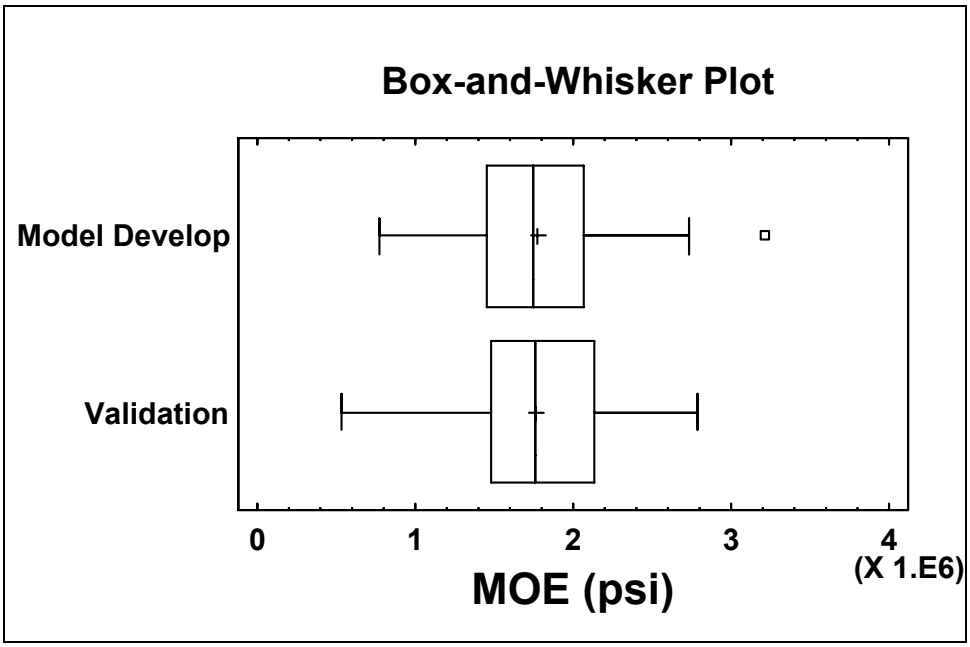

Figure 7.2. Box and whisker plots for veneer tensile MOE test results from the model development and validation studies.

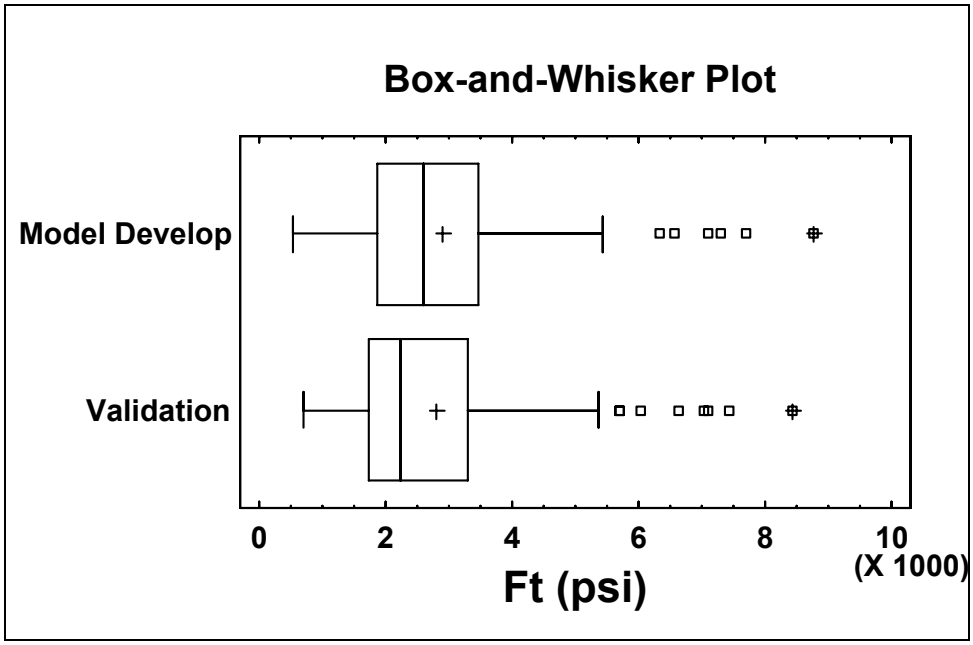

Figure 7.3. Box and whisker plots for veneer F_t test results from the model development and validation studies.

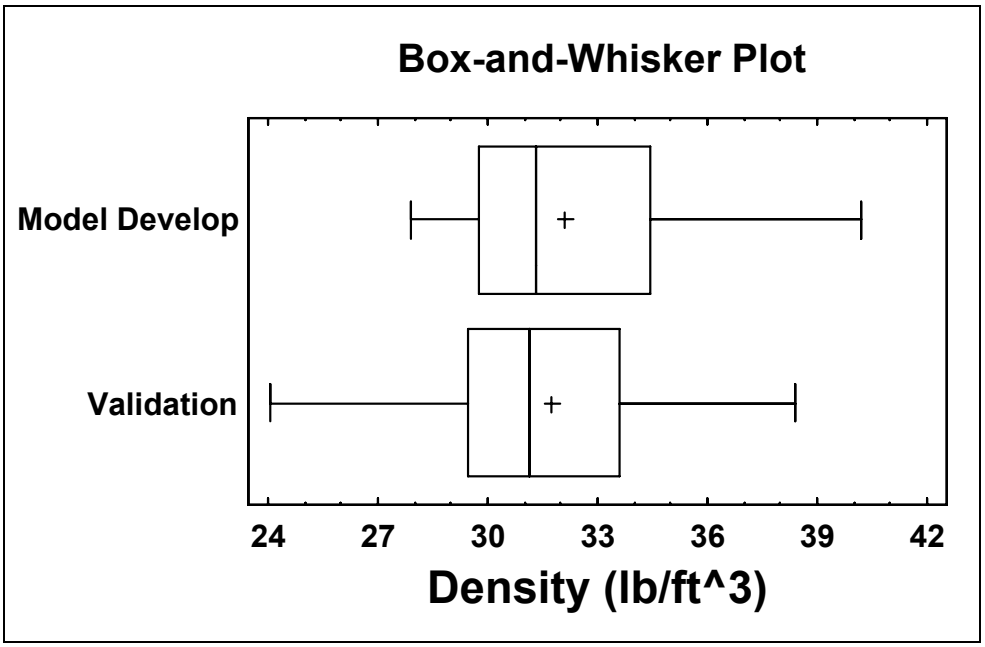

Figure 7.4. Box and whisker plots for veneer density test results from the model development and validation studies.

The ability to validate the prediction models using this set of data was sufficient, given the two populations used for the model and validation study were similar. Given the two populations (i.e., data sets) were similar, it allowed for comparing the validity of each system's prediction model.

7.2.3 Model Validation Prediction Results and Discussion

Using veneer measures determined by non-destructive testing, veneer tensile MOE and F_t values were predicted using the nine different prediction models developed in Chapter 6. Results of veneer static tensile MOE and F_t were then compared to predicted values using each system. Analysis of R-squared values of the prediction models (Chapter 6) were compared to R-squared values of predicted versus

actual regressions determined in this section. This analysis allowed for determining how well each model was able to predict future values and also explain the variation in veneer mechanical properties. Specifically, the lower the reduction in R-squared values between model development and validation studies, the more reliable the model. Furthermore, the higher the model R-squared value from the validation study, the better it did in explaining the variation in veneer static properties.

While comparison of R-squared values gave some indication of how well each system performed in predicting future veneer mechanical properties, other comparisons were also performed. A comparison was needed on each system's ability to predict both the veneer population average and each individual value. One-way analysis of variance (ANOVA) tests were performed to determine if any differences existed in average veneer tensile MOE and F_t values between the nine prediction models and destructive test values. Further evaluation was performed to determine the percent error of each model as compared to veneer static tensile properties. Finally, percent error for each individually predicted value from each model as compared to individual veneer static properties was determined. The overall average percent error within each model was then calculated and each model was compared.

7.2.3.1 Veneer Tensile MOE Model Validation

Table 7.2 shows the resulting R-squared values for the prediction model and validation model test, respectively, under each system for veneer tensile MOE.

Table 7.2. Comparison of R-squared values of the prediction model and validation model test when predicting veneer tensile MOE.

Veneer Tensile MOE Prediction Model Validation Comparison Table				
System	Model (included variables)	R-Squared Values		Difference Validation - Model %
		Model	Validation	
Basic Property	**Density** (v3)	0.48	0.34	-14.0
Optical	**Basic Optical** (v13, v23)	0.24	0.24	0.0
	Optical + Density (v3, v16, v20)	0.66	0.50	-16.0
	Optical + GRP (v23, v25, v31, v33, v34)	0.42	0.33	-9.0
	Optical + Density + GRP (v3, v16, v20, v25, v31, v33, v34)	0.72	0.48	-24.0
Ultrasonic	**Average MOE_d** (v7)	0.61	0.47	-14.0
	Average UPT (v4)	0.34	0.29	-5.0
	Ultrasonic + Spectral Analysis (v7, v35, v36)	0.65	0.50	-15.0
Combined	**All Combined Systems** (v7, v22, v36)	0.68	0.51	-17.0

In analyzing R-squared values, density showed a weaker relationship to veneer tensile MOE in the validation study as compared to the model development section. In turn, every prediction model which included density as either a predictor variable or as part of a variable calculation (e.g., MOE_d) showed a weaker relationship to veneer tensile MOE in the validation study. While not specifically tested, it was likely density measurements do not adequately account for changes in growth ring angle, slope of grain around defects, and diving grain which would influence veneer tensile MOE results. Models which did not include density (i.e., basic optical with growth

ring pattern measures and average UPT) did not show as much reduction in R-squared values between the model development and validation study.

The combined system (i.e., integration of optical and ultrasonic system measures) resulted in the highest R-squared value in the validation study. Specifically, the combined model performed best in terms of explaining the variation in veneer tensile MOE as compared to other models. The optical with density model and ultrasonic with waveform spectral analysis (FFT) model performed equally well and were more reliable as compared to MOE_d prediction of veneer tensile MOE.

The basic optical model showed no change in R-squared value when predicting veneer tensile MOE value between the model development and validation study. This suggests the optical system was not influenced by evaluating a different set of veneer. Additionally, the system was able to correctly identify and quantify influential veneer measures from one set of tests to the next. The basic optical system was still weaker, in terms of explaining the variation in veneer tensile MOE, as compared to other models.

Results from one-way ANOVA testing showed no statistically significant difference (p-value = 0.431) existed for average veneer tensile MOE between all ten groups tested (nine prediction models and veneer static tensile MOE). Figure 7.5 provides a box and whisker plot of veneer tensile MOE predicted by each system's model and from destructive testing. The basic optical and UPT models, while they could predict average veneer tensile MOE, did not do well in terms of explaining the overall variation in veneer tensile MOE, as previously determined from Table 7.2.

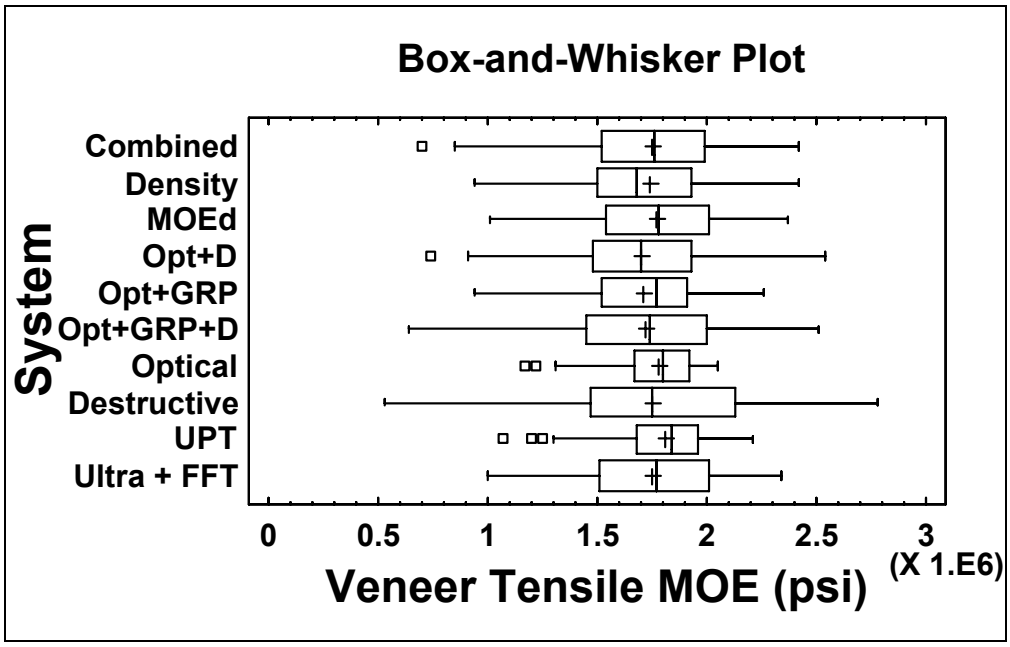

Figure 7.5. Box and whisker plots for veneer tensile MOE from all prediction models and static (destructive) results.

Table 7.3 shows the average predicted veneer tensile MOE value from the validation study population as determined by each system. Additionally, the average percent error (from veneer static tensile MOE) and rank for each system was identified (Table 7.3). The ultrasonic (with spectral analysis included) and combined optical and ultrasonic models were the two best predictors, respectively, of average veneer population tensile MOE. The optical (with density included) and UPT models were the two worst predictors, respectively, of average veneer population tensile MOE.

Table 7.4 shows the overall average percent error when comparing predicted versus veneer static tensile MOE on an individual specimen basis, rather than the population average. On average, the optical (with density included) and optical (with

density and growth ring pattern measures included) models were the two best predictors, respectively, of individual veneer static tensile MOE.

The combined system and ultrasonic (with spectral analysis included) system models appeared to be the two best predictors of overall population average of veneer static tensile MOE. The optical (with density and growth ring pattern measures included) model did, however, perform rather well considering both the ability to predict individual and the average population veneer static tensile MOE. As evident from Figure 7.5, the optical (with density and growth ring pattern measures included) model also had a similar spread in terms of variation of the 50 percentile range and lower and upper quartiles, in comparison with veneer static tensile MOE values.

Table 7.3. Comparison of percent error of predicted average veneer tensile MOE from each model as compared to average veneer static tensile MOE.

Model (included variables)	**Predicted Average Veneer Tensile MOE (psi)**	**Comparison to Average Veneer Static Tensile MOE (1,754,206 psi)**	
		Error (%)	**Rank**
Ultrasonic + Spectral Analysis (v7, v35, v36)	1,750,028	0.2	1
All Combined Systems (v7, v22, v36)	1,745,341	0.5	2
Average MOE_d (v7)	1,772,171	-1.0	3
Density (v3)	1,735,114	1.1	4
Basic Optical (v13, v23)	1,780,961	-1.5	5
Optical + Density + GRP (v3, v16, v20, v25, v31, v33, v34)	1,717,994	2.1	6
Optical + GRP (v23, v25, v31, v33, v34)	1,712,574	2.4	7
Optical + Density (v3, v16, v20)	1,697,253	3.2	8
Average UPT (v4)	1,813,722	-3.4	9

Table 7.4. Comparison of average percent error for each prediction model on an individual veneer specimen basis as related to veneer static tensile MOE.

Model (included variables)	**Overall Average of Individual Specimen Veneer Static Tensile MOE Comparisons**	
	Error (%)	**Rank**
Optical + Density (v3, v16, v20)	-0.5	1
Optical + Density + GRP (v3, v16, v20, v25, v31, v33, v34)	-1.4	2
Optical + GRP (v23, v25, v31, v33, v34)	-2.9	3
Combined Systems (v7, v22, v36)	-3.8	4
Ultrasonic + Spectral Analysis (v7, v35, v36)	-4.5	5
Density (v3)	-5.1	6
Average MOE$_d$ (v7)	-6.4	7
Basic Optical (v13, v23)	-9.1	8
Average UPT (v4)	-10.5	9

7.2.3.2 Veneer F_t Model Validation

Table 7.5 shows the resulting R-squared values for the prediction model and validation model test, respectively, under each system for veneer F_t. Upon analysis of R-squared values, density showed a weaker relationship to veneer static F_t in the validation study as compared to the model development section. Furthermore, density resulted in the weakest predictor of veneer static F_t in the validation study. In turn, every prediction model which included density as either a predictor variable or as part of a variable calculation showed a weaker relationship to veneer static tensile F_t in the validation study. Again, it was likely density measurements do not adequately account for changes in growth ring angle, slope of grain around defects, and diving grain which would highly influence veneer F_t results.

Table 7.5. Comparison of R-squared values of the prediction model and validation model test when predicting veneer F_t.

Veneer F_t Prediction Model Validation Comparison Table				
System	Model (included variables)	R-Squared Values		Difference Validation - Model %
		Model	Validation	
Basic Property	**Density** (v3)	0.31	0.16	-15
Optical	**Basic Optical** (v13, v18)	0.28	0.26	-2
	Optical + Density (v3, v21, v24)	0.50	0.30	-20
	Optical + GRP (v13, v18, v33)	0.39	0.46	7
	Optical + Density + GRP (v3, v21, v29, v32, v34)	0.56	0.41	-15
Ultrasonic	**Average MOE_d** (v7)	0.45	0.27	-18
	Average UPT (v4)	0.26	0.18	-8
	Ultrasonic + Spectral Analysis (v7, v37)	0.51	0.43	-8
Combined	**Combined Systems** (v7, v21, v24, v32, v33, v38)	0.63	0.51	-12

The optical including growth ring pattern measurements model, which did not include density, showed an improvement in R-squared values during the validation study when predicting veneer static F_t (Table 7.5). Other models which did not include density (basic optical and Average UPT) did not show as much reduction in R-squared values between the model development and validation study. The combined system model and optical including growth ring pattern measurements model showed the first and second highest R-squared values in the validation study, respectively. Specifically, these two prediction models were best in terms of explaining the

variation in veneer static F_t as compared to other models. With the exception of the basic optical system, all other optical systems outperformed the MOE_d model when predicting veneer static F_t during the validation study.

The basic optical model showed the lowest change, of those which were reduced, in R-squared value when predicting veneer F_t between the model development and validation study. This suggests the optical system was less influenced by evaluating a different set of veneer than the ultrasonic systems. The basic optical system was able to outperform the density and UPT models, and was just slightly lower (1 percent) in terms of explaining the variation in veneer static F_t as compared to the MOE_d model.

Results from one-way ANOVA testing showed no statistically significant difference (p-value = 0.383) existed for average veneer F_t between all ten groups tested (nine prediction models and veneer static F_t). Figure 7.6 provides a box and whisker plot of veneer F_t predicted by each system's model and from destructive testing. The basic optical and UPT models could predict average veneer static F_t, but did not do well in terms of explaining overall variation in veneer static F_t, as previously determined from Table 7.5.

It was also noted the optical (with growth ring and density measures included) model predicted values below zero. In further investigation, only one specimen's veneer F_t value was predicted to be below zero (predicted as -128 psi). In looking at the entropy image for this specimen, there were two very small knots within the circular growth ring pattern area of a large defect. In measuring the number of defects for this specimen, these two small knots were considered part of the larger defect.

This resulted in a much higher average defect width than if these small knots had been considered separate defects. Further calculation when counting these two knots as separate defects resulted in a positive prediction of veneer F_t.

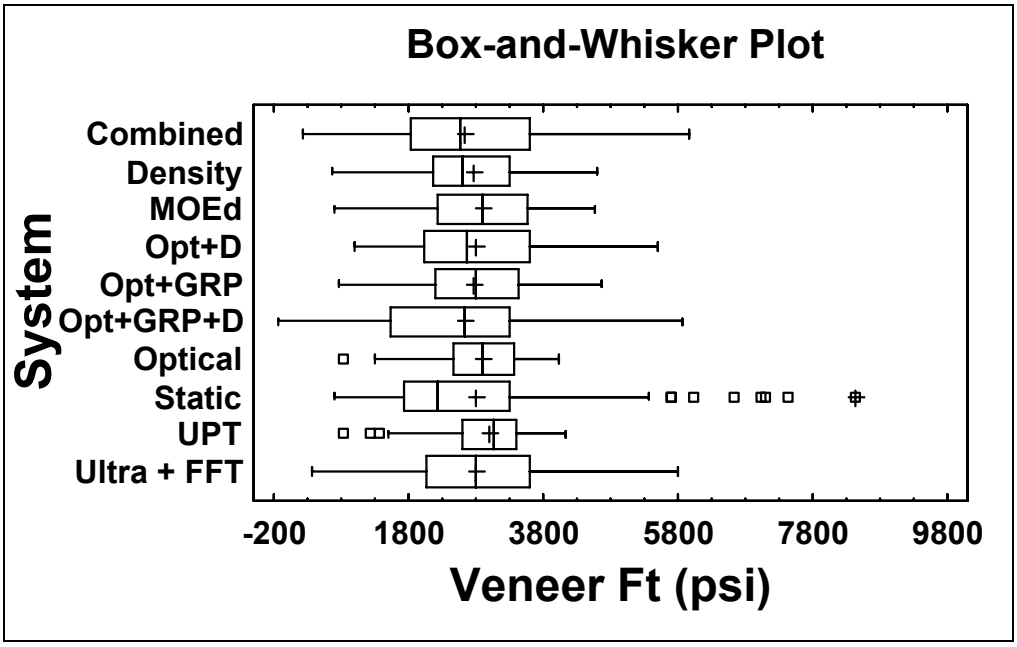

Figure 7.6. Box and whisker plots for veneer F_t from all prediction models and static results.

Table 7.6 shows the average predicted veneer F_t value from the validation study population as determined by each system. Additionally, the average percent error (from the actual veneer F_t) and rank for each system was determined (Table 7.6). Table 7.7 shows the overall average percent error when comparing the predicted versus veneer static F_t on an individual specimen basis, rather than the population average.

Table 7.6. Comparison of average population predictions to static values of veneer tensile F_t.

Model (included variables)	**Predicted Veneer F_t (psi)**	**Comparison to Veneer static F_t (population average = 2,796 psi)**	
		Error (%)	**Rank**
Ultrasonic + Spectral Analysis (v7, v37)	2,800	-0.2	1
Optical + Density (v3, v21, v24)	2,791	0.2	2
Density (v3)	2,773	0.8	3
Optical + GRP (v13, v18, v33)	2,772	0.9	4
Average MOE_d (v7)	2,886	-3.2	5
Basic Optical (v13, v18)	2,911	-4.1	6
Combined Systems (v7, v21, v24, v32, v33, v38)	2,636	5.7	7
Optical + Density + GRP (v3, v21, v29, v32, v34)	2,618	6.4	8
Average UPT (v4)	2,991	-7.0	9

Table 7.7. Comparison of average percent error for each prediction model on an individual veneer specimen basis as related to veneer static F_t.

Model (included variables)	**Overall Average of Individual Specimen Veneer F_t Comparisons**	
	Error (%)	**Rank**
Combined Systems (v7, v21, v24, v32, v33, v38)	-2.2	1
Optical + Density + GRP (v3, v21, v29, v32, v34)	-4.5	2
Ultrasonic + Spectral Analysis (v7, v37)	-11.1	3
Optical + Density (v3, v21, v24)	-15.2	4
Optical + GRP (v13, v18, v33)	-15.2	5
Density (v3)	-19.9	6
Average MOE_d (v7)	-21.6	7
Basic Optical (v13, v18)	-26.0	8
Average UPT (v4)	-29.7	9

The combined system model appeared to provide the best prediction of veneer static F_t. The combined system model best explained the variation (i.e., highest R-

squared value) in veneer static F_t during both the model development and validation studies. Additionally, the combined systems model performed the best in terms of predicting individual veneer static specimen F_t (Table 7.7) on an average basis. The optical (with growth ring and density measures included) model showed the second best prediction in terms of average percent error when predicting individual veneer static specimen F_t, but did under predict some individual specimens as compared to other models (Figure 7.6). The MOE_d model, on average, appeared to over predict veneer static tensile F_t as compared to the combined system model.

The first and second ranked model in Table 7.7 included measures of density (included in calculation of MOE_d in the combined model), basic optical (defect), and growth ring pattern measures. Of note from Table 7.7 was the significant increase in percent error when the combination of basic optical, density, and growth ring patterns measures were removed (i.e., models ranked three to nine). This suggested the combination of basic optical, density, and growth ring patterns measures is much more important for the reliable prediction of individual veneer F_t values; as opposed to individual veneer tensile MOE. Specifically, the change in percent error on individual predictions of veneer tensile MOE using various models was much more gradual (Table 7.4).

7.2.3.3 Improvements in Veneer Grading and Property Predictions

All models tested showed no statistically significant difference in average predicted veneer tensile MOE and F_t. Improvements in prediction of veneer tensile

MOE and F_t were made, however, by including extra measures in with currently used industrial methods of ultrasonic grading (i.e., MOE_d). In terms of predicting both veneer static tensile MOE and F_t, the validation study results indicated the ultrasonic system of grading could benefit from inclusion of some spectral analysis measures, as well as, optically determined measures (i.e., as in the combined system model).

The validation study results indicated non-destructive evaluation (NDE) systems not having to rely solely or highly on density measurements were more reliable from one set of tests to the next. This result suggests an NDE optical system which also includes, along with density, some measure of veneer defects and growth ring patterns has potential for grading veneer. Specifically, in terms of veneer F_t, this suggests an optical system, even without density included, may likely outperform the ultrasonic system utilizing solely either MOE_d or UPT. This finding was validated by the fact that optical systems including some measure of growth ring pattern were more reliable than MOE_d and UPT systems when evaluating veneer static F_t. In some cases, however, inclusion of growth ring pattern measures resulted in under predicted veneer static F_t values. In this study, just one means of attempting to quantify growth ring measures was studied. The optical system may likely have benefited by using a growth ring pattern measurement system to measure actual pattern angles, rather than summation of pixel values within a line along the length and across the width of veneer images. Inclusion of actual angle values (zero to 180-degrees) should likely improve veneer F_t prediction.

The results suggest the optical system which was developed for this study shows promise in performing as well as, if not better, than traditional ultrasonic

grading systems. The developed optical system proved reliable in terms of repeatability in locating and quantifying influential veneer measures. Furthermore, results from small veneer specimen grading via a non-destructive optical system provides justification for future research on full-size veneer sheets.

By using an optical system to locate and quantify veneer measures, manufacturers of veneer composites (LVL and plywood) could improve final product properties. Specifically, by knowing the location and influence of specific veneer defects and characteristics, manufacturers would be able to make better decisions in regard to veneer selection and placement within a composite. In regard to plywood manufacturers, the ability of the optical system to locate defects may be of even greater importance in today's environment. With the advent of increased LVL production, some plywood manufacturers are left with a reduced supply of what is considered high grade veneer material (e.g., G1, G2, and G3 grade veneer). By using information acquired by an optical scanning system, plywood manufacturers could also better select and orient veneers in a manner which maximizes product strength performance.

7.3 Laminated Veneer Lumber Assembly and Property Prediction Study

Given that the majority of ultrasonically graded veneer is utilized by LVL manufacturers, research was needed to determine the relationship between individually predicted veneer properties via the different scanning methods (optical,

ultrasonic, and combined optical and ultrasonic), and their respective predictions of final LVL material properties.

7.3.1 Veneer for LVL: Non-Destructive Testing and Property Prediction

The resulting three-hundred and ten (310) veneer specimens for producing LVL specimens were first non-destructively tested using the optical system and ultrasonic system setup described in Chapter 5. In terms of testing procedures, with one exception, the exact same methods were followed as outlined in Section 5.2.2.1 for non-destructive testing. The one exception was the distance over which specimens were tested for ultrasonic properties. Because the LVL was being tested in tension, it was determined the amount of grip length needed to be increased 12-inches in length on each end, as opposed to the 3.5-inches used when testing individual veneer. The increase in length was determined to be necessary, after some preliminary testing on 5-layer LVL with a 3.5-inch grip length resulted in the LVL being crushed within the grip area. Once the increased grip area was incorporated into the final veneer specimen size (to maintain the 24-inches between grips), the overall distance for measuring ultrasonic stress waves increased to 40-inches.

In terms of optical scanning, only the area which underwent tension testing (i.e., the 24-inch long center area) was scanned on each veneer. Optical scanning was performed using the procedures and system as outlined in Section 5.2.2.2. After being non-destructively tested, specimens were placed back in the conditioning room set at 60 percent relative humidity and 20^{o}C.

Using veneer measures determined by non-destructive testing, tensile MOE and F_t values for each individual veneer was predicted using the nine different prediction models developed in Chapter 6. Again, in this section, only those veneer measurements needed for each model were used for predicting individual veneer properties. All other remaining veneer measurements were determined and saved, however. The resulting nine different prediction values for tensile MOE and F_t on each individual veneer were then recorded and saved for use in calculating a prediction of LVL material properties.

7.3.2 LVL Assembly Procedures and Property Predictions

7.3.2.1 LVL Sorting and Property Predictions

Veneer specimens non-destructively tested in Section 7.3.1 were then randomly selected and assigned to be manufactured into a specific LVL specimen. Each LVL specimen was comprised of five layers (nominal 0.625-inch total thickness). To further randomize the veneer within each LVL specimen, individual veneers were randomized in regard to layer location from top to bottom (layer 1 to 5, respectively). Veneer sorting was performed randomly, rather than in a manner to meet some target LVL tensile MOE value. Sorting to meet some specific target or groups of targets based on the nine separate model predictions would have reduced the sample size within each group too small for making statistically valid comparisons. Sorting randomly allowed for a large enough sample size to statistically compare how well each of the nine models predicted LVL properties.

Predicted LVL tensile MOE and F_t properties were calculated using the average value of the individually predicted veneer tensile MOE and F_t values comprising each specimen. As a result, there were nine separate predictions of LVL specimen tensile MOE and F_t, which were based on the previously developed models in Chapter 6. Predicted LVL specimen tensile MOE was calculated using Equation 7.1 (Bodig and Jayne 1993). The same methodology was used to calculate LVL specimen F_t using equation 7.2.

$$E_{L\,avg} = \frac{1}{A_1}\sum_{i=1}^{5} E_L^i A_1^i \qquad \textbf{Equation 7.1}$$

$$F_{L\,avg} = \frac{1}{A_1}\sum_{i=1}^{5} F_L^i A_1^i \qquad \textbf{Equation 7.2}$$

Where:

$E_{L\,avg}$ = predicted LVL specimen tensile MOE (psi)

$F_{L\,avg}$ = predicted LVL specimen F_t (psi)

A_1 = final LVL specimen cross sectional area (in^2)

E_L^i = predicted individual veneer tensile MOE (psi)

F_L^i = predicted individual veneer F_t (psi)

A_1^i = cross sectional area of individual veneer (in^2)

Note: When determining cross sectional area for A_1^i, final LVL specimen width and individual veneer thickness was used. Final width was used, as specimens were trimmed prior to testing (Section 7.3.3.2).

7.3.2.2 LVL Specimen Assembly Procedures

Based on the assigned specimen number and layer location from Section 7.3.2.1, veneers were sorted into their appropriate LVL arrangement. A total of 62 LVL specimens were manufactured. All LVL specimens were laid up at Hexion Specialty Chemicals in Springfield, Oregon. The adhesive system used to manufacture the LVL was Hexion's WONDERBOND® EPI EL-70 with WONDERBOND® EPI CL-1. This adhesive is an Emulsion Polymer Isocyanate (EPI) adhesive used for wood laminating applications (e.g., LVL). This particular adhesive was selected based on the ability to cold press the LVL, as a sufficient hot-press of this size was not readily available. Adhesive was applied to the veneer by a laboratory-scale roller glue spreader (Figure 7.7).

Each 6-inch by 48-inch specimen was aligned in parallel with each other to achieve a loose-side to tight-side interface. Individual LVL specimens were stacked in a specially designed fixture (Figure 7.8) and pressed within 20-minutes after adhesive was applied. To simulate the pressing process of manufacturing facilities, specimens were pressed to pressure (using a torque wrench) rather than final thickness (Figure 7.9). The LVL specimens remained in the pressing fixture for 24-hours. All pressing variables were held constant for each specimen produced. Table 7.8 outlines the process variables maintained throughout the LVL lay-up based on the adhesive manufacturer's (i.e., Hexion) recommendations for the EPI adhesive utilized.

Figure 7.7. EPI adhesive application using laboratory-style adhesive spreader.

Figure 7.8. Assembled LVL specimens prior to cold pressing.

Figure 7.9. Cold pressed LVL specimens during manufacturing.

Table 7.8. Outline of LVL specimen assembly process variables.

Station	Process Variable
Adhesive Application	Veneer MC – Equilibrium MC obtained in 60% relative humidity and 20 ^{o}C condition (approximately 11.5-12.5% MC, O.D. basis)
	WONDERBOND® EPI EL-70 with WONDERBOND® EPI CL-1
	Laboratory adhesive-spreader
	Viscosity 6,000-6,500 centipoise @ 21 ^{o}C
	60 lbs./Mft^2 spread rate (single glue-line)
	Max. 20 minute assembly time after application
Cold Press	24 hour press time
	Room Temperature – approximately 21 ^{o}C
	175 psi pressure
Cold Stacking	7-day stacking time at approximately 21 ^{o}C

Upon completion of pressing (i.e., after the 24-hour cold pressing), each individual LVL specimen was processed into a tension specimen. Because some misalignment occurred during LVL manufacturing, specimens were edge trimmed to a nominal width of 5.800-inches and end trimmed as long as possible to maximize grip area (approximately 47.750-inches in length). After seven (7) days of cold stacking, LVL tension specimens were conditioned to equilibrium at 60 percent relative humidity and 20^{o}C.

7.3.3 LVL Specimen Destructive Tension Testing

After the LVL specimens prepared in Section 7.3.2.2 reached equilibrium moisture content, they were tested destructively in tension. Both axial tension static strength (F_t) and axial static modulus of elasticity (MOE) was evaluated. Tension testing was performed following procedures outlined in ASTM D4761 (2005). Specimen width, thickness, and length measurements were measured and recorded prior to testing each individual LVL specimen. LVL specimens were tested in tension parallel to grain at a rate of 0.250-inches per minute of hydraulic ram motion controlled by a MTS 407 Controller. The grip area was set at 12-inches on each end, leaving 24-inches as the overall length between the variable thickness wedge-type grips.

Testing was performed using a special tension testing apparatus located at Oregon State University's Wood Science and Engineering Department (Figure 7.10 and 7.11). Failure was generally achieved in four to six minutes. Load was measured

by an Interface 200K load cell. Strain (i.e., deformation) was recorded on one face of the specimens over a gauge length of 4.1-inches using an extensometer (350-ohm strain gauge). Due to the constraints of the setup, deformation was measured over this shorter distance (as compared when testing individual veneer). Because the grips were variable thickness wedge-type grips, a considerable distance (approximately eight-inches at each grip) of the actual test area was inside the grip assembly. This made measuring deformation over the entire 24-inches impossible. During testing, load and displacement data was measured and recorded using a data acquisition system controlled by a LabVIEW program. After testing was completed, static tension strength (F_t) and static tensile modulus of elasticity (MOE) was calculated using Equation 3.2 and 3.3, respectively. Additionally, LVL specimen density (at test condition) was calculated.

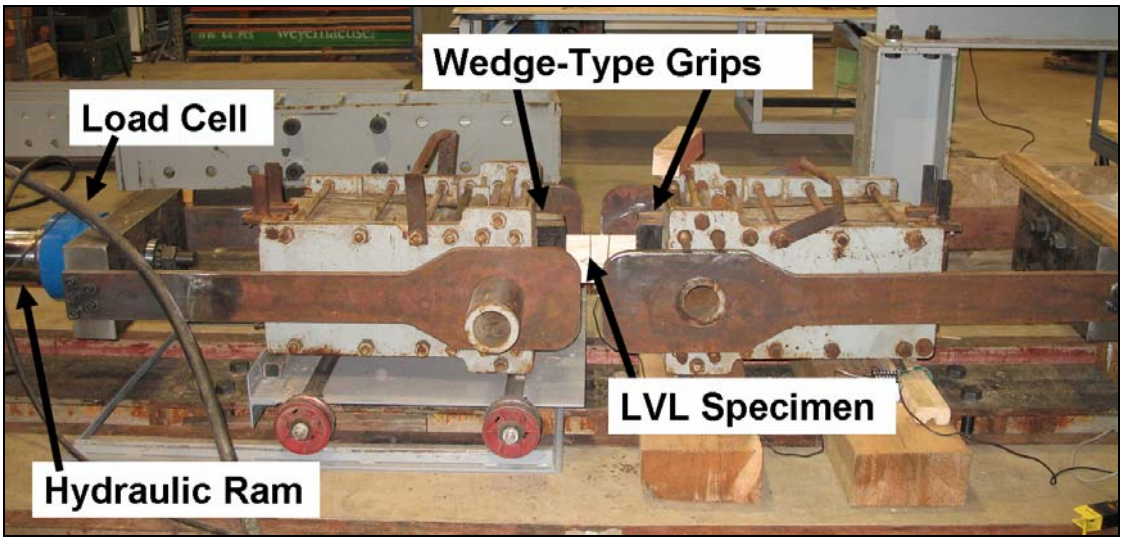

Figure 7.10. LVL tension test setup.

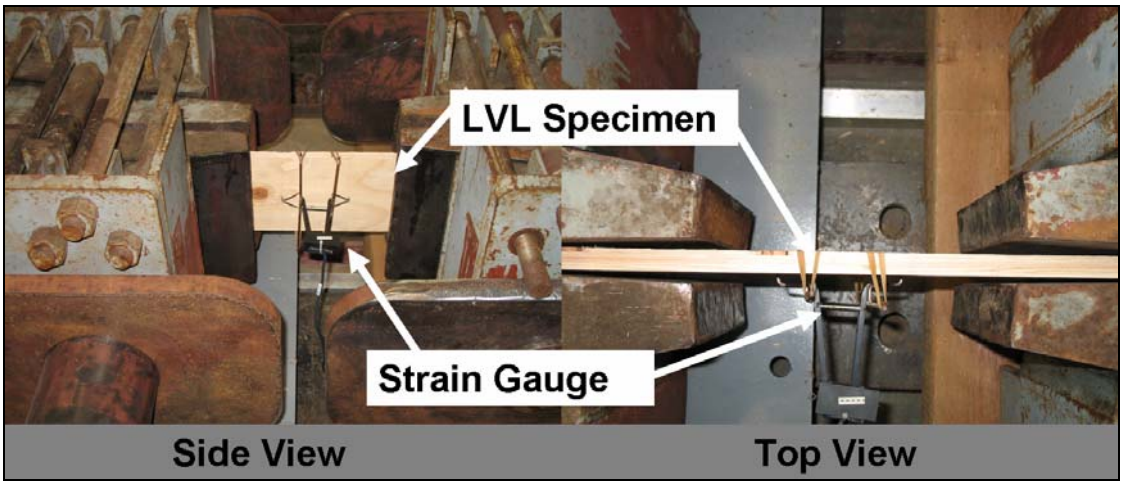

Figure 7.11. LVL specimen and strain gauge placement during tension tests.

Immediately after each individual tension test was completed, a six-inch long specimen was prepared from the end of each LVL specimen for determining moisture content. Moisture content was evaluated following procedures in ASTM D4442, Method B (2007). Original specimen weight was measured and recorded immediately after testing. Moisture content specimens were then placed in an oven set at 212 ± 2 ^{o}F until there was no more change in weight. The final oven-dry weight was then measured and recorded and moisture content at the time of testing was calculated.

7.3.4 LVL Property Prediction Results and Discussion

7.3.4.1 LVL Test Results

Table 7.9 provides a summary of destructively determined LVL tensile MOE and F_t. Complete results for each individual specimen are located in Appendix C.

Table 7.9. LVL destructively determined tension test results.

Summary Statistic	Density (lb/ft^3)	Moisture Content (%)	Tensile MOE (psi)	F_t (psi)
Average	33.8	12.0	1,749,764	5,821
St. Dev.	1.4	0.3	218,309	1,202
COV %	4.1	2.1	12.5	20.6
Min.	30.6	11.4	1,269,798	3,049
Max.	36.9	12.7	2,303,577	8,492
Sample Size	62	62	62	62

The coefficient of variation (COV%), for both tensile MOE and F_t, was much lower as compared to the individual veneer test results. This reduction in COV% assured the sorting method suitably randomized strength reducing features (e.g., defects and highly sloped growth ring patterns) when manufacturing the LVL specimens. Furthermore, the coefficient of variation from the LVL tests were more in line with the average 25 percent coefficient of variation reported for tensile parallel to grain of clear wood (Forest Products Laboratory 1999). The coefficient of variation, however, was higher than the 10-12 percent for LVL when using UPT as a sorting method (Sharp 1985). The higher coefficient of variation in this study was likely due to the purposely selected random veneer sorting, rather than sorting by any of the prediction models to reduce the variation. This also suggests that some means of sorting (e.g., via average UPT) into groups is likely to result in lower variation, as compared to random sorting.

Figure 7.12 shows the relationship between LVL static tensile MOE and F_t. In this regression, 13.5 percent of the variation (R-squared = 0.135) in LVL F_t was explained by LVL tensile MOE. This low R-squared value was in agreement with

results from past research, as Jung (1982) reported that static MOE did not correlate well with static strength (r-squared from 8.1% to 37.1%).

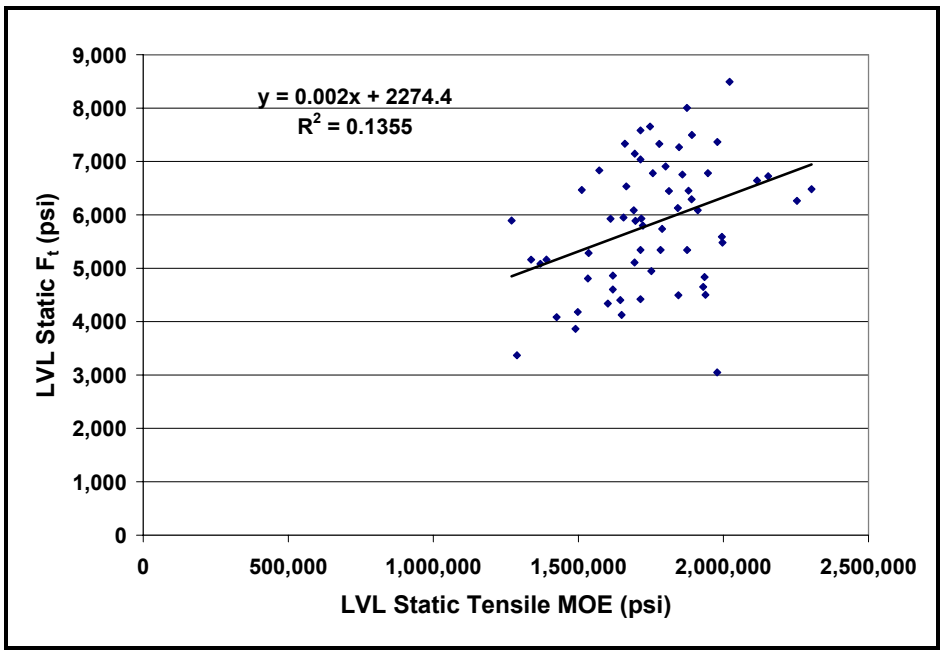

Figure 7.12. LVL static F_t versus static tensile MOE as destructively determined.

As evident from Figure 7.12, the relationship between static tensile MOE and F_t was very weak. It was also much weaker than the relationship found between veneer static F_t and tensile MOE. Due to the grip arrangement used, deformation could only be measured over a small distance, rather than over the entire 24-inch length undergoing tension. It is likely that using such a small gage length failed to incorporate movement in areas which ultimately failed, especially when failure was located outside the region measured for MOE. This likely influenced LVL tensile MOE results, but to what extent is unknown.

Given this, some caution was needed when comparing each system's model in terms of its ability to predict LVL tensile MOE. Specifically, caution was needed when analyzing the optical scanning, ultrasonic (when including spectral measurements), and combined systems models, which included predictor variables which were measures of total, minimum, and maximum values. Prediction models which used only measures of average veneer properties (e.g., MOE_d, Density, and UPT) were probably less influenced by the measuring of LVL tensile MOE over a short distance. The amounts by which these models may have been less influenced, however, was not investigated.

Failure of every LVL specimen occurred outside the grip area. No glue-line failures were observed, so the LVL assembly process was successful in bonding the veneer layers together to form an adequate composite material. Figure 7.13, 7.14, and 7.15 show examples of typical LVL tension failures. Failure typically occurred in different areas within each layer in a given specimen (Figure 7.13).

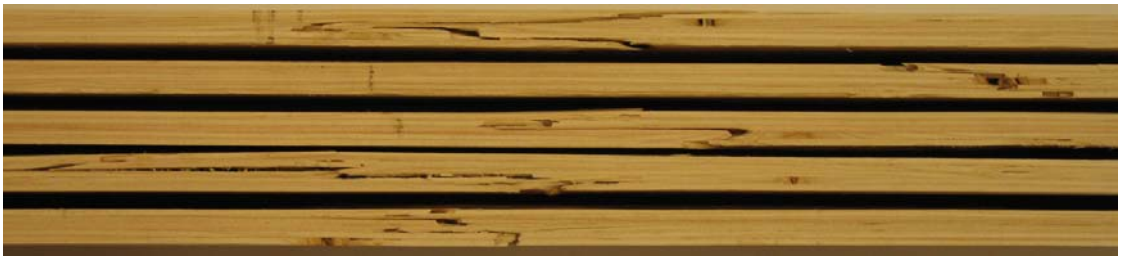

Figure 7.13. Typical LVL tension failures showing failure through layers.

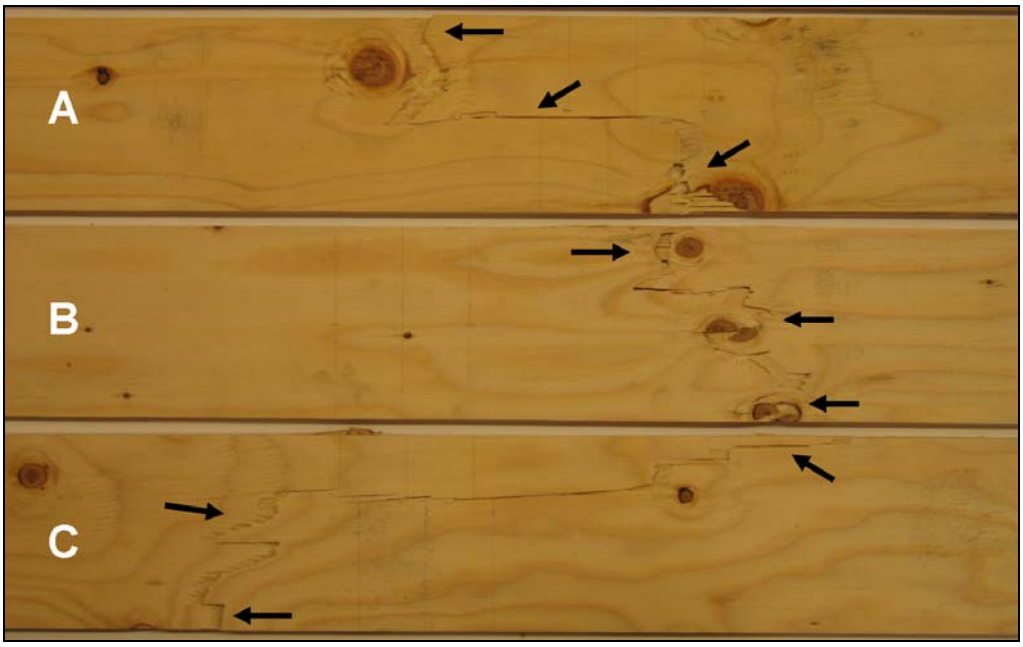

Figure 7.14. Typical LVL tension failures observed on surface layers (A-large defects spaced apart, B-grouping of defects, C-small defect combined with diving grain).

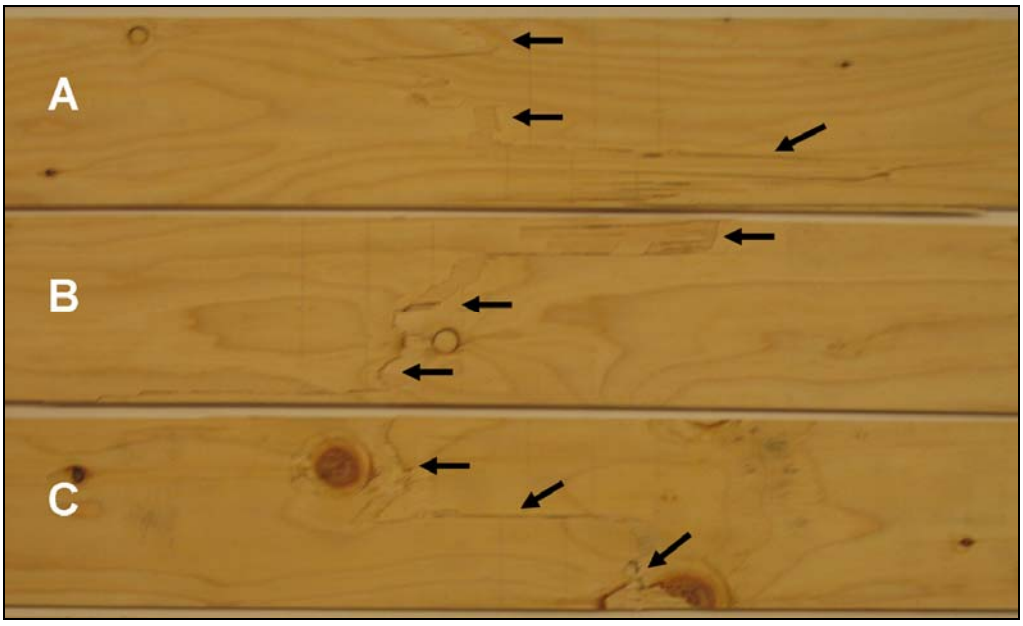

Figure 7.15. Additional typical LVL tension failures observed on surface layers (A-relatively free of defects and fairly straight grain pattern, B- highly sloped grain pattern, C-two large defects combined with diving grain).

In the surface layer, many failures tended to occur in areas with a highly sloped growth ring pattern (indicator of diving grain), large defects, and groups of defects (Figure 7.14 and 7.15). Furthermore, many of the failures noted at the LVL surface layers followed similar patterns as in the individual veneer tension test failures. This suggests the influence of localized defects and diving grain of individual veneers, while reduced by the composite nature of LVL, are still important variables in determining veneer F_t values.

Because one of the objectives of this study was to compare veneer grading methods, the LVL specimens manufactured did not include joints between adjacent veneers (e.g., scarf, crushed-lap) and comprised of less layers than industrial LVL. Lee et al. (1999) reported yellow-poplar LVL with crushed-lap veneer-joints was as strong in edgewise bending, as compared to LVL which were free of veneer joints. Yellow-poplar LVL with scarf veneer-joints, however, showed a statistically significant lower mean value of edgewise bending strength when compared to LVL with crushed-lap and no veneer-joints (Lee et al. 1999). Given this, LVL manufactured on an industrial basis, may show slightly different failure modes when certain types of veneer-joints are included in LVL billets.

7.3.4.2 LVL Tensile MOE Property Prediction Using Developed Models

Table 7.10 shows the resulting R-squared values of the relationship between predicted values obtained using each model and LVL static tensile MOE. Predicted versus LVL static tensile MOE plots are shown in Appendix C. Based on the R-

squared values in Table 7.10, the MOE_d model performed the best in terms of explaining the variation in LVL tensile MOE. None of the models, however, performed well in terms of explaining the variation in LVL tensile MOE. As previously noted, the measurement of tensile MOE over a small gauge length could have impacted prediction of LVL tensile MOE.

Table 7.10. Comparison of R-squared values of each prediction model in comparison to LVL static tensile MOE.

System	Model (included variables)	Prediction of LVL Static Tensile MOE	
		R^2	Rank
Material Property	**Density** (v3)	0.074	7
Optical	**Basic Optical** (v13, v23)	0.003	9
	Optical + Density (v3, v16, v20)	0.117	6
	Optical + GRP (v23, v25, v31, v33, v34)	0.042	8
	Optical + Density + GRP (v3, v16, v20, v25, v31, v33, v34)	0.121	4
Ultrasonic	**Average MOE_d** (v7)	0.150	1
	Average UPT (v4)	0.119	5
	Ultrasonic + Spectral Analysis (v7, v35, v36)	0.131	3
Combined	**Combined Systems** (v7, v22, v36)	0.140	2

One-way ANOVA testing was used to further analyze the ability of each prediction model to successfully determine average LVL static tensile MOE. When

performing this analysis, LVL static tensile MOE was also included (labeled as Destructive). Results from one-way ANOVA testing showed there was a statistically significant difference (p-value < 0.0001) for average LVL tensile MOE between the groups. Figure 7.16 provides a box and whisker plot of LVL tensile MOE determined by each system.

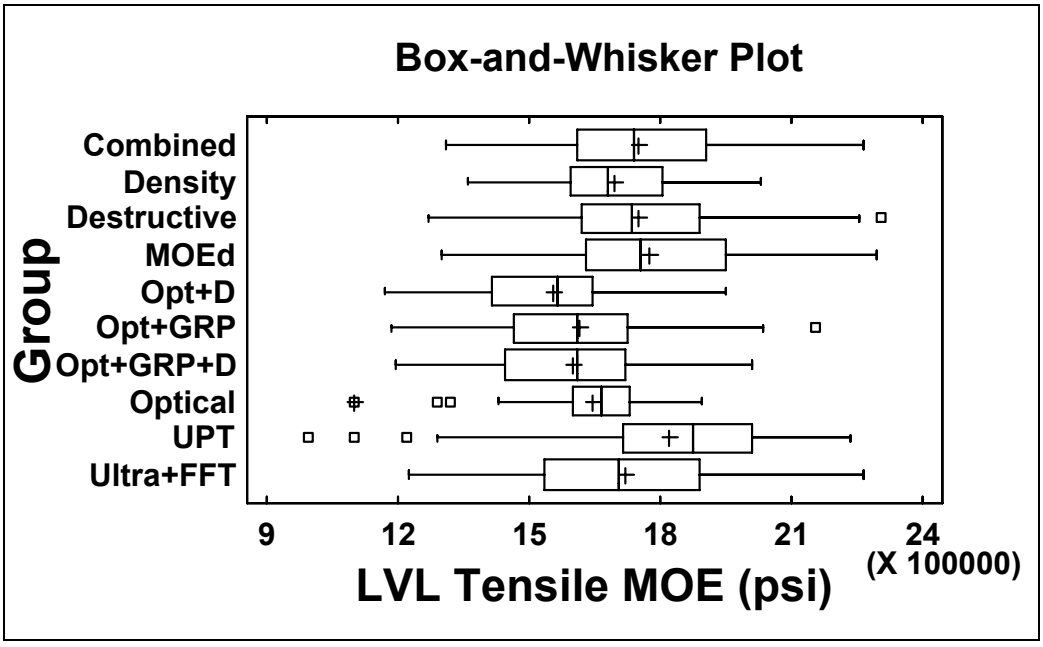

Figure 7.16. Box and whisker plots for LVL tensile MOE from all prediction models and static (destructive) results.

Multiple range tests indicated a statistically significant difference between many different groups in terms of average LVL tensile MOE. Of interest were comparisons of each group in relation to LVL static (destructive) tensile MOE. Table 7.11 shows the results of multiple range comparison tests. Average predicted LVL tensile MOE from three optical system models; optical (including density), optical

(including growth ring pattern and density measures, and optical (including growth ring pattern measures) were determined as being statistically different in comparison to average LVL static tensile MOE. The remaining models were not statistically different in their average prediction of LVL tensile MOE in comparison with average LVL static tensile MOE (Table 7.11).

Table 7.11. Multiple range comparison output on tests for differences in average LVL tensile MOE between groups, showing homogeneous groups (those in bold were not statistically different from LVL static tensile MOE).

System	Average LVL Tensile MOE (psi)	Homogeneous Groups					
Optical + Density (v3, v16, v20)	1,553,124	X					
Optical + Density + GRP (v3, v16, v20, v25, v31, v33, v34)	1,597,728	X	X				
Optical + GRP (v23, v25, v31, v33, v34)	1,613,279	X	X	X			
Basic Optical (v13, v23)	1,647,057	X	X	X	**X**		
Density (v3)	1,695,169		X	X	**X**	**X**	
Ultrasonic + Spectral Analysis (v7, v35, v36)	1,719,183			X	**X**	**X**	**X**
Destructive Tensile MOE	1,749,764				**X**	**X**	**X**
Combined Systems (v7, v22, v36)	1,751,945				**X**	**X**	**X**
Average MOE_d (v7)	1,774,993					**X**	**X**
Average UPT (v4)	1,818,341						**X**

Table 7.12 shows the overall average percent error when comparing the predicted versus LVL static tensile MOE on an individual specimen basis, rather than the population average. On average, the ultrasonic (with spectral analysis included) system and the combined system models were the two best predictors, respectively, of individual LVL tensile MOE. As evident from Figure 7.16, the combined system model had a similar spread, in comparison with LVL static tensile MOE values, in terms of variation of the 50 percentile range and lower and upper quartiles.

Table 7.12. Comparison of average percent error for each prediction model on an individual LVL specimen basis as related to LVL static tensile MOE.

Model (included variables)	**Overall Average of Individual Specimen LVL Static Tensile MOE Comparisons**	
	Error (%)	**Rank**
Ultrasonic + Spectral Analysis (v7, v35, v36)	0.8	1
Combined Systems (v7, v22, v36)	-1.1	2
Density (v3)	1.9	3
Average MOE_d (v7)	-2.4	4
Basic Optical (v13, v23)	4.4	5
Average UPT (v4)	-4.9	6
Optical + GRP (v23, v25, v31, v33, v34)	6.7	7
Optical + Density + GRP (v3, v16, v20, v25, v31, v33, v34)	7.7	8
Optical + Density (v3, v16, v20)	10.3	9

Further analysis of the 50 percentile range (Figure 7.16) indicated the MOE_d system and the ultrasonic (with spectral analysis included) system models tended to over predict and under predict LVL tensile MOE, respectively. This helps explain why the combined system model performed better, as it included measures of MOE_d

and spectral analysis, along with some optical measures. The differences in over prediction in the MOE_d model and under prediction of the ultrasonic (with spectral analysis included) were reduced under the combined systems model.

Again, some caution needs to be taken with regard to prediction of LVL tensile MOE given the small area over which it was measured. It is also likely that many of optical methods performed poorly because they were based on individual veneer specimens. Due to lamination effects, optically determined measures which highly influenced tensile MOE on an individual basis may have less effect on a composite material. A better approach for the optical system may be to average all the optically measured properties within a given LVL specimen and develop regression equations to predict LVL tensile MOE. This approach is investigated in Section 7.3.5.

7.3.4.3 LVL F_t Property Prediction Using Developed Models

Due to lamination effects discussed in Section 2.1, predicting LVL specimen tensile strength by calculating the average of the individual veneers in a specimen did not prove to be a highly reliable method. One-way ANOVA testing was used to analyze the ability of each prediction model to successfully determine average LVL static F_t. When performing this analysis, LVL static F_t was also used as one of the groups (labeled as Destructive). Results from one-way ANOVA testing showed that there was a statistically significant difference (p-value < 0.0001) for average LVL F_t between the groups. Multiple range tests indicated all models showed a statistically significant difference to average LVL static F_t. Additionally, multiple range tests

indicated various models as being different from one another in terms of predicted average LVL specimen F_t. Figure 7.17 provides a box and whisker plot of LVL F_t determined by each prediction model using the average of individually predicted veneer F_t approach.

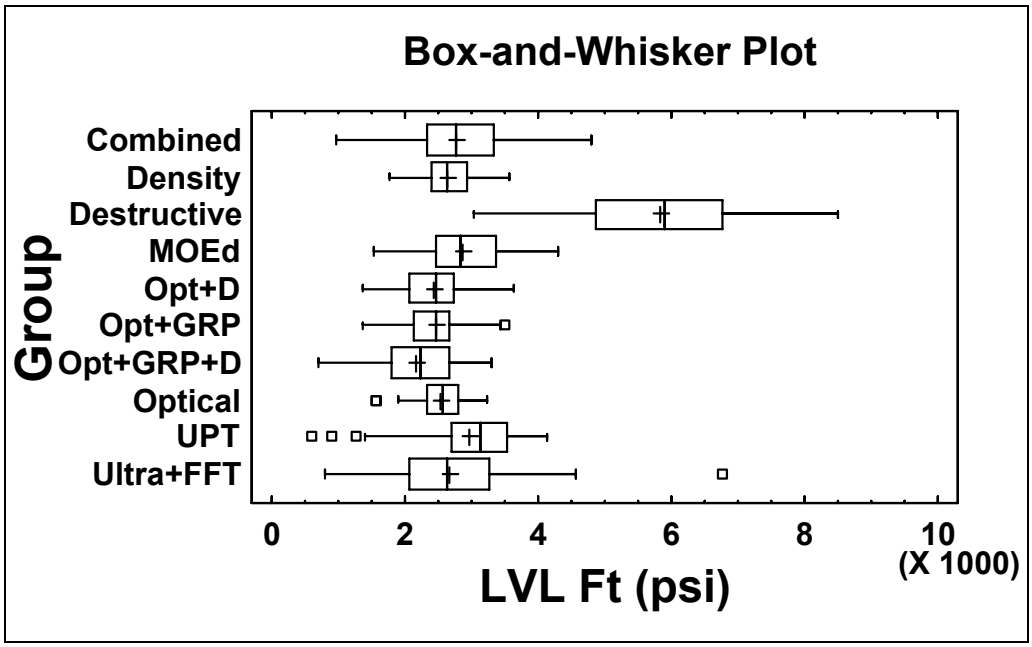

Figure 7.17. Box and whisker plots for predicted LVL F_t using the average of individually predicted veneer F_t values under each model as compared to static (destructive) test results.

The poor results found when using the average of predicted values of individual veneer strength to predict LVL strength are in agreement with discussion by Uskoski and Bechtel (1993), who suggested it was not valid to assume that LVL possesses a tensile strength equivalent to average strength of the laminates. The poor results also are in agreement on the impact of the laminate effect discussed by Serrano et al. (1996).

Due to the lamination effect, a better approach, when predicting LVL F_t, was to perform linear regression using predicted LVL values obtained using each model plotted against LVL static F_t values. Examination of the resulting R-squared values would allow for determining which system was most capable of explaining the variation in LVL static F_t. Table 7.13 shows the resulting R-squared values for the relationship between each model's predicted LVL F_t value and LVL static F_t. Plots of predicted versus actual LVL tensile F_t (including regression equations) are shown in Appendix C. Additionally, Figure 7.18 provides a box and whisker plot of fitted LVL F_t values determined for each system from linear regression analysis.

Based on the R-squared values in Table 7.13, the MOE_d model performed the best in terms of predicting LVL static F_t. Models comprised solely of average measures of individual veneer properties (e.g., MOE_d and density), performed best in explaining the variation in LVL F_t values. The basic optical, optical including growth ring pattern, and optical including growth ring pattern measures and density measures models were the three worst performing models, respectively. The optical including density, while weaker in terms of explaining the variation in LVL F_t, outperformed the UPT model. The combined system and ultrasonic including spectral analysis models were slightly weaker, as compared to the MOE_d model.

While the MOE_d model best explained the variation in LVL F_t values, it was evident that from analysis of the 50 percentile range (Figure 7.18), neither the lower or upper ends were predicted well. Typically, LVL F_t design values are based on the lower 5th percentile, as compared to MOE values which are based on average results. The lower 5th percentile is usually determined from parametric or non parametric

analysis of a set of data under the guidance of ASTM D2915 (2003). The intent of this study was not to predict LVL characteristic values. It was apparent, however, that using the MOE_d, and, for that matter, any model developed, would have over-predicted the characteristic value given the random specimen lay-up used. This result may not hold true when LVL lay-up is performed to meet a certain target, rather than randomly as done in this study. It was evident future research is needed to better explain the variation in observed LVL F_t values.

Table 7.13. Comparison of R-squared values of each prediction model in comparison to LVL static F_t.

System	Model (included variables)	Prediction of LVL Static F_t	
		R^2	Rank
Material Property	**Density** (v3)	0.40	4
Optical	**Basic Optical** (v13, v18)	0.03	9
	Optical + Density (v3, v21, v24)	0.37	5
	Optical + GRP (v13, v18, v33)	0.20	8
	Optical + Density + GRP (v3, v21, v29, v32, v34)	0.25	7
Ultrasonic	**Average MOE_d** (v7)	0.52	1
	Average UPT (v4)	0.31	6
	Ultrasonic + Spectral Analysis (v7, v37)	0.46	3
Combined	**All Combined Systems** (v7, v21, v24, v32, v33, v38)	0.50	2

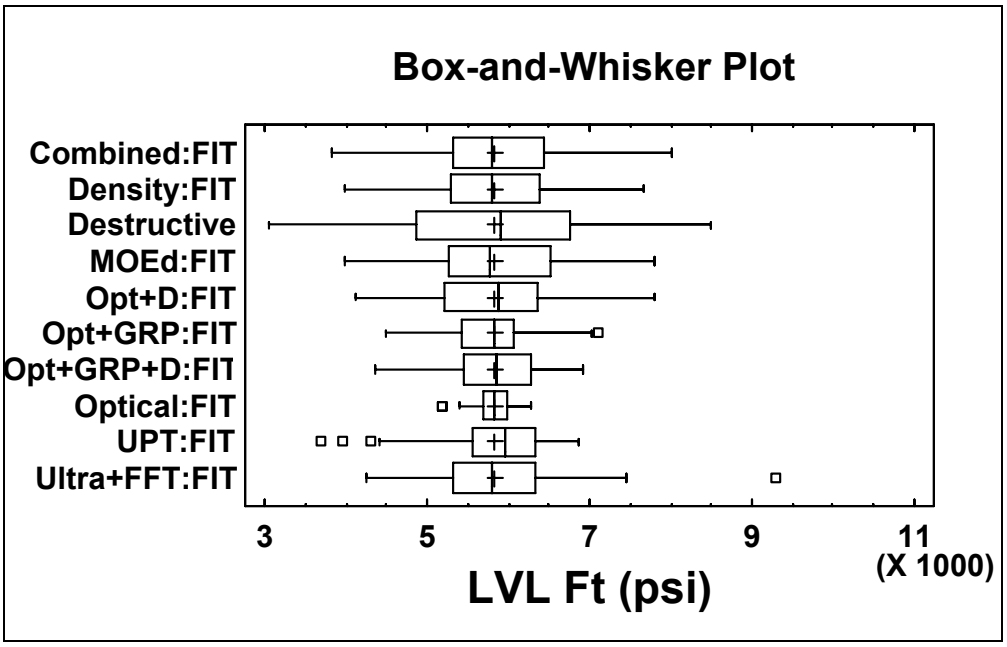

Figure 7.18. Box and whisker plots of fitted LVL F_t values from all prediction models in comparison to static (destructive) results.

7.3.5 LVL Property Prediction via Overall Average Veneer Measures Within a Specimen

In an attempt to determine a better means to use optical system data to better explain the variation observed in LVL tensile MOE and F_t values, prediction analysis was performed using average veneer measures comprising an entire LVL specimen, rather than predicting individual veneer layers and calculating a predicted value for the specimen. To do so, all optically determined measures for all five veneers within a specimen were averaged. The average optical measures, along with density, were used to predict static LVL tensile MOE and F_t. Regression analysis for LVL tensile MOE, however, did not improve the explanation of variability (i.e., R-squared value)

in LVL static tensile MOE, as found for the optical system in Section 7.3.4.2. The focus for this section then was limited to prediction of LVL static F_t.

Regression results using the average of all optical measures (basic optical and growth ring pattern measures) and density indicated six average characteristics were statistically significant (at an alpha level = 0.05) in predicting static LVL F_t (Table 7.14). Figure 7.19 shows the relationship between predicted LVL F_t using statistically significant average optical (including growth ring pattern measures) and density measures versus LVL static F_t. In this regression, 57.5 percent of the variation (R-squared = 0.575) in LVL F_t was explained by the linear regression coefficients.

Table 7.14. Statistically significant variables, regression coefficients, and p-values from regression analysis on average optical (including growth ring pattern measures) and density data for predicting LVL static F_t.

Independent Variable	Regression Coefficient	p-value
Constant	-7,329.2	0.015
Average Density (v3), lb/ft^3	363.5	0.001
Average Maximum Defect Width (v18), in	7,139.6	0.015
Average Total Defect Width (v20), in	-4,955.4	0.000
Average Total Defect Volume (v22), in^3	9,192.6	0.002
Average Maximum Defect Volume (v23), in^3	-34,069	0.012
Average E Minimum (v28)	0.7075	0.007

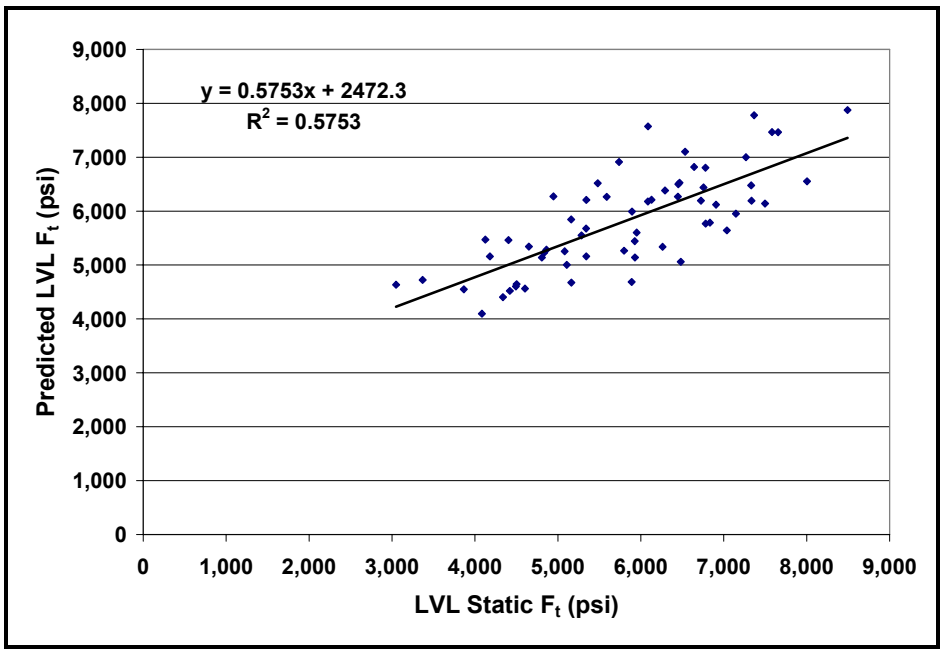

Figure 7.19. Predicted LVL F_t from average optical measures (including growth ring pattern measures) and density versus LVL static F_t.

Regression results using average basic optical measures and density (no growth ring pattern measures included) indicated five average characteristics were statistically significant (at an alpha level = 0.05) in predicting LVL static F_t (Table 7.15). Figure 7.20 shows the relationship between predicted LVL F_t using statistically significant average optical and density measures versus LVL static F_t. In this regression, 53.0 percent of the variation (R-squared = 0.530) in LVL F_t was explained by the linear regression coefficients.

Table 7.15. Statistically significant variables, regression coefficients, and p-values from regression analysis on average basic optical and density data for predicting LVL static F_t.

Independent Variable	Regression Coefficient	p-value
Constant	-7,765.1	0.008
Average Density (v3), lb/ft^3	502.3	0.000
Average Number of Defects (v16)	723.4	0.028
Average Total Defect Width (v20), in	-5,805.4	0.001
Overall Average Defect Width (v21), in	4,130.0	0.027
Average Total Defect Volume (v22), in^3	8,598.6	0.004

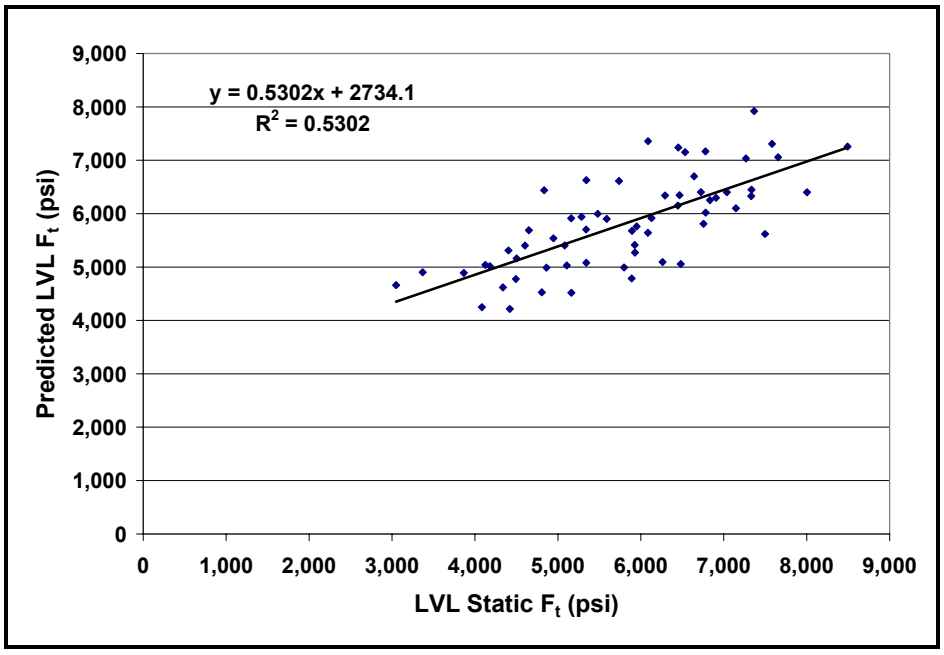

Figure 7.20. Predicted LVL F_t from average optical (no growth ring pattern) and density measures versus LVL static F_t.

The basic ultrasonic and ultrasonic including spectral analysis models are comprised solely of average measures, so no improvements were found by using average values comprising an entire LVL specimen. The combined system model for

individual veneer predictions, however, did include two growth ring pattern measures (E90 Minimum and Maximum) which were not average values. The average optical measures of veneer in a given LVL specimen were combined with statistically significant values from the individual combined model (i.e., average MOE_d and Average Peak Variance – dB Scale). Analysis was then performed to look at any improvements in predicting static LVL F_t when using this combined system approach.

Regression results using the combined system (i.e., average basic optical, growth ring pattern, average MOE_d, and average peak variance - dB scale) measures indicated five average characteristics were statistically significant (at an alpha level = 0.05) in predicting LVL static F_t (Table 7.16). Figure 7.21 shows the relationship between predicted LVL F_t using statistically significant combined system measures versus LVL static F_t. In this regression, 64.5 percent of the variation (R-squared = 0.645) in LVL F_t was explained by the linear regression coefficients.

Table 7.16. Statistically significant variables, regression coefficients, and p-values from regression analysis on combined system measures for predicting LVL static F_t.

Independent Variable	Regression Coefficient	p-value
Constant	-1,589.4	0.293
Average MOE_d (v7), psi	0.0041	0.000
Average Total Defect Width (v20), in	-3,503.3	0.001
Overall Average Defect Width (v21), in	2,038.9	0.024
Average Total Defect Volume (v22), in^3	6,505.4	0.006
E90 Minimum (v33)	1.8058	0.021

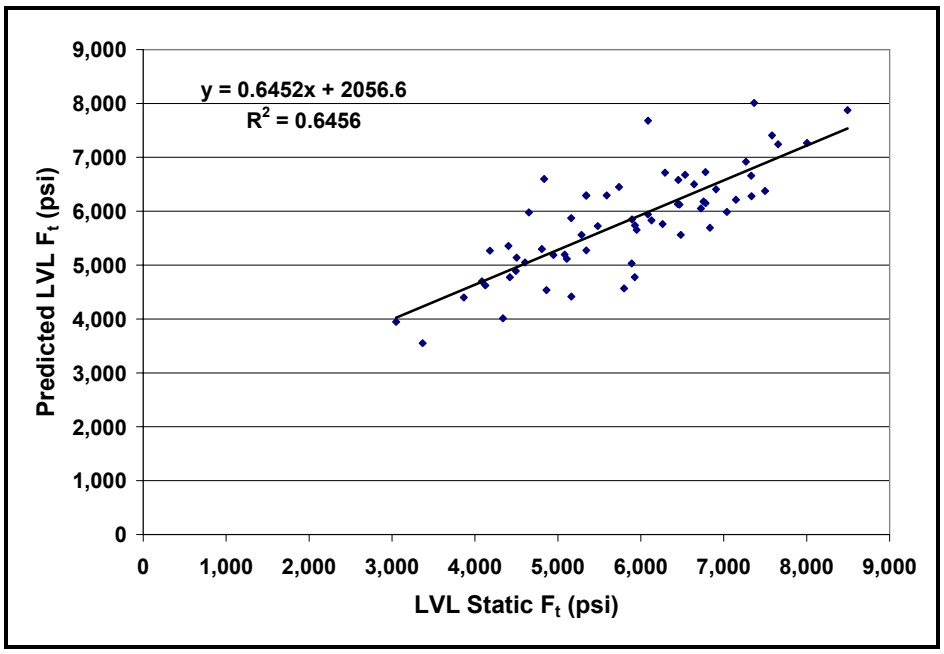

Figure 7.21. Predicted LVL F_t from average combined system measures (average basic optical, growth ring pattern, MOE_d, and peak variance - dB scale) versus LVL static F_t.

The combined systems model which included average optical, growth ring pattern, and MOE_d comprising an LVL specimen, rather than predicted F_t of each individual veneer laminate, best explained the variation in LVL static F_t values as compared to all other models (Table 7.17). The results indicated LVL static F_t could best be predicted by combining average MOE_d and optical values together. This finding suggests improved LVL F_t predictions could be achieved by integrating the existing ultrasonic and optical systems found in many manufacturing facilities.

In terms of the optical system, models which included average measures comprising an LVL specimen, rather than predicted F_t of each individual veneer laminate, explained more of the variation in LVL static F_t values. The prediction

including average optical, growth ring pattern, and density measures performed the best, and was better than the MOE_d model in explaining the variation in LVL static F_t. The prediction including average optical and density measures performed slightly better than the MOE_d model.

Table 7.17. Comparison of R-squared values of models using average of predicted individual veneers in comparison when using average measures within an LVL specimen to predict LVL static F_t.

Model Type	Model (included variables)	Prediction of LVL Static F_t	
		R^2	Rank
Predictions Based on Average of Individually Predicted Veneer Layers in LVL Specimens	**Density** (v3)	0.40	7
	Basic Optical (v13, v18)	0.03	12
	Basic Optical + Density (v3, v21, v24)	0.37	8
	Basic Optical + GRP (v13, v18, v33)	0.20	11
	Basic Optical + Density + GRP (v3, v21, v29, v32, v34)	0.25	10
	Average MOE_d (v7)	0.52	4
	Average UPT (v4)	0.31	9
	Ultrasonic + Spectral Analysis (v7, v37)	0.46	6
	All Combined Systems (v7, v21, v24, v32, v33, v38)	0.50	5
Predictions Based on Average Veneer Measures in LVL Specimens	**Average Basic Optical + Density** (v3, v16, v20, v21, v22)	0.53	3
	Average Basic Optical + Density + GRP (v3, v18, v20, v22, v23, v28)	0.58	2
	Average Combined Systems (v7, v20, v21, v22, v33)	0.65	1

From these results, the optical system (with density included) was as capable, if not better, as compared to the MOE_d model when predicting static LVL F_t. Additionally, the inclusion of growth ring measures significantly improved the prediction of LVL static F_t. It was also noted within a given system that different veneer measures were statistically significant when performing regression analysis using the average veneer measures within a specimen versus individual veneer sheet predictions (Table 7.17). This suggests that different veneer defect and growth ring pattern measures are more influential on an individual veneer versus LVL basis. While this occurred in the relatively small size individual veneer sheets utilized in this study, it is hypothesized future optical scanning on full-size veneer sheets may not show such a difference between influential individual veneer and LVL optically determined measures.

Given the results for predicting LVL static F_t when using average veneer measures within a specimen, it was determined the optical system showed promise as a suitable method to predict LVL F_t properties. Further improvement on the optical system, in particular measurement of growth ring pattern angles and quantifying the amount of diving grain, would likely improve the explanation of variability in LVL F_t values.

7.3.6 LVL Property Prediction via NDE on LVL Material

Past research reported conflicting results for correlations between LVL billet measured UPT and various LVL properties. In terms of tensile strength, Pieters

(1979) reported correlations between average billet UPT to LVL tensile of 0.80. Jung (1982) reported that UPT prediction provided poor correlation to strength (r-squared from 0.4% to 30.6%). To investigate these findings in terms of this study, ultrasonic testing was also performed on final LVL specimens prior to tension testing. Procedures in Section 5.2.2.1 for ultrasonic non-destructive testing were used, except the transit time was measured over a distance of 40-inches. This matched the transit distance for which each individual veneer was measured. Additionally, ultrasonic testing was performed on the LVL specimens at approximately the same locations as in the individual veneer testing. When comparing LVL static F_t to average LVL UPT (Figure 7.22), results from this study (R-squared = 0.167) agreed with Jung (1982), who reported poor correlations between UPT and LVL strength.

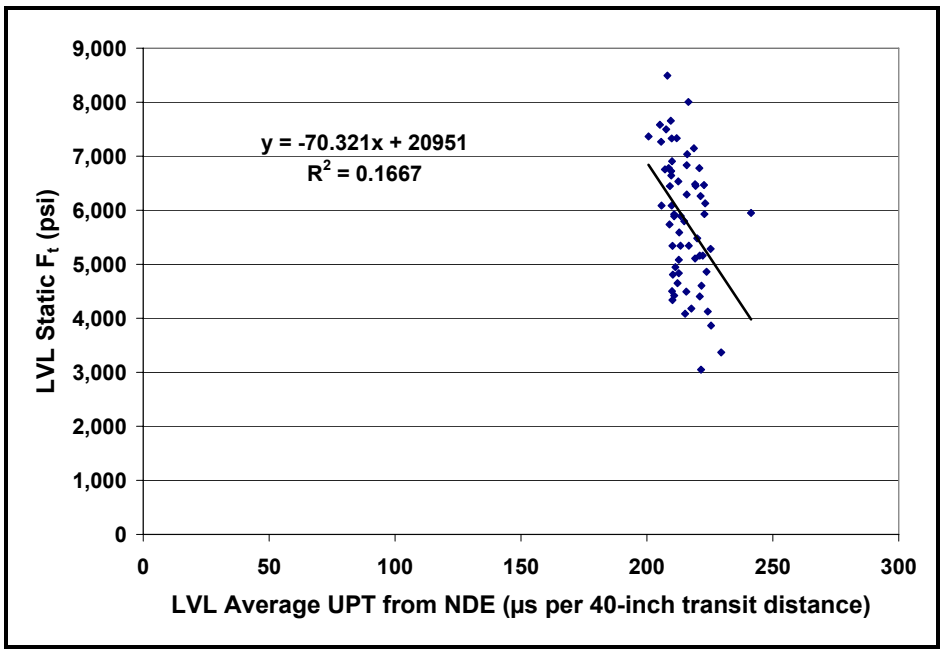

Figure 7.22. LVL static F_t versus non-destructively measured UPT on LVL specimens.

Additionally, the correlation between non-destructively determined LVL MOE_d (Figure 7.23) showed a weaker relationship to LVL static F_t, as compared to the relationship found in Section 7.3.4.3 when using the average MOE_d values measured on individual veneers to predict LVL specimen F_t (Table 7.13).

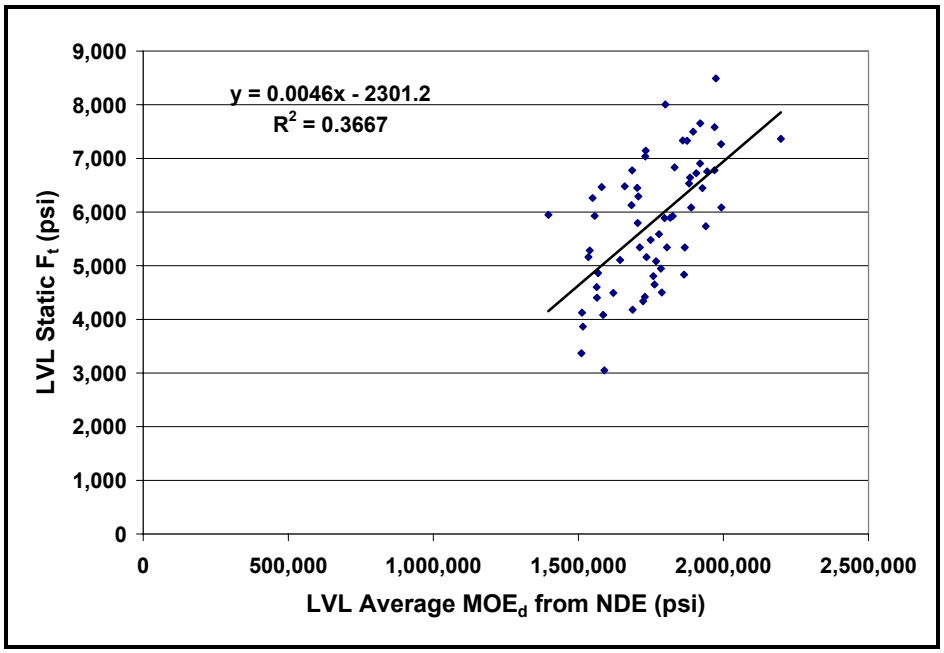

Figure 7.23. LVL static F_t versus non-destructively measured MOE_d on LVL specimens.

The results of this research found a much weaker relationship between measured LVL MOE_d and LVL static F_t, than the R-squared value of 0.92 reported by Kunesh (1978b). This research did demonstrate, however, that individually measured veneer MOE_d provided better predictions of LVL F_t as compared to actual non-destructive ultrasonic testing of the LVL material. While not specifically tested, this

may show a weakness of the ultrasonic stress wave system in adequately recognizing defects or other features throughout the various layers of the LVL. It may be likely that the stress wave travels only through the layers near the surface when longitudinal stress wave testing is performed.

7.3.7 Improvements in LVL Property Predictions

None of the models developed in Chapter 6 performed well in explaining the variation of LVL static tensile MOE. The poor performance was likely more related to LVL tensile MOE being measured over a very small distance, rather than over the entire 24-inch length being tested. Many models, however, were able to predict the LVL population average. Specifically, average LVL static tensile MOE was best predicted by using the combined optical and ultrasonic model.

In terms of LVL static F_t prediction, due to lamination effects, using the average prediction of individual veneers comprising a LVL specimen as the prediction of strength was not appropriate. Under this system, none of the nine models were able to predict LVL static F_t. Using the average prediction of individual veneers comprising a LVL specimen and developing a new prediction model was more appropriate and resulted in better prediction of LVL static F_t. Prediction models which included measures of average veneer properties performed the best. Specifically, of the nine models from Chapter 6, the MOE_d model performed the best in terms of explaining the variation of LVL static F_t values when using the average of individual veneer predictions within a specimen.

The optical system models developed in Chapter 6, while they worked well in predicting individual veneer strength, did not perform as well as the MOE_d, density, ultrasonic (including spectral analysis), and combined systems models. The benefit of manufacturing LVL is the ability to minimize the influence of large defects within a veneer sheet by randomizing the defects throughout the billet. This helps explain why the individual veneer optical system predictions which included values of maximum and total defects, performed more poorly when predicting LVL F_t.

The best predictions of LVL static F_t were determined to be those which used overall average veneer measures comprising a LVL specimen, as opposed to the average of individually predicted veneers within a specimen. The combined systems model which included overall average optical, growth ring pattern, and MOE_d comprising a LVL specimen, rather than predicted F_t of each individual veneer laminate, best explained the variation in LVL static F_t values as compared to all other models. Additionally, by using measures from the optical system, in conjunction with density, and determining the overall average of each measure comprising the entire LVL specimen, more of the variation in LVL static F_t was explained, as compared to the average MOE_d model.

The optical system outperformed the MOE_d model when new models were developed specifically for LVL (Table 7.14 and 7.15). Furthermore, these two models outperformed MOE_d values obtained by non-destructive ultrasonic testing on the actual LVL specimens when predicting LVL static F_t. Based on these findings, an optical system, which includes measures of density, appears to show promise as an

improved means of grading veneer for use in LVL, as compared to current systems based on MOE_d or UPT.

Logan (2000) suggested optical systems which have been introduced, at that time, could be effective in helping visual sorting, but have not demonstrated a means in controlling veneer physical properties. The optical scanning system developed in this research appears to have bridged this gap in terms of the inability of optical scanning to control veneer properties used in LVL. Specifically, this research proved the developed optical scanning system performed equally as well as the ultrasonic system when grading veneer and predicting LVL tensile mechanical properties. Furthermore, when combined with existing ultrasonic veneer grading information, the developed combined system (ultrasonic and optical) resulted in improved veneer grading and LVL mechanical property predictions.

Furthermore, utilization of an optical system could likely benefit LVL manufacturers in other ways in terms of sorting LVL material. For example, LVL billets are typically made in widths of 4-foot and vary in length, as many processes allow for manufacturing continuous length LVL. Current ultrasonic grading provides an average prediction of the 4-foot wide by "x" length LVL properties. When making a final product, the LVL billet is cut further into smaller width pieces. The resulting pieces are assumed to be equivalent to the average value of the LVL billet from which they were processed. Rather than using the average properties from the billet, sorting processed LVL material based on optical measures contained within the smaller piece could result in better predictions of LVL properties and improved sorting and grading.

A second benefit of using optically determined information would be when a production run is downgraded due to results of quality control sample testing. It is likely not all the material cut from the billets possessed poor strength values for the intended grade. Rather than downgrading the whole production run, further sorting could be performed by using the optical system measures and LVL predictions. The downgraded material could be sorted into different groups based on optical system measurements and predicted LVL properties and re-tested. The likely result would be that much of the processed LVL pieces would meet the original intended properties.

CHAPTER 8 CONCLUSIONS AND FUTURE RESEARCH RECOMMENDATIONS

This study investigated various non-destructive evaluation (NDE) techniques in an attempt to improve Douglas-fir veneer and laminated veneer lumber (LVL) tensile modulus of elasticity (MOE) and strength (F_t) property predictions. The NDE techniques investigated included veneer density, optical scanning, ultrasonic stress wave, and an integrated optical and ultrasonic system. The optical scanning system was developed by using existing equipment to acquire veneer images which were then analyzed for quantifying various veneer characteristics. The ultrasonic stress wave system used was a commercially available system which uses the same principles to grade veneer at a production facility. The ultrasonic system also consisted of a second component which was developed during this study for capturing and analyzing waveforms generated by the commercially available equipment when testing veneer. Additionally, the combined system utilized information obtained from the optical and ultrasonic systems and investigated any improvements resulting by combining these methods.

Non-destructive and destructive testing of veneer was performed to develop nine different prediction models for both veneer tensile MOE and F_t. One prediction model was based solely on density. The remaining prediction models were from the optical system (four models), ultrasonic (three models), and combined optical and ultrasonic system (one model). The reliability of each prediction model was then evaluated by performing non-destructive and destructive testing on a second set of

veneer and comparing predicted versus experimental results. Additionally, NDE was performed on a set of veneer which was used to manufacture LVL specimens. The reliability of each prediction model was then evaluated in terms of predicting LVL tensile MOE and F_t values.

8.1 Conclusions on Each System's Ability to Predict Veneer Tensile MOE and F_t

Based on the results of the veneer model development and validation studies, the following conclusions were made:

1. All models tested showed no statistically significant difference in average predicted veneer tensile MOE and F_t.
2. Many models performed equally well in predicting veneer static tensile MOE.
3. The basic optical model performed the worst in explaining the variation in veneer static tensile MOE.
4. The combined optical and ultrasonic system model best explained the variation in veneer static tensile MOE and F_t.
    - By combining information acquired by both the optical and ultrasonic system, improved tensile property prediction was achieved. As evident from the study's results, non-destructive evaluation (NDE) systems that did not rely solely or highly on density measurements were more reliable in predicting veneer tensile properties from one set of tests to the next. Specifically, in terms of veneer F_t, this suggests a combined system

grading approach may likely outperform the ultrasonic system utilizing solely density, MOE_d or UPT.

5. The optical scanning system appeared to be a viable means of grading veneer and resulted in improved prediction of veneer F_t values, as compared to current industrial practices.
    - The optical system was reliable in terms of correctly identifying and quantifying veneer characteristics that influence veneer tensile MOE and F_t properties. All optical models, performed equally well or better in explaining the variation in veneer static F_t values, as compared to the average MOE_d model. The optical model including growth ring pattern measures (no density included) was second best in explaining the variation in veneer static F_t, as compared to the average density and UPT models which performed the worst, respectively, in explaining the variation in veneer static F_t.
6. Improvement in the ultrasonic system for predicting veneer static tensile properties could be made by including measures obtained by spectral analysis of waveform data.
    - The ultrasonic model with spectral analysis included, was second and third best in explaining the variation in veneer static tensile MOE and F_t values, respectively. As a result, it was apparent the current industrial ultrasonic system of grading could benefit from inclusion of some specific spectral analysis measures.

7. The existing optical scanning systems used in production facilities were able to produce images of sufficient quality to quantify defect and other veneer measures on full-size veneer sheets.

8.2 Conclusions on Each System's Ability to Predict LVL Tensile MOE and F_t

Based on the results of the LVL study, the following conclusions were made:

1. Many developed models accurately predicted the average LVL MOE of the population tested, but none of the models performed well in terms of explaining the variation in LVL static tensile MOE.
    - The combined optical and ultrasonic model best predicted average LVL static tensile MOE. The poor results in explaining the variation in LVL static tensile MOE was likely due to LVL MOE being measured over a very small distance, rather than over the 24-inch length being tested.
2. Due to lamination effects, the calculated average of individually predicted veneers comprising a billet determined by each model performed poorly when predicting average LVL static F_t.
3. To account for the lamination effect, better results were obtained by using a linear regression of predicted values (average of individual veneers in a LVL specimen) for each model versus LVL static F_t values.
    - Under this scenario, models which included measures of average veneer properties, as compared to maximum and minimum values, performed the best. Specifically, the MOE_d model performed the best in terms of

explaining the variation of LVL static F_t values, followed closely by the combined system model. Because of the lamination effect, optical models which included measures of maximum defect properties, performed poorly when predicting LVL F_t. The optical model that included density measures, however, outperformed the UPT model, as the model did not include measures of maximum defect properties; rather it contained a measure of average defect width and volume.

4. LVL static F_t was best predicted by using overall average veneer measures comprising the entire LVL specimen, rather than averaging the individual veneer laminate predictions of F_t.
5. The combined systems model which included average optical, growth ring pattern, and MOE_d measures comprising an LVL specimen, rather than predicted F_t of each individual veneer laminate, best explained the variation in LVL static F_t values as compared to all other models.
    - Results indicated LVL static F_t could best be predicted by combining average MOE_d and optical values together. This finding suggests improved LVL F_t predictions could be achieved by integrating the existing ultrasonic and optical systems found in many manufacturing facilities.
6. The optical system, which included average measures of density and specific defect and growth ring pattern measures comprising and LVL specimen, showed promise as an improved means of grading veneer for use in LVL, as compared to current systems based only on average MOE_d or average UPT.

- Development of optical system prediction equations by averaging all measured defect and growth ring patterns within a given LVL specimen, rather than using individual veneer predictions, resulted in the second best predictor of LVL static F_t values. Under this scenario, the optical system outperformed the MOE_d model. Specifically, the optical model which included average defect, growth ring, and density measurements within a LVL specimen better explained the variation in LVL static F_t values, as compared to the MOE_d and UPT model. Additionally, this model outperformed average MOE_d values obtained by non-destructive ultrasonic testing on the actual LVL specimens when predicting LVL static F_t.

8.3 Conclusions on Implications for Veneer and LVL Manufacturers

It was evident that inclusion of optically determined measures improved the prediction of both veneer and LVL tensile MOE and F_t values. By including measures determined by the optical system with density and ultrasonic information (i.e., combined system), improvements could be made in veneer grading and LVL property predictions. By using an optical system to locate and quantify veneer measures, manufacturers of veneer composites (LVL and plywood) could improve final product properties. Specifically, by knowing the location and influence of specific veneer defects and characteristics, manufacturers would be able to make better decisions in regard to veneer selection and placement within a composite. By using information

acquired with an optical scanning system, manufacturers could better select and orient veneers in a manner which maximizes product strength performance.

Furthermore, use of an optical system would likely benefit LVL manufacturers when processing large LVL billets into smaller final products. Better prediction of LVL grades may be achievable by using prediction equations based on optical and density and/or combined optical and ultrasonic properties of the final cut to size product, rather than average full-size billet property predictions. Additionally, the optical including density prediction models may likely allow manufactures to sort LVL material from a downgraded production run into different groups. Further quality control sample testing may then likely result in much of the processed LVL pieces meeting the original intended mechanical properties and grade designation.

8.4 Recommendations for Future Research

The developed optical system showed potential as being an improved method for individually grading veneer and predicting LVL tensile properties. It was evident that inclusion of optically determined measures with current ultrasonic veneer grading information likely would improve veneer grading. While this study focused on research using smaller veneer specimens than typically used in manufacturing LVL, further research is needed to determine how optically obtained information influences full-size veneer sheet properties. In doing so, maximum defect measures found influential in determining individual veneer strength properties may not be as

significant in terms of full-size veneer sheet properties. This would likely result in better prediction of LVL mechanical properties when using an optical system.

To fully utilize an optical system as a means to grade veneer, more research is needed to quantify growth ring pattern angles and diving grain, rather than the image pixel color summation approach used in this study. A quantified measure of growth ring pattern angle and diving grain would likely result in better prediction of veneer and LVL mechanical properties. One possible method for locating and quantifying diving grain within veneer would be to image both surfaces of the veneer. Once images of both sides were obtained, differences in growth ring pattern between the top and bottom (i.e., tight and loose side) could be analyzed. Given the relatively thin nature of veneer, areas with very similar growth ring patterns at the same location on both veneer sides could indicate areas with diving grain. Additionally, further research is needed to determine if latewood percentage measured on full-size veneer sheets is a better indicator of overall veneer density. While density alone was not the best predictor of veneer and LVL properties, it was significant in many of the prediction equations.

Finally, further research is needed to determine prediction equations for other LVL mechanical properties. Research on full-size sheets would allow for prediction of individual veneer properties via optical methods. Following this, full-size LVL billets could be manufactured and specimens could be prepared to test for edge and flat-wise bending, tension, and shear. Then, optically determined measures could be studied to see if they perform well in predicting various destructively determined LVL properties. It is likely defects may play a more important role in outer LVL layers in

bending specimens, rather than tension specimens. The optical system would then allow for better identifying influential veneer defect measures and likely provide an improved means of sorting veneer for outer LVL layers.

BIBLIOGRAPHY

American Society for Testing and Materials. 2007. Standard Test Methods for Direct Moisture Content Measurement of Wood and Wood-Base Material. D4442-07 (2007). Ann. Book of Standards, Section 4, Vol. 04-10. ASTM, West Conshohocken, PA.

American Society for Testing and Materials. 2005. Standard Test Methods for Mechanical Properties of Lumber and Wood-Base Structural Material. D4761-05 (2005). Ann. Book of Standards, Section 4, Vol. 04-10. ASTM, West Conshohocken, PA.

American Society for Testing and Materials. 2003. Standard Practice for Evaluating Allowable Properties for Grades of Structural Lumber. D2719-03 (2003). Ann. Book of Standards, Section 4, Vol. 04-10. ASTM, West Conshohocken, PA.

American Society for Testing and Materials. 2003. Standard Test Methods for Structural Panels in Tension. D3500-90 (2003). Ann. Book of Standards, Section 4, Vol. 04-10. ASTM, West Conshohocken, PA.

Barnes, D. 2000. An integrated model of the effect of processing parameters on the strength properties of oriented strand wood products. Forest Prod. J. 50(11/12):33-42.

Beall, F.C. 1996. Application of ultrasonic technology to wood and wood-based materials. Second International Conference on the Development of Wood Science/Technology and Forestry. Hungary. 10pp.

Beall, F.C. 2002. Overview of the use of ultrasonic technologies in research on wood properties. Wood Science and Technology 36(2002):197-212.

Bejo, L. and E.M. Lang. 2004. Simulation based modeling of the elastic properties of structural composite lumber. Wood Fiber Sci. 36(3):395-410.

Berndt, H., A.P. Schniewind, and G.C. Johnson. High resolution ultrasonic imaging of wood. Wood Science and Technology 38(1999):185-198.

Berthholf, L.D. 1965. Use of elementary stress wave theory for prediction of dynamic strain in wood. Washington State Institute of Technology, Bulletin 291. Washington State University, Pullman, WA.

Biernacki, J.M. and F.C. Beall. 1993. Development of an acousto-ultrasonic scanning system for nondestructive evaluation of wood and wood laminates. Wood Fiber Sci. 23(5):289-297.

Boardman, B.E., J.F. Senft, G.P. McCabe, and C.M. Ladisch. 1992. Colorimetric analysis in grading black walnut veneer. Wood Fiber Sci. 24(1):99-107.

Bodig, J. 2000. The process of NDE research for wood and wood composites. In: Proceedings, 12th international symposium on nondestructive testing of wood. 2000 September 13-15, University of Western Hungary, Sopron. Sopron, Hungary: University of Western Hungary: 7-22.

Bodig, J. and B.A. Jayne. 1992. Mechanics of Wood and Wood Composites. Reprint ed. Krieger Publishing Company, Malabar, Florida. 712pp.

Brashaw, B.K., R.J. Ross, and R.F. Pellerin. 1996. Stress wave nondestructive evaluation of green veneer: southern pine and Douglas fir. In: Nondestructive Evaluation of Materials and Composites. Steve Doctor, Carol A. Lebowitz, George Y. Baaklini, Editors. Proc. SPIE 2944. 296-306.

Brashaw, B.K., X. Wang, R.J. Ross, and R.F. Pellerin. 2004. Relationship between stress wave velocities of green and dry veneer. Forest Prod. J. 54(6):85-89.

Brunner, C.C., G.B. Shaw, D.A. Butler, and J.W. Funck. 1990. Using color in machine vision systems for wood processing. Wood Fiber Sci. 22(4):413-428.

Brunner, C.C., A.G. Maristany, D.A. Butler, D. VanLeeuwen, and J.W. Funck. 1992. An evaluation of color spaces for detecting defects in Douglas-fir veneer. Industrial Metrology 2(1992):169-184.

Burmester, A. 1967. Detection of knots in pinewood by ultrasonics. Holz Als Roh- Und Werkstoff 25(4):157-163.

Butler, D.A., C.C. Brunner, and J.W. Funck. 2001. Wood-surface classification using extended-color information. Holz als Roh- und Werkstoff 59(2001):475-482.

Butler, D.A., C.C. Brunner, and J.W. Funck. 2002. Wood-surface feature classification via extended-color imagery. Forest Prod. J. 52(6):80-84.

Chang, S.J., J.R. Olsen, and P.C. Wang. 1989. NMR imaging of internal features in wood. Forest Prod. J. (39)6:43-49.

Forest Products Laboratory. 1999. Wood handbook—Wood as an engineering material. Gen. Tech. Rep. FPL–GTR–113. Madison, WI: U.S. Department of Agriculture, Forest Service, Forest Products Laboratory. 463pp.

Fuller, J.J., R.J. Ross and J.R. Dramm. 1994. Honeycomb and surface check detection using ultrasonic nondestructive evaluation. Research Note FPL-RN-0261. U.S. Department of Agriculture Forest Product Laboratory, Madison, WI.

Fuller, J.J., R.J. Ross and J.R. Dramm. 1995. Nondestructive evaluation of honeycomb and surface checks in red oak lumber. Forest Prod. J. (45)5:413-416.

Funck, J.W., C.C. Brunner, and D.A. Butler. 1991. Softwood veneer defect detection using machine vision. Pages 113 to 120. In: Proceedings of the Process Control/Production Management of Wood Products: Technology for the 90's Symposium. Southeastern Section Annual Meeting, Athens, GA. Forest Products Research Society, Madison, WI. Oct. 30 - Nov. 1, 1990.

Galligan, W.L. and R.W. Courteau. 1965. Measurement of elasticity of lumber with longitudinal stress waves and the piezoelectric effect of wood. 1965 April. Spokane, WA. Pullman, WA. Washington State University:223-244.

Gerhards, C.C. 1975. Stress wave speed and MOE of sweetgum ranging from 150 to 15 percent MC. Forest Prod. J. 25(4):51-57.

Gerhards, C.C. 1982a. Effect of knots on stress waves in lumber. Research Paper FPL-RP-384. U.S. Department of Agriculture Forest Product Laboratory, Madison, WI.

Gerhards, C.C. 1982b. Longitudinal stress waves for lumber stress grading: factors affecting applications: state of the art. Forest Prod. J. 32(2):20-25.

Green, D.W., R.F. Pellerin, J.W. Evans, and D.E. Kretschmann. 1990. Moisture content and tensile strength of Douglas Fir dimension lumber. Res. Pap. FPL-RP-497. Madison, WI, U.S. Department of Agriculture, Forest Service, Forest Products Laboratory, 1990. 33pp.

Hoover, W.L., J.M. Ringe, C.A. Eckelman, and J.A. Youngquist. 1988. Design and specification of hardwood laminated-veneer-lumber for furniture applications. Forest Prod. J. 38(1):31-34.

Hunt, M.O., M.H. Triche, G.P. McCabe, anb W.L. Hoover. 1989. Tensile properties of yellow-poplar veneer strands. Forest Prod. J. 39(9):31-33.

James, W.J. 1961. Effect of temperature and moisture content on internal friction and speed of sound in Douglas-fir. Forest Prod. J. 11(9):383-390.

James, W.L. 1964. Vibration, static strength, and elastic properties of clear Douglas-fir at various levels of moisture content. Forest Prod. J. 14(9):409-413.

Jayne, B.A. 1959. Indices of quality. Vibrational properties of wood. Forest Prod. J. 9(11):413-416.

Jung, J. 1979. Stress-wave grading techniques on veneer sheets. General Technical Report FPL-GTR-27. U.S. Department of Agriculture Forest Product Laboratory, Madison, WI.

Jung, J. 1982. Properties of parallel-laminated veneer from stress-wave-tested veneers. Forest Prod. J. 32(7):30-35.

Kaiserlik, J.H., and R.F. Pellerin. 1977. Stress wave attenuation as an indicator of lumber strength. Forest Prod. J. 27(6):39-43.

Kang, H. and R.E. Booker. 2002. Variation of stress wave velocity with MC and temperature. Wood Science and Technology. 36(2002):40-54.

Kawamoto, S. and R. Sam. Williams. 2002. Acoustic emissions and acousto-ultrasonic techniques for wood and wood-based composites. A review. General Technical Report FPL-GTR-134. U.S. Department of Agriculture Forest Product Laboratory, Madison, WI.

Kimmel, J.D. and J.J. Janowiak. 1995. Red maple and yellow-poplar LVL from ultrasonically rated veneer. Forest Prod. J. 45(7/8):54-58.

Koch, P. and G.E. Woodson. 1968. Laminating butt-jointed, long-run southern pine veneers into long beams of uniform high strengths. Forest Prod. J. 18(10):45-51.

Kunesh, R.H. 1978a. Micro=Lam: Structural laminated veneer lumber. Forest Prod. J. 28(7):41-44.

Kunesh, R.H. 1978b. Using ultrasonic energy to grade veneer. In: Proceedings, 4th symposium on nondestructive testing of wood. 1978 August 28-30. Vancouver, WA. Pullman, WA: Washington State University:275-278.

Lang, E.M., L. Bejo, F. Divos, Z. Kovacs, and R.B. Anderson. 2003. Orthotropic strength and elasticity of hardwoods in relation to composite manufacture. Part III: Orthotropic elasticity of structural veneers. Wood Fiber Sci. 35(2):308-320.

Lebow, P.K., C.C. Brunner, A.G. Maristany, and D.A. Butler. 1996. Classification of wood surface features by spectral reflectance. Wood Fiber Sci. 28(1):74-90.

Lee, J.N., R.C. Tang, and J. Kaiserlik. 1999. Edgewise static bending properties of yellow-poplar laminated veneer lumber: Effect of veneer-joint design. Forest Prod. J. 49(7/8):64-70.

Lee, J.N., R.C. Tang, and J. Kaiserlik. 2001. Nondestructive evaluation of modulus of elasticity of yellow-poplar LVL: Effect of veneer-joint design and relative humidity. Wood Fiber Sci. 33(4):510-521.

Logan, J.D. 1978. Machine stress rating. In: Proceedings, 4th symposium on nondestructive testing of wood. 1978 August 28-30. Vancouver, WA. Pullman, WA. Washington State University:285-303.

Logan, J.D. 2000. Machine sorting of wood veneer for structural LVL applications. In: Proceedings, 34th International Particleboard/Composite Materials Symposium. 2000, April 4-6. Pullman, WA. Washington State University:67-77.

Marra, G.G., R.F. Pellerin and W.L. Galligan. 1966. Nondestructive determination of wood strength and elasticity by vibration. Holz als Rohund Werkstoff. October 1966:460:466.

McAlister, R.H. 1976. Modulus of elasticity distribution of loblolly pine veneer as related to location within the stem and specific gravity. Forest Prod. J. 26(10):37-40.

McAlister, R.H. 1982. MOE and tensile strength distribution of veneer of four commercially imported southeastern hardwoods. COM-PLY Rept. 23. USDA Forest Service, Southeastern Forest Expt. Sta., Asheville, N.C.
McDonald, K.A. 1978. Lumber defect detection by ultrasonics. Research Paper FPL-RP-311. U.S. Department of Agriculture Forest Product Laboratory, Madison, WI.

Meder, R., A.Thumm, and H. Bier. 2002. Veneer stiffness predicted by NIR spectroscopy calibrated using mini-LVL test panels. Holz als Roh-und Werkstoff 60(2002):159-164.

NIST. 2007. Voluntary Product Standard PS 1-07, Structural Plywood. National Institute of Standards and Technology, Technology Administration, U.S. Department of Commerce, Gaithersburg, MD. 52pp.

Panshin, A.J. and P. deZeeuw. 1964. Textbook of Wood Technology - Vol. I. New York: McGraw-Hill Inc., p.187.

Pellerin, R.F. 1965. A vibrational approach to nondestructive testing of structural lumber. Forest Prod. J. XV(3):93-101.

Pellerin, R.F. and W.L. Galligan. 1973. Nondestructive method of grading wood materials. Canadian Patent No. 918286.

Pellerin, R.F. and R.J. Ross, eds. 2002. Nondestructive evaluation of wood. Forest Products Society, Madison, WI. 129pp.

Pieters, A.R. 1979. Ultrasonic energy: a new method for veneer grading. ASCE convention and exposition. Preprint. 1979, April 2-6. Boston, MA:17pp.

Preston, S.B. 1950. Beam strength as affected by placement of laminae. Forest Prod. J. Proc. Forest Prod. Res. Soc. (4):228-240.

Pu, J. and R.C. Tang. 1997. Nondestructive evaluation of modulus of elasticity of southern pine LVL: Effect of veneer grad and relative humidity. Wood Fiber Sci. 29(3):249-263.

Ross, R.J. 1985. Stress wave propagation in wood products. In: Proceedings, 5th Nondestructive testing of wood symposium. 1985 September 9-11. Pullman, WA. Pullman, WA:Washington State University:291-318.

Ross, R.J. and R.F. Pellerin. 1988. NDE of wood-based composites with longitudinal stress waves. Forest Prod. J. 38(5):39-45.

Ross, R.J. and R.F. Pellerin. 1994. Nondestructive testing for assessing wood members in structures. General Technical Report FPL-GTR-70. U.S. Department of Agriculture Forest Product Laboratory, Madison, WI.

Ross, R.J., B.K. Brashaw, and R.F. Pellerin. 1998. Nondestructive evaluation of wood. Forest Prod. J. 48(1):14-19.

Ross, R.J., J.R. Erickson, B.K. Brashaw, X. Wang, S.A. Verhey, J.W. Forsman, and C.L. Pilon. 2004. Yield and ultrasonic modulus of elasticity of red maple veneer. Forest Prod. J. 54(12):220-225.

Sakai, H., A. Minanisawa, and K. Takagi. 1990. Effect of moisture content on ultrasonic velocity and attenuation in woods. Ultrasonics. 28(November):382-385.

Schmidt, T. 1978. Scanning/computing methods for measuring knots and other defects in lumber and veneers. In: Proceedings, 4th symposium on nondestructive testing of wood. 1978 August 28-30. Vancouver, WA. Pullman, WA: Washington State University:23-25.

Serrano, E., P.J. Gustafsson, and H.J. Larsen. 1996. Lamination effect and finger joints analysed by fracture mechanics. In: Proceedings, International Wood Engineering Conference. Vol. 4. Oct. 28-31, 1996. New Orleans, LA. pp. 295-302.

Sharp, D.J. 1985. Non-destructive testing techniques for manufacturing LVL and predicting performance. In: Proceedings, 5th symposium on nondestructive testing of wood. 1985 September 9-11. Pullman, WA. Pullman, WA: Washington State University:99-108.

Uskoski, D.A. and F.K. Bechtel. 1993. Ultrasonic stress graded veneer. In: Proceedings, The international panel and engineered-wood technology exposition. 1993, October 19-21. Atlanta, GA:9pp.

Wang, J., J.M. Biernacki and F. Lam. 2001. Nondestructive evaluation of veneer quality using acoustic wave measurements. Wood Science and Technology 34(2001):505-516.

Wang, P.C. and S.J. Chang. 1986. Nuclear magnetic resonance imaging of wood. Wood Fiber Sci. 18(2):308-314.

Wang, X., R.J. Ross, B.K. Brashaw, S.A. Verhey, J.W. Forsman, and J.R. Erickson. Flexural properties of laminated veneer lumber manufactured from ultrasonically rated red maple veneer. Research Note FPL-RN-0288. U.S. Department of Agriculture Forest Product Laboratory, Madison, WI.

APPENDICES

Appendix A. Model Development Study:

Individual Veneer Tension Test Results

Cross Correlation Between Basic Optical, Growth Ring Pattern, Basic Ultrasonic, and Veneer Static Tensile MOE and F_t Values

And

Cross Correlation Between Defect and Waveform Measures

Table A-1. Individual veneer static tension MOE and F_t test results from model development study.

Veneer Tension Test Results - Model Development Study									
Specimen Number	**Width (inch)**	**Length (inch)**	**Thickness (inch)**	**Weight (g)**	**Slope (lbf/in)**	**Pmax (lbf)**	**Density (lb/ft^3)**	**MOE (lbf/in^2)**	**F_t (lbf/in^2)**
53a	6.148	31.000	0.128	235.3	190,077	2,352	36.8	2,178,218	2,995
53b	6.123	31.000	0.128	229.0	190,032	2,266	35.8	2,178,072	2,886
53c	6.138	31.000	0.132	232.1	137,242	1,327	35.3	1,530,297	1,644
53d	6.157	31.000	0.126	228.1	146,804	3,106	36.3	1,709,888	4,020
53e	6.139	31.000	0.125	219.7	185,779	6,692	35.3	2,187,736	8,756
53f	6.126	31.000	0.129	227.4	161,089	2,308	35.5	1,841,639	2,932
139a	6.096	31.000	0.134	195.1	121,650	1,988	29.3	1,337,814	2,429
139b	6.070	31.000	0.138	200.0	130,131	1,561	29.3	1,398,074	1,863
139c	6.110	31.000	0.130	190.4	135,294	2,068	29.5	1,536,020	2,609
139d	6.085	31.000	0.134	196.5	212,593	2,175	29.7	2,355,320	2,677
139e	6.115	31.000	0.124	205.9	156,717	2,294	33.3	1,856,372	3,019
139f	6.077	31.000	0.129	179.6	108,060	1,463	28.2	1,243,069	1,870
126a	6.127	31.000	0.128	183.3	139,125	1,905	28.8	1,599,791	2,434
126b	6.075	31.000	0.126	190.6	129,644	928	30.6	1,527,272	1,215
126c	6.121	31.000	0.127	192.6	150,678	1,629	30.6	1,751,371	2,104
126d	6.110	31.000	0.123	184.1	113,151	1,305	30.2	1,357,807	1,740
126e	6.098	31.000	0.125	199.1	160,957	1,726	32.0	1,896,754	2,260
126f	6.102	31.000	0.132	201.2	153,152	1,694	30.7	1,714,514	2,107
8a	6.158	31.000	0.128	195.3	167,399	1,219	30.6	1,918,763	1,552
8b	6.152	31.000	0.132	186.3	109,950	1,610	28.2	1,218,500	1,982
8c	6.159	31.000	0.131	194.2	144,878	2,808	29.6	1,616,084	3,480
8d	6.148	31.000	0.131	197.4	94,696	960	30.2	1,062,258	1,197
8e	6.134	31.000	0.131	182.9	164,307	2,481	28.1	1,847,432	3,100
8f	6.118	31.000	0.128	193.0	158,378	2,161	30.3	1,820,192	2,760
16a	6.126	31.000	0.132	214.1	166,301	2,506	32.5	1,850,916	3,099
16b	6.115	31.000	0.135	214.7	169,097	2,819	31.9	1,843,416	3,415
16c	6.128	31.000	0.135	220.8	100,926	1,137	32.7	1,096,005	1,372
16d	6.142	31.000	0.122	201.1	150,072	1,265	32.9	1,798,897	1,685
16e	6.133	31.000	0.131	205.1	122,532	1,797	31.3	1,369,920	2,232
16f	6.134	31.000	0.135	216.2	154,767	2,945	32.1	1,682,155	3,557
49a	6.156	31.000	0.129	245.2	216,229	4,243	38.0	2,455,332	5,353
49b	6.144	31.000	0.131	239.8	167,117	3,028	36.7	1,875,868	3,777
49c	6.101	31.000	0.118	235.1	213,799	5,235	40.2	2,678,326	7,287
49d	6.169	31.000	0.124	239.0	231,646	5,436	38.4	2,725,546	7,107
49e	6.150	31.000	0.125	240.4	232,725	5,041	38.5	2,730,050	6,571
49f	6.164	31.000	0.122	234.5	268,910	5,797	38.2	3,211,719	7,693
60a	6.122	31.000	0.127	190.8	134,135	1,460	30.1	1,552,619	1,878
60b	6.125	31.000	0.126	182.5	123,767	1,888	29.0	1,440,483	2,442
60c	6.102	31.000	0.129	179.9	90,998	1,420	28.0	1,038,478	1,801
60d	6.109	31.000	0.129	183.6	123,122	1,754	28.6	1,406,033	2,226

Table A-1 (continued). Individual veneer static tension MOE and F_t test results from model development study.

Veneer Tension Test Results - Model Development Study (continued)									
Specimen Number	**Width (inch)**	**Length (inch)**	**Thickness (inch)**	**Weight (g)**	**Slope (lbf/in)**	**Pmax (lbf)**	**Density (lb/ft^3)**	**MOE (lbf/in^2)**	**F_t (lbf/in^2)**
60e	6.113	31.000	0.129	185.7	127,207	2,071	28.9	1,451,807	2,626
60f	6.107	31.000	0.128	192.4	144,482	2,118	30.4	1,669,912	2,720
125a	6.097	31.000	0.141	216.9	135,595	2,413	30.9	1,417,118	2,802
125b	6.077	31.000	0.136	211.9	154,448	1,575	31.6	1,688,188	1,913
125c	6.089	31.000	0.132	192.6	117,542	1,265	29.4	1,313,768	1,571
125d	6.106	31.000	0.133	205.8	166,276	1,528	31.1	1,839,183	1,878
125e	6.083	31.000	0.134	200.4	147,337	2,128	30.2	1,626,702	2,611
125f	6.067	31.000	0.136	189.0	71,209	957	28.1	775,341	1,158
98a	6.208	31.000	0.135	221.6	172,211	3,444	32.5	1,849,342	4,109
98b	6.212	31.000	0.143	220.3	186,861	1,927	30.4	1,889,884	2,165
98c	6.155	31.000	0.134	222.0	142,185	2,456	33.2	1,557,353	2,989
98d	6.187	31.000	0.142	217.9	122,714	1,201	30.5	1,259,243	1,369
98e	6.201	31.000	0.136	221.2	128,913	2,501	32.3	1,380,900	2,977
98f	6.186	31.000	0.140	224.5	196,566	5,498	31.8	2,042,849	6,349
44a	6.138	31.000	0.126	235.8	170,962	1,924	37.4	1,985,454	2,483
44b	6.161	31.000	0.127	232.7	181,792	2,855	36.7	2,099,192	3,663
44c	6.174	31.000	0.135	255.5	213,667	3,110	37.8	2,315,877	3,745
44d	6.144	31.000	0.130	232.2	165,904	1,154	35.7	1,869,510	1,445
44e	6.131	31.000	0.129	244.8	225,997	4,269	38.2	2,581,868	5,419
44f	6.157	31.000	0.126	236.6	176,372	2,837	37.4	2,042,187	3,650
96a	6.125	31.000	0.128	199.6	117,828	1,169	31.3	1,355,336	1,494
96b	6.143	31.000	0.129	217.9	182,084	1,011	33.8	2,067,969	1,276
96c	6.142	31.000	0.124	216.0	184,222	1,657	34.9	2,181,488	2,180
96d	6.139	31.000	0.136	201.6	106,658	1,542	29.8	1,154,045	1,854
96e	6.151	31.000	0.137	220.1	229,403	3,236	32.1	2,449,914	3,840
96f	6.143	31.000	0.132	232.4	215,292	1,607	35.3	2,398,767	1,989
74a	6.163	31.000	0.126	218.1	117,018	1,985	34.4	1,353,536	2,551
74b	6.101	31.000	0.134	227.5	133,576	3,146	34.2	1,470,419	3,848
74c	6.173	31.000	0.131	226.4	204,214	3,934	34.5	2,277,143	4,874
74d	6.170	31.000	0.133	236.7	202,217	2,182	35.4	2,217,802	2,659
74e	6.159	31.000	0.132	224.1	207,355	3,966	33.9	2,295,480	4,878
74f	6.149	31.000	0.132	226.8	203,107	2,985	34.3	2,247,851	3,671
150a	6.081	31.000	0.131	197.3	128,495	1,352	30.4	1,449,034	1,694
150b	6.069	31.000	0.131	187.9	113,221	2,061	29.0	1,279,176	2,587
150c	6.097	31.000	0.135	213.8	179,065	3,866	31.9	1,954,447	4,688
150d	6.098	31.000	0.137	211.5	177,987	2,845	31.0	1,913,951	3,399
150e	6.074	31.000	0.130	184.5	90,121	1,949	28.7	1,027,245	2,468
150f	6.089	31.000	0.136	209.1	183,406	2,416	31.1	2,000,760	2,928
38a	6.126	31.000	0.122	187.7	123,899	1,147	30.9	1,495,156	1,538
38b	6.132	31.000	0.120	188.0	177,822	2,330	31.3	2,170,517	3,160

Table A-1 (continued). Individual veneer static tension MOE and F_t test results from model development study.

Veneer Tension Test Results - Model Development Study (continued)									
Specimen Number	**Width (inch)**	**Length (inch)**	**Thickness (inch)**	**Weight (g)**	**Slope (lbf/in)**	**Pmax (lbf)**	**Density (lb/ft^3)**	**MOE (lbf/in^2)**	**F_t (lbf/in^2)**
38c	6.151	31.000	0.125	179.4	162,404	2,952	28.8	1,908,639	3,855
38d	6.128	31.000	0.124	185.6	137,952	1,995	30.1	1,637,213	2,631
38e	6.126	31.000	0.109	180.9	131,196	1,085	33.4	1,772,287	1,629
38f	6.167	31.000	0.123	177.9	185,260	2,902	28.8	2,193,515	3,818
42a	6.131	31.000	0.124	207.5	174,802	2,103	33.5	2,065,191	2,761
42b	6.136	31.000	0.119	209.8	204,789	1,550	35.4	2,529,476	2,127
42c	6.153	31.000	0.121	205.0	180,767	2,811	33.8	2,180,805	3,768
42d	6.141	31.000	0.124	216.8	131,310	1,155	34.9	1,548,837	1,514
42e	6.146	31.000	0.121	213.2	210,150	3,714	35.1	2,538,038	4,984
42f	6.144	31.000	0.117	209.4	175,108	2,456	35.7	2,187,680	3,409
54a	6.138	31.000	0.132	211.8	185,379	931	32.1	2,059,219	1,149
54b	6.138	31.000	0.126	192.3	162,283	3,438	30.7	1,896,033	4,463
54c	6.145	31.000	0.124	190.6	140,774	2,244	30.7	1,659,472	2,939
54d	6.154	31.000	0.127	202.1	148,233	1,848	31.8	1,707,065	2,365
54e	6.154	31.000	0.132	209.2	115,801	1,575	31.8	1,287,935	1,946
54f	6.144	31.000	0.129	207.1	184,879	2,610	32.1	2,099,368	3,293
194a	6.113	31.000	0.131	181.4	132,176	435	27.9	1,491,184	545
194b	6.106	31.000	0.134	195.4	155,925	1,809	29.3	1,715,128	2,211
194d	6.114	31.000	0.138	196.4	138,694	1,403	28.6	1,479,516	1,663
194e	6.091	31.000	0.133	189.6	157,502	1,726	28.8	1,749,900	2,131
194f	6.100	31.000	0.134	185.8	107,870	1,190	27.9	1,187,764	1,456
196a	6.117	31.000	0.132	190.3	142,589	2,068	29.0	1,589,247	2,561
196b	6.147	31.000	0.135	203.8	75,871	1,175	30.2	822,855	1,416
196c	6.108	31.000	0.134	200.7	140,621	2,171	30.1	1,543,399	2,648
196d	6.123	31.000	0.131	185.5	131,242	1,676	28.4	1,469,699	2,085
196f	6.102	31.000	0.132	200.2	102,402	1,582	30.5	1,142,049	1,960
Average	6.130	31.000	0.130	207.5	156,313	2,283	32.1	1,776,568	2,884
St. Deviation	0.031	0.000	0.006	18.8	37,805	1,146	3.0	447,488	1,481
COV %	0.5	0.0	4.3	9.0	24.2	50.2	9.4	25.2	51.4
Minimum	6.067	31.000	0.109	177.9	71,209	435	27.9	775,341	545
Maximum	6.212	31.000	0.143	255.5	268,910	6,692	40.2	3,211,719	8,756
Range	0.145	0.000	0.035	77.6	197,700	6,257	12.3	2,436,378	8,211

Table A-2. Cross correlation table (correlation and p-values) for variables 1-7.

	Veneer Tensile MOE	Veneer F_t	Veneer Density	Average UPT	Minimum UPT	Maximum UPT	Average MOE_d
Veneer Tensile MOE	1.000 0.000	0.681 0.000	0.697 0.000	-0.583 0.000	-0.523 0.000	-0.520 0.000	0.780 0.000
Veneer F_t	0.681 0.000	1.000 0.000	0.561 0.000	-0.505 0.000	-0.444 0.000	-0.472 0.000	0.670 0.000
Veneer Density	0.697 0.000	0.561 0.000	1.000 0.000	-0.398 0.000	-0.378 0.000	-0.325 0.001	0.866 0.000
Average UPT	-0.583 0.000	-0.505 0.000	-0.398 0.000	1.000 0.000	0.860 0.000	0.897 0.000	-0.792 0.000
Minimum UPT	-0.523 0.000	-0.444 0.000	-0.378 0.000	0.860 0.000	1.000 0.000	0.672 0.000	-0.710 0.000
Maximum UPT	-0.520 0.000	-0.472 0.000	-0.325 0.001	0.897 0.000	0.672 0.000	1.000 0.000	-0.697 0.000
Average MOE_d	0.780 0.000	0.670 0.000	0.866 0.000	-0.792 0.000	-0.710 0.000	-0.697 0.000	1.000 0.000
Minimum MOE_d	0.745 0.000	0.658 0.000	0.784 0.000	-0.793 0.000	-0.644 0.000	-0.828 0.000	0.953 0.000
Maximum MOE_d	0.749 0.000	0.628 0.000	0.888 0.000	-0.692 0.000	-0.753 0.000	-0.549 0.000	0.960 0.000
St. Deviation of MOE_d	-0.032 0.744	-0.107 0.274	0.152 0.119	0.233 0.016	-0.160 0.102	0.578 0.000	-0.039 0.691
Latewood Percentage - Single Threshold	0.023 0.812	0.045 0.647	0.229 0.018	-0.005 0.958	0.017 0.860	0.007 0.943	0.150 0.125
Latewood Percentage - Dual Threshold Green + Black	0.078 0.426	0.178 0.067	0.178 0.068	-0.103 0.292	-0.032 0.748	-0.113 0.249	0.163 0.094
Latewood Percentage - Dual Threshold Black	0.336 0.000	0.390 0.000	0.310 0.001	-0.174 0.074	-0.070 0.475	-0.204 0.036	0.317 0.001
Latewood Percentage - Dual Threshold Green	-0.235 0.015	-0.162 0.097	-0.083 0.398	0.042 0.668	0.030 0.763	0.059 0.546	-0.108 0.271
Defect Percentage	-0.356 0.000	-0.383 0.000	-0.037 0.706	0.274 0.004	0.137 0.162	0.358 0.000	-0.195 0.046
Number of Defects	-0.080 0.418	-0.134 0.172	-0.036 0.715	-0.023 0.818	-0.065 0.507	0.060 0.542	-0.040 0.684
Average Surface Area/Defect	-0.259 0.007	-0.357 0.000	-0.041 0.676	0.280 0.004	0.170 0.081	0.353 0.000	-0.190 0.051

Table A-2 (continued). Cross correlation table (correlation and p-values) for variables 1-7.

	Veneer Tensile MOE	Veneer F_t	Veneer Density	Average UPT	Minimum UPT	Maximum UPT	Average MOE_d
Maximum Defect Width	-0.391 0.000	-0.439 0.000	-0.090 0.361	0.379 0.000	0.265 0.006	0.462 0.000	-0.284 0.003
Minimum Defect Width	-0.041 0.675	-0.167 0.087	0.064 0.516	0.135 0.168	0.117 0.230	0.143 0.144	-0.031 0.750
Total Defect Width	-0.333 0.000	-0.347 0.000	0.002 0.987	0.267 0.006	0.162 0.097	0.351 0.000	-0.172 0.078
Average Defect Width	-0.311 0.001	-0.394 0.000	-0.008 0.931	0.366 0.000	0.269 0.005	0.437 0.000	-0.222 0.022
Total Defect Volume	-0.336 0.000	-0.287 0.003	0.005 0.963	0.235 0.015	0.131 0.181	0.286 0.003	-0.143 0.144
Maximum Defect Volume	-0.434 0.000	-0.412 0.000	-0.140 0.152	0.411 0.000	0.289 0.003	0.484 0.000	-0.323 0.001
Average Defect Volume	-0.317 0.001	-0.334 0.000	-0.029 0.769	0.401 0.000	0.292 0.002	0.458 0.000	-0.245 0.011
GRP E:Mean	0.318 0.001	0.257 0.008	0.574 0.000	-0.240 0.013	-0.276 0.004	-0.105 0.286	0.495 0.000
GRP E:St. Dev.	0.294 0.002	0.164 0.094	0.347 0.000	-0.238 0.014	-0.249 0.010	-0.196 0.044	0.356 0.000
GRP E:Max	0.317 0.001	0.221 0.023	0.455 0.000	-0.289 0.003	-0.287 0.003	-0.211 0.030	0.450 0.000
GRP E:Min	0.271 0.005	0.209 0.032	0.561 0.000	-0.220 0.024	-0.261 0.007	-0.079 0.421	0.474 0.000
GRP E:median	0.316 0.001	0.277 0.004	0.559 0.000	-0.228 0.019	-0.261 0.007	-0.088 0.367	0.478 0.000
GRP E90:Mean	0.318 0.001	0.257 0.008	0.574 0.000	-0.240 0.013	-0.276 0.004	-0.105 0.286	0.495 0.000
GRP E90:St. Dev.	-0.198 0.042	-0.255 0.008	0.171 0.079	0.105 0.285	0.040 0.681	0.133 0.173	0.038 0.696
GRP E90:Max	-0.019 0.849	-0.098 0.319	0.347 0.000	-0.046 0.641	-0.102 0.299	0.046 0.636	0.232 0.017
GRP E90:Min	0.393 0.000	0.345 0.000	0.515 0.000	-0.277 0.004	-0.295 0.002	-0.127 0.196	0.481 0.000
GRP E90:median	0.371 0.000	0.297 0.002	0.579 0.000	-0.275 0.004	-0.305 0.001	-0.139 0.154	0.521 0.000

Table A-3. Cross correlation table (correlation and p-values) for variables 8-14.

	Minimum MOE_d	Maximum MOE_d	St. Deviation of MOE_d	Latewood Percentage - Single Threshold	Latewood Percentage - Dual Threshold Green + Black	Latewood Percentage - Dual Threshold Black	Latewood Percentage - Dual Threshold Green
Veneer Tensile MOE	0.745 0.000	0.749 0.000	-0.032 0.744	0.023 0.812	0.078 0.426	0.336 0.000	-0.235 0.015
Veneer F_t	0.658 0.000	0.628 0.000	-0.107 0.274	0.045 0.647	0.178 0.067	0.390 0.000	-0.162 0.097
Veneer Density	0.784 0.000	0.888 0.000	0.152 0.119	0.229 0.018	0.178 0.068	0.310 0.001	-0.083 0.398
Average UPT	-0.793 0.000	-0.692 0.000	0.233 0.016	-0.005 0.958	-0.103 0.292	-0.174 0.074	0.042 0.668
Minimum UPT	-0.644 0.000	-0.753 0.000	-0.160 0.102	0.017 0.860	-0.032 0.748	-0.070 0.475	0.030 0.763
Maximum UPT	-0.828 0.000	-0.549 0.000	0.578 0.000	0.007 0.943	-0.113 0.249	-0.204 0.036	0.059 0.546
Average MOE_d	0.953 0.000	0.960 0.000	-0.039 0.691	0.150 0.125	0.163 0.094	0.317 0.001	-0.108 0.271
Minimum MOE_d	1.000 0.000	0.869 0.000	-0.308 0.001	0.124 0.207	0.155 0.113	0.324 0.001	-0.126 0.198
Maximum MOE_d	0.869 0.000	1.000 0.000	0.193 0.048	0.163 0.095	0.146 0.136	0.276 0.004	-0.090 0.361
St. Deviation of MOE_d	-0.308 0.001	0.193 0.048	1.000 0.000	0.090 0.357	-0.025 0.799	-0.103 0.292	0.071 0.470
Latewood Percentage - Single Threshold	0.124 0.207	0.163 0.095	0.090 0.357	1.000 0.000	0.773 0.000	0.507 0.000	0.476 0.000
Latewood Percentage - Dual Threshold Green + Black	0.155 0.113	0.146 0.136	-0.025 0.799	0.773 0.000	1.000 0.000	0.633 0.000	0.638 0.000
Latewood Percentage - Dual Threshold Black	0.324 0.001	0.276 0.004	-0.103 0.292	0.507 0.000	0.633 0.000	1.000 0.000	-0.192 0.049
Latewood Percentage - Dual Threshold Green	-0.126 0.198	-0.090 0.361	0.071 0.470	0.476 0.000	0.638 0.000	-0.192 0.049	1.000 0.000
Defect Percentage	-0.274 0.004	-0.101 0.301	0.357 0.000	0.403 0.000	0.155 0.114	-0.321 0.001	0.516 0.000
Number of Defects	-0.093 0.344	-0.015 0.881	0.187 0.055	0.186 0.056	0.040 0.682	-0.128 0.192	0.178 0.068
Average Surface Area/Defect	-0.267 0.006	-0.107 0.273	0.339 0.000	0.292 0.002	0.113 0.249	-0.189 0.053	0.331 0.001

Table A-3 (continued). Cross correlation table (correlation and p-values) for variables 8-14.

	Minimum MOE_d	Maximum MOE_d	St. Deviation of MOE_d	Latewood Percentage - Single Threshold	Latewood Percentage - Dual Threshold Green + Black	Latewood Percentage - Dual Threshold Black	Latewood Percentage - Dual Threshold Green
Maximum Defect Width	-0.367 0.000	-0.197 0.043	0.362 0.000	0.336 0.000	0.131 0.181	-0.252 0.009	0.417 0.000
Minimum Defect Width	-0.062 0.529	-0.001 0.990	0.128 0.192	-0.020 0.841	-0.023 0.815	-0.026 0.789	-0.003 0.976
Total Defect Width	-0.255 0.008	-0.094 0.340	0.333 0.000	0.367 0.000	0.159 0.103	-0.268 0.006	0.468 0.000
Average Defect Width	-0.307 0.001	-0.137 0.160	0.344 0.000	0.243 0.012	0.120 0.221	-0.183 0.061	0.334 0.000
Total Defect Volume	-0.199 0.040	-0.074 0.453	0.255 0.008	0.329 0.001	0.136 0.163	-0.294 0.002	0.466 0.000
Maximum Defect Volume	-0.396 0.000	-0.239 0.014	0.336 0.000	0.327 0.001	0.109 0.265	-0.288 0.003	0.425 0.000
Average Defect Volume	-0.323 0.001	-0.155 0.112	0.339 0.000	0.246 0.011	0.136 0.163	-0.144 0.140	0.317 0.001
GRP E:Mean	0.383 0.000	0.538 0.000	0.262 0.007	0.379 0.000	0.312 0.001	0.232 0.016	0.164 0.093
GRP E:St. Dev.	0.330 0.001	0.369 0.000	0.060 0.544	0.160 0.101	0.031 0.755	0.106 0.280	-0.066 0.499
GRP E:Max	0.396 0.000	0.463 0.000	0.113 0.248	0.325 0.001	0.165 0.090	0.172 0.077	0.038 0.697
GRP E:Min	0.354 0.000	0.524 0.000	0.301 0.002	0.444 0.000	0.386 0.000	0.240 0.013	0.251 0.009
GRP E:median	0.364 0.000	0.520 0.000	0.259 0.007	0.353 0.000	0.318 0.001	0.229 0.018	0.175 0.073
GRP E90:Mean	0.384 0.000	0.538 0.000	0.262 0.007	0.379 0.000	0.311 0.001	0.233 0.016	0.164 0.094
GRP E90:St. Dev.	0.002 0.987	0.092 0.346	0.183 0.060	0.371 0.000	0.106 0.278	-0.241 0.013	0.374 0.000
GRP E90:Max	0.149 0.126	0.286 0.003	0.252 0.009	0.414 0.000	0.234 0.016	-0.048 0.625	0.345 0.000
GRP E90:Min	0.365 0.000	0.508 0.000	0.251 0.009	0.245 0.011	0.251 0.009	0.271 0.005	0.049 0.620
GRP E90:median	0.411 0.000	0.558 0.000	0.241 0.013	0.354 0.000	0.320 0.001	0.286 0.003	0.121 0.218

Table A-4. Cross correlation table (correlation and p-values) for variables 15-21.

	Defect Percentage	Number of Defects	Average Surface Area / Defect	Maximum Defect Width	Minimum Defect Width	Total Defect Width	Average Defect Width
Veneer Tensile MOE	-0.356 0.000	-0.080 0.418	-0.259 0.007	-0.391 0.000	-0.041 0.675	-0.333 0.000	-0.311 0.001
Veneer F_t	-0.383 0.000	-0.134 0.172	-0.357 0.000	-0.439 0.000	-0.167 0.087	-0.347 0.000	-0.394 0.000
Veneer Density	-0.037 0.706	-0.036 0.715	-0.041 0.676	-0.090 0.361	0.064 0.516	0.002 0.987	-0.008 0.931
Average UPT	0.274 0.004	-0.023 0.818	0.280 0.004	0.379 0.000	0.135 0.168	0.267 0.006	0.366 0.000
Minimum UPT	0.137 0.162	-0.065 0.507	0.170 0.081	0.265 0.006	0.117 0.230	0.162 0.097	0.269 0.005
Maximum UPT	0.358 0.000	0.060 0.542	0.353 0.000	0.462 0.000	0.143 0.144	0.351 0.000	0.437 0.000
Average MOE_d	-0.195 0.046	-0.040 0.684	-0.190 0.051	-0.284 0.003	-0.031 0.750	-0.172 0.078	-0.222 0.022
Minimum MOE_d	-0.274 0.004	-0.093 0.344	-0.267 0.006	-0.367 0.000	-0.062 0.529	-0.255 0.008	-0.307 0.001
Maximum MOE_d	-0.101 0.301	-0.015 0.881	-0.107 0.273	-0.197 0.043	-0.001 0.990	-0.094 0.340	-0.137 0.160
St. Deviation of MOE_d	0.357 0.000	0.187 0.055	0.339 0.000	0.362 0.000	0.128 0.192	0.333 0.000	0.344 0.000
Latewood Percentage - Single Threshold	0.403 0.000	0.186 0.056	0.292 0.002	0.336 0.000	-0.020 0.841	0.367 0.000	0.243 0.012
Latewood Percentage - Dual Threshold Green + Black	0.155 0.114	0.040 0.682	0.113 0.249	0.131 0.181	-0.023 0.815	0.159 0.103	0.120 0.221
Latewood Percentage - Dual Threshold Black	-0.321 0.001	-0.128 0.192	-0.189 0.053	-0.252 0.009	-0.026 0.789	-0.268 0.006	-0.183 0.061
Latewood Percentage - Dual Threshold Green	0.516 0.000	0.178 0.068	0.331 0.001	0.417 0.000	-0.003 0.976	0.468 0.000	0.334 0.000
Defect Percentage	1.000 0.000	0.415 0.000	0.718 0.000	0.780 0.000	0.146 0.135	0.861 0.000	0.634 0.000
Number of Defects	0.415 0.000	1.000 0.000	-0.104 0.289	0.298 0.002	-0.300 0.002	0.688 0.000	-0.013 0.897
Average Surface Area/Defect	0.718 0.000	-0.104 0.289	1.000 0.000	0.707 0.000	0.599 0.000	0.403 0.000	0.834 0.000

Table A-4 (continued). Cross correlation table (correlation and p-values) for variables 15-21.

	Defect Percentage	Number of Defects	Average Surface Area / Defect	Maximum Defect Width	Minimum Defect Width	Total Defect Width	Average Defect Width
Maximum Defect Width	0.780 0.000	0.298 0.002	0.707 0.000	1.000 0.000	0.288 0.003	0.766 0.000	0.838 0.000
Minimum Defect Width	0.146 0.135	-0.300 0.002	0.599 0.000	0.288 0.003	1.000 0.000	0.030 0.759	0.703 0.000
Total Defect Width	0.861 0.000	0.688 0.000	0.403 0.000	0.766 0.000	0.030 0.759	1.000 0.000	0.558 0.000
Average Defect Width	0.634 0.000	-0.013 0.897	0.834 0.000	0.838 0.000	0.703 0.000	0.558 0.000	1.000 0.000
Total Defect Volume	0.838 0.000	0.568 0.000	0.340 0.000	0.631 0.000	-0.008 0.931	0.939 0.000	0.455 0.000
Maximum Defect Volume	0.754 0.000	0.200 0.040	0.673 0.000	0.955 0.000	0.200 0.040	0.713 0.000	0.766 0.000
Average Defect Volume	0.578 0.000	-0.114 0.243	0.831 0.000	0.747 0.000	0.720 0.000	0.473 0.000	0.951 0.000
GRP E:Mean	0.273 0.005	0.182 0.061	0.137 0.160	0.262 0.007	0.023 0.817	0.353 0.000	0.229 0.018
GRP E:St. Dev.	0.115 0.242	-0.017 0.860	0.160 0.100	0.104 0.290	0.086 0.383	0.059 0.551	0.109 0.267
GRP E:Max	0.243 0.012	0.151 0.122	0.175 0.073	0.172 0.078	0.033 0.736	0.237 0.015	0.155 0.113
GRP E:Min	0.297 0.002	0.230 0.018	0.156 0.111	0.246 0.011	0.020 0.836	0.374 0.000	0.222 0.022
GRP E:median	0.257 0.008	0.186 0.057	0.112 0.252	0.257 0.008	0.021 0.830	0.353 0.000	0.228 0.019
GRP E90:Mean	0.273 0.005	0.182 0.061	0.137 0.161	0.262 0.007	0.023 0.817	0.353 0.000	0.229 0.018
GRP E90:St. Dev.	0.734 0.000	0.323 0.001	0.495 0.000	0.638 0.000	0.028 0.775	0.708 0.000	0.499 0.000
GRP E90:Max	0.634 0.000	0.359 0.000	0.371 0.000	0.593 0.000	0.005 0.960	0.675 0.000	0.447 0.000
GRP E90:Min	0.072 0.463	0.121 0.216	0.027 0.782	0.133 0.173	0.085 0.387	0.187 0.056	0.153 0.117
GRP E90:median	0.189 0.052	0.139 0.155	0.073 0.456	0.184 0.059	0.009 0.924	0.269 0.005	0.162 0.098

Table A-5. Cross correlation table (correlation and p-values) for variables 22-28.

	Total Defect Volume	Maximum Defect Volume	Average Defect Volume	GRP E Mean	GRP E St. Dev.	GRP E Max	GRP E Min
Veneer Tensile MOE	-0.336 0.000	-0.434 0.000	-0.317 0.001	0.318 0.001	0.294 0.002	0.317 0.001	0.271 0.005
Veneer F_t	-0.287 0.003	-0.412 0.000	-0.334 0.000	0.257 0.008	0.164 0.094	0.221 0.023	0.209 0.032
Veneer Density	0.005 0.963	-0.140 0.152	-0.029 0.769	0.574 0.000	0.347 0.000	0.455 0.000	0.561 0.000
Average UPT	0.235 0.015	0.411 0.000	0.401 0.000	-0.240 0.013	-0.238 0.014	-0.289 0.003	-0.220 0.024
Minimum UPT	0.131 0.181	0.289 0.003	0.292 0.002	-0.276 0.004	-0.249 0.010	-0.287 0.003	-0.261 0.007
Maximum UPT	0.286 0.003	0.484 0.000	0.458 0.000	-0.105 0.286	-0.196 0.044	-0.211 0.030	-0.079 0.421
Average MOE_d	-0.143 0.144	-0.323 0.001	-0.245 0.011	0.495 0.000	0.356 0.000	0.450 0.000	0.474 0.000
Minimum MOE_d	-0.199 0.040	-0.396 0.000	-0.323 0.001	0.383 0.000	0.330 0.001	0.396 0.000	0.354 0.000
Maximum MOE_d	-0.074 0.453	-0.239 0.014	-0.155 0.112	0.538 0.000	0.369 0.000	0.463 0.000	0.524 0.000
St. Deviation of MOE_d	0.255 0.008	0.336 0.000	0.339 0.000	0.262 0.007	0.060 0.544	0.113 0.248	0.301 0.002
Latewood Percentage - Single Threshold	0.329 0.001	0.327 0.001	0.246 0.011	0.379 0.000	0.160 0.101	0.325 0.001	0.444 0.000
Latewood Percentage - Dual Threshold Green + Black	0.136 0.163	0.109 0.265	0.136 0.163	0.312 0.001	0.031 0.755	0.165 0.090	0.386 0.000
Latewood Percentage - Dual Threshold Black	-0.294 0.002	-0.288 0.003	-0.144 0.140	0.232 0.016	0.106 0.280	0.172 0.077	0.240 0.013
Latewood Percentage - Dual Threshold Green	0.466 0.000	0.425 0.000	0.317 0.001	0.164 0.093	-0.066 0.499	0.038 0.697	0.251 0.009
Defect Percentage	0.838 0.000	0.754 0.000	0.578 0.000	0.273 0.005	0.115 0.242	0.243 0.012	0.297 0.002
Number of Defects	0.568 0.000	0.200 0.040	-0.114 0.243	0.182 0.061	-0.017 0.860	0.151 0.122	0.230 0.018
Average Surface Area/Defect	0.340 0.000	0.673 0.000	0.831 0.000	0.137 0.160	0.160 0.100	0.175 0.073	0.156 0.111

Table A-5 (continued). Cross correlation table (correlation and p-values) for variables 22-28.

	Total Defect Volume	Maximum Defect Volume	Average Defect Volume	GRP E Mean	GRP E St. Dev.	GRP E Max	GRP E Min
Maximum Defect Width	0.631 0.000	0.955 0.000	0.747 0.000	0.262 0.007	0.104 0.290	0.172 0.078	0.246 0.011
Minimum Defect Width	-0.008 0.931	0.200 0.040	0.720 0.000	0.023 0.817	0.086 0.383	0.033 0.736	0.020 0.836
Total Defect Width	0.939 0.000	0.713 0.000	0.473 0.000	0.353 0.000	0.059 0.551	0.237 0.015	0.374 0.000
Average Defect Width	0.455 0.000	0.766 0.000	0.951 0.000	0.229 0.018	0.109 0.267	0.155 0.113	0.222 0.022
Total Defect Volume	1.000 0.000	0.641 0.000	0.422 0.000	0.313 0.001	0.038 0.696	0.211 0.030	0.331 0.001
Maximum Defect Volume	0.641 0.000	1.000 0.000	0.738 0.000	0.207 0.033	0.045 0.648	0.110 0.261	0.205 0.035
Average Defect Volume	0.422 0.000	0.738 0.000	1.000 0.000	0.189 0.052	0.039 0.691	0.098 0.319	0.220 0.024
GRP E:Mean	0.313 0.001	0.207 0.033	0.189 0.052	1.000 0.000	0.553 0.000	0.798 0.000	0.880 0.000
GRP E:St. Dev.	0.038 0.696	0.045 0.648	0.039 0.691	0.553 0.000	1.000 0.000	0.857 0.000	0.222 0.022
GRP E:Max	0.211 0.030	0.110 0.261	0.098 0.319	0.798 0.000	0.857 0.000	1.000 0.000	0.490 0.000
GRP E:Min	0.331 0.001	0.205 0.035	0.220 0.024	0.880 0.000	0.222 0.022	0.593 0.000	1.000 0.000
GRP E:median	0.308 0.001	0.201 0.039	0.192 0.048	0.991 0.000	0.490 0.000	0.748 0.000	0.877 0.000
GRP E90:Mean	0.312 0.001	0.207 0.033	0.189 0.052	1.000 0.000	0.553 0.000	0.798 0.000	0.880 0.000
GRP E90:St. Dev.	0.684 0.000	0.629 0.000	0.466 0.000	0.421 0.000	0.113 0.248	0.317 0.001	0.462 0.000
GRP E90:Max	0.608 0.000	0.541 0.000	0.377 0.000	0.744 0.000	0.314 0.001	0.551 0.000	0.696 0.000
GRP E90:Min	0.127 0.193	0.072 0.464	0.118 0.229	0.895 0.000	0.501 0.000	0.700 0.000	0.757 0.000
GRP E90:median	0.235 0.015	0.129 0.188	0.122 0.212	0.989 0.000	0.564 0.000	0.795 0.000	0.862 0.000

Table A-6. Cross correlation table (correlation and p-values) for variables 29-34.

	GRP E median	GRP E90 Mean	GRP E90 St. Dev.	GRP E90 Max	GRP E90 Min	GRP E90 median
Veneer Tensile MOE	0.316 0.001	0.318 0.001	-0.198 0.042	-0.019 0.849	0.393 0.000	0.371 0.000
Veneer F_t	0.277 0.004	0.257 0.008	-0.255 0.008	-0.098 0.319	0.345 0.000	0.297 0.002
Veneer Density	0.559 0.000	0.574 0.000	0.171 0.079	0.347 0.000	0.515 0.000	0.579 0.000
Average UPT	-0.228 0.019	-0.240 0.013	0.105 0.285	-0.046 0.641	-0.277 0.004	-0.275 0.004
Minimum UPT	-0.261 0.007	-0.276 0.004	0.040 0.681	-0.102 0.299	-0.295 0.002	-0.305 0.001
Maximum UPT	-0.088 0.367	-0.105 0.286	0.133 0.173	0.046 0.636	-0.127 0.196	-0.139 0.154
Average MOE_d	0.478 0.000	0.495 0.000	0.038 0.696	0.232 0.017	0.481 0.000	0.521 0.000
Minimum MOE_d	0.364 0.000	0.384 0.000	0.002 0.987	0.149 0.126	0.365 0.000	0.411 0.000
Maximum MOE_d	0.520 0.000	0.538 0.000	0.092 0.346	0.286 0.003	0.508 0.000	0.558 0.000
St. Deviation of MOE_d	0.259 0.007	0.262 0.007	0.183 0.060	0.252 0.009	0.251 0.009	0.241 0.013
Latewood Percentage - Single Threshold	0.353 0.000	0.379 0.000	0.371 0.000	0.414 0.000	0.245 0.011	0.354 0.000
Latewood Percentage - Dual Threshold Green + Black	0.318 0.001	0.311 0.001	0.106 0.278	0.234 0.016	0.251 0.009	0.320 0.001
Latewood Percentage - Dual Threshold Black	0.229 0.018	0.233 0.016	-0.241 0.013	-0.048 0.625	0.271 0.005	0.286 0.003
Latewood Percentage - Dual Threshold Green	0.175 0.073	0.164 0.094	0.374 0.000	0.345 0.000	0.049 0.620	0.121 0.218
Defect Percentage	0.257 0.008	0.273 0.005	0.734 0.000	0.634 0.000	0.072 0.463	0.189 0.052
Number of Defects	0.186 0.057	0.182 0.061	0.323 0.001	0.359 0.000	0.121 0.216	0.139 0.155
Average Surface Area/Defect	0.112 0.252	0.137 0.161	0.495 0.000	0.371 0.000	0.027 0.782	0.073 0.456

Table A-6 (continued). Cross correlation table (correlation and p-values) for variables 29-34.

	GRP E median	GRP E90 Mean	GRP E90 St. Dev.	GRP E90 Max	GRP E90 Min	GRP E90 median
Maximum Defect Width	0.257 0.008	0.262 0.007	0.638 0.000	0.593 0.000	0.133 0.173	0.184 0.059
Minimum Defect Width	0.021 0.830	0.023 0.817	0.028 0.775	0.005 0.960	0.085 0.387	0.009 0.924
Total Defect Width	0.353 0.000	0.353 0.000	0.708 0.000	0.675 0.000	0.187 0.056	0.269 0.005
Average Defect Width	0.228 0.019	0.229 0.018	0.499 0.000	0.447 0.000	0.153 0.117	0.162 0.098
Total Defect Volume	0.308 0.001	0.312 0.001	0.684 0.000	0.608 0.000	0.127 0.193	0.235 0.015
Maximum Defect Volume	0.201 0.039	0.207 0.033	0.629 0.000	0.541 0.000	0.072 0.464	0.129 0.188
Average Defect Volume	0.192 0.048	0.189 0.052	0.466 0.000	0.377 0.000	0.118 0.229	0.122 0.212
GRP E:Mean	0.991 0.000	1.000 0.000	0.421 0.000	0.744 0.000	0.895 0.000	0.989 0.000
GRP E:St. Dev.	0.490 0.000	0.553 0.000	0.113 0.248	0.314 0.001	0.501 0.000	0.564 0.000
GRP E:Max	0.748 0.000	0.798 0.000	0.317 0.001	0.551 0.000	0.700 0.000	0.795 0.000
GRP E:Min	0.877 0.000	0.880 0.000	0.462 0.000	0.696 0.000	0.757 0.000	0.862 0.000
GRP E:median	1.000 0.000	0.991 0.000	0.400 0.000	0.734 0.000	0.899 0.000	0.980 0.000
GRP E90:Mean	0.991 0.000	1.000 0.000	0.421 0.000	0.744 0.000	0.895 0.000	0.989 0.000
GRP E90:St. Dev.	0.400 0.000	0.421 0.000	1.000 0.000	0.825 0.000	0.129 0.189	0.317 0.001
GRP E90:Max	0.734 0.000	0.744 0.000	0.825 0.000	1.000 0.000	0.554 0.000	0.667 0.000
GRP E90:Min	0.899 0.000	0.895 0.000	0.129 0.189	0.554 0.000	1.000 0.000	0.893 0.000
GRP E90:median	0.980 0.000	0.989 0.000	0.317 0.001	0.667 0.000	0.893 0.000	1.000 0.000

Table A-7. Cross correlation table (correlation and p-values) between defect and waveform measures.

	Defect Percentage	Number of Defects	Average Surface Area / Defect	Max. Defect Width	Min. Defect Width	Total Defect Width	Average Defect Width	Total Defect Volume	Max. Defect Volume	Average Defect Volume
PS Arith. Mean: Linear	-0.344 0.000	-0.058 0.557	-0.367 0.000	-0.342 0.000	-0.134 0.172	-0.266 0.006	-0.323 0.001	-0.230 0.018	-0.360 0.000	-0.327 0.001
PS Std Dev: Linear	-0.353 0.000	-0.067 0.493	-0.371 0.000	-0.365 0.000	-0.167 0.088	-0.295 0.002	-0.353 0.000	-0.257 0.008	-0.365 0.000	-0.342 0.000
PS Variance: Linear	-0.299 0.002	0.006 0.950	-0.343 0.000	-0.328 0.001	-0.200 0.039	-0.249 0.010	-0.357 0.000	-0.219 0.024	-0.313 0.001	-0.327 0.001
PS Kurtosis: Linear	-0.188 0.053	-0.136 0.165	-0.117 0.231	-0.170 0.081	-0.083 0.399	-0.195 0.045	-0.117 0.232	-0.175 0.073	-0.157 0.109	-0.102 0.300
PS Median: Linear	-0.399 0.000	-0.123 0.208	-0.293 0.002	-0.439 0.000	-0.089 0.362	-0.374 0.000	-0.344 0.000	-0.362 0.000	-0.459 0.000	-0.319 0.001
PS Mode: Linear	-0.351 0.000	-0.059 0.547	-0.353 0.000	-0.350 0.000	-0.160 0.101	-0.295 0.002	-0.335 0.000	-0.262 0.007	-0.351 0.000	-0.322 0.001
PS Summation: Linear	-0.344 0.000	-0.058 0.556	-0.367 0.000	-0.342 0.000	-0.134 0.172	-0.266 0.006	-0.323 0.001	-0.230 0.018	-0.360 0.000	-0.327 0.001
PS Skewness: Linear	-0.214 0.027	-0.165 0.091	-0.124 0.205	-0.202 0.038	-0.077 0.433	-0.234 0.016	-0.138 0.159	-0.210 0.031	-0.186 0.057	-0.118 0.230
PS Maximum: Linear	-0.351 0.000	-0.059 0.546	-0.353 0.000	-0.350 0.000	-0.160 0.101	-0.295 0.002	-0.335 0.000	-0.262 0.007	-0.351 0.000	-0.322 0.001
PS Minimum: Linear	-0.037 0.708	-0.003 0.972	-0.095 0.331	-0.049 0.621	-0.084 0.393	-0.009 0.925	-0.059 0.549	-0.025 0.803	-0.079 0.422	-0.092 0.349
PS Arith. Mean: Decibel	-0.447 0.000	-0.048 0.626	-0.370 0.000	-0.473 0.000	-0.100 0.306	-0.374 0.000	-0.387 0.000	-0.378 0.000	-0.544 0.000	-0.413 0.000
PS Std Dev: Decibel	-0.226 0.020	0.037 0.707	-0.198 0.042	-0.218 0.024	-0.015 0.882	-0.151 0.122	-0.171 0.079	-0.145 0.137	-0.293 0.002	-0.218 0.025
PS Variance: Decibel	-0.225 0.020	0.040 0.685	-0.199 0.041	-0.219 0.024	-0.015 0.878	-0.149 0.126	-0.172 0.078	-0.143 0.144	-0.293 0.002	-0.217 0.025
PS Kurtosis: Decibel	0.351 0.000	-0.004 0.969	0.220 0.023	0.368 0.000	0.024 0.811	0.317 0.001	0.289 0.003	0.353 0.000	0.450 0.000	0.316 0.001
PS Median: Decibel	-0.455 0.000	-0.164 0.094	-0.318 0.001	-0.487 0.000	-0.076 0.438	-0.437 0.000	-0.378 0.000	-0.418 0.000	-0.504 0.000	-0.350 0.000
PS Mode: Decibel	-0.167 0.087	-0.088 0.370	-0.177 0.069	-0.146 0.135	-0.031 0.754	-0.133 0.173	-0.106 0.278	-0.145 0.139	-0.190 0.051	-0.138 0.159
PS Summation: Decibel	-0.447 0.000	-0.048 0.626	-0.370 0.000	-0.473 0.000	-0.100 0.306	-0.374 0.000	-0.387 0.000	-0.378 0.000	-0.544 0.000	-0.413 0.000
PS Skewness: Decibel	0.420 0.000	0.041 0.674	0.247 0.011	0.424 0.000	0.039 0.689	0.397 0.000	0.341 0.000	0.408 0.000	0.464 0.000	0.330 0.001
PS Maximum: Decibel	-0.314 0.001	-0.148 0.129	-0.271 0.005	-0.301 0.002	-0.077 0.431	-0.281 0.004	-0.237 0.015	-0.238 0.014	-0.315 0.001	-0.245 0.011
PS Minimum: Decibel	-0.018 0.852	-0.019 0.843	-0.055 0.577	-0.001 0.991	0.008 0.939	0.003 0.979	0.009 0.924	-0.035 0.722	-0.046 0.643	-0.023 0.815
PSD Arith. Mean: Linear	-0.344 0.000	-0.058 0.557	-0.367 0.000	-0.342 0.000	-0.134 0.172	-0.266 0.006	-0.323 0.001	-0.230 0.018	-0.360 0.000	-0.327 0.001
PSD Std Dev: Linear	-0.353 0.000	-0.067 0.494	-0.371 0.000	-0.365 0.000	-0.167 0.087	-0.295 0.002	-0.353 0.000	-0.257 0.008	-0.365 0.000	-0.342 0.000

Table A-7 (continued). Cross correlation table (correlation and p-values) between defect and waveform measures.

	Defect Percentage	Number of Defects	Average Surface Area / Defect	Max. Defect Width	Min. Defect Width	Total Defect Width	Average Defect Width	Total Defect Volume	Max. Defect Volume	Average Defect Volume
PSD Variance: Linear	0.049 0.616	0.015 0.881	0.028 0.776	0.185 0.057	-0.087 0.377	0.090 0.357	0.088 0.369	0.069 0.482	0.244 0.012	0.078 0.426
PSD Kurtosis: Linear	-0.188 0.053	-0.136 0.165	-0.117 0.231	-0.170 0.081	-0.083 0.399	-0.195 0.045	-0.117 0.232	-0.175 0.073	-0.157 0.109	-0.102 0.300
PSD Median: Linear	-0.400 0.000	-0.158 0.105	-0.283 0.003	-0.460 0.000	-0.090 0.361	-0.394 0.000	-0.355 0.000	-0.365 0.000	-0.472 0.000	-0.321 0.001
PSD Mode: Linear	-0.351 0.000	-0.059 0.547	-0.354 0.000	-0.350 0.000	-0.160 0.100	-0.295 0.002	-0.335 0.000	-0.262 0.007	-0.351 0.000	-0.322 0.001
PSD Summation: Linear	-0.344 0.000	-0.058 0.557	-0.367 0.000	-0.342 0.000	-0.134 0.172	-0.266 0.006	-0.323 0.001	-0.230 0.018	-0.360 0.000	-0.327 0.001
PSD Skewness: Linear	-0.214 0.027	-0.165 0.091	-0.124 0.205	-0.202 0.038	-0.077 0.433	-0.234 0.016	-0.138 0.159	-0.210 0.031	-0.186 0.057	-0.118 0.230
PSD Maximum: Linear	-0.351 0.000	-0.059 0.547	-0.354 0.000	-0.350 0.000	-0.160 0.100	-0.295 0.002	-0.335 0.000	-0.262 0.007	-0.351 0.000	-0.322 0.001
PSD Minimum: Linear	0.049 0.616	0.015 0.881	0.028 0.776	0.185 0.057	-0.087 0.377	0.090 0.357	0.088 0.369	0.069 0.482	0.244 0.012	0.078 0.426
PSD Arith. Mean: Decibel	-0.447 0.000	-0.048 0.626	-0.370 0.000	-0.473 0.000	-0.100 0.306	-0.374 0.000	-0.387 0.000	-0.378 0.000	-0.544 0.000	-0.413 0.000
PSD Std Dev: Decibel	-0.226 0.020	0.037 0.707	-0.198 0.042	-0.218 0.024	-0.015 0.882	-0.151 0.122	-0.171 0.079	-0.145 0.137	-0.293 0.002	-0.218 0.025
PSD Variance: Decibel	-0.225 0.020	0.040 0.685	-0.199 0.041	-0.219 0.024	-0.015 0.878	-0.149 0.126	-0.172 0.078	-0.143 0.144	-0.293 0.002	-0.217 0.025
PSD Kurtosis: Decibel	0.351 0.000	-0.004 0.969	0.220 0.023	0.368 0.000	0.024 0.811	0.317 0.001	0.289 0.003	0.353 0.000	0.450 0.000	0.316 0.001
PSD Median: Decibel	-0.455 0.000	-0.164 0.094	-0.318 0.001	-0.487 0.000	-0.076 0.438	-0.437 0.000	-0.378 0.000	-0.418 0.000	-0.504 0.000	-0.350 0.000
PSD Mode: Decibel	-0.167 0.087	-0.088 0.370	-0.177 0.069	-0.146 0.135	-0.031 0.754	-0.133 0.173	-0.106 0.278	-0.145 0.139	-0.190 0.051	-0.138 0.159
PSD Summation: Decibel	-0.447 0.000	-0.048 0.626	-0.370 0.000	-0.473 0.000	-0.100 0.306	-0.374 0.000	-0.387 0.000	-0.378 0.000	-0.544 0.000	-0.413 0.000
PSD Skewness: Decibel	0.420 0.000	0.041 0.674	0.247 0.011	0.424 0.000	0.039 0.689	0.397 0.000	0.341 0.000	0.408 0.000	0.464 0.000	0.330 0.001
PSD Maximum: Decibel	-0.314 0.001	-0.148 0.129	-0.271 0.005	-0.301 0.002	-0.077 0.431	-0.281 0.004	-0.237 0.015	-0.238 0.014	-0.315 0.001	-0.245 0.011
PSD Minimum: Decibel	-0.018 0.852	-0.019 0.843	-0.055 0.577	-0.001 0.991	0.008 0.939	0.003 0.979	0.009 0.924	-0.035 0.722	-0.046 0.643	-0.023 0.815
Peak Arith. Mean: Linear	-0.310 0.001	-0.024 0.808	-0.315 0.001	-0.303 0.002	-0.071 0.469	-0.216 0.026	-0.254 0.009	-0.194 0.046	-0.361 0.000	-0.292 0.002
Peak Std Dev: Linear	-0.328 0.001	-0.079 0.421	-0.343 0.000	-0.325 0.001	-0.110 0.262	-0.256 0.008	-0.292 0.002	-0.215 0.027	-0.347 0.000	-0.305 0.001
Peak Variance: Linear	-0.342 0.000	-0.060 0.543	-0.366 0.000	-0.341 0.000	-0.136 0.164	-0.266 0.006	-0.324 0.001	-0.229 0.018	-0.356 0.000	-0.326 0.001
Peak Kurtosis: Linear	-0.224 0.021	-0.150 0.126	-0.199 0.040	-0.273 0.005	-0.132 0.178	-0.258 0.008	-0.240 0.013	-0.211 0.030	-0.226 0.020	-0.205 0.035

Table A-7 (continued). Cross correlation table (correlation and p-values) between defect and waveform measures.

	Defect Percentage	Number of Defects	Average Surface Area / Defect	Max. Defect Width	Min. Defect Width	Total Defect Width	Average Defect Width	Total Defect Volume	Max. Defect Volume	Average Defect Volume
Peak Median: Linear	-0.434 0.000	-0.148 0.131	-0.309 0.001	-0.470 0.000	-0.082 0.401	-0.412 0.000	-0.366 0.000	-0.396 0.000	-0.488 0.000	-0.338 0.000
Peak Mode: Linear	-0.353 0.000	-0.113 0.248	-0.332 0.001	-0.345 0.000	-0.124 0.205	-0.304 0.002	-0.302 0.002	-0.263 0.007	-0.351 0.000	-0.298 0.002
Peak Summation: Linear	-0.310 0.001	-0.024 0.807	-0.315 0.001	-0.303 0.002	-0.071 0.470	-0.216 0.026	-0.254 0.009	-0.194 0.047	-0.361 0.000	-0.292 0.002
Peak Skewness: Linear	-0.229 0.018	-0.170 0.082	-0.187 0.056	-0.263 0.007	-0.109 0.264	-0.268 0.006	-0.225 0.020	-0.222 0.022	-0.214 0.027	-0.190 0.051
Peak Maximum: Linear	-0.353 0.000	-0.113 0.248	-0.332 0.001	-0.345 0.000	-0.124 0.206	-0.304 0.002	-0.302 0.002	-0.263 0.007	-0.351 0.000	-0.298 0.002
Peak Minimum: Linear	-0.015 0.880	0.016 0.870	-0.081 0.408	-0.021 0.834	-0.056 0.568	0.017 0.866	-0.030 0.757	-0.011 0.911	-0.056 0.569	-0.063 0.520
Peak Arith. Mean: Decibel	-0.447 0.000	-0.048 0.626	-0.370 0.000	-0.473 0.000	-0.100 0.306	-0.374 0.000	-0.387 0.000	-0.378 0.000	-0.544 0.000	-0.413 0.000
Peak Std Dev: Decibel	-0.226 0.020	0.037 0.707	-0.198 0.042	-0.218 0.024	-0.015 0.882	-0.151 0.122	-0.171 0.079	-0.145 0.137	-0.293 0.002	-0.218 0.025
Peak Variance: Decibel	-0.225 0.020	0.040 0.685	-0.199 0.041	-0.219 0.024	-0.015 0.878	-0.149 0.126	-0.172 0.078	-0.143 0.144	-0.293 0.002	-0.217 0.025
Peak Kurtosis: Decibel	0.351 0.000	-0.004 0.969	0.220 0.023	0.368 0.000	0.024 0.811	0.317 0.001	0.289 0.003	0.353 0.000	0.450 0.000	0.316 0.001
Peak Median: Decibel	-0.455 0.000	-0.164 0.094	-0.318 0.001	-0.487 0.000	-0.076 0.438	-0.437 0.000	-0.378 0.000	-0.418 0.000	-0.504 0.000	-0.350 0.000
Peak Mode: Decibel	-0.167 0.087	-0.088 0.370	-0.177 0.069	-0.146 0.135	-0.031 0.754	-0.133 0.173	-0.106 0.278	-0.145 0.139	-0.190 0.051	-0.138 0.159
Peak Summation: Decibel	-0.447 0.000	-0.048 0.626	-0.370 0.000	-0.473 0.000	-0.100 0.306	-0.374 0.000	-0.387 0.000	-0.378 0.000	-0.544 0.000	-0.413 0.000
Peak Skewness: Decibel	0.420 0.000	0.041 0.674	0.247 0.011	0.424 0.000	0.039 0.689	0.397 0.000	0.341 0.000	0.408 0.000	0.464 0.000	0.330 0.001
Peak Maximum: Decibel	-0.314 0.001	-0.148 0.129	-0.271 0.005	-0.301 0.002	-0.077 0.431	-0.281 0.004	-0.237 0.015	-0.238 0.014	-0.315 0.001	-0.245 0.011
Peak Minimum: Decibel	-0.018 0.852	-0.019 0.843	-0.055 0.577	-0.001 0.991	0.008 0.939	0.003 0.979	0.009 0.924	-0.035 0.722	-0.046 0.643	-0.023 0.815
RMS Arith. Mean: Linear	-0.310 0.001	-0.024 0.809	-0.315 0.001	-0.303 0.002	-0.071 0.470	-0.216 0.026	-0.254 0.009	-0.194 0.047	-0.361 0.000	-0.292 0.002
RMS Std Dev: Linear	-0.328 0.001	-0.079 0.421	-0.343 0.000	-0.326 0.001	-0.110 0.262	-0.256 0.008	-0.292 0.002	-0.215 0.027	-0.347 0.000	-0.305 0.001
RMS Variance: Linear	-0.342 0.000	-0.060 0.543	-0.366 0.000	-0.341 0.000	-0.136 0.164	-0.266 0.006	-0.324 0.001	-0.229 0.018	-0.356 0.000	-0.326 0.001
RMS Kurtosis: Linear	-0.224 0.021	-0.150 0.126	-0.199 0.040	-0.273 0.005	-0.132 0.178	-0.258 0.008	-0.240 0.013	-0.211 0.030	-0.226 0.020	-0.205 0.035
RMS Median: Linear	-0.434 0.000	-0.147 0.131	-0.309 0.001	-0.470 0.000	-0.082 0.401	-0.412 0.000	-0.366 0.000	-0.396 0.000	-0.488 0.000	-0.338 0.000
RMS Mode: Linear	-0.353 0.000	-0.113 0.248	-0.332 0.001	-0.345 0.000	-0.124 0.205	-0.304 0.002	-0.302 0.002	-0.263 0.007	-0.351 0.000	-0.298 0.002

Table A-7 (continued). Cross correlation table (correlation and p-values) between defect and waveform measures.

	Defect Percentage	Number of Defects	Average Surface Area / Defect	Max. Defect Width	Min. Defect Width	Total Defect Width	Average Defect Width	Total Defect Volume	Max. Defect Volume	Average Defect Volume
RMS Summation:	-0.310 0.001	-0.024 0.807	-0.315 0.001	-0.303 0.002	-0.071 0.470	-0.216 0.026	-0.254 0.009	-0.194 0.047	-0.361 0.000	-0.292 0.002
RMS Skewness: Linear	-0.229 0.018	-0.170 0.082	-0.187 0.056	-0.263 0.007	-0.109 0.264	-0.268 0.006	-0.225 0.020	-0.222 0.022	-0.214 0.027	-0.190 0.051
RMS Maximum: Linear	-0.353 0.000	-0.113 0.248	-0.332 0.001	-0.345 0.000	-0.124 0.205	-0.304 0.002	-0.302 0.002	-0.263 0.007	-0.351 0.000	-0.298 0.002
RMS Minimum: Linear	-0.015 0.880	0.016 0.870	-0.081 0.408	-0.021 0.834	-0.056 0.568	0.017 0.866	-0.030 0.757	-0.011 0.911	-0.056 0.569	-0.063 0.520
RMS Arith. Mean: Decibel	-0.344 0.000	-0.058 0.556	-0.367 0.000	-0.342 0.000	-0.134 0.172	-0.266 0.006	-0.323 0.001	-0.230 0.018	-0.360 0.000	-0.327 0.001
RMS Std Dev: Decibel	-0.353 0.000	-0.067 0.493	-0.371 0.000	-0.365 0.000	-0.167 0.088	-0.295 0.002	-0.353 0.000	-0.257 0.008	-0.365 0.000	-0.342 0.000
RMS Variance: Decibel	-0.299 0.002	0.006 0.950	-0.343 0.000	-0.329 0.001	-0.200 0.039	-0.249 0.010	-0.357 0.000	-0.219 0.024	-0.313 0.001	-0.327 0.001
RMS Kurtosis: Decibel	-0.188 0.053	-0.136 0.165	-0.117 0.231	-0.170 0.081	-0.083 0.399	-0.195 0.045	-0.117 0.232	-0.175 0.073	-0.157 0.109	-0.102 0.300
RMS Median: Decibel	-0.399 0.000	-0.123 0.208	-0.293 0.002	-0.439 0.000	-0.090 0.361	-0.374 0.000	-0.345 0.000	-0.362 0.000	-0.460 0.000	-0.319 0.001
RMS Mode: Decibel	-0.351 0.000	-0.059 0.547	-0.353 0.000	-0.350 0.000	-0.160 0.101	-0.295 0.002	-0.335 0.000	-0.262 0.007	-0.351 0.000	-0.322 0.001
RMS Summation:	-0.344 0.000	-0.058 0.556	-0.367 0.000	-0.342 0.000	-0.134 0.172	-0.266 0.006	-0.323 0.001	-0.230 0.018	-0.360 0.000	-0.327 0.001
RMS Skewness: Decibel	-0.214 0.027	-0.165 0.091	-0.124 0.205	-0.202 0.038	-0.077 0.433	-0.234 0.016	-0.138 0.159	-0.210 0.031	-0.186 0.057	-0.118 0.230
RMS Maximum: Decibel	-0.351 0.000	-0.059 0.546	-0.353 0.000	-0.350 0.000	-0.160 0.101	-0.295 0.002	-0.335 0.000	-0.262 0.007	-0.351 0.000	-0.322 0.001
RMS Minimum: Decibel	-0.018 0.853	0.032 0.747	-0.100 0.306	-0.039 0.692	-0.093 0.344	0.018 0.854	-0.060 0.543	-0.002 0.985	-0.067 0.496	-0.089 0.363
Raw Waveform Arith. Mean	0.241 0.013	-0.194 0.046	0.393 0.000	0.344 0.000	0.282 0.003	0.144 0.141	0.417 0.000	0.124 0.205	0.343 0.000	0.430 0.000
Raw Waveform Std Dev	-0.323 0.001	-0.079 0.419	-0.353 0.000	-0.396 0.000	-0.209 0.032	-0.290 0.003	-0.380 0.000	-0.253 0.009	-0.429 0.000	-0.394 0.000
Raw Waveform Variance	-0.328 0.001	-0.078 0.425	-0.357 0.000	-0.395 0.000	-0.217 0.025	-0.297 0.002	-0.389 0.000	-0.262 0.007	-0.422 0.000	-0.397 0.000
Raw Waveform Kurtosis	0.220 0.023	0.126 0.200	0.108 0.273	0.127 0.195	-0.113 0.249	0.184 0.058	0.061 0.537	0.129 0.188	0.092 0.348	0.021 0.830
Raw Waveform Median	-0.137 0.161	-0.120 0.220	-0.102 0.296	-0.162 0.097	0.033 0.738	-0.117 0.231	-0.088 0.367	-0.090 0.359	-0.185 0.057	-0.078 0.424
Raw Waveform Mode	0.090 0.360	0.018 0.858	0.187 0.055	0.209 0.032	0.203 0.037	0.089 0.367	0.266 0.006	0.026 0.793	0.200 0.040	0.258 0.007
Raw Waveform Summation	0.241 0.013	-0.194 0.046	0.393 0.000	0.344 0.000	0.282 0.003	0.144 0.141	0.417 0.000	0.124 0.205	0.343 0.000	0.430 0.000
Raw Waveform Skewness	0.065 0.509	0.060 0.541	0.094 0.340	0.215 0.027	0.070 0.478	0.100 0.308	0.187 0.056	0.055 0.576	0.216 0.026	0.145 0.139
Raw Waveform Maximum	-0.227 0.019	-0.015 0.880	-0.286 0.003	-0.283 0.003	-0.204 0.036	-0.180 0.064	-0.273 0.005	-0.183 0.060	-0.339 0.000	-0.319 0.001
Raw Waveform Minimum	0.215 0.027	0.020 0.841	0.307 0.001	0.315 0.001	0.253 0.009	0.179 0.066	0.336 0.000	0.151 0.123	0.353 0.000	0.367 0.000

Appendix B. Model Validation Study:

Individual Veneer Tension Test Results

And

Plots of Predicted Veneer Tensile MOE and F_t Values via Each Model
Versus Static (actual) Tensile MOE and F_t Values

Table B-1. Individual veneer static tension MOE and F_t test results from model validation study.

Veneer Tension Test Results - Model Validation Study									
Specimen Number	**Width (inch)**	**Length (inch)**	**Thickness (inch)**	**Weight (g)**	**Slope (lbf/in)**	**Pmax (lbf)**	**Density (lb/ft^3)**	**MOE (lbf/in^2)**	**F_t (lbf/in^2)**
002a	6.082	31.000	0.126	184.3	68,776	795	29.5	806,077	1,035
002c	6.080	31.000	0.133	182.1	141,940	2,093	27.8	1,585,730	2,598
004c	6.051	31.000	0.124	195.4	136,561	1,989	32.1	1,644,750	2,662
004d	6.068	31.000	0.129	204.9	157,074	2,240	32.3	1,813,097	2,873
004e	6.024	31.000	0.127	201.4	236,063	1,060	32.4	2,782,359	1,388
005a	6.071	31.000	0.130	216.9	181,554	1,657	33.8	2,074,227	2,103
005b	6.083	31.000	0.138	224.0	214,271	5,070	32.7	2,293,098	6,029
005d	6.088	31.000	0.135	219.3	175,188	3,754	32.7	1,914,712	4,559
006c	6.102	31.000	0.134	226.7	201,502	3,412	34.2	2,226,104	4,188
006d	6.100	31.063	0.135	218.4	154,290	2,107	32.5	1,683,202	2,554
010a	6.091	31.000	0.140	253.3	196,860	3,132	36.5	2,077,594	3,673
010b	6.091	31.000	0.131	238.7	215,738	6,738	36.8	2,433,510	8,445
011c	6.048	31.000	0.126	192.8	150,104	3,236	31.1	1,772,672	4,246
011d	6.077	31.000	0.134	192.6	149,504	3,944	29.2	1,658,628	4,862
014a	6.041	31.000	0.128	187.2	111,734	1,017	29.7	1,298,035	1,313
014b	6.030	31.063	0.126	171.1	44,604	532	27.7	529,433	702
021a	6.079	31.000	0.122	231.3	188,562	4,229	38.4	2,292,958	5,714
021b	6.080	31.000	0.133	238.5	181,661	2,823	36.4	2,029,479	3,504
021c	6.061	31.000	0.140	254.8	209,202	4,081	37.0	2,226,962	4,827
025b	6.027	31.000	0.139	185.9	87,264	1,899	27.2	935,846	2,263
025c	6.066	31.000	0.123	188.0	179,011	1,579	31.1	2,168,245	2,125
031a	6.052	31.063	0.131	186.8	134,752	1,826	28.8	1,526,705	2,299
031d	6.073	31.063	0.129	180.9	114,092	1,485	28.3	1,310,710	1,896
032c	6.072	31.000	0.126	201.2	184,349	1,331	32.2	2,164,434	1,736
032d	6.062	31.000	0.130	211.9	174,410	2,510	33.1	1,995,790	3,191
033a	6.085	31.000	0.118	221.6	221,950	1,374	37.9	2,781,840	1,913
033b	6.097	31.000	0.125	230.1	86,486	1,571	37.0	1,019,344	2,057
037a	6.035	31.000	0.134	208.1	132,144	2,204	31.7	1,473,389	2,730
037b	6.054	31.000	0.128	208.3	102,432	1,212	33.0	1,189,739	1,564
037c	6.071	31.000	0.127	209.5	204,874	4,379	33.5	2,400,788	5,702
039c	6.085	31.000	0.134	200.2	172,145	1,532	30.3	1,907,301	1,886
039d	6.045	31.000	0.127	194.3	136,932	1,456	31.1	1,605,185	1,896
040a	6.065	31.000	0.122	191.0	100,825	2,467	31.7	1,226,428	3,334
040b	6.078	31.000	0.126	200.5	134,650	2,981	32.2	1,585,469	3,900
040d	6.039	31.000	0.127	194.4	133,104	2,535	31.1	1,562,031	3,305
045a	6.072	31.000	0.129	188.5	170,146	5,200	29.5	1,951,092	6,625
045b	6.067	31.000	0.132	198.7	202,943	4,278	30.6	2,289,371	5,362
048a	6.082	31.000	0.119	205.4	107,519	1,097	35.0	1,342,729	1,522
048c	6.086	31.000	0.122	205.8	167,727	1,068	34.0	2,032,965	1,438
051a	6.102	31.000	0.125	231.4	225,446	1,701	37.3	2,665,316	2,234
051c	6.084	31.000	0.128	230.5	134,874	1,622	36.3	1,555,698	2,079
051d	6.101	31.000	0.131	226.4	150,434	3,172	34.8	1,693,914	3,969
057a	6.086	31.000	0.124	198.7	147,129	1,906	32.3	1,754,636	2,526
057c	6.083	31.000	0.124	200.8	165,292	1,082	32.8	1,976,094	1,437
058b	6.072	31.063	0.129	190.8	190,730	1,585	30.0	2,200,022	2,031
058c	6.077	31.000	0.133	199.7	207,443	1,370	30.4	2,309,939	1,695
059a	6.067	31.000	0.129	195.3	184,906	2,129	30.7	2,130,343	2,725

Table B-1 (continued). Individual veneer static tension MOE and F_t test results from model validation study.

Veneer Tension Test Results - Model Validation Study (continued)									
Specimen Number	**Width (inch)**	**Length (inch)**	**Thickness (inch)**	**Weight (g)**	**Slope (lbf/in)**	**Pmax (lbf)**	**Density (lb/ft^3)**	**MOE (lbf/in^2)**	**F_t (lbf/in^2)**
059b	6.054	31.000	0.125	179.3	103,764	1,622	29.0	1,231,530	2,139
059d	6.070	31.000	0.125	180.1	185,374	1,632	29.2	2,198,831	2,151
061a	6.055	31.000	0.135	190.6	145,534	1,524	28.7	1,605,414	1,868
061b	6.067	31.000	0.121	174.1	138,407	1,524	29.1	1,696,743	2,076
062a	6.101	31.000	0.137	231.0	202,476	6,210	34.0	2,180,194	7,430
062b	6.087	31.000	0.137	239.7	224,218	2,740	35.4	2,424,275	3,292
064a	6.073	31.000	0.126	217.5	178,115	1,126	34.9	2,094,817	1,471
064c	6.104	31.000	0.130	222.5	189,380	2,219	34.5	2,151,940	2,802
064e	6.096	31.000	0.128	209.2	158,779	2,082	32.9	1,831,490	2,668
092b	6.103	31.000	0.127	227.4	231,230	5,483	36.1	2,690,419	7,088
092c	6.118	31.000	0.138	233.3	215,158	5,940	34.0	2,297,858	7,049
094a	6.125	31.063	0.130	202.2	n/a	2,014	31.2	n/a	2,534
094b	6.122	31.000	0.127	191.9	156,325	1,938	30.4	1,816,713	2,502
094d	6.096	31.000	0.131	206.7	181,689	2,183	31.9	2,055,600	2,744
101a	6.129	31.000	0.136	225.4	214,942	3,901	33.2	2,320,786	4,680
101b	6.135	31.000	0.136	228.8	178,075	2,175	33.6	1,917,424	2,602
102b	6.064	31.000	0.134	225.2	155,683	1,898	34.1	1,727,550	2,340
102e	6.070	31.000	0.120	196.2	103,171	1,510	33.2	1,280,173	2,082
103c	6.073	31.000	0.123	188.8	155,406	1,345	31.0	1,868,715	1,797
103e	6.057	31.063	0.130	199.0	105,554	1,086	31.0	1,208,861	1,382
140c	6.040	31.063	0.130	191.9	133,299	1,597	30.0	1,527,960	2,034
140d	6.044	31.063	0.131	191.8	110,973	1,388	29.8	1,263,771	1,756
149c	6.045	31.000	0.136	199.9	169,533	1,413	29.9	1,859,353	1,722
149e	6.049	31.000	0.132	214.8	n/a	1,852	33.2	n/a	2,328
158c	6.032	31.063	0.131	191.0	105,366	1,298	29.7	1,204,679	1,649
158d	6.052	31.000	0.133	184.6	139,562	1,697	28.3	1,566,368	2,116
159a	6.026	31.063	0.126	179.3	152,592	1,496	29.0	1,812,233	1,974
159d	6.024	31.000	0.131	198.2	156,832	2,330	30.8	1,785,230	2,947
163a	6.055	31.000	0.128	189.1	147,124	1,431	29.9	1,705,207	1,843
163b	6.041	31.000	0.132	184.6	146,408	1,344	28.4	1,652,344	1,685
164a	6.044	31.000	0.135	194.0	109,218	2,815	29.2	1,204,768	3,450
164b	6.056	31.000	0.132	190.8	152,203	2,686	29.4	1,720,097	3,373
164d	6.059	31.000	0.135	194.2	137,808	2,492	29.1	1,513,400	3,041
213a	6.073	31.063	0.126	189.7	142,691	1,719	30.3	1,674,965	2,242
213d	6.005	31.063	0.127	178.2	93,336	1,176	28.8	1,105,766	1,548
234a	5.991	31.000	0.131	182.4	71,357	1,241	28.7	821,476	1,587
234b	5.996	31.000	0.129	185.1	103,840	827	29.3	1,205,977	1,067
235a	6.020	31.000	0.132	155.8	96,061	1,172	24.0	1,085,974	1,472
235b	6.059	31.000	0.134	180.9	83,487	762	27.5	928,923	942
253a	6.005	31.000	0.123	175.8	125,149	1,193	29.2	1,521,931	1,612
256a	6.002	31.000	0.122	204.0	144,228	1,211	34.2	1,768,977	1,650
256b	5.998	31.063	0.129	190.9	102,428	1,075	30.2	1,189,184	1,387
Average	6.066	31.010	0.129	202.6	153,057	2,212	31.7	1,754,206	2,796
St. Deviation	0.030	0.023	0.005	19.6	42,385	1,302	2.8	475,619	1,591
COV %	0.5	0.1	3.8	9.7	27.7	58.9	8.9	27.1	56.9
Minimum	5.991	31.000	0.118	155.8	44,604	532	24.0	529,433	702
Maximum	6.135	31.063	0.140	254.8	236,063	6,738	38.4	2,782,359	8,445
Range	0.144	0.063	0.022	99.0	191,459	6,206	14.4	2,252,926	7,743

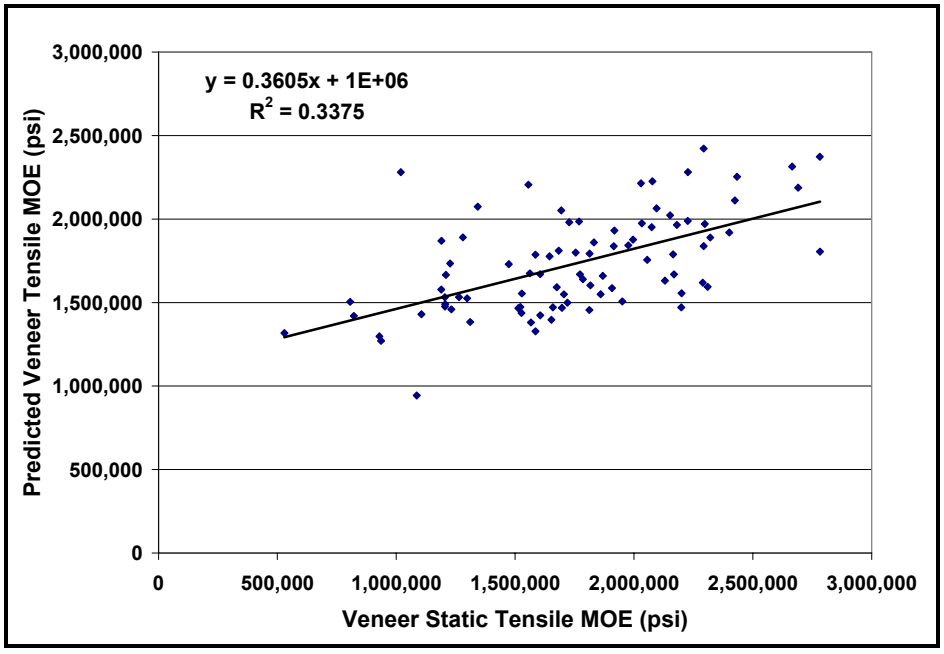

Figure B-1. Density model: Predicted veneer tensile MOE vs. static MOE.

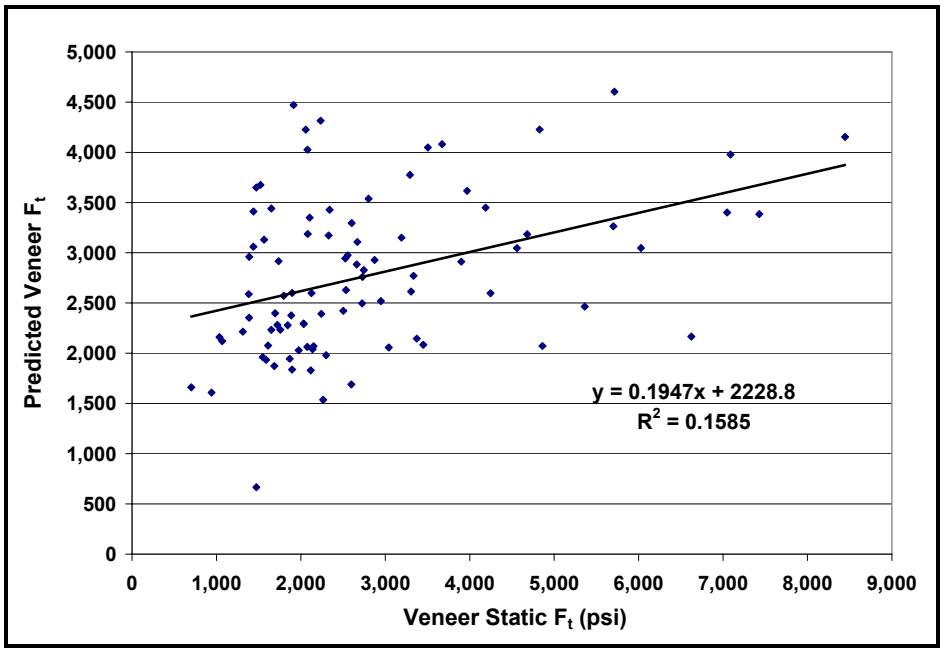

Figure B-2. Density model: Predicted veneer F_t vs. static F_t.

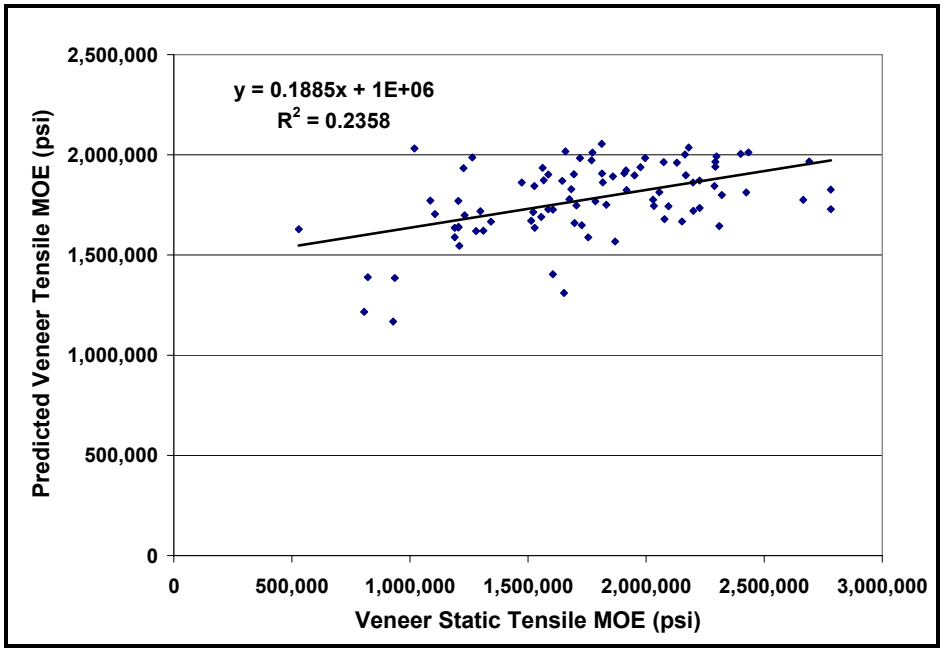

Figure B-3. Basic optical model: Predicted veneer tensile MOE vs. static MOE.

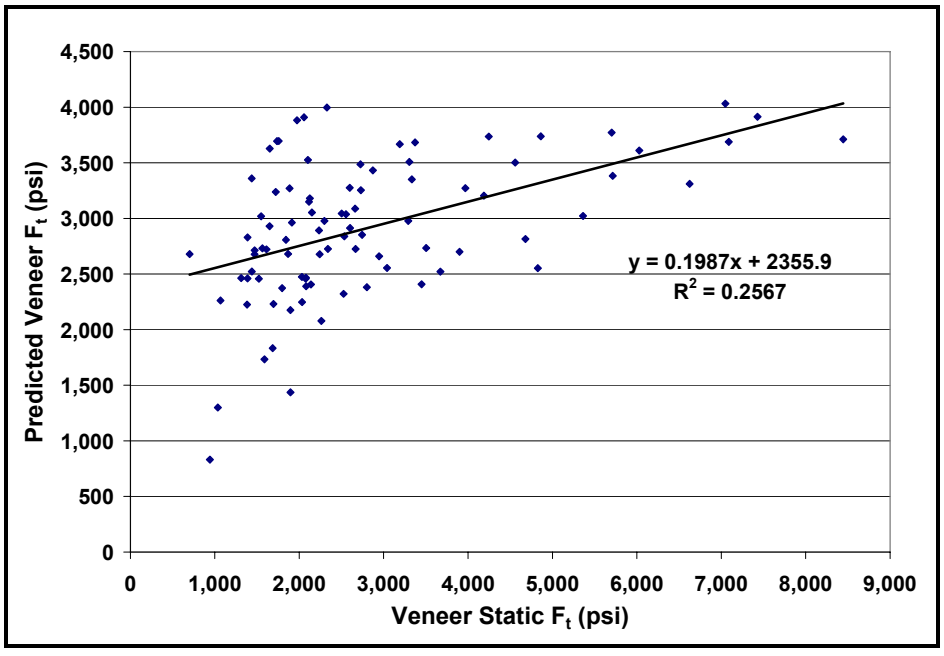

Figure B-4. Basic optical model: Predicted veneer F_t vs. static F_t.

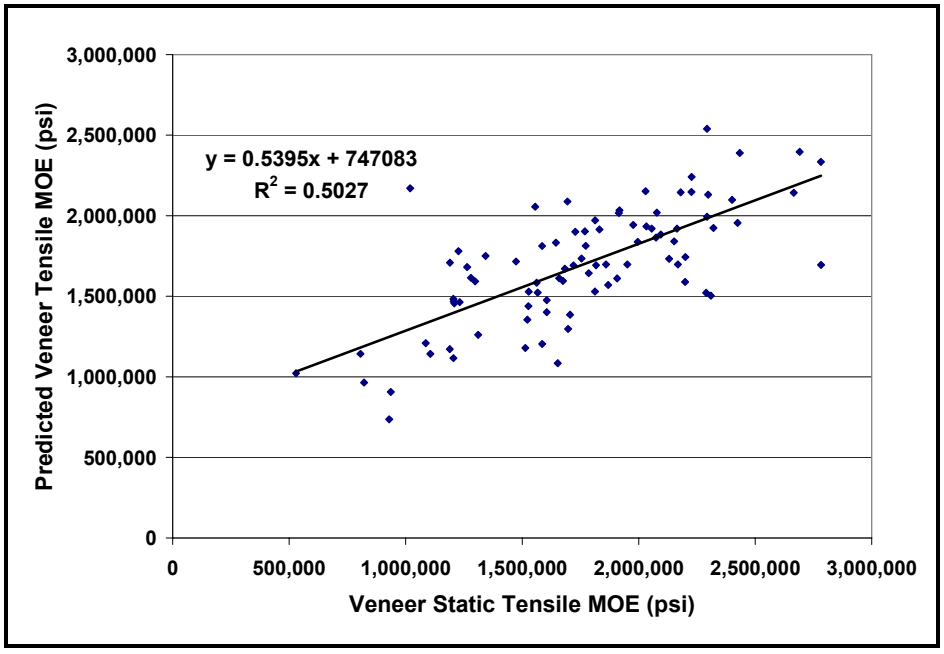

Figure B-5. Optical + density model: Predicted veneer tensile MOE vs. static MOE.

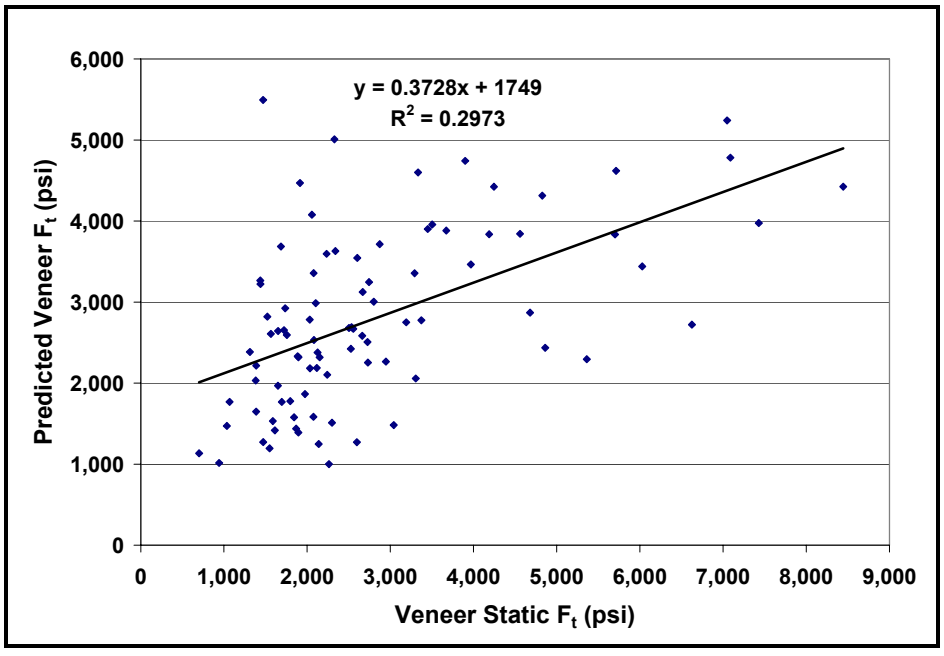

Figure B-6. Optical + density model: Predicted veneer F_t vs. static F_t.

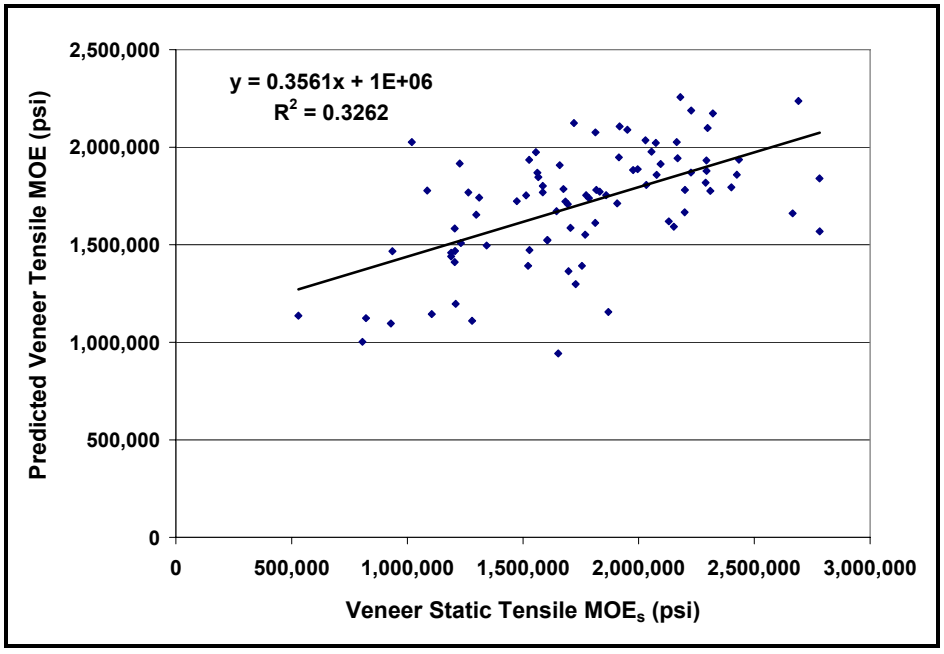

Figure B-7. Optical + GRP model: Predicted veneer tensile MOE vs. static MOE.

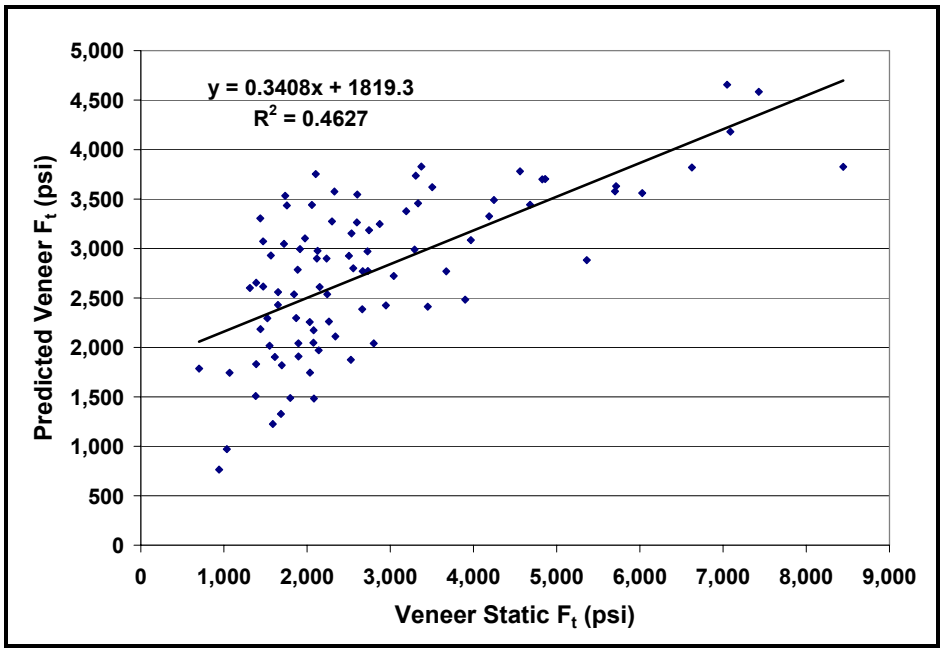

Figure B-8. Optical + GRP model: Predicted veneer F_t vs. static F_t.

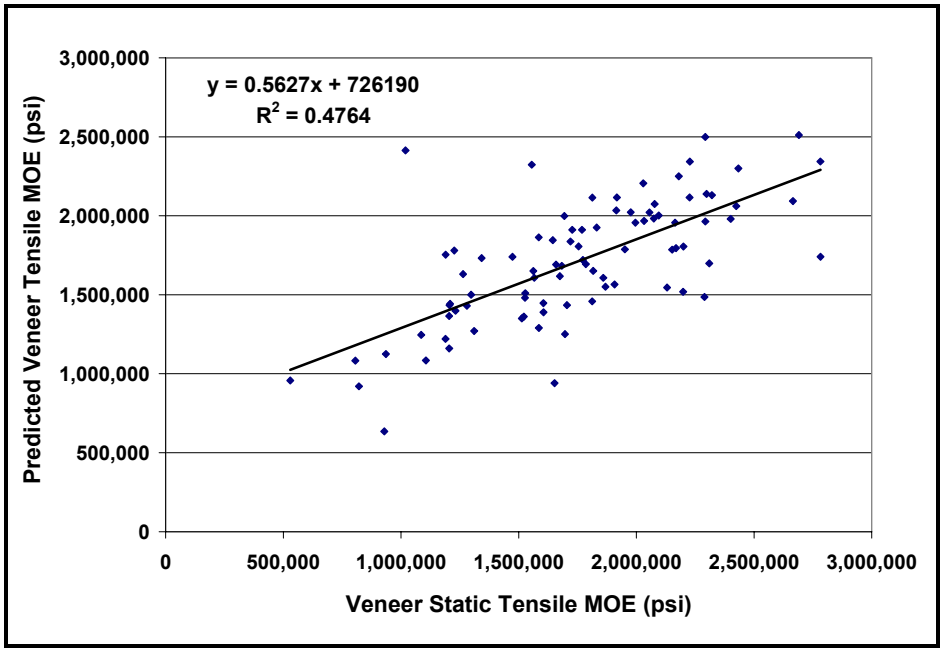

Figure B-9. Optical + GRP + density model: Predicted veneer tensile MOE vs. static MOE.

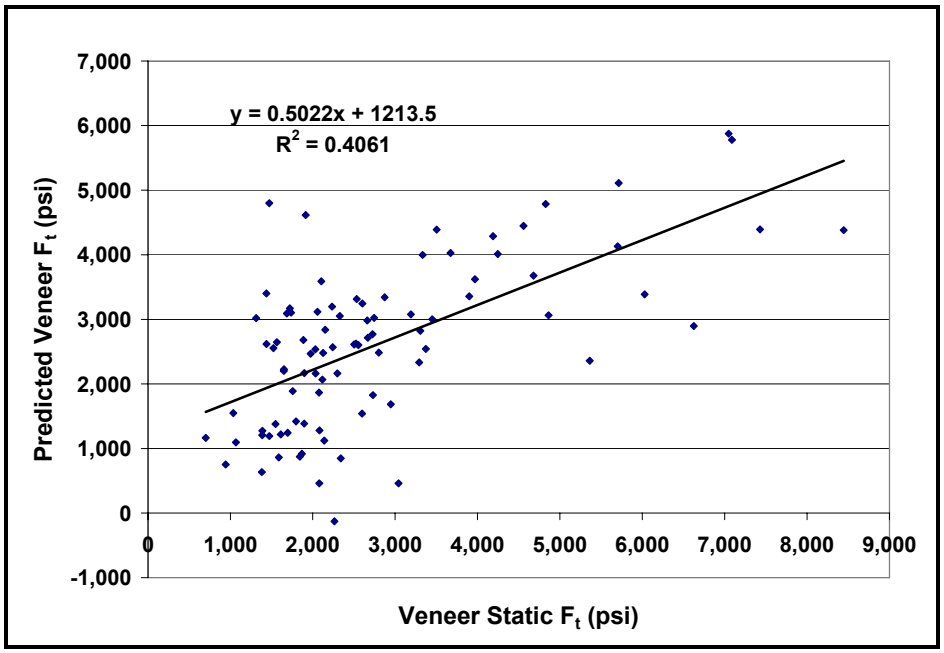

Figure B-10. Optical + GRP + density model: Predicted veneer F_t vs. static F_t.

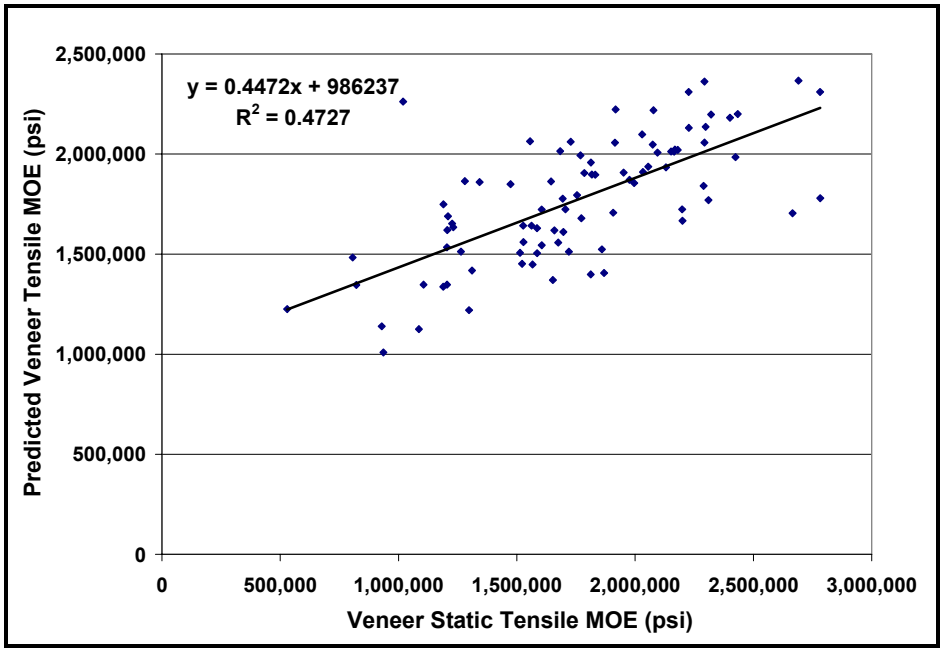

Figure B-11. Average MOE_d model: Predicted veneer tensile MOE vs. static MOE.

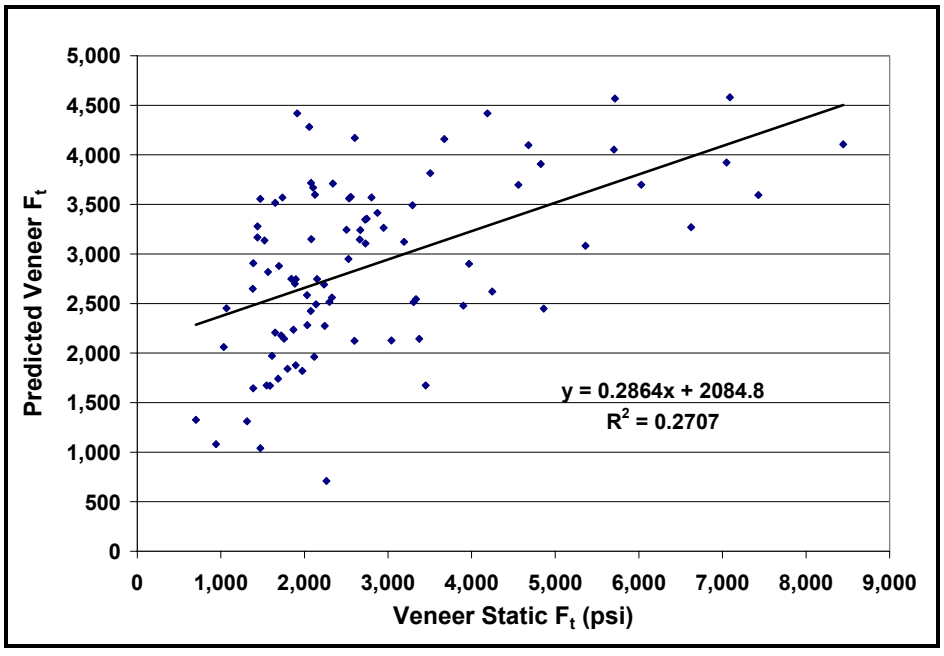

Figure B-12. Average MOE_d model: Predicted veneer F_t vs. static F_t.

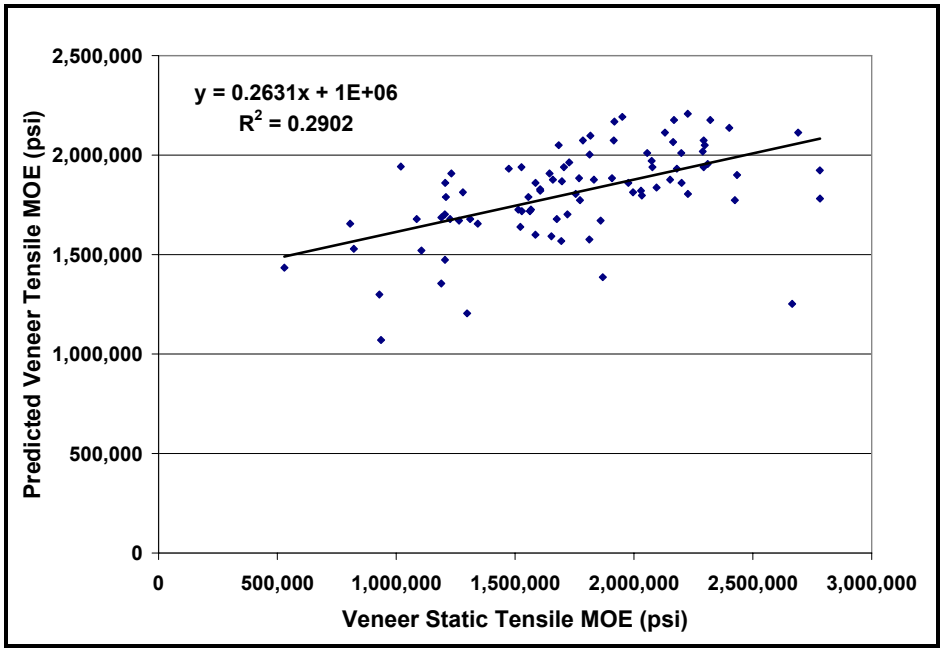

Figure B-13. Average UPT model: Predicted veneer tensile MOE vs. static MOE.

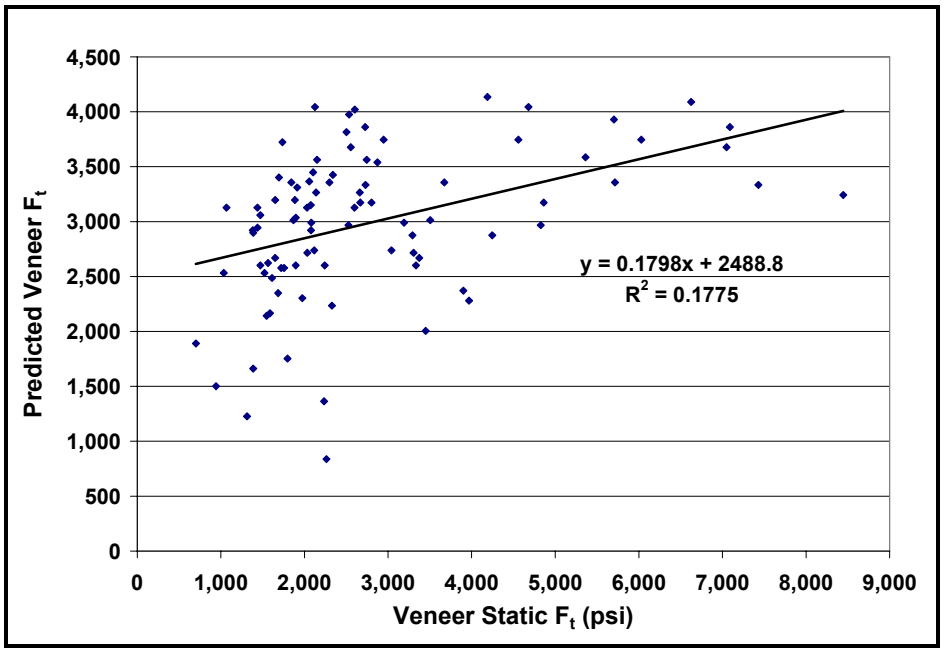

Figure B-14. Average UPT model: Predicted veneer F_t vs. static F_t.

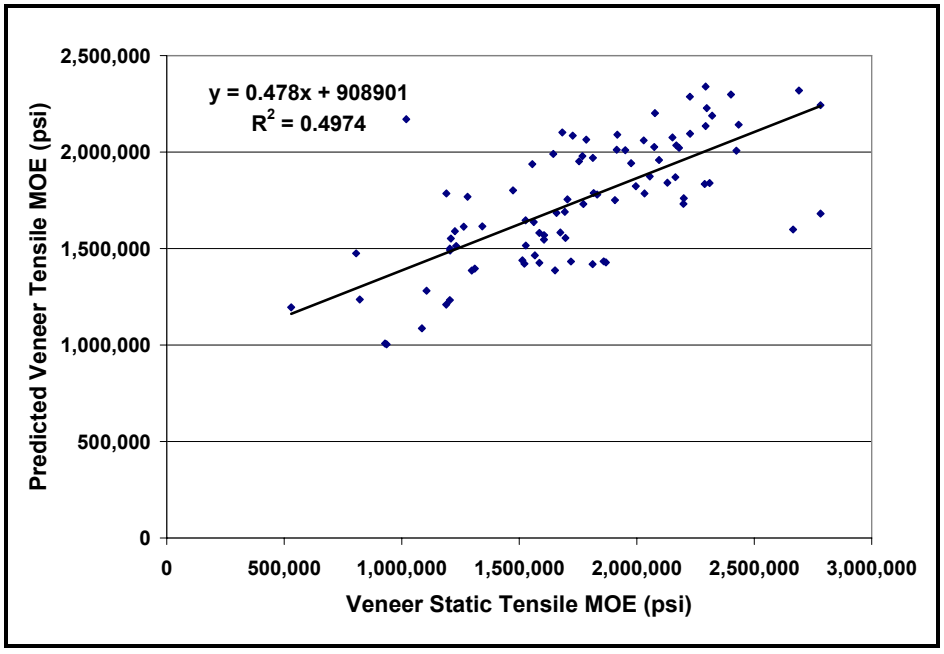

Figure B-15. Ultrasonic + spectral analysis model: Predicted veneer tensile MOE vs. static MOE.

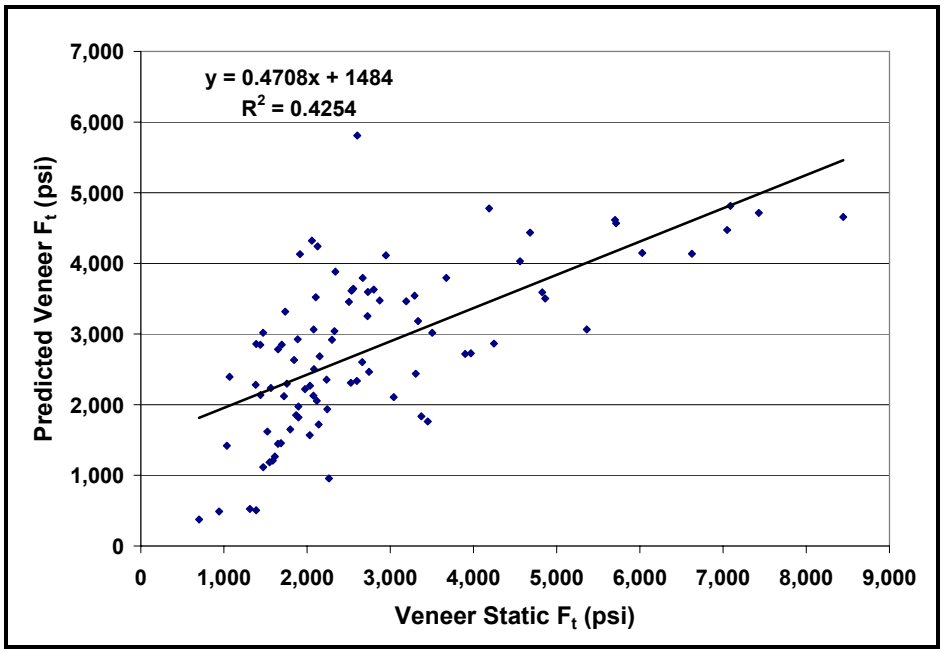

Figure B-16. Ultrasonic + spectral analysis model: Predicted veneer F_t vs. static F_t.

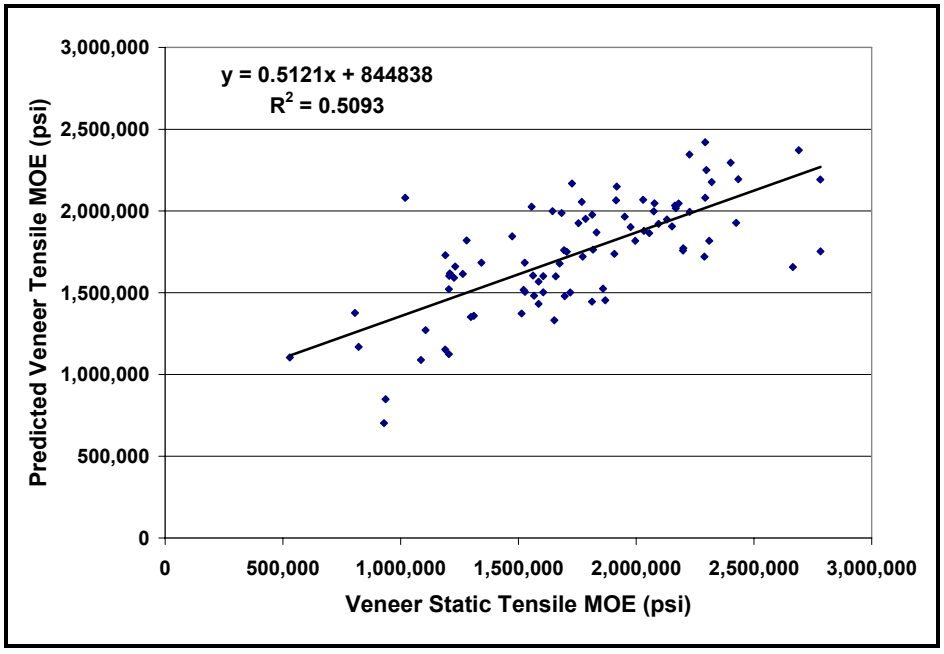

Figure B-17. Combined Optical + ultrasonic model: Predicted veneer tensile MOE vs. static MOE.

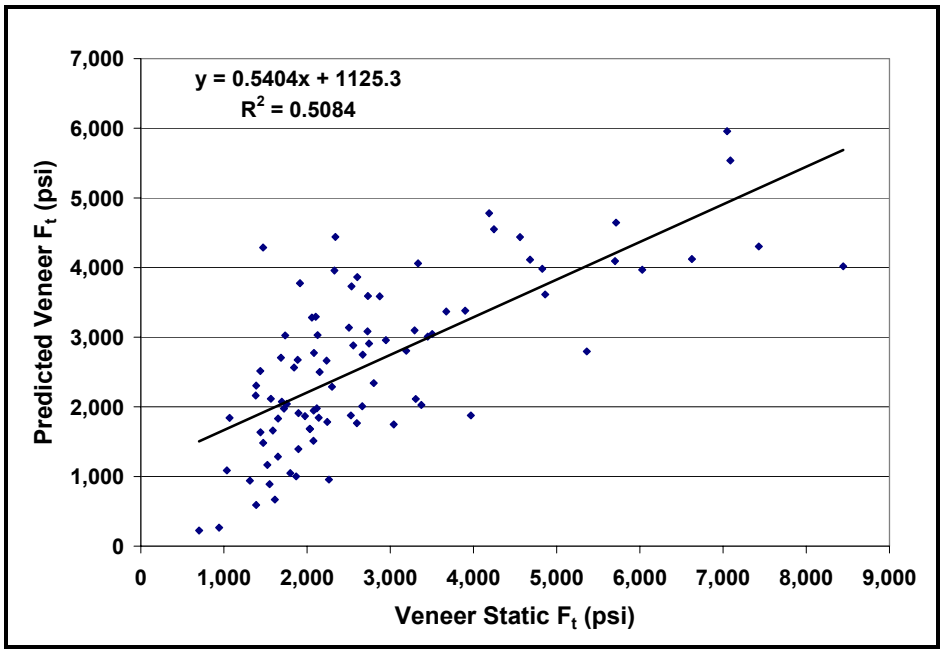

Figure B-18. Combined optical + ultrasonic model: Predicted veneer F_t vs. static F_t.

Appendix C. Laminated Veneer Study:

Individual LVL Tension Test Results

Plots of Predicted LVL Tensile MOE via Each Model
Versus Static (actual) Tensile MOE

And

Linear Regression Plots for Prediction
of LVL Static F_t for Each System Model

Table C-1. Individual LVL static tension MOE and F_t test results.

LVL Tension Test Results										
Specimen Number	**Width (inch)**	**Length (inch)**	**Thickness (inch)**	**Weight [1] (g)**	**Slope (lbf/in)**	**Pmax (lbf)**	**Density (lb/ft^3)**	**M.C. (%)**	**MOE (lbf/in^2)**	**F_t (lbf/in^2)**
LVL1	5.815	47.500	0.646	1636.6	1,973,202	25,264	34.9	12.0	2,154,113	6,725
LVL2	5.808	47.688	0.648	1662.9	1,651,472	25,993	35.3	11.8	1,800,497	6,906
LVL3	5.822	47.813	0.640	1615.7	1,925,642	24,750	34.5	11.7	2,115,990	6,642
LVL4	5.830	47.813	0.627	1640.2	1,723,955	24,786	35.7	12.1	1,946,271	6,781
LVL5	5.832	47.750	0.652	1647.4	1,588,930	28,830	34.6	11.7	1,713,971	7,582
LVL6	5.828	47.750	0.646	1573.1	1,253,166	19,133	33.3	11.4	1,368,870	5,082
LVL7	5.832	47.750	0.637	1656.5	1,423,060	25,386	35.6	11.8	1,571,962	6,833
LVL8	5.831	47.813	0.658	1682.8	1,724,245	23,514	34.9	11.6	1,842,527	6,129
LVL9	5.825	47.875	0.623	1501.4	1,485,255	18,532	32.9	12.1	1,693,424	5,107
LVL10	5.821	47.750	0.626	1613.0	1,578,688	20,903	35.3	11.9	1,788,441	5,736
LVL11	5.818	47.750	0.643	1506.8	1,347,356	14,459	32.1	12.0	1,489,810	3,865
LVL12	5.812	47.750	0.656	1583.9	1,755,771	23,987	33.1	12.1	1,890,160	6,291
LVL13	5.848	47.875	0.643	1660.1	1,691,518	27,327	35.1	11.5	1,846,909	7,267
LVL14	5.828	47.875	0.645	1532.2	1,402,316	18,069	32.4	11.8	1,532,749	4,807
LVL15	5.833	47.500	0.646	1527.7	1,814,571	11,490	32.5	11.6	1,978,196	3,049
LVL16	5.832	47.813	0.644	1495.9	1,458,059	16,293	31.7	12.4	1,601,423	4,338
LVL17	5.823	47.625	0.645	1573.1	1,565,814	20,064	33.5	11.9	1,714,091	5,342
LVL18	5.824	47.813	0.648	1571.2	1,181,800	12,714	33.2	12.2	1,288,003	3,369
LVL19	5.816	47.813	0.645	1486.9	1,265,186	19,363	31.6	12.0	1,389,967	5,162
LVL20	5.818	47.750	0.634	1589.4	1,673,538	19,698	34.4	11.9	1,874,705	5,340
LVL21	5.831	47.938	0.630	1637.5	1,487,202	23,999	35.4	11.5	1,665,280	6,533
LVL22	5.830	47.750	0.651	1624.8	1,737,317	24,487	34.1	12.0	1,879,434	6,452
LVL23	5.805	47.750	0.649	1660.1	1,769,400	18,213	35.1	11.6	1,934,604	4,834
LVL24	5.801	47.750	0.642	1495.9	1,542,360	16,464	32.0	12.0	1,713,632	4,421
LVL25	5.810	47.813	0.638	1550.4	1,351,022	15,495	33.3	12.0	1,497,802	4,180
LVL26	5.822	47.875	0.631	1514.1	1,530,395	21,298	32.8	12.1	1,722,073	5,797
LVL27	5.800	47.813	0.644	1605.7	1,614,246	19,955	34.2	12.3	1,783,181	5,342
LVL28	5.805	47.813	0.662	1635.7	1,541,165	22,865	33.9	12.3	1,655,217	5,950
LVL29	5.821	47.875	0.645	1543.1	1,474,674	18,256	32.7	12.7	1,618,960	4,862
LVL30	5.817	47.688	0.660	1653.8	1,652,541	28,140	34.4	12.2	1,778,478	7,330
LVL31	5.820	47.688	0.644	1620.2	1,156,912	22,086	34.5	12.3	1,269,798	5,893
LVL32	5.820	47.625	0.638	1458.8	1,663,355	16,684	31.4	12.2	1,844,663	4,493
LVL33	5.803	47.938	0.650	1692.8	1,850,148	32,031	35.7	11.9	2,020,818	8,492
LVL34	5.815	47.875	0.629	1566.7	1,678,150	27,423	34.1	12.1	1,891,204	7,497

1. Weight measured at time of testing and at moisture condition as reported.

Table C-1 (continued). Individual LVL static tension MOE and F_t test results.

LVL Tension Test Results (continued)										
Specimen Number	**Width (inch)**	**Length (inch)**	**Thickness (inch)**	**Weight [1] (g)**	**Slope (lbf/in)**	**Pmax (lbf)**	**Density (lb/ft^3)**	**M.C. (%)**	**MOE (lbf/in^2)**	**F_t (lbf/in^2)**
LVL35	5.826	47.750	0.665	1634.7	1,604,221	27,266	33.7	11.9	1,714,036	7,038
LVL36	5.812	47.813	0.668	1544.0	1,552,124	16,016	31.7	12.2	1,648,825	4,125
LVL37	5.804	47.688	0.651	1541.3	1,406,179	19,969	32.6	12.2	1,535,057	5,285
LVL38	5.848	47.688	0.642	1505.0	1,472,341	17,281	32.0	12.1	1,618,611	4,603
LVL39	5.817	47.688	0.643	1572.2	1,810,096	20,901	33.6	12.0	1,994,511	5,588
LVL40	5.838	47.688	0.641	1617.5	1,528,641	26,741	34.5	11.7	1,694,179	7,146
LVL41	5.813	47.563	0.655	1504.1	2,073,676	23,845	31.6	12.4	2,253,231	6,263
LVL42	5.818	47.813	0.647	1522.3	1,564,675	22,318	32.2	12.0	1,716,831	5,929
LVL43	5.829	47.750	0.634	1629.3	1,676,248	29,581	35.2	11.8	1,874,015	8,004
LVL44	5.835	47.750	0.649	1736.4	1,752,635	23,048	36.6	11.7	1,911,327	6,086
LVL45	5.818	47.875	0.659	1651.1	1,637,461	25,992	34.3	12.1	1,756,463	6,779
LVL46	5.810	47.688	0.643	1626.6	1,687,742	25,238	34.8	11.9	1,858,363	6,756
LVL47	5.845	47.875	0.660	1544.0	1,538,585	16,988	31.8	12.2	1,644,436	4,404
LVL48	5.807	47.875	0.645	1537.7	1,372,010	24,219	32.7	12.0	1,511,494	6,466
LVL49	5.840	47.750	0.648	1675.6	1,224,974	19,527	35.3	11.7	1,336,967	5,160
LVL50	5.855	47.938	0.636	1653.8	1,804,132	20,407	35.3	11.9	1,996,436	5,480
LVL51	5.828	47.750	0.662	1589.4	1,806,829	17,368	32.9	11.7	1,937,753	4,502
LVL52	5.835	47.750	0.661	1613.0	1,569,880	23,470	33.4	12.0	1,690,794	6,085
LVL53	5.810	47.750	0.631	1406.1	1,263,718	14,971	30.6	12.2	1,424,690	4,084
LVL54	5.822	47.875	0.662	1701.9	1,630,407	29,504	35.1	11.7	1,746,754	7,655
LVL55	5.821	47.813	0.627	1549.5	1,419,528	21,629	33.8	11.7	1,610,742	5,926
LVL56	5.838	47.750	0.641	1649.3	1,632,300	24,126	35.1	11.8	1,812,116	6,447
LVL57	5.848	47.813	0.627	1522.3	1,712,996	17,050	33.1	12.3	1,929,955	4,650
LVL58	5.862	47.688	0.656	1599.4	1,621,987	19,019	33.2	12.0	1,751,320	4,946
LVL59	5.845	47.813	0.651	1662.0	1,529,971	27,905	34.8	11.8	1,660,048	7,334
LVL60	5.809	47.813	0.634	1539.5	1,515,599	21,687	33.3	12.3	1,696,748	5,889
LVL61	5.816	47.750	0.638	1716.4	1,789,596	27,332	36.9	11.8	1,978,844	7,366
LVL62	5.840	47.875	0.630	1536.8	2,073,676	23,845	33.2	11.9	2,303,577	6,481
Average	5.824	47.772	0.645	1,590.3	1,593,623	21,858	33.8	12.0	1,749,764	5,821
St. Dev.	0.014	0.093	0.011	69.1	200,110	4,545	1.4	0.3	218,309	1,202
COV %	0.2	0.2	1.7	4.3	12.6	20.8	4.1	2.1	12.5	20.6
Minimum	5.800	47.500	0.623	1,406.1	1,156,912	11,490	30.6	11.4	1,269,798	3,049
Maximum	5.862	47.938	0.668	1,736.4	2,073,676	32,031	36.9	12.7	2,303,577	8,492
Range	0.062	0.438	0.045	330.2	916,764	20,541	6.3	1.3	1,033,779	5,443

1. Weight measured at time of testing and at moisture condition as reported.

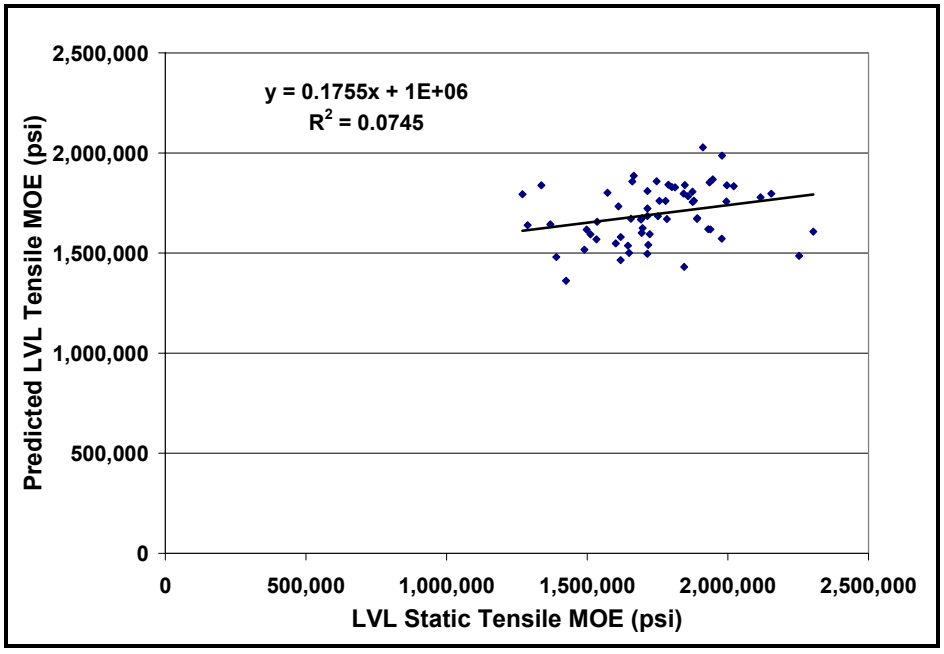

Figure C-1. Density model: Predicted LVL tensile MOE vs. static MOE.

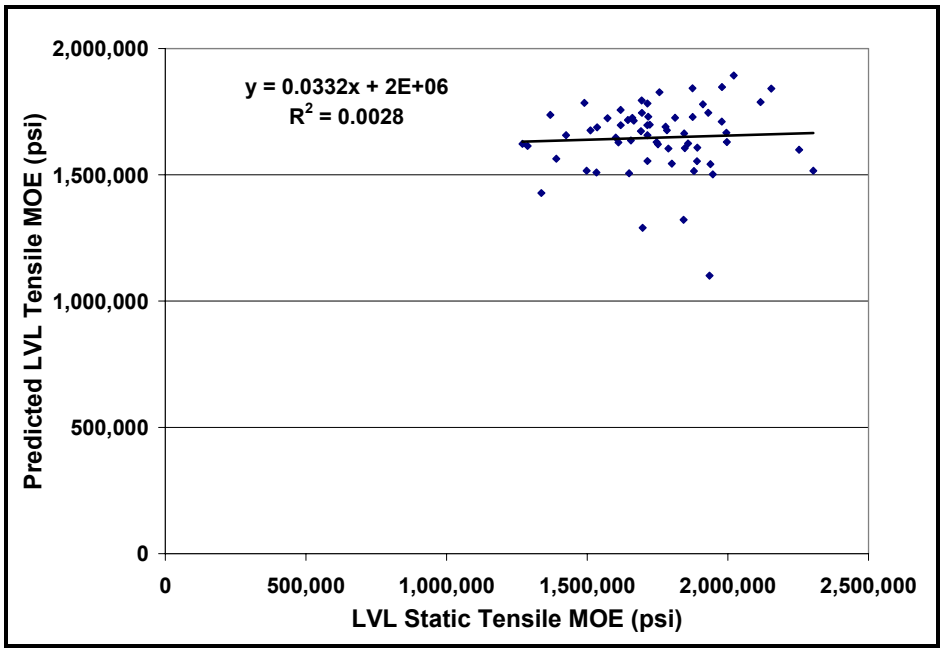

Figure C-2. Basic optical model: Predicted LVL tensile MOE vs. static MOE.

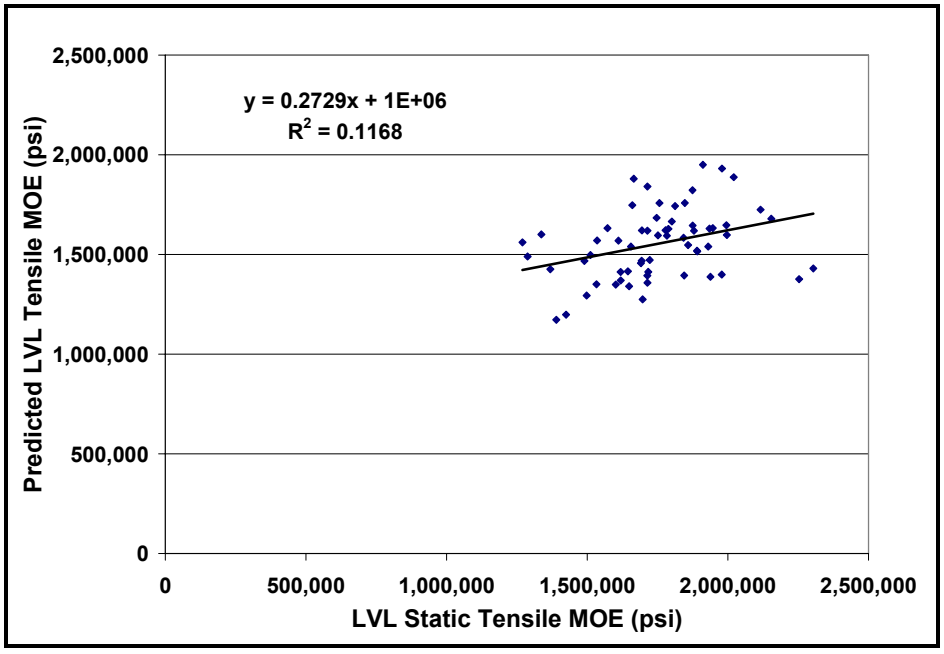

Figure C-3. Optical + density model: Predicted LVL tensile MOE vs. static MOE.

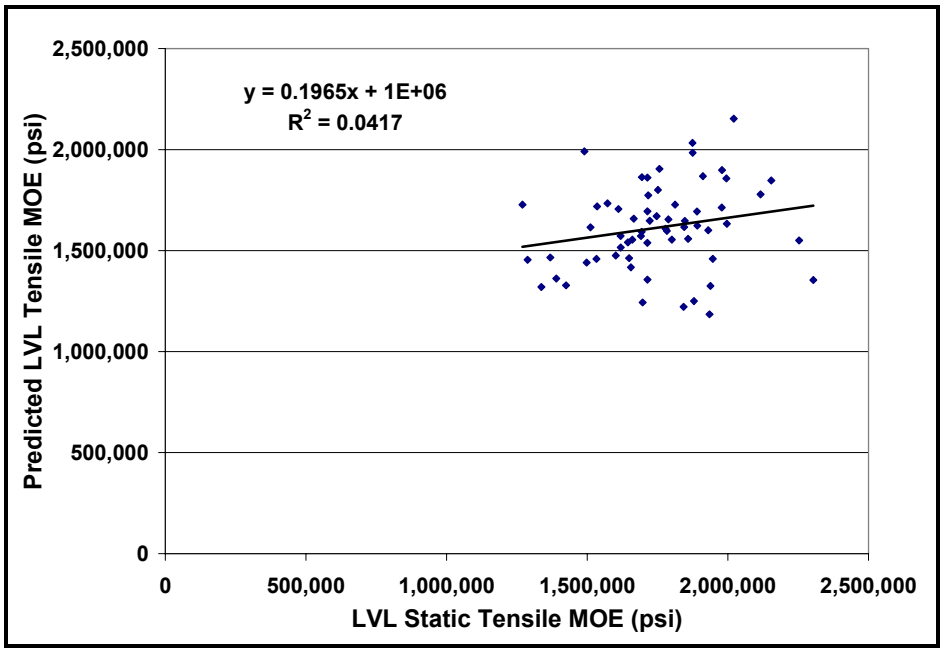

Figure C-4. Optical + GRP model: Predicted LVL tensile MOE vs. static MOE.

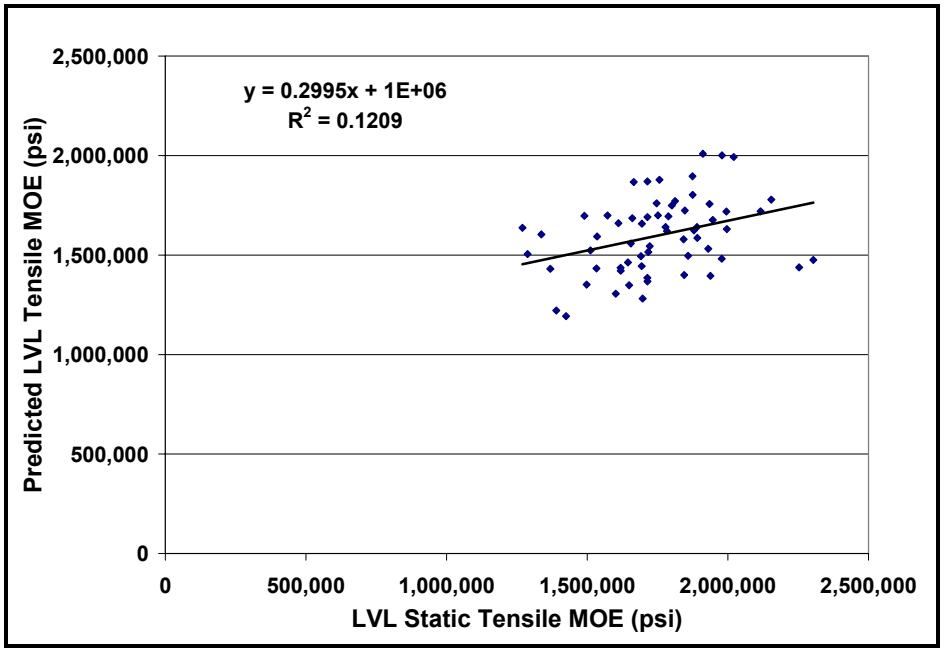

Figure C-5. Optical + GRP + density model: Predicted LVL tensile MOE vs. static MOE.

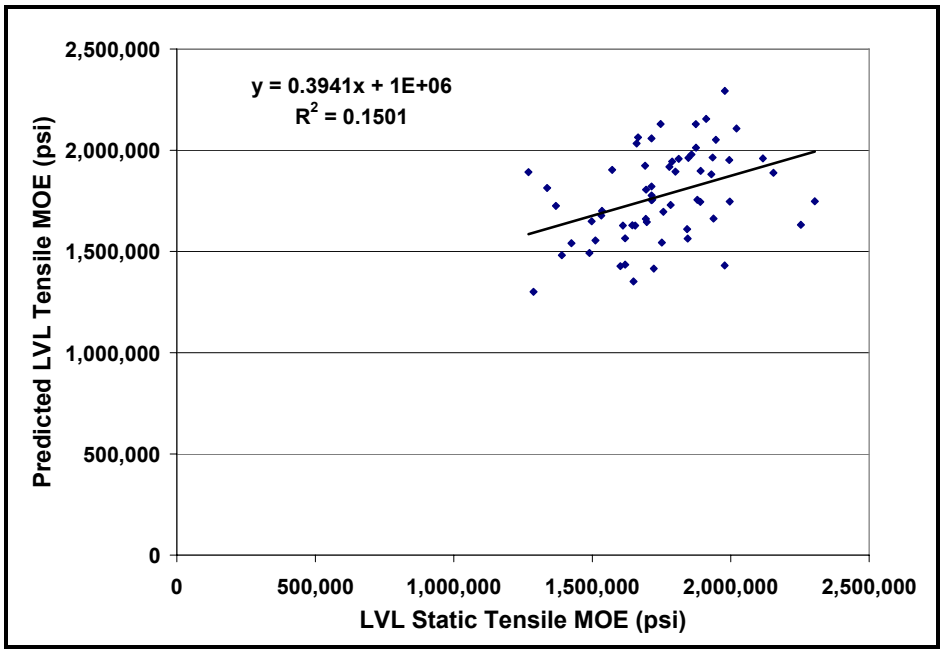

Figure C-6. Average MOE_d model: Predicted LVL tensile MOE vs. static MOE.

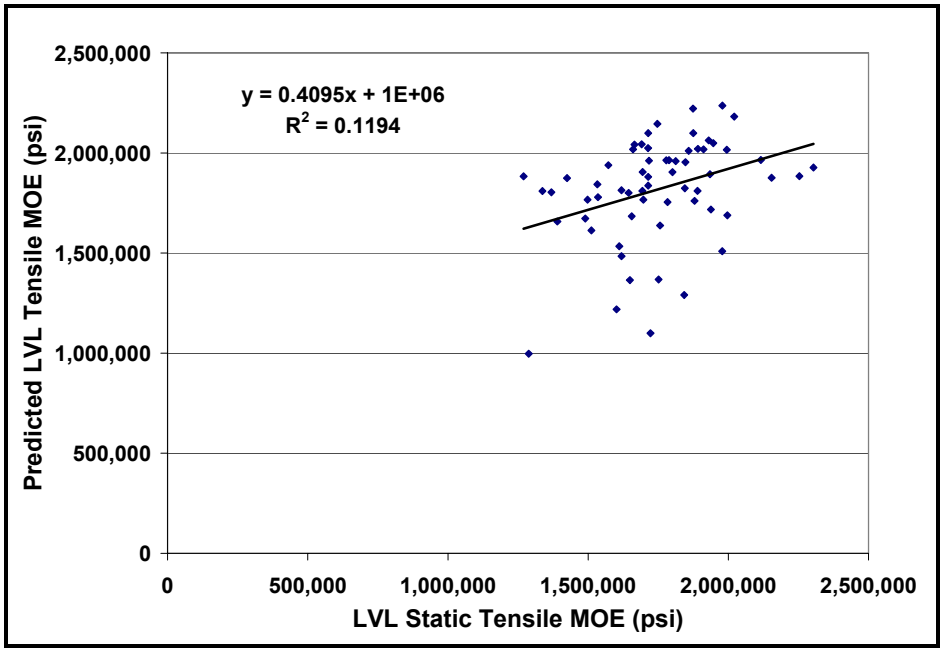

Figure C-7. Average UPT model: Predicted LVL tensile MOE vs. static MOE.

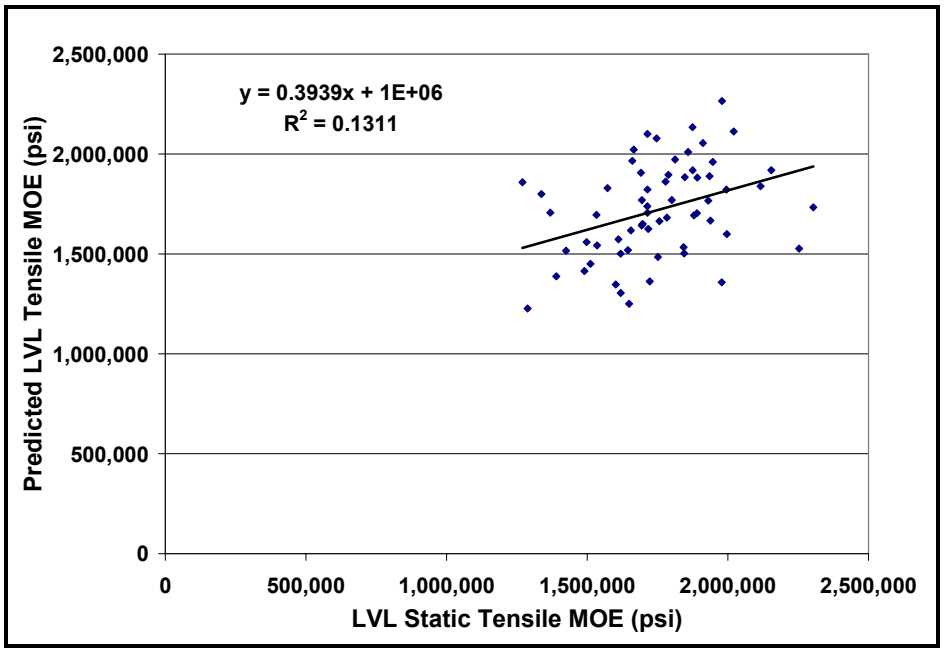

Figure C-8. Ultrasonic + spectral analysis model: Predicted LVL tensile MOE vs. static MOE.

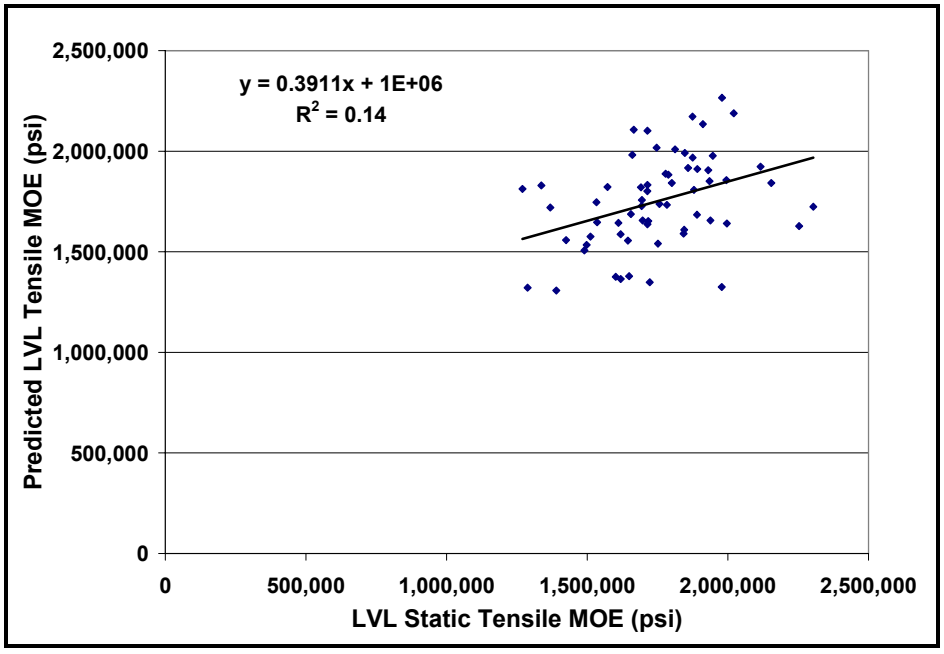

Figure C-9. Combined optical + ultrasonic model: Predicted LVL tensile MOE vs. static MOE.

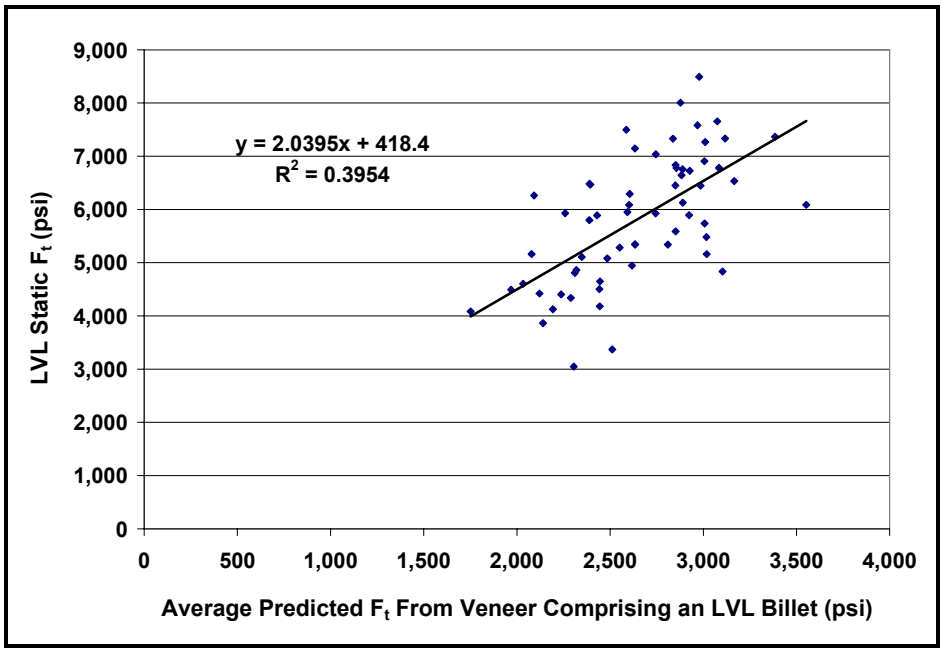

Figure C-10. Density model: Regression equation for predicting LVL static F_t based on calculated average of predicted F_t for veneer comprising a LVL specimen.

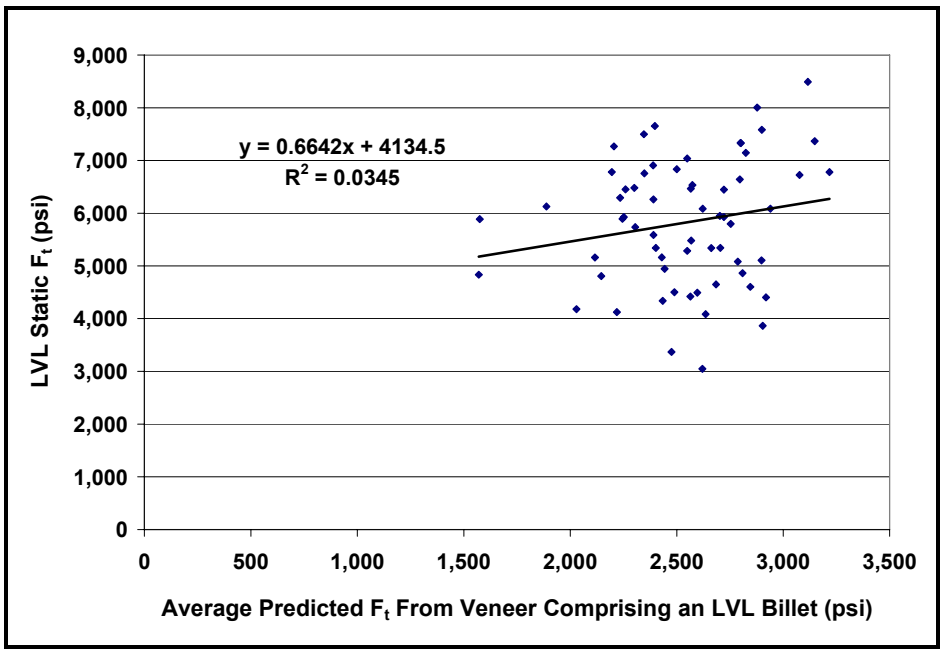

Figure C-11. Basic optical model: Regression equation for predicting LVL static F_t based on calculated average of predicted F_t for veneer comprising a LVL specimen.

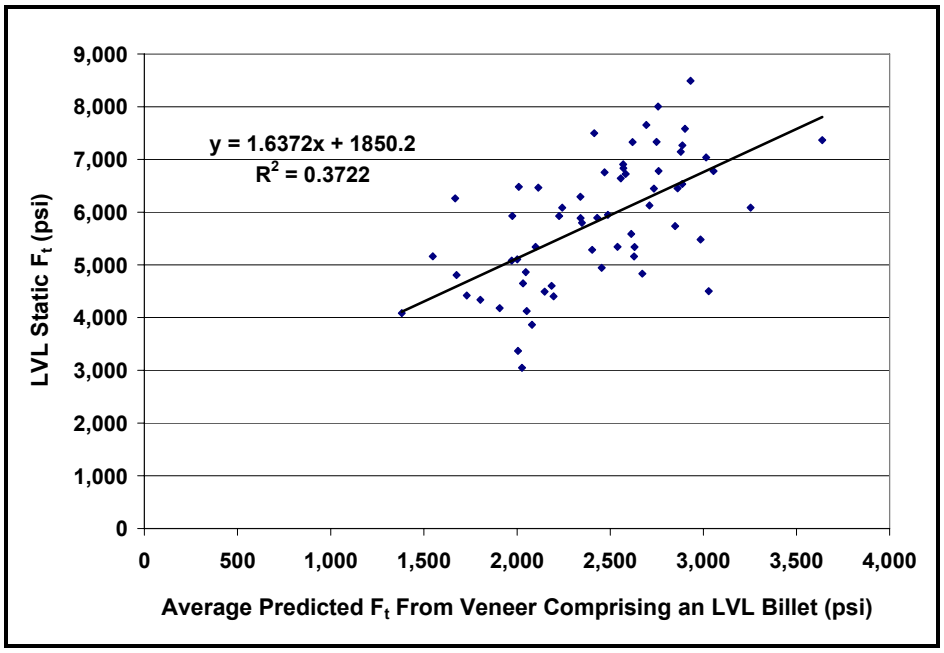

Figure C-12. Optical + density model: Regression equation for predicting LVL static F_t based on calculated average of predicted F_t for veneer comprising a LVL specimen.

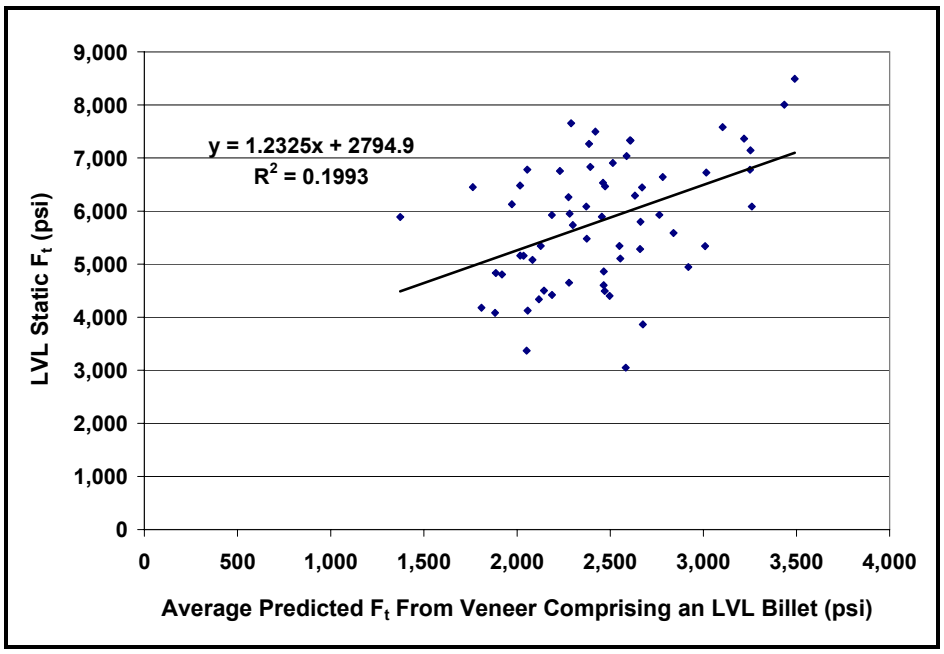

Figure C-13. Optical + GRP model: Regression equation for predicting LVL static F_t based on calculated average of predicted F_t for veneer comprising a LVL specimen.

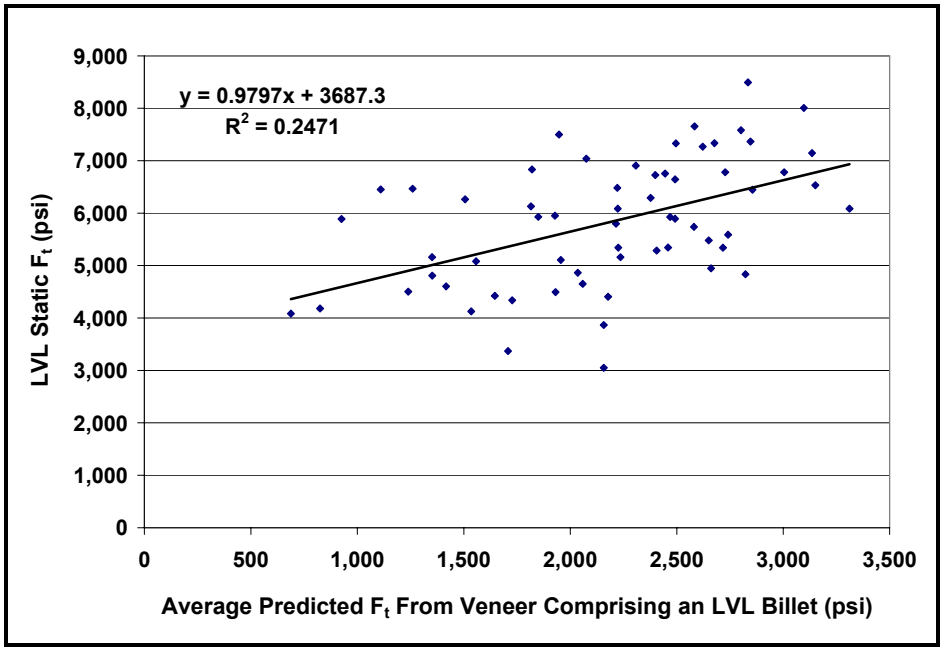

Figure C-14. Optical + GRP + density model: Regression equation for predicting LVL static F_t based on calculated average of predicted F_t for veneer comprising a LVL specimen.

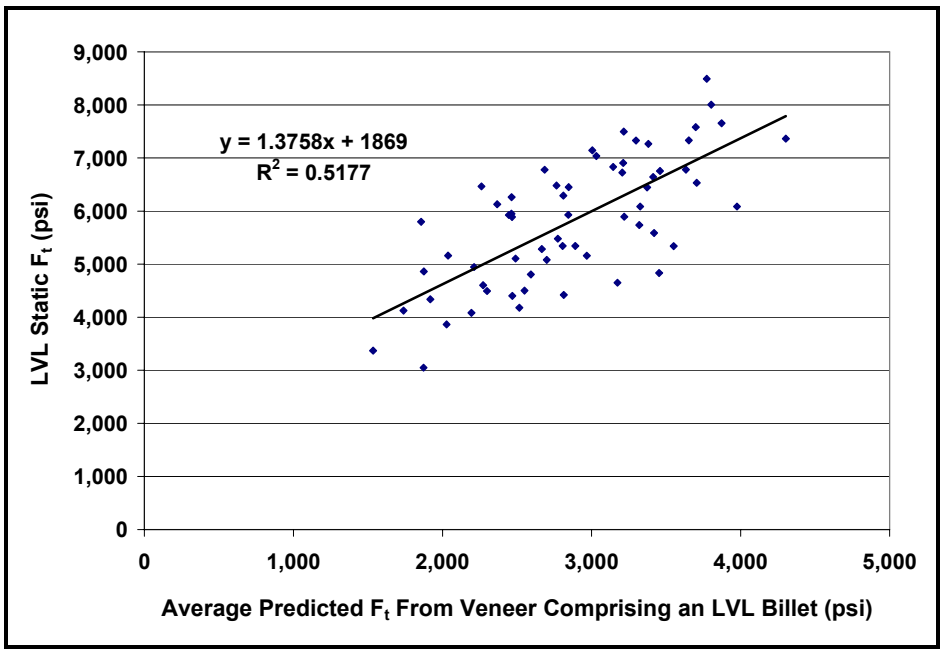

Figure C-15. Average MOE_d model: Regression equation for predicting LVL static F_t based on calculated average of predicted F_t for veneer comprising a LVL specimen.

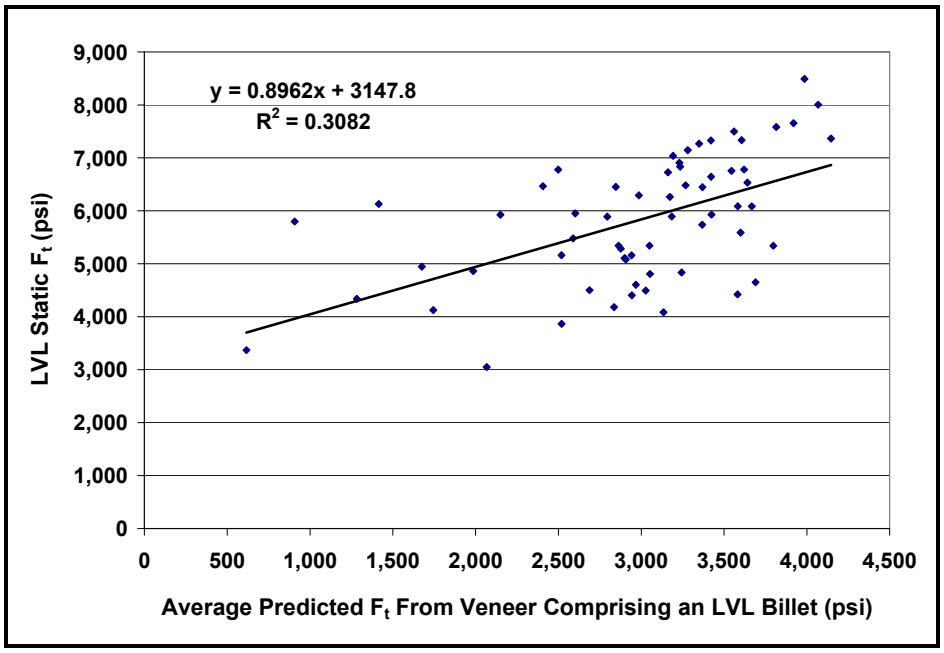

Figure C-16. Average UPT model: Regression equation for predicting LVL static F_t based on calculated average of predicted F_t for veneer comprising a LVL specimen.

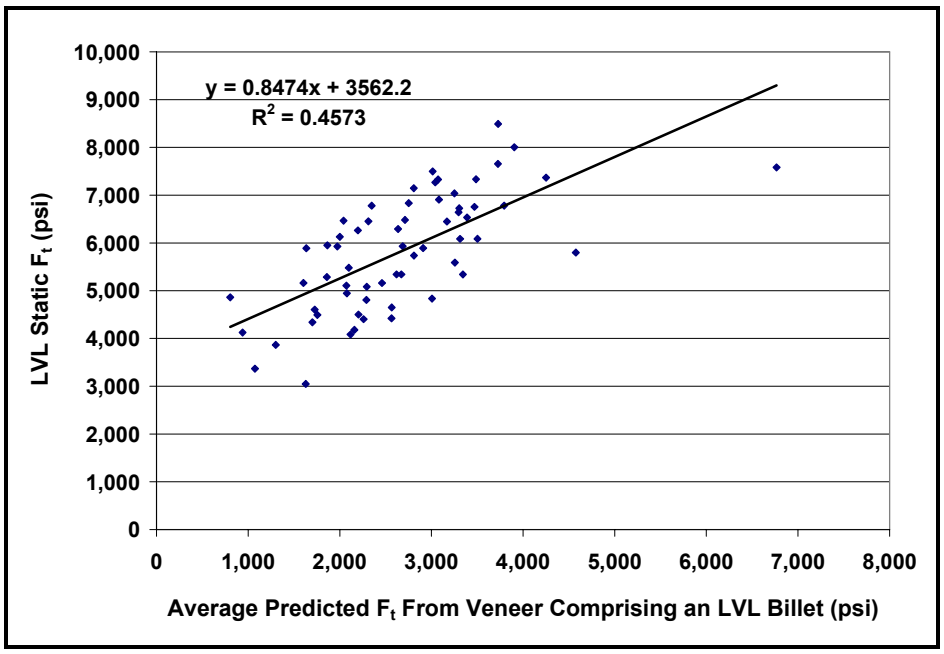

Figure C-17. Ultrasonic + spectral analysis model: Regression equation for predicting LVL static F_t based on calculated average of predicted F_t for veneer comprising a LVL specimen.

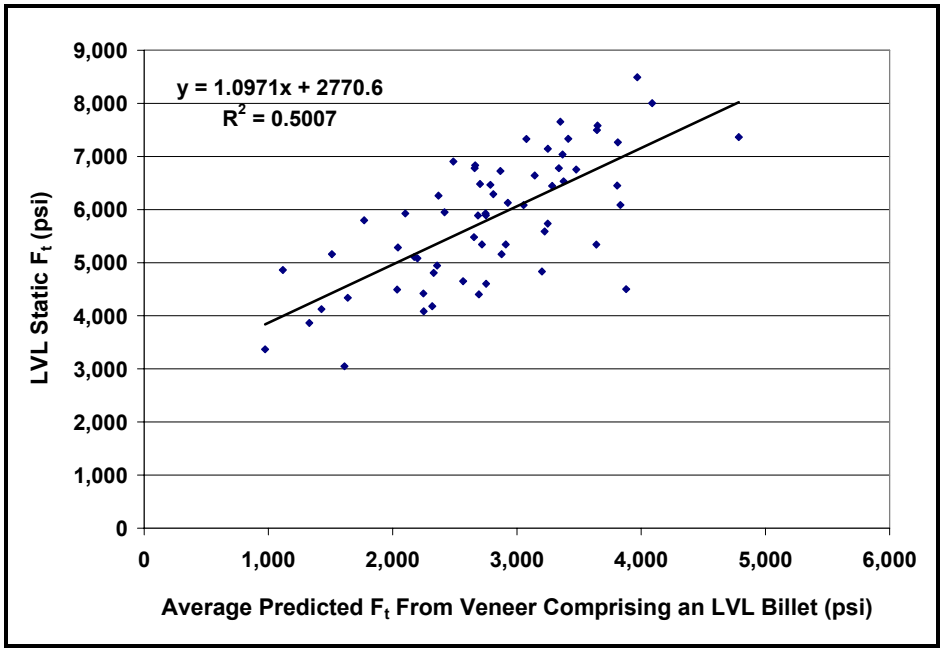

Figure C-18. Combined Optical + ultrasonic model: Regression equation for predicting LVL static F_t based on calculated average of predicted F_t for veneer comprising a LVL specimen.